

# **Development of tissue engineering strategies for supporting regeneration after injuries of the nervous system**

Von der Fakultät für Mathematik, Informatik und Naturwissenschaften der RWTH Aachen University zur Erlangung des akademischen Grades einer Doktorin der Naturwissenschaften genehmigte Dissertation

vorgelegt von

Diplom-Chemikerin

Kristina Belladonna Klinkhammer (geb. Feil)

aus Herdecke

Berichter: Universitätsprofessor Dr. Martin Möller

Universitätsprofessor Dr. Doris Klee

Tag der mündlichen Prüfung: 05.12.2011

Diese Dissertation ist auf den Internetseiten der Hochschulbibliothek online verfügbar.

---

---

## Acknowledgment

Diese Arbeit entstand in der Zeit von Juni 2005 bis Mai 2009 am DWI e. V. an der RWTH Aachen und wäre ohne die großartige Hilfe vieler Menschen nicht möglich gewesen.

Zunächst danke ich Herrn Prof. Martin Möller für die Möglichkeit, dieses interessante Thema bearbeiten zu dürfen. Frau Prof. Doris Klee danke ich für die Betreuung meiner Arbeit und die Anregungen und Diskussionen hierzu. Ich danke ihr für ihre Unterstützung und ihren Rückhalt. Ich danke außerdem PD Dr. Gary Brook und Prof. Dr. Jörg Mey für die Assistenz bei der Betreuung meiner Arbeit. Durch sie habe ich wertvolle Einblicke in biologische und medizinische Fragestellungen bekommen und gelernt, über den „chemischen“ Tellerrand zu schauen. Ein besonderer Dank gilt PD Dr. Paul Dalton für die Einführung in das Thema und seine Ratschläge bei den verschiedensten Fragen.

Ich danke allen Kollegen im AK Klee für die freundliche Atmosphäre und die wissenschaftliche Gespräche, die meine Arbeit immer wieder bereichert haben. Insbesondere bedanke ich mich bei Dirk Grafahrend für seine Hilfe bei allerlei chemischen Fragestellungen.

Ich bedanke mich bei allen Mitarbeitern am Universitätsklinikum Aachen und am Lehrstuhl für Biologie II der RWTH Aachen, die zum Gelingen dieser Arbeit beigetragen haben. Dies gilt insbesondere für Eva Schnell, Nadine Seiler, José Gerardo-Nava und Julia Bockelmann, die durch die gute Zusammenarbeit und die Durchführung der zellbiologischen Versuche diese Arbeit überhaupt erst möglich gemacht haben.

Ein großes Dankeschön geht an meine Forscher Sebastian Kühl und Holger Leonards für die Bearbeitung wichtiger Themen im Rahmen dieser Arbeit. Hara Simitzis danke ich besonders für ihren großartigen Fleiß, ihr Durchhaltevermögen und insbesondere für ihre Freundschaft.

Ich bedanke mich bei allen HiWi-Studenten, die wertvolle Arbeit zum Gelingen dieser Arbeit geleistet haben und nicht müde geworden sind, unzählige Substrate vorzubereiten und Daten auszuwerten.

Den Mitarbeitern des DWI und der MC danke ich für die angenehme Arbeitsatmosphäre und die stetige Bereitschaft, bei Problemen auszuhelfen. Mein ganz besonderer Dank gilt Stefan

---

Rütten für die tausenden von REM-Aufnahmen, die er für mich gemacht hat. Außerdem danke ich Dr. Robert Kaufmann für die XPS-Messungen und Dr. Ahmed Mourran für die Aufnahmen mit dem konfokalen Raman-Mikroskop und die wertvollen Diskussionen über die Interpretation der Ergebnisse. Meinen Büronachbarn Dr. Petra Mela und Dr. Rostislav Vinokur danke ich für die gute Stimmung im Büro. Vielen lieben Dank an meine Auszubildende Jana Wiese für ihre große Hilfe bei der Probenvorbereitung und den Spaß, den wir zusammen hatten.

Heidrun, Melanie, Mona, Haika, Priya, vielen lieben Dank für eure Freundschaft!

Ich danke allen, die diese Arbeit Korrektur gelesen haben und sie durch ihre Anregungen entscheidend verbessert haben. Hierbei ist besonders Dr. David Martin zu nennen, der mir stets schnell und zuverlässig geholfen hat.

Ganz besonders bedanke ich mich bei meiner Familie; ich danke meinen Eltern, meiner Schwester und meinen Schwiegereltern für die langjährige Unterstützung und das Interesse an meiner Arbeit. Meinem Mann danke ich für seine Liebe, für seine Geduld und dafür, dass er mich immer unterstützt.

---

## Table of Content

<b>List of Abbreviations</b>		<b>vi</b>
<b>Summary</b>		<b>x</b>
<b>Zusammenfassung</b>		<b>xiii</b>
<b>Chapter 1</b>	Introduction	<b>1</b>
<b>Chapter 2</b>	State of the art	<b>7</b>
<b>I Blends of poly(<math>\epsilon</math>-caprolactone) and collagen</b>		
<b>Chapter 3</b>	Electrospinning and investigation of fibres of poly( $\epsilon$ -caprolactone) (PCL)/collagen blends	<b>42</b>
<b>Chapter 4</b>	2-dimensional substrates of poly( $\epsilon$ -caprolactone) and PCL/collagen blends for <i>in vitro</i> investigations	<b>68</b>
<b>Chapter 5</b>	<i>In vitro</i> investigations on electrospun fibres of poly( $\epsilon$ -caprolactone) and poly( $\epsilon$ -caprolactone) /collagen	<b>90</b>
<b>II Poly(<math>\epsilon</math>-caprolactone)-<i>block</i>-poly(ethylene oxide) block copolymers</b>		
<b>Chapter 6</b>	Synthesis and electrospinning of poly( $\epsilon$ -caprolactone)- <i>b</i> -poly(ethylene oxide) block copolymers	<b>119</b>
<b>Chapter 7</b>	Synthesis and electrospinning of a GRGDS-functionalised poly( $\epsilon$ -caprolactone)- <i>b</i> -poly(ethylene oxide) block copolymer	<b>156</b>
<b>III Blends from star shaped NCO-poly(ethylene glycol)-<i>stat</i>-poly(propylene glycol) and poly(<math>\epsilon</math>-caprolactone)</b>		
<b>Chapter 8</b>	Functionalisation of electrospun fibres of poly( $\epsilon$ -caprolactone) and star shaped NCO-poly(ethylene glycol)- <i>stat</i> -poly(propylene glycol) for neuronal cell guidance	<b>175</b>
<b>CV</b>		<b>210</b>
<b>List of publications</b>		<b>211</b>

---

## List of Abbreviation

°C	degree Celsius
3D	three dimensional
Å	angstrom
ABD	antibody diluent
Ala	alanine
Arg	arginine
Asp	aspartatic acid
<i>b</i>	block
BHT	2,6-di- <i>tert</i> -butyl-4-methylphenol
Boc-PEO-OH	di- <i>tert</i> -butylcarbonate mono-protected poly(ethylene oxide)
CDCl <sub>3</sub>	deuterated chloroform
cFN	cellular fibronectin
cm	centimetre
CNS	central nervous system
CO <sub>2</sub>	carbon dioxide
CPCL25	a blend of PCL with 25 wt% type I collagen from calf skin
d	days
DAPI	4',6-diamidino-2 phenylindole dihydrochloride
DCM	dichloromethane
DFG	German research society (Deutsche Forschungsgemeinschaft)
DIV	days <i>in vitro</i>
DMEM	Dulbecco's modified Eagle medium
DMF	dimethylformamide
DMSO	dimethyl sulfoxide
DRG	dorsal root ganglia
DSC	differential scanning calorimetry
DWI	Deutsches Wollforschungsinstitut
ECM	extracellular matrix
EDC	1-ethyl-3-[3-dimethylaminopropyl]carbodiimide
eq	equivalent
Et <sub>2</sub> Zn	diethyl zinc
eV	electron volt

## Abbreviation

---

FCS	fetal calf serum
fig	figure
g	gram
ga	gauge
Gly	glycine
GPC	gel permeation chromatography
GRGDS	one letter code of the peptide sequence glycine-arginine-glycine-aspartic acid-serine
H <sub>2</sub> N-PEO	$\alpha$ -amino-hydroxy poly(ethylene oxide)
HCl*Et <sub>2</sub> O	HCl*diethyl ether
Ile	isoleucine
k	kilo
kDa	kilodalton
kV	kilovolt
Lys	lysine
M	molar
mA	milliampere
MES	2-(N-morpholino)ethanesulfonic acid
min	minute
mL	millilitre
mm	millimetre
Mn	molecular weight (number average)
MPEO 10k	MPEO with a molecular weight of 10000 g/mol
MPEO 5k	MPEO with a molecular weight of 5000 g/mol
MPEO	mono methyl ether poly(ethylene oxide) (=MeO-PEO-OH)
Mw	molecular weight (weight average)
NaCl	sodium chloride
NaOH	sodium hydroxide
NCO	isocyanate
NF200	antibody against neurofilament 200 kDa
NFG	nerve growth factor
NGS	normal goat serum
NHS	N-hydroxysuccinimide
NMP	N-methylpyrrolidone

---

NMR	nuclear magnetic resonance
p.a.	per analysis
PBS	phosphate buffered saline buffer
PCL	poly( $\epsilon$ -caprolactone)
PCL-ol	PCL-diol
PDI	polydispersity index (=Mw/Mn)
PEG	poly(ethylene glycol)
PEO	poly(ethylene oxide)
PEO- <i>b</i> -PCL	poly(ethylene oxide)- <i>b</i> -poly( $\epsilon$ -caprolactone)
pFN	plasma fibronectin
PLLA	poly(L-lactic acid)
PNS	peripheral nervous system
P-PEG	abbreviation for PCL/sPEG blends
PMMA	poly(methyl methacrylate)
PPol-PEG	abbreviation for PCL/PCL-diol/sPEG blends
<i>p</i> TSA	<i>para</i> -toluene sulfonic acid
RGD	one letter code of the peptide sequence arginine-glycine-aspartic acid
RT	room temperature
RWTH	Rheinisch-Westfälische Technische Hochschule
S100	antibody to mark Schwann cells
SC	Schwann cell
sec	second
SEM	scanning electron microscope
Sn(Oct) <sub>2</sub>	stannous II octoate
sPEG	star-shaped poly(ethylene oxide)- <i>stat</i> -poly(propylene oxide)
TBS-T	tris-buffered saline with Triton X
T <sub>c</sub>	crystallisation temperature
TE	tissue engineering
THF	tetrahydrofuran
T <sub>m</sub>	melting temperature
TMS	tetramethyl silane
Tyr	tyrosine
UV	ultraviolet
Val	valine



## Abbreviation

---

v/v	volume per volume
vs	versus
w/v	weight per volume
wt%	weight percent
XPS	X-ray photoelectron spectroscopy
YIGSR	one letter code of the peptide sequence tyrosine-isoleucine-glycine-serine-arginine
μg	microgram
μl	microlitre

---

## Summary

This thesis deals with the preparation of artificial guiding structures for supporting regeneration after nerve injuries. Injuries of the nervous system can have serious consequences such as the loss of motoric and sensoric function. As existing treatment methods for the peripheral nervous system (PNS) include several unsatisfying deficits and due to the absence of efficient treatment for injuries of the central nervous system (CNS), the development of an artificial scaffold for supporting nerve regeneration in both the PNS and CNS is highly desirable. Chemical composition, mechanical properties and oriented structures for aligned guidance of recovering nerves are important issues for such scaffolds.

The method of electrospinning was applied to produce highly oriented fibres from different materials with low densities to achieve oriented cell growth and aligned extensions from a variety of neuronal and non-neuronal cells. For *in vitro* experiments fibres were collected onto glass cover slips which were surface functionalised with a thin hydrogel layer based on star-shaped poly(ethylene glycol)-*stat*-poly(propylene glycol) (sPEG). The sPEG layer demonstrated non-adhesive properties towards cells and proteins which enabled controlled investigation of the effects actuated by the fibres. Additionally the sPEG layer allowed durable adhesion of the electrospun fibres on the substrates during several analytics and *in vitro* experiments.

Three different polymeric materials were developed and electrospun into fibres. Blends of poly( $\epsilon$ -caprolactone) (PCL) and the extracellular matrix protein (ECM) collagen were prepared by mixing and dissolving different ratios of the two polymers in a sufficient solvent. Electrospinning of the mixtures demonstrated a high dependency of the fibre quality on solution concentration and PCL-collagen ratio. High quality electrospun fibres were homogeneous, defect-free and had a small fibre diameter distribution. For oriented fibres, the degree of orientation and the absence of junctions between single fibres were important criteria. While high quality random fibres could be obtained at a certain electrospinning solution concentration from all PCL-collagen mixtures, reproducible high qualities of oriented suspended fibres were only obtained at a PCL-collagen ratio of 3:1. Fibre diameters were between 0.4 – 2.4  $\mu\text{m}$ . Several analytical methods including antibody staining against collagen, x-ray photoelectron spectroscopy, infra red spectroscopy, and confocal raman spectroscopy demonstrated the existence of collagen at the fibre surface. In a first approach of *in vitro* experiments, oriented electrospun fibres of PCL/collagen blend containing 25 wt% of collagen were applied directly onto sPEG coated cover slips. Pure PCL fibres served as

control. Experiments with cells important in the nervous system including neurons, Schwann cells, astrocytes, oligodendrocytes and olfactory ensheathing cells showed an affinity of the cells to the collagen containing fibres. Neurites were longer and cells migrated further and showed a higher alignment according the fibre direction with these fibres.

In a second approach random and oriented PCL/collagen and PCL fibres were collected on the coverslips which were surface functionalised with a cell repellent sPEG hydrogel layer or on coverslips coated with a sPEG hydrogel which was functionalised with the ECM peptide sequence Gly-Arg-Gly-Asp-Ser (GRGDS) enabling cellular adhesion. Within this system the orientation and the chemistry of fibres and the underlying substrate can be varied independently which allows the investigation of competitive cell/surface and cell/fibre interactions. It turned out, that culture of dissociated DRGs behaved with regard to the competitive functionality of the fibre and substrate surfaces. The combination of aligned PCL/collagen fibres on non-adhesive surfaces was most efficient in guiding neurite outgrowth.

In the second part of the thesis, amphiphilic poly(ethylene oxide)-*b*-poly( $\epsilon$ -caprolactone) (PEO-*b*-PCL) block copolymers with molecular weights between 34000 to 76000 g/mol and different block length ratios were prepared. The synthesis performed with tin-octoate as catalyst in the melt allowed good control of molecular weight and high yields up to 90 %. The majority of the polymers could be electrospun into suspended oriented fibres and the polymers with the highest molecular weights showed the lowest dependency on electrospinning parameters. Surface analysis of the electrospun fibres demonstrated a hydrophilic character and reduced protein adsorption properties. With respect to these results, a GRGDS-functionalised PEO<sub>230</sub>-*b*-PCL<sub>560</sub> block copolymer was prepared in a three step synthesis starting from di-*tert*-butylcarbonate (Boc)-protected PEO as macroinitiator. Analytics verified the success of each preparation step. The functionalisation with the peptide sequence should allow cellular adhesion and guidance of neuronal cells similar to the results with PCL/collagen as described before. Simultaneously it should inhibit undesired protein adsorption due to the PEO block, which makes the polymers suitable as implantable biomaterials with controlled material/body interactions. However, impurities and degradation processes during the synthesis prevented oriented electrospinning and therefore cell experiments which could confirm the theoretical considerations were not performed.

In the third part of the thesis blends of sPEG, PCL and poly- $\epsilon$ -caprolactone-diol (PCL-diol) were prepared and functionalised either with the peptide sequence GRGDS or the ECM protein fibronectin. Oriented suspended fibres could be electrospun. A reduced protein

---

affinity of PCL/sPEG/PCL-diol blends demonstrated the existence of sPEG at the fibre surface. Unfunctionalised PCL/sPEG fibres showed minimal cellular migration and axonal outgrowth while in contrast, the biologically functionalised fibres increased cellular response significantly. Thus, these fibres combine protein repellent properties with simultaneous cell attracting functionality.

Oriented suspended and biological functionalised electrospun fibres encouraged cell adhesion and migration and induced alignment of cells and extensions according to the fibre direction. Thus, the fibres developed in this thesis are a promising tool for the preparation of scaffolds for neuronal regeneration after nerve injuries.

### Zusammenfassung

Diese Doktorarbeit beschäftigt sich mit der Entwicklung von künstlichen richtungsangebenen Gerüststrukturen, die zur Regeneration von Nerven nach Verletzungen des Nervensystems eingesetzt werden sollen. Verletzungen des zentralen und des peripheren Nervensystems (ZNS, bzw. PNS) haben unter anderem den Verlust von motorischen und sensorischen Funktionen zur Folge. Die aktuellen Behandlungsmethoden für PNS-Verletzungen weisen eine Vielzahl von Unzulänglichkeiten auf und für ZNS-Verletzungen gibt es momentan gar keine Behandlungsmethode. Daher besteht ein großer Bedarf, künstliche Implantate zu entwickeln, die durch ihre chemische Zusammensetzung, mechanische Eigenschaften und durch strukturgebende Parameter Nervenwachstum leiten und unterstützen können.

Innerhalb dieser Doktorarbeit wurde die Methode des Elektrosinnens verwendet, um freischwebende, orientierte Fasern aus verschiedenen Materialien in einer geringen Dichte herzustellen. Die Fasern wurden auf Deckgläsern gesammelt, die mit einer speziellen Hydrogelschicht aus sternförmigen Poly(ethylenoxid)-*stat*-poly(propylenoxid) (sPEG) beschichtet wurden. Diese Hydrogelschicht wirkt abweisend auf Zellen und Proteine, so dass diese sich dort nicht anlagern können. Dadurch kann gezielt der Einfluss der Fasern auf das Zellverhalten untersucht werden. Zusätzlich ermöglicht die sPEG Schicht die permanente Bindung der Fasern an die Glasoberfläche, so dass die Fasern in nachfolgenden Experimenten nicht abgespült werden. Drei verschiedene polymere Materialien wurden in dieser Arbeit entwickelt und zu Fasern versponnen.

Im ersten Teil wurden orientierte und randomisierte Fasern aus Blends aus Poly( $\epsilon$ -caprolacton) (PCL) und Kollagen Typ I mit verschiedenen Mischungsverhältnissen hergestellt. Es zeigte sich, dass die Faserqualität stark von der Konzentration der Spinnlösung und vom Verhältnis von PCL zu Kollagen abhing. Qualitativ hochwertige Fasern sind homogen, defektfrei und haben eine geringe Faserdurchmesserverteilung. Bei orientierten Fasern spielen auch noch der Grad der Orientierung und die Abwesenheit von Vernetzungspunkten zwischen den einzelnen Fasern eine Rolle. Während es möglich war, aus sämtlichen PCL-Kollagen-Mischungen randomisierte Fasern herzustellen, konnten hochwertige und reproduzierbare orientierte Fasern nur bei einem PCL:Kollagen-Verhältnis von 3:1 erzielt werden. Hierbei wurden Faserdurchmesser von 0.4 – 2.4  $\mu\text{m}$  erreicht. Zahlreiche Analytikmethoden (z. B. Antikörper-Färbung, Röntgenphotoelektronen-Spektroskopie, Infrarot-Spektroskopie und konfokale Raman-Spektroskopie) bestätigten die Anwesenheit von Kollagen an der Fa-

---

seroberfläche. In einer ersten Reihe von Zellversuchen wurden Deckgläser mit sPEG beschichtet und hierauf orientierte PCL-Kollagenfasern mit einem Kollagengehalt von 25 Gew.-% gesammelt. Es wurde eine Vielzahl verschiedener Zellen aus den beiden Nervensystemen (u.a. Neuronen, Astrozyten und Schwannzellen) auf die Fasern appliziert. Fasern aus reinem PCL dienten zudem als Kontrolle. Es zeigte sich eine hohe Affinität der Zellen zu den kollagenhaltigen Fasern. So waren Neurite länger und besser orientiert und Zellen migrierten weiter und streckten sich deutlich mehr entlang der PCL/Kollagen-Fasern.

In einer zweiten Versuchsreihe wurden orientierte und nicht-orientierte PCL/Kollagen und PCL Fasern miteinander verglichen. Sie wurden auf sPEG-Hydrogelschichten und zusätzlich auf sPEG-Hydrogelschichten, die mit Gly-Arg-Gly-Asp-Ser (GRGDS), einem Zellbindungspeptid aus der Extrazellulären Matrix (EZM), funktionalisiert wurden, gesammelt. Dieser Versuchsaufbau ermöglichte die Variation einzelner Komponenten des Systems und die Untersuchung des Einflusses der konkurrierenden Komponenten auf die zelluläre Antwort. Es stellte sich heraus, dass dissoziierte Zellen aus Dorsalwurzelganglien (DRGs) auf die Konkurrenz aus funktionalisierten Fasern und Substratoberfläche reagierten und dass die Kombination aus orientierten PCL/Kollagenfasern auf proteinabweisenden Oberflächen am effektivsten waren, um gerichtetes Neuritenwachstum zu generieren.

Im zweiten Teil dieser Arbeit wurden Blockcopolymer aus Poly(ethylenoxid)-*block*-( $\epsilon$ -caprolacton) (PEO-*b*-PCL) mit einem Molekulargewicht zwischen 34000 und 76000 g/mol und verschiedenen Blocklängenverhältnissen hergestellt. Die Synthese aus der Schmelze mit Zinnoctoat als Katalysator erwies sich als die beste Methode und erlaubte eine gute Kontrolle über das Molekulargewicht und Ausbeuten bis zu 90 %. Fast alle Polymere konnten zu orientierten Fasern gesponnen werden, wobei die Faserqualität bei Polymeren mit hohen Molekulargewichten weniger von den Elektrosinnbedingungen beeinflusst wurde. Die Oberflächenanalyse dieser Fasern zeigte eine deutliche Hydrophilie und eine verminderte Adsorption von Proteinen aus Lösung, was darauf hindeutete, dass sich der PEO-Block an der Faseroberfläche befand. Basierend auf diesen Ergebnissen wurde anschließend ein GRGDS-funktionalisiertes PEO<sub>230</sub>-*b*-PCL<sub>560</sub> Blockcopolymer hergestellt. Die 3-schrittige Synthese wurde mit einem Boc-geschützten PEO-Block als Makroinitiator gestartet und die einzelnen Schritte analytisch bestätigt. Die Funktionalisierung mit der Peptidsequenz sollte Zelladhäsion und Führung von neuronalen Zellen ermöglichen und der PEO-Block gleichzeitig unerwünschte Proteinadsorption unterdrücken. Diese Eigenschaften würden diese Fasern zu geeigneten Kandidaten für die Herstellung von Implantaten machen, bei denen bestimmte Körper/Biomaterial-Wechselwirkungen erzielt werden sollen. Während der Synthese traten

jedoch Abbaureaktionen des Polymers auf. Dadurch, und durch synthesebedingte Verunreinigungen war es nicht möglich, aus diesem Material freischwebende, orientierte Fasern zu spinnen, so dass die Theorie nicht in Zellversuchen bestätigt werden konnte.

Im dritten Teil dieser Dissertation wurden Blends aus PCL, sPEG und PCL-Diol hergestellt und mit GRGDS bzw. Fibronectin funktionalisiert. Es wurden orientierte, freischwebende Fasern erzeugt und die Existenz des sPEGs an der Faseroberfläche durch eine reduzierte Proteinadsorption dieser Fasern bestätigt. Unfunktionalisierte Fasern zeigten verminderte Zelladhäsion und reduziertes Neuritenwachstum. Die biologische Funktionalisierung mit GRGDS oder Fibronectin zeigte im Gegensatz dazu eine signifikante positive Zellreaktion. Dies bestätigte die hervorragenden Eigenschaften dieser Fasern, nämlich unerwünschte Proteinadsorption zu verhindern und gleichzeitig spezielle Zellreaktion anzuregen.

Orientierte, freischwebende und biologisch funktionalisierte Fasern erwiesen sich als besonders geeignet für die Zelladhäsion und Migration und induzierten die Ausrichtung von Zellen und orientiertes Extensionswachstum entlang der Faserrichtung. Damit sind diese Fasern ein viel versprechendes Mittel zur Herstellung von Gerüststrukturen für die neuronale Regeneration nach Nervenverletzungen.





## INTRODUCTION

### 1.1 Concept

The aim of this thesis was the development of artificial guiding structures as a tissue engineering strategy for supporting nerve regeneration after nerve injuries.

In nervous systems, neurons are the basic structural and functional elements. They consist of a cell body (soma) and its extensions (axons and dendrites) and have the task to transmit electrical signals for information transport. Glial cells which are e. g. Schwann cells (SC) in the peripheral nervous system (PNS) and oligodendrocytes in the central nervous system (CNS) surround the axons and support their functions. Several axons are bundled to form fascicles and several fascicles finally form the nerve cable<sup>1</sup>.

Injuries of the PNS and CNS occur thousand folds worldwide every year and result in serious loss of motoric and sensory functions distal the lesion site and additional often in neurotic pain. While small PNS injuries often recover by themselves due to self-healing processes of the patients body<sup>2</sup>, bigger injuries require the usage of nerve autografts, mainly from the *nervus seralis*. This raises a range of other problems such as multiple surgeries, neuroma pain and function loss at the donor site. In contrast to the PNS, injuries of the CNS do not regenerate by themselves due to several reasons. One main problem is the formation of a glial scar by activated astrocytes. This scar protects the healthy tissue from infections and further physical damage but is also a barrier for regenerating axons<sup>3,4</sup>. Additionally astrocytes express inhibiting molecules which prevent axonal growth and result in failure of regeneration<sup>5</sup>. At present no treatment for regeneration of CNS injuries exists.

Tissue engineering has evolved from biomaterials to produce cell/scaffold constructs that permit cellular organisation before scaffold degradation. It combines medical, mechanical, chemical and biological aspects and was defined, as “the recognition of biological tissue through the use of cells with the aid of supporting structures and/or biomolecules” by the European Commission in 2001<sup>6</sup>. Biocompatible artificial implants with oriented structures may guide regenerating nerve fibres and may help to overcome the disadvantages involved by nerve autografts in injuries of the PNS. They also may be used to overcome the glial scar and help to induce axonal regeneration in the CNS by providing specific signals.

## Introduction

---

Two main concepts are in consideration for the development of such bridging implants for supporting nerve recovery. The first uses tubes or channels embedded in a surrounding matrix as guiding structures<sup>1, 7</sup>. The purpose of this thesis is another concept in which oriented fibres guide regenerating nerves, mimicking the fibrillar structure of nerve fibres similar to autografts. It was already shown that oriented structures are able to guide axonal growth followed by SCs which preferentially migrate on axons<sup>8-10</sup>. These mutual interactions between Schwann cells and neurites make oriented fibres ideal candidates for supporting nerve regeneration because they mimic the structure of axons.

In this thesis, fibres in the nanometre range were produced by electrospinning. The gap method of alignment<sup>11, 12</sup> enables the production of aligned fibres in controlled densities for the investigation of single cell-fibre interaction. However this method requires high polymer purity, intensive investigation of electrospinning parameters and mechanical stability of the resulting fibres.

Of course not only structural aspects play an important role in nerve regeneration but also chemical and biological ones. First of all, the artificial implant must consist of a biomaterial which itself is not cytotoxic and neither its degradation products. The surface of such an implant must be biologically or chemical functionalised to induce specific bioreactions necessary for nerve regeneration<sup>13</sup>. This can be achieved by targeted introduction of biologically active molecules to the bulk material. From the broad range of possible biomaterials, poly( $\epsilon$ -caprolactone) (PCL) was chosen as the main polymer in this thesis. PCL is a semicrystal synthetic polyester and was employed in several biomedical studies<sup>14, 15</sup>. It can be electrospun into mechanical stable oriented fibres necessary for the concept of this thesis. Although PCL itself is cell attractive, biological activation is necessary for specific bioreactions. This thesis deals with three different ways of biological functionalisation of PCL. The bioactive function was verified by spectroscopic analysis and *in vitro* experiments with a wide range of cells important for nerve regeneration including neurons, SC and astrocytes.

In the first part, PCL was blended with the extracellular matrix (ECM) protein collagen which has mainly structural functions in the ECM but also mediates cell adhesion and migration<sup>16</sup>. Since the proliferation of human fibroblasts increased by inclusion of collagen in PCL/collagen fibres<sup>17</sup>, the presence of collagen in the oriented fibres of the implant should be advantageous for ECM building in nerve grafts *in vivo*.

A more controllable but also more complicated way includes the full synthesis of a biologically active synthetic polymer. Block copolymers of PCL and poly(ethylene oxide) (PEO) were synthesised and the peptide sequence GRGDS was bound to the polyether to mediate biological activity in the second part of this thesis. As GRGDS is the cell binding domain in ECM proteins such as fibronectin, collagen and laminin,<sup>18</sup> a similar function as by the inclusion of collagen is introduced to the fibres but with a much smaller molecule. PEO was shown to prevent the adhesion of cells and proteins,<sup>19</sup> which is a desired property because immuno reactions such as inflammation and encapsulation can be suppressed and also the adhesion of cells which disturb the regeneration processes. Thus, the inclusion of this polymer into the biomaterial offers a high control of cell reactions when the biomaterial is simultaneously activated with cell attractive cues. This effect was already shown by Grafahrend *et al.*<sup>20</sup> with PEO-*b*-PCL block copolymers, but in contrast to this thesis, they prepared block copolymers with a maximum molecular weight of 27 kDa, while in this thesis molecular weights were minimum 34 kDa, but preferential around 70 kDa, necessary for the preparation of oriented electrospun fibres.

Star-shaped poly(ethylene oxide)-*stat*-poly(propylene oxide) (sPEG) has similar or even better cell and protein repellent properties than linear PEO<sup>19</sup>. In the third part of this thesis a six-arm sPEG polymer with isocyanate (NCO) end groups was used for the preparation of PCL/sPEG blends. The combination of the star-like structure and reactive NCO groups, allows crosslinking of the molecules resulting in the formation of a three-dimensional network. Beside the possibility for crosslinking, the NCO groups allow a wide range of (bio)functionalisation by reaction with amino or hydroxyl groups in biological active molecules. Here biological functionalisation was forced by addition of GRGDS or fibronectin. This enables controlled cellular reactions as previously described for part two of the thesis. Thus, the inclusion of these polymers offers a high control of cell reactions and therefore nerve regeneration.

### 1.2 Content of this thesis

This thesis deals with the preparation of artificial guiding structures for supporting nerve regeneration after nerve injuries by the method of electrospinning.

**Chapter 2** gives an overview of the state of the art and introduces the topic of tissue engineering. The method of electrospinning is explained and polymers used in electrospinning experiments for tissue engineering applications are presented. Important extracellular matrix proteins which can serve as biological functionalisation of tissue engineering constructs are named and their role in the body described.

**Chapter 3** deals with the preparation of blends of PCL/collagen and their electrospinning into random and oriented fibres. Effects on fibre morphologies in dependency on electrospinning conditions are discussed and surface and bulk properties of the fibres are analysed.

In **chapter 4** oriented and random fibres of pure PCL and of a PCL/collagen blend with 25 wt% collagen are applied on the one hand onto glass coverslips which are coated with a cell and protein repellent hydrogel layer based on poly(ethylene oxide)-*stat*-poly(propylene oxide) (sPEG) and on the other hand onto sPEG-coated hydrogel layers which are surface functionalised with the cell adhesive peptide sequence GRGDS. The competitive influences of surface coating, fibre material and fibre alignment on behaviour of dissociated cells from dorsal root ganglia are investigated.

In **chapter 5** the cellular behaviour of a wide range of neuronal and non-neuronal cells is investigated in *in vitro* experiments on the fibres which were found to be the best for oriented cell growth from chapter 4. These fibres, namely oriented biological functionalised collagen containing fibres on repellent surfaces are compared with oriented PCL fibres on the same surface. The experiments presented in this chapter were performed in collaboration with Eva Schnell<sup>21</sup>, Nadine Seiler<sup>22</sup> and José Gerardo-Nava<sup>23</sup> during two diploma theses and one doctoral thesis.

**Chapter 6** deals with the preparation of amphiphilic poly(ethylene oxide)-*b*-poly( $\epsilon$ -caprolactone) (PEO-*b*-PCL) block copolymers and comparison of different ways of synthesis. Oriented electrospinning of the polymers is performed and the influences of block lengths, block length ratios and electrospinning conditions on the resulting fibres described. Surface and bulk properties are analysed.

With respect to the results of chapter 6, in **chapter 7** the preparation of a GRGDS-functionalised PEO-*b*-PCL block copolymer is described including the influence of synthesis parameters on fibre preparation by electrospinning.

**Chapter 8** presents the preparation and electrospinning of blends from PCL, PCL-diol and sPEG. Fibres from different polymer mixtures are produced and fibre morphology in dependency of polymer concentration and applied solvents are investigated. Functionalisation of the blends with GRGDS or the protein fibronectin is described. It is shown, that the biological functionalisation influences the behaviour of dissociated cells from dorsal root ganglia in comparison with fibres from an unfunctionalised blend.

### 1.3 References

1. Schmidt, C. E.; Leach, J. B., Neural tissue engineering: strategies for repair and regeneration. *Annual Review of Biomedical Engineering* **2003**, 5, 293 - 347.
2. Reichert, H., *Neurobiologie*. 2nd edition ed.; Georg Thieme Verlag: Stuttgart, 2000.
3. Busch, S. A.; Silver, J., The role of extracellular matrix in CNS regeneration. *Current opinion in neurobiology* **2007**, 1, (17), 120 - 127.
4. Klapka, N.; Müller, H. W., Collagen matrix in spinal cord injury. *Journal of Neurotrauma* **2006**, 23, 422 - 435.
5. Fawcett, J. W.; Asher, R. A., The glial scar and central nervous system repair. *Brain Research Bulletin* **1999**, 49, (6), 377 - 391.
6. Devices, T. S. C. o. M. P. a. M. *Opinion on The State of the Art concerning Tissue Engineering, SANCO/SCMPMD/2001/0006 Final*; European Commission: 2001.
7. Lundborg, G., A 25-year perspective of peripheral nerve surgery: evolving neuroscientific concepts and clinical significance. *The Journal of Hand Surgery* **2000**, 25A, 391 - 413.
8. Son, Y. J.; Thompson, W. J., Schwann cell processes guide regeneration of peripheral axons. *Neuron* **1995**, 14, 125 - 32.
9. Thompson, D. M.; Buettner, H. M., Neurite outgrowth is directed by Schwann cell alignment in the absence of other guidance cues. *Annals of Biomedical Engineering* **2006**, 34, 161 - 168.
10. Ide, C.; Tohyama, K.; Yokota, R.; Nitatori, T.; Onodera, S., Schwann cell basal lamina and nerve regeneration. *Brain Reseach* **1983**, 288, 61 - 75.
11. Dalton, P. D.; Klee, D.; Möller, M., Electrospinning with dual collection rings. *Polymer* **2005**, 46, (3), 611 - 614.
12. Li, D.; Wang, Y. L.; Xia, Y. N., Electrospinning of polymeric and ceramic nanofibers as uniaxially aligned arrays. *Nano Letters* **2003**, 3, (8), 1167 - 1171.

13. Ratner, B. D., Correlation, surfaces and biomaterial science. In *Biomaterials Science: An introduction to materials in medicine*, 2 nd ed.; Ratner, B. D., Hoffman, A. S., Schoen, F. J., Lemons, J. E., Ed. Elsevier: San Diego, 2004; pp 765 - 771.
14. Chew, S. Y.; Mi, R.; Hoke, A.; Leong, K. W., The effect of the alignment of electrospun fibrous scaffolds on Schwann cell maturation. *Biomaterials* **2008**, 29, 653 - 661.
15. Johnson, J.; Nowicki, M. O.; Lee, C. H.; Antonio Chiocca, E. A.; Viapiano, M. S.; Lawler, S. E.; Lannutti, J. L., Quantitative analysis of complex glioma cell migration on electrospun polycaprolactone using time-lapse microscopy. *Tissue Engineering, Part C* **2009**, 15, (4), 531 - 540.
16. Geiger, B.; Bershadsky, A.; Pankov, R.; Yamada, K. M., Transmembrane extracellular matrix - cytoskeleton crosstalk. *Nature Reviews Molecular Cell Biology* **2001**, 2, (11), 793 - 805.
17. Venugopal, J.; Zhang, Y.; Ramakrishna, S., *In vitro* culture of human dermal fibroblasts on electrospun polycaprolactone collagen nanofibrous membrane. *Artificial Organs* **2006**, 30, 440 - 445.
18. Hersel, U., Dahmen, C., Kessler, H., RGD modified polymers: biomaterials for stimulated cell adhesion and beyond. *Biomaterials* **2003**, 24, 4385 - 4415.
19. Gasteier, P.; Reska, A.; Schulte, P.; Salber, J.; Offenhausser, A.; Moeller, M.; Groll, J., Surface grafting of PEO-based star-shaped molecules for bioanalytical and biomedical applications. *Macromolecular Bioscience* **2007**, 7, (8), 1010 - 1023.
20. Grafahrend, D.; Calvet, J. L.; Salber, J.; Dalton, P. D.; Moeller, M.; Klee, D., Biofunctionalized poly(ethylene glycol)-block-poly(epsilon-caprolactone) nanofibers for tissue engineering. *Journal of Materials Science-Materials in Medicine* **2008**, 19, (4), 1479 - 1484.
21. Schnell, E. Guidance of glial cell migration and axonal growth by electrospun nanofibers of poly-epsilon-caprolactone and a collagen/poly-epsilon-caprolactone blend. Diploma thesis at RWTH Aachen, Aachen, 2006.
22. Seiler, N. Elektrospun nanofibers as guidance structures for migration of Schwann cells and astrocytes. Diploma Thesis at RWTH Aachen, Aachen, 2007.
23. Gerrardo-Nava, J. Doctoral Thesis at RWTH Aachen, in preparation.

### STATE OF THE ART

Injuries of peripheral nerves (PN) may cause lasting sensory or motor deficits and sometimes they are also accompanied by intractable neuropathic pain<sup>1</sup>. Until now, the best available treatment of peripheral nerve lesions involves the transplantation of an autologous nerve. However, several limitations of this approach have motivated the search for a bioengineering solution in order to design artificial implants. Artificial implants for nerve regeneration have to be biocompatible with suitable mechanical properties, but also have to promote several specific physiological reactions<sup>2,3</sup>: (1) They should guide and promote axonal elongation of motor and sensory neurons, (2) endogenous Schwann cells from the host have to migrate into the implant as these cells are needed to provide trophic support and remyelination of regenerated fibers, and (3) the implant must allow vascularisation, diffusion of metabolites and oxygen while preventing the infiltration of scar forming fibroblasts.

Oriented nanofibres of the right biomaterial fulfil important criteria for neurite guidance and aligned axon growth and offer a great opportunity for the development of artificial nerve implants. Preparation of these highly aligned fibres is possible using the method of electrospinning from a wide range of materials.

#### 2.1 Tissue Engineering

Cells in native tissue live in a three-dimensional environment, embedded in the extracellular matrix (ECM) which consists predominantly of a network of filaments with biological cues. Proliferation, migration and guiding of the cells are mainly dictated by interactions with the ECM. Loss or damage of tissue and organs requires special treatments including transplantation, tissue implantation from the patient himself, application of medical devices and/or pharmaceuticals. Often the body reacts allergically or immunologically and inflammations occur. In general the diseased organ or tissue is only imperfectly replaced and the number of required transplants is much higher than the available.

Tissue engineering (TE) strategies include the preparation of cell-scaffold devices for the development of implants to support or replace certain body functions, e.g. after injuries of the nervous system. It combines medical, mechanical, chemical and biological aspects and permits cellular organisation before scaffold degradation<sup>4</sup>. Figure 1 illustrates the concept of TE.

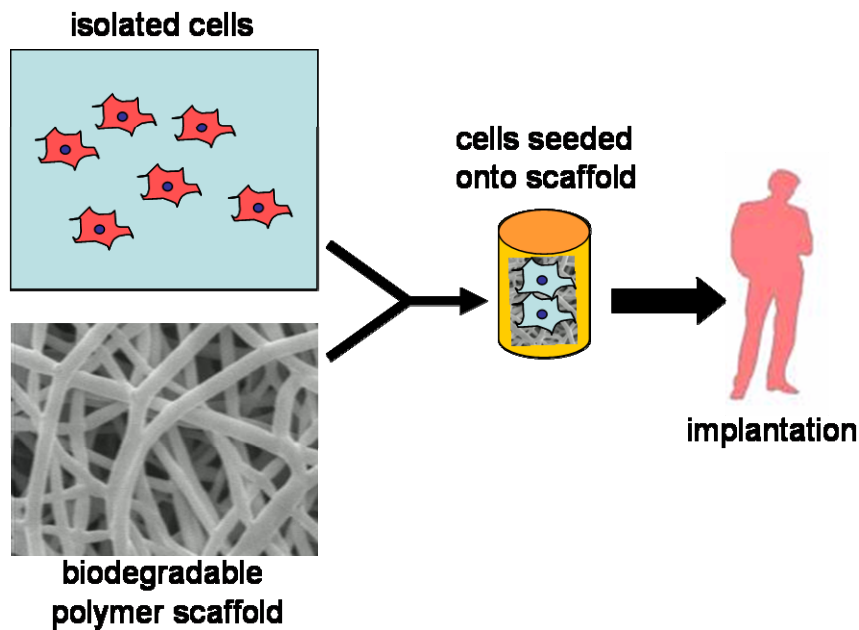


**Figure 1: Concept of tissue engineering.** Isolated cells, mostly from the patient himself are seeded onto a scaffold from a biodegradable polymer. This seeded scaffold is implanted into the patient and cells start to reorganise.

It is of significance that the structure of the scaffold is similar to the morphology of the natural tissue. For neuronal tissue engineering strategies an oriented nanometre scaled fibrillar structure is therefore required.

## 2.2 Electrospun fibres for tissue engineering

Fibres with diameters less than 500 nm are called nanofibres. They have several extraordinary characteristics compared to larger fibres (e.g. above 20  $\mu\text{m}$ ): a very large surface area to volume ratio, high bending performance and flexible surface functionalities. Fibres with similar structures and diameters than those of fibrils in the ECM are very interesting for biomedical applications as cells can attach and organise well around fibres of diameters smaller than themselves.

Nanofibres can be produced by several different techniques including drawing<sup>5</sup>, template synthesis<sup>6,7</sup>, phase separation<sup>8</sup> or self-assembly<sup>9,10</sup>. Another simple, fast and inexpensive method is electrospinning which enables the production of continuous fibres. Different fibre types for various applications can be obtained: high density mats of random fibres as well as single oriented fibres.



### 2.2.1 The electrospinning process

In the electrospinning process continuous fibres are formed by charging a polymer melt or solution which moves towards a counter electrode. The polymer solution gets charged by pressing it through a spinneret with a certain speed. The spinneret is connected with a high voltage source and the applied voltage leads to the formation of a polymer drop at the end of the spinneret. If the voltage is high enough to overcome the surface tension of the droplet, it changes its shape, becomes stretched and the so called “Taylor cone” is formed (see figure 2). The cone is not oriented vertical but has an angle of  $\delta = 49.3^\circ$ , detected by Taylor in the 1960s<sup>11-13</sup>. When the voltage reaches a certain limit, the surface tension of the polymer cone at the tip of the spinneret is countervailed by the electrostatic force and elongating and stretching of the cone occurs, resulting in the formation of a polymer jet. The jet moves towards the nearest counter electrode (grounded target). Charged elements inside the jet create electrostatic forces which cause whipping and bending of the jet with the result that it does not move straight towards the target but in loops, the so-called “bending instability”<sup>14</sup>. Several parameters such as viscosity, surface tension, electrostatic forces, air friction and gravity are involved in this process. The diameter of the loops increases with rising instability and distance from the spinneret. Bigger loop diameters result in elongation and thinning of the jet. However, the jet diameter is limited<sup>15</sup>. During the jet’s way towards the target, the solvent evaporates and small fibres are collected onto a target. Depending on the desired product, different targets can be used. A schematic view of an electrospinning apparatus is shown in Figure 2. It typically consists of three components: a high voltage source, a spinneret and a grounded target as collector.

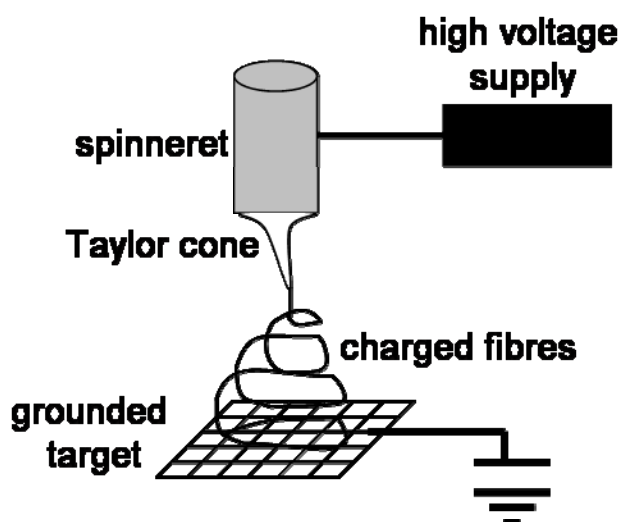


**Figure 2: Scheme of electrospinning setup.** The setup consists of a high voltage supply, a spinneret and a grounded target where the fibres are collected.

### 2.2.2 Parameters affecting electrospun fibres

The electrospinning process is very complex and many parameters influence the ability to electrospin fibres of a specific polymer/solvent composition and thus the morphology of the resulting fibres as well as the spinning efficiency. For polymers which can be electrospun into fibres, it is desirable that (1) the fibre diameter is consistent and controllable, (2) the surface is defect-free or defect-controllable and (3) continuous single electrospun fibres can be collected. Figure 3 summarises the different morphologies which can be obtained via electrospinning including (a) homogeneous oriented fibres, (b) homogeneous random fibres, (c) beaded fibres and (d) beads.

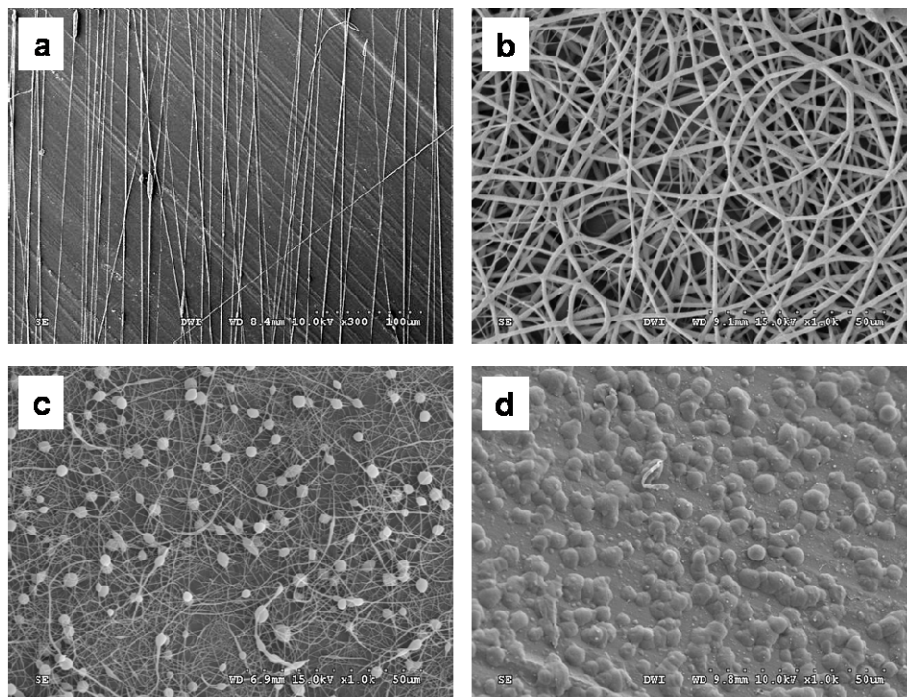


**Figure 3: Different products obtained by electrospinning:** (a) homogeneous oriented fibres, (b) homogeneous random fibres, (c) beaded fibres, and (d) beads.

The effective parameters can be divided into three main aspects:

- **solution properties:** e.g. viscosity, boiling temperature, vapour pressure, surface tension, dielectric constant, and conductivity,
- **ambient parameters:** e.g. (solution) temperature, humidity and air velocity in the electrospinning chamber,

- **governing parameters:** e.g. pump rate to the spinneret, electric field strength, electric potential at the tip of the spinneret, working distance (distance between the tip and the target), length and diameter of the spinneret and solution flow rate.

Although exceptions can be found for all cases, some general findings can help to explain the electrospinning phenomena: The **solution parameters** have the biggest effects on the electrospinning process. On the jet's path from the spinneret to the target, the polymer content in the jet and jet size primarily influence the fibre diameter. Splitting of the jet in several sub-jets may,<sup>16</sup> or may not<sup>14, 17, 18</sup> occur and results in different fibre diameters. When no splitting is involved, the molecular weight of the polymer and the solution viscosity, which is a function of the polymer concentration and the molecular weight, are one of the most significant parameters influencing the fibre morphology. Below a critical polymer concentration, the jet in the electrospinning process breaks up into small droplets due to Rayleigh instabilities ("electrospraying")<sup>19</sup>. As the polymer concentration is increased, a mixture of beads and fibres is obtained<sup>20</sup>. Higher polymer concentration results in continuous fibres. Their diameters rise when concentration is increased, but too high concentrations prevent electrospinning due to too high viscosities. The jet formation relies on the entanglement of polymer chains and continuous fibres can only be obtained using polymer contents above a critical concentration which allows chain overlap. This concentration is directly proportional to the molecular weight of the polymer. This means that for longer chain lengths (= higher molecular weight), lower concentrations are needed for chain overlapping and therefore for the formation of continuous fibres<sup>21, 22</sup>. Figure 4 visualises the correlations between molecular weight, polymer concentration and fibre formation.

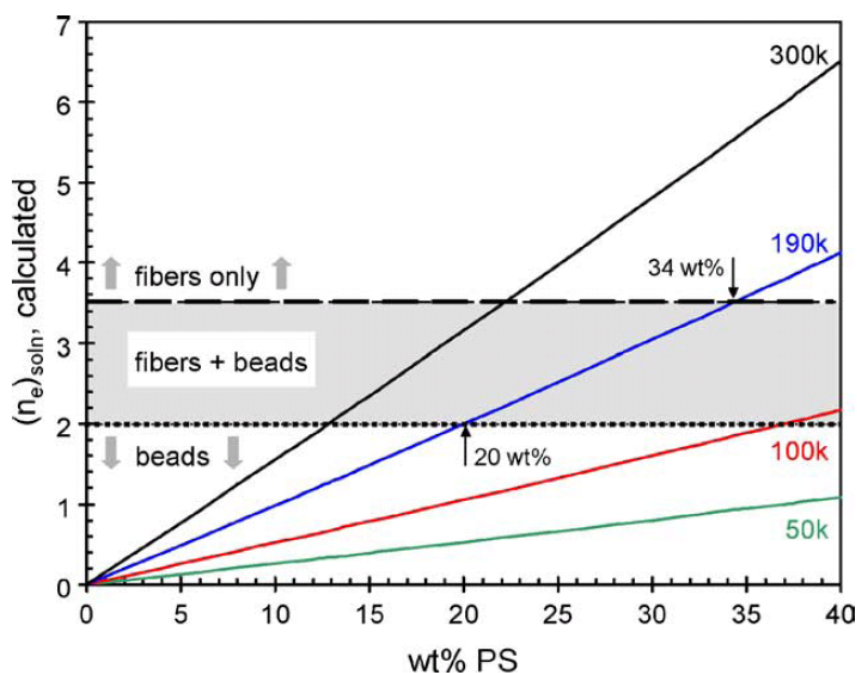


**Figure 4:** Number of entanglement  $(n_e)_{\text{soln}}$  as function of polymer concentration for polystyrene (PS) in tetrahydrofuran. The solid lines are calculated for different average molecular weights. In the grey region fibres and beads are obtained. Above the dashed line electrospinning of continuous fibres is possible. Reprinted from literature<sup>21</sup>. Copyright (2005) with permission from Elsevier.

Besides the molecular weight of the polymer and the solution concentration, the solvent properties play an important role in the formation of electrospun fibres, too. The *surface tension*  $\gamma$  is the opposite force to the coulomb repulsion and the balance between these two forces determines the curvature of the bending jet during instabilities. The surface tension together with the viscosity of the spinning solution is often the key factor determining if a specific polymer/solvent combination can be electrospun<sup>16</sup>. Beads and beaded fibres are less likely to be formed with lower surface tension<sup>20</sup>. Normally small surface tensions are desired, because this requires smaller applied voltages. However, the surface tension of a solvent changes after dissolution of a polymer in dependency on the concentration<sup>16</sup>, the nature of the polymer<sup>23</sup> and the solvent composition<sup>24</sup>. Thus, low surface tension of a solvent will not necessarily result in better nanofibres.

The *dielectric constant*  $\epsilon$  indicates how much electrical charge a solvent can hold. High electrical constants induce a more homogeneous distribution of surface charge density on the jet which yields higher quality fibres with smaller diameters<sup>25</sup>.

Another important factor is the *volatility* of the solvent. The evaporation of the solvent creates the solid fibre on the target. Ideally all of the solvent is evaporated during travelling from the spinneret to the target. Otherwise residual solvent may cause fusion of “wet” fibres<sup>26</sup>. An example of this fibre morphology is shown in figure 5.

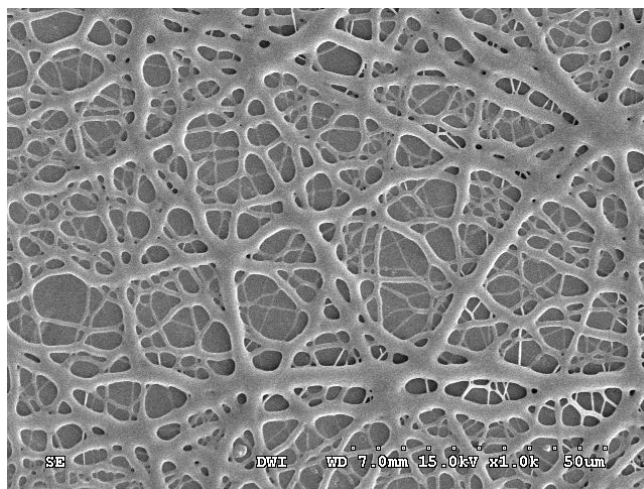


**Figure 5:** Example of wet fibres obtained if the solvent is not fully evaporated during the electrospinning process.

Low boiling points and high vapour pressure assist fast solvent evaporation and improve fibre quality. However, rapid evaporation may result in drying of the polymer solution at the spinneret tip and causes blocking<sup>27</sup>.

The *conductivity* of the polymer solution also has an influence. It can be increased by the introduction of small amounts of ions (salt) in percentages of around 1 %<sup>20</sup>. This generates a higher charge density on the surface of the solution jet during electrospinning and induces elongating forces in the jet resulting in smaller beads and thinner fibres. However, too high salt concentrations prevent electrospinning<sup>28</sup>.

The **ambient parameters** mainly have influence on the velocity of solvent evaporation and correlate for example with the volatility of the solvent and the resulting effects. Mostly electrospinning is not performed in a conditioned room which makes it very difficult to precisely control these parameters.

From the **governing parameters** the applied voltage and the flow rate have the biggest effect on fibre morphology. The applied *voltage* provides the surface charge on the

electrospinning jet. With higher voltages instability and stretching of the jet occur which generally yield smaller fibre diameters<sup>29</sup>. However, in the literature contradictory results have been presented, ranging from no significant effect<sup>30</sup> to the opposite effect<sup>31</sup>. This discrepancy shows that the influence of the voltage can not be considered alone but in combination with other parameters as for example the flow rate (the rate at which the polymer solution is pumped through the spinneret). The ideal flow rate matches the rate of removal of the solution from the tip of the spinneret. Higher flow rates often result in larger fibre diameters and beads.

It must be pointed out, that some of these parameters are not independent from each other and some are hard to control. Practical experiments for each polymer/solvent combination are therefore essential for evaluating parameters for high quality fibres. The influences of electrospinning parameters on fibre morphology are summarised in several good reviews and books<sup>25, 32-35</sup>.

### 2.2.3 Collector geometry for electrospinning

Different collector geometries allow the collection of different fibre arrangements which can be used for a range of applications. Figure 6 demonstrates the common collection targets with (a) single plate, (b) rotating mandrel, (c) dual rings, and (d) parallel bars.

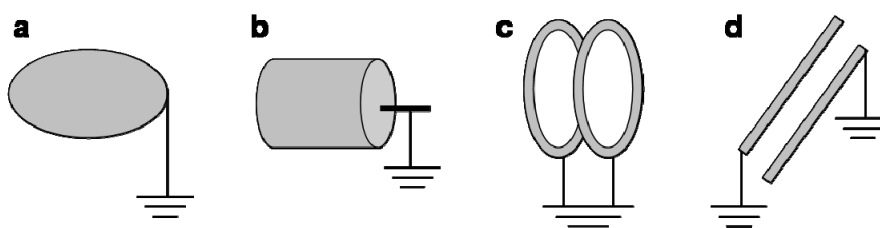


**Figure 6: Commonly used collection targets in electrospinning** including (a) single plate, (b) rotating mandrel, (c) dual rings, and (d) parallel bars.

The simplest and most frequently used configuration is a grounded single plate (fig. 6a) which is placed at a fixed distance from the tip of the spinneret. The residual charges on the as-spun fibres are rapidly removed and a dense sheet of random fibres is formed (see fig. 3b). To orientate the fibres within these sheets (see fig. 3a), a rotating mandrel can be used (fig. 6b). The degree of orientation can be controlled by the rotation-velocity. This configuration allows for example the production of tubular nanofibre constructs used for

development of tissue engineering applications such as vascular grafts<sup>36,37</sup>. A development in spinning orientated fibres is through the use of dual collection rings (fig. 6c). Here single, orientated fibres can be obtained, suspended between the rings<sup>38</sup>. A similar configuration which allows the collection of highly aligned nanofibres with more space between them represents the use of two parallel bars (fig. 6d)<sup>39</sup>. This arrangement induces splitting of the electric field into two and is directed by each of the electrodes. The jet is attracted first to the closest electrode and then stretched rapidly to the other electrode resulting in a perpendicular alignment<sup>39,40</sup>. This effect is illustrated in figure 7.

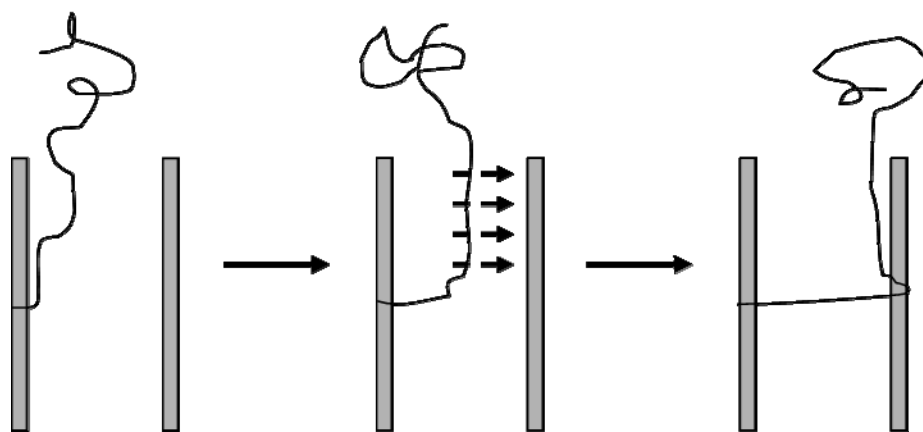


**Figure 7: Jet stretching across two parallel electrodes.**

Polymer nanofibres have poor electrical conductivity and therefore the fibre in the gap between the electrodes loses its residual charges very slowly<sup>24</sup> which results in fibre repulsion. In contrast to the collection on a rotating mandrel, very thin nanofibres cannot be collected with this method because of their fragility. The same is expected for fibres from polymers with low mechanical stability.

### 2.2.4 Electrospun fibres in biomedical applications

For the development of bioengineered implants it is of significance, that the structure of the biomaterial is similar to the morphology of the natural tissue. Thus, woven and non-woven fibre mats are used for the production of tissue templates and wound dressings where excellent cell penetration is required, while oriented structures guide cells in nerve regeneration. The potential of electrospun fibres from different polymers and composites have already been investigated for a broad range of possible biomedical applications. Table 1 gives an overview.

**Table 1: Polymers electrospun into fibres and used for tissue engineering applications** with PLGA: poly(lactide-*co*-glycolic acid); PCL: poly( $\epsilon$ -caprolactone); PLA: poly(lactide acid); PLLA: poly(L-lactide acid); PEO: poly(ethylene oxide). References taken from<sup>41, 42</sup>.

Application	Polymer	Cell type	Reference
<b>skin graft</b>	PLGA/dextran	dermal fibroblasts	43
	PCL/collagen type I	dermal fibroblasts	44, 45
	collagen type I	keratinocytes	46
	PLGA/chitin nanoparticles/collagen type I	keratinocytes	47
<b>bone graft</b>	PCL	mesenchymal stem cells	48
	PCL	<i>in vivo</i> implantation	49
	PCL/hydroxyapatite	osteoblasts	50
<b>vascular graft</b>	poly(L-lactide- <i>co</i> -caprolactone)/collagen type I	human coronary artery endothelial cells	51
	PLA/collagen type I	arterial smooth muscle cells	52
	PLGA/collagen/elastin	smooth muscle cells	53
<b>cartilage graft</b>	collagen type II	chondrocytes	54, 55
	PLGA	chondrocytes	56
	PCL	chondrocytes	57
<b>cardiac graft</b>	PCL coated with collagen type I	cardiomyocytes	58
	polyaniline/gelatin	cardiac myoblasts	59
<b>nerve graft</b>	PLLA	neural stem cells	60, 61
	PLGA	<i>in vivo</i> implantation	62
<b>drug delivery</b>	PCL/PEO		63, 64
	PCL/PEO/dextran		65

Table 1 shows that mainly electrospun fibres from polyesters, especially PCL and poly(lactide acid)s have been used in tissue engineering applications, independent from the site of action. Combinations with biological active molecules such as collagen enhanced cellular recognition and improved the function of the graft.

### 2.3 Polymers for tissue engineering

Polymers play an important role in tissue engineering and natural polymers such as the ECM proteins collagen and fibrin<sup>66</sup>, as well as synthetic ones have already been applied. Polyesters from the poly( $\alpha$ -hydroxy) family are often used if bioresorbable and degradable



materials are needed. Poly( $\epsilon$ -caprolactone) (PCL) is used for long-term applications due to its slow degradation rate while poly(L-lactide acid) (PLA, stereoisomers PLLA and PDLA) degrades much faster. Other prominent polymers for TE are poly(glycolic acid) (PGA), poly(lactide-*co*-glycolic acid) (PLGA) and poly(ethylene oxide) (PEO)<sup>67</sup>. In order to mimic the ECM and induce cell recognition, growth factors, peptides or proteins can be incorporated into the scaffold. For this purpose several methods including blending and covalent binding by chemical reactions are available.

### 2.3.1 Block copolymers

Block copolymers are special kinds of polymers consisting of blocks of different polymerised monomers and offer the opportunity to profit from the advantages of all involved polymers. Type of monomer, block lengths, block ratio and structure define a broad range of properties including solubility and degradation rate but require monitored synthesis. Figure 8 shows examples for possible architectures such as AB-diblock, ABA-triblock and ABC-triblock polymers.

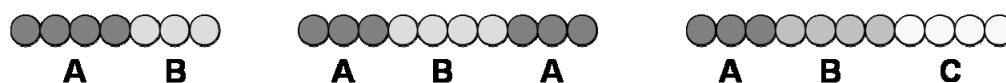


**Figure 8: Variations of block copolymers.** Several combinations including AB, ABA and ABC block copolymers are possible.

Numerous combinations of polymer blocks are possible, for example the preparation of copolymers with two hydrophobic blocks such as P(LLA-CL) diblocks<sup>68</sup> as well as those from a hydrophilic block and a hydrophobic one e.g. PEO-*b*-PLA<sup>69</sup> or PEO-*b*-PCL<sup>70, 71</sup>. Such amphiphiles are of particular interest for tissue engineering, as the various block insolubilities can assist in drug delivery due to spontaneous formation of micelles through self-assembly in a selective solvent. The PEO component is soluble in water and is present at the shell or corona of the micelle in aqueous solutions while the hydrophobic PCL comprises the core.

For the synthesis of block copolymers generally three strategies are of importance: In the first method, a block coupling reaction or condensation between two different polymers with functional end groups is performed. The second method uses ionic initiators with a terminal active centre of the starting block which stays “alive” and can reinitiate the

polymerisation of a second monomer. This initiator can be cationic or anionic as for example in the anionic-ring-opening polymerisation. Thirdly, a bifunctional radical initiator can be used to initiate a second potential active centre at the end of an already grown polymer chain. This results in the formation of a macroinitiator which can start a new chain in a further reaction<sup>72</sup>.

Ring-opening polymerisation of cyclic esters such as  $\epsilon$ -caprolactone with alcohols demonstrated good control of molecular weights and high yields. Such a synthesis of PEO-*b*-PCL copolymers can be performed in solution or from the melt. A PEO block with a certain block length serves as macroinitiator and can be activated by a broad range of catalysts (non-metallic or metallic). Although non-metallic activation with HCl\*diethyl ether<sup>73, 74</sup> is possible, syntheses are mostly performed with metallic catalysts. Especially stannous II octoate<sup>70, 71</sup> is often used resulting in PEO-*b*-PCL block copolymers with molecular weights between 1500 and 25000 Da. The mechanism of the ring-opening polymerisation with stannous II octoate as catalyst has been well investigated and confirmed by mass spectroscopic analysis<sup>75</sup>. It is illustrated in figures 9 and 10: The synthesis of PEO-*b*-PCL block copolymers with  $\epsilon$ -caprolactone as monomer and PEO as macroinitiator starts with the activation of the catalyst **1** (fig. 9) by the alcohol function of PEO. Hydrogen bonds between the octoate and alcoholate groups from the PEO results in formation of a stannous alcoholate as active species **3**, a stable initiator complex.

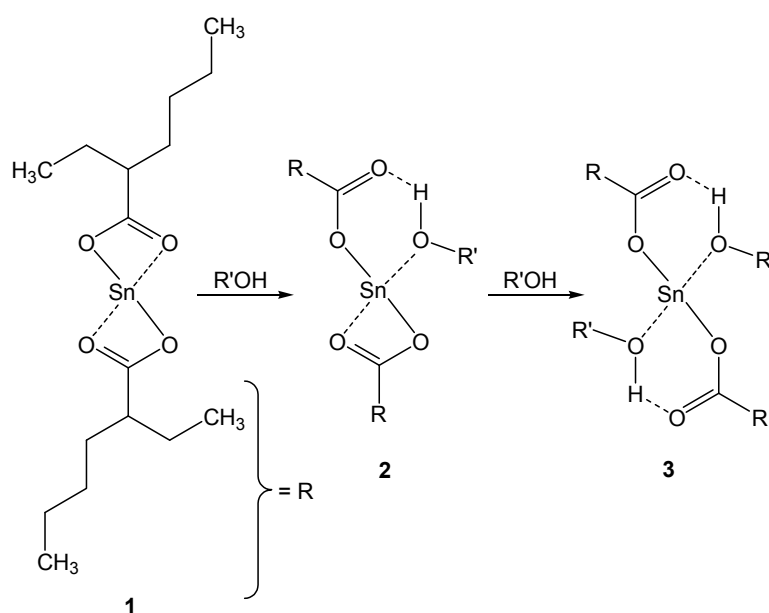


**Figure 9: Activation of the catalyst (1) by an alcohol.** The stannous alcoholate (3) serves as active species.

The subsequent ring-opening polymerisation follows a coordination-insertion mechanism (see fig. 10). In the first step, the monomer ( $\epsilon$ -caprolactone) is slightly complexed by the initiator resulting in complex **4** (fig. 10). In the next step, a nucleophilic attack to the carbonyl carbon of the monomer occurs, resulting in a four-member transition state **TS1** which transforms into a molecule with a new C-O bond **5**. After final rotation and coordination of the endo-cyclic oxygen the ring-opening occurs, ending in another four-member transition state **TS2**. A complex **6** is formed, analogous to the starting complex **3**.

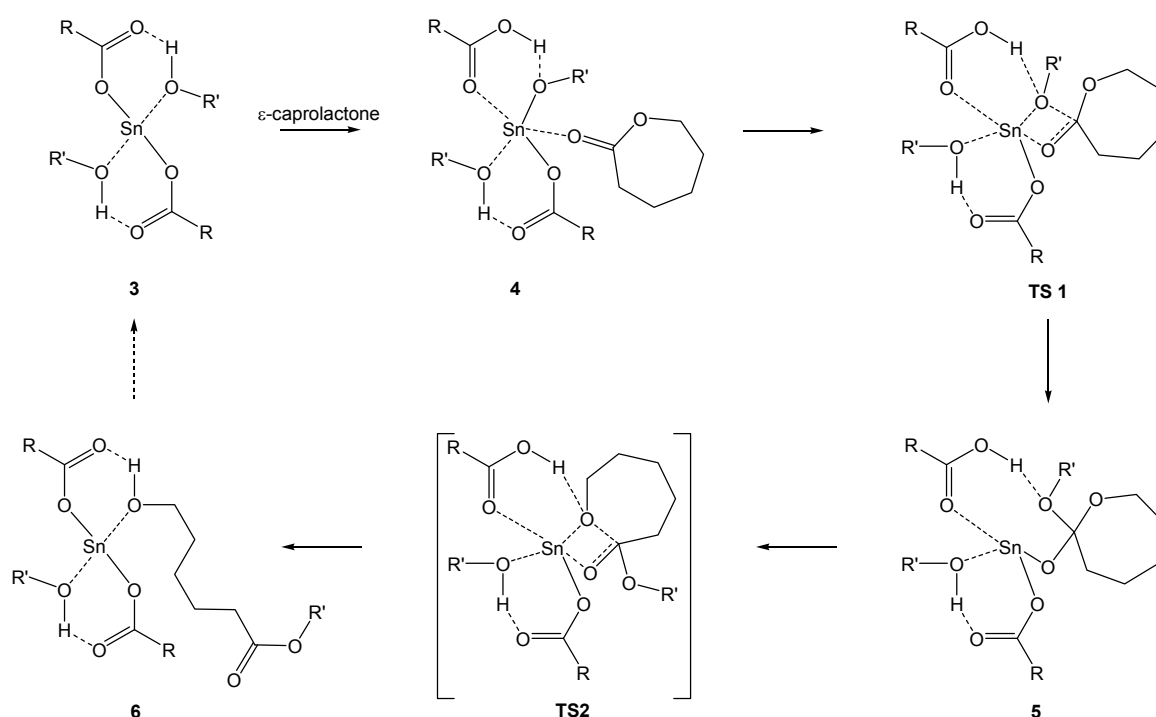


**Figure 10: Coordination-insertion mechanism of the ring-opening polymerisation of  $\epsilon$ -caprolactone with PEO.**

Stannous II octoate is a potentially cytotoxic agent if not removed. However PEO-*b*-PCL block copolymers have already been synthesised with this initiator and successfully used in drug delivery systems<sup>76</sup> and as non-woven fibres for cell attachment, which demonstrates that the amount of eventually remaining catalyst is too small to affect cellular reactions.

## 2.4 Proteins in biomedical applications

Proteins are omnipresent in the body and exist in a wide variety of chemical structures. Soluble ones are components of all biological fluids, for example in such as blood plasma. But they are also structure building compounds of the extracellular matrix (ECM) which is abundant in all tissue and organs. Interactions of cells with proteins have significant influence

on adhesion, proliferation, migration and guidance of cells. Thus, the knowledge of protein properties and behaviour is very important for the development of tissue engineered artificial implants.

### 2.4.1 Cell receptors

Cells interact with ECM proteins via specific cell surface receptors. The best-known and most characterised receptors belong to the integrin superfamily. Receptors for extracellular adhesion proteins (collagen, fibronectin and laminin) are mainly responsible for cell-substrate adhesion. Integrins can also form direct transmembrane links between adhesive ECM proteins and intracellular components like actin-filaments at focal adhesions<sup>77</sup>. Beside ECM proteins, growth factors and cytokines as well as cell-cell-contacts have been identified to regulate the phenotypes of the cells.

### 2.4.2 ECM proteins

One main goal of tissue engineering is mimicking the properties of the extracellular matrix (ECM) to obtain optimum conditions for tissue and organ replacement or recovery. The ECM is a complex three-dimensional network of extracellular macromolecules whose functional composition and structural integrity are important for tissue architecture and function. Four classes of macromolecules exist which form the ECM: collagens, structural glycoproteins, proteoglycans and elastin<sup>78</sup>. Collagen is the most abundant protein in the body and important for cell adhesion. Fibronectin is a very prominent glycoprotein and plays a role in nerve regeneration. These both proteins are highly important in the context of this thesis.

Collagen represents approximately 30 % of all vertebrate body proteins. More than 90 % of the extracellular proteins in bone and tendon and more than 50 % in the skin consist of collagen. It is the main structural protein and is organised into fibres. All members of the collagen family have a unique triple-helix configuration with three polypeptides as subunits, called  $\alpha$ -chains. These  $\alpha$ -chains consist predominantly of the amino acid repeating unit glycine-X-Y with X and Y often being proline and hydroxyproline. Crosslinking between the subunits and the molecules themselves makes collagen insoluble in water and most organic solvents.

At least 19 types of collagen have been identified, differing in lengths of helix and nature and size of non-helical sections. The different types of collagen are required to fulfil different biological features in the different parts of the body. The diameter of the natural

aggregated collagen fibril is between 10 and 500 nm, depending on tissue type and stage of development. The predominant collagen type in higher order animals is collagen type I. It consists of two identical chains ( $\alpha 1(I)$ ) and one chain with a different amino acid composition ( $\alpha 2(I)$ ). It is present in nearly all connective tissue and has supporting functions but also has positive influence on fibre growth, even within the central nervous system<sup>79</sup>. Nerve guides prepared from collagen have demonstrated regeneration of peripheral nerves and dorsal roots<sup>80-82</sup>.

Collagen I has already been electrospun into fibres, alone or in combination with other (synthetic) polymers<sup>53, 54, 83-85</sup>. Recent publications have indicated that collagen degrades to gelatin during the electrospinning process, especially when fluoroalcohols are used as solvent<sup>86, 87</sup>. The loss of collagen was described to be between 45 %<sup>86</sup> and 99 %<sup>87</sup>. However, the positive effect of collagen has already been confirmed in several *in vitro* experiments with fibres of this protein alone<sup>54</sup> or of PCL/collagen blends, resulting in increased cell proliferation compared to pure PCL fibres<sup>88-90</sup>.

Fibronectin (FN) is an extracellular matrix glycoprotein with two nearly identical polypeptide chains, each with a molecular weight of approximately 250 kDa. Two types of FN exist: soluble plasma FN (pFN) and less-soluble cellular FN (cFN). pFN is involved in the processes of blood clotting, wound healing and phagocytosis while cFN is a major component of the ECM and serves as linker between different molecules. Fibronectin has several binding sites including two major heparin-binding sites, a collagen-binding domain and binding sites for integrin receptors for cell attachment. The best-known integrin-recognition sequence is the amino acid sequence Arg-Gly-Asp (RGD) which is located near the middle of the molecule. Additionally, a second distinct region was identified that acts synergistically with the RGD sequence. Both are important for cell adhesion and migration mediated by integrin receptors. Figure 11 shows a model of the fibronectin molecule with three different types of homologous repeats I, II and III<sup>77, 91</sup>.

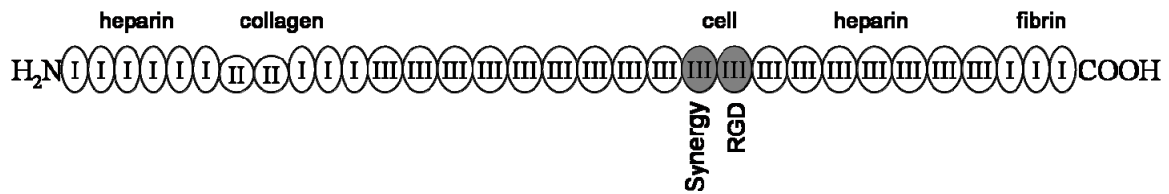


**Figure 11: Model of the structure of fibronectin.** It consists of 12 type I repeats, 2 type II repeats and 18 type III repeats. The approximate relative locations of some binding sites are indicated. Image redrawn after<sup>77</sup>. Copyright (1994) with permission from Elsevier.

FN is known to play a role in neuronal migration and nerve regeneration after injury. It is expressed along the pathway of neural crest migration and nerve outgrowth in the peripheral nervous system (PNS). Fibronectin and at least one of its receptors have been suggested to be important for nerve regeneration possibly by facilitating of Schwann cells<sup>92</sup>. Surfaces patterned with fibronectin or its binding-domain peptide RGD have been shown to enhance neuronal outgrowth compared to controls without these molecules<sup>93</sup>.

The laminin family also belongs to the group of extracellular glycoproteins and is localised in the basement membrane which separates epithelial cells and cell layers from connective tissue around or underneath them. Laminin is a large (800 kDa) cross-shaped protein consisting of three polypeptide chains ( $\alpha$ ,  $\beta$ ,  $\gamma$ ). It is multifunctional and can bind to other common basement membrane components as for example collagen IV, but also promotes many biological activities such as cell growth and migration, tumour growth and metastases, nerve regeneration and neurite outgrowth and wound repair. Three specific peptide sequences have been identified as cell adhesive sites: RGD at the half of the  $\alpha$  chain, Tyr-Ile-Gly-Ser-Arg (YIGSR) in the  $\beta$  chain, promoting cell adhesion and migration, and Ser-Ile-Lys-Val-Ala-Val (SIKVAV) which is known to induce neurite outgrowth.<sup>77, 94</sup> Figure 12 illustrates the cross-shape structure of laminin.

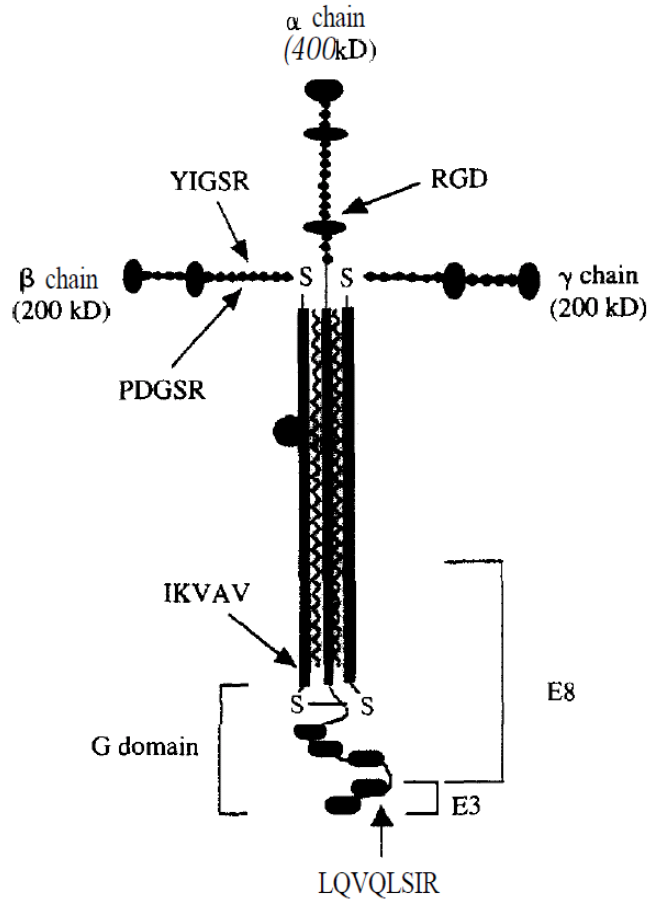


**Figure 12: Model of the structure of laminin.** Image taken from Reference <sup>94</sup>. Copyright 1996) with permission from Elsevier.

Several *in vitro* experiments with PC12 cells<sup>95</sup> and dorsal root ganglia (DRG)<sup>96</sup> on laminin or with dorsal root ganglia (DRG) on surfaces modified with the laminin cell-binding peptides (RGD, IKVAV and YIGSR)<sup>97</sup> demonstrated increased neurite extension.

### 2.4.3 Proteins and peptides in biomaterial-body-interactions

Proteins and peptides have been incorporated into tissue engineering scaffolds to achieve biofunctionality of the scaffold material several times. These biomolecules can induce a range of cell reactions including adhesion, proliferation or neurite outgrowth. On the other hand, soluble proteins which are always present in body fluids, such as blood plasma, adsorb within seconds to implanted materials. The relative bulk concentration of the proteins and their intrinsic surface activities are the two major driving forces for the adsorption. The pH value of the fluid is important too, because it influences the net charge of the protein. Proteins adsorb in monolayers on the surface and therefore compete for available adsorption sites. Due to their chemical nature, proteins have different affinities to the biomaterial,

resulting in different outcomes of the competition between the proteins on each surface<sup>98</sup>. The protein monolayer transforms the, often inert, biomaterial surface into a biologically active one which mediates body reaction. This can cause a range of problems such as acute and chronic inflammation<sup>99</sup> or fibrous encapsulation of the implanted scaffold<sup>100</sup>.

Masking of implanted biomaterials with a protein repellent and thus cell repellent surface can prevent these undesired body reactions. Protein resistant surfaces should be hydrophilic, uncharged and flexible. Several polymers fulfil these demands and are used for the preparation of non-fouling surfaces such as poly(acrylamide), poly(hydroxyethyl methacrylate), poly(*N,N*-dimethyl acrylamide), dextran, poly(oxazoline) and poly(ethylene oxide) (PEO). PEO is nontoxic and nonimmunogenic and is the most effective of these polymers<sup>101</sup>. It was found to prevent protein adsorption as a thin hydrogel coating<sup>102</sup> as well as part of electrospun fibres consisting of PEO-*b*-PCL block copolymers<sup>103</sup>. Pure PCL on the other hand was also shown to be biocompatible<sup>104, 105</sup> but it induces protein adsorption. On surfaces with grafted PEO, the protein resistance increases with grafting density and chain length<sup>106</sup>. In aqueous solutions and with low grafting densities, the neighbouring polymer chains do not overlap and only parts of the surface are covered (mushroom-regime). Higher concentrations result in the formation of a so-called brush structure due to chain stretching away from the surface and high water solubility of the polymer. Very high coating density however is not possible because of steric hindrance caused by already grafted chains. In contrast, star-shaped PEO (PEO star) offers the possibility to prepare high-density layers of PEO molecules on a surface. These molecules have a central core from which the PEO arms extend. These arms are preferentially located near the substrate surface and the possibility of surface binding by functionalised end groups is increased<sup>107</sup>. Several types of PEO stars (e.g. 30 arms, 10000 g/mol per arm; 70 arms, 5200 g/mol per arm; 24 arms, 9700 g/mol per arm and 70 arms, 4500 g/mol per arm) have been grafted onto surfaces in the past and demonstrated protein repellence in dependence on molecular weights and number of arms<sup>108, 109</sup>. A detailed overview about the different PEO star molecules and their properties is given in a review by Gasteier *et al.*<sup>110</sup>. Often, the star-shaped PEO prevented proteins better from surface adsorption than comparative linear PEO polymers. It turned out that star molecules with a low number of arms, a low molecular weight per arm and a flexible core molecule were the most effective ones. Following this strategy and furthermore enabling crosslinking of the star-molecules with each other by end group functionalisation led to the development of a specific PEO-based star-molecule by the group of Möller *et al.*<sup>111, 112</sup>. They



synthesised a statistical copolymer of ethylene oxide (EO) and propylene oxide (PO) with a ratio of 4:1 as backbone of 6 arms with a molecular weight of 2000 g/mol per arm and with a sorbitol core. The arms were functionalised with isophorone diisocyanate (IPDI) to yield isocyanate (NCO) end groups. In this thesis, this polymer is referred as “sPEG” instead of the chemically more correct abbreviation of (star-NCO-poly(EO-*stat*-PO)), because the name “sPEG” has been predominately used in former publications. Figure 13 shows the chemical structure of the polymer and possible reactions of the NCO-end group with water and amine groups.

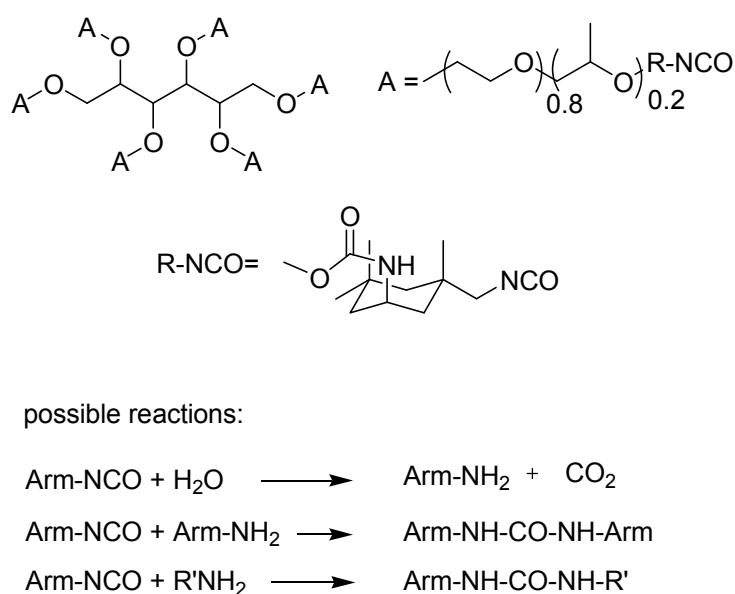


**Figure 13: Chemical composition of the sPEG polymer.** The reactions occur in aqueous environment and result in crosslinking of the sPEG molecules. Arm = arm of sPEG molecule. Redrawn after<sup>110</sup>.

Dissolution of sPEG in water results in hydrolysis of the isocyanate groups to carbamic acid which leads to the formation of amine groups at neutral pH. These can react with unreacted NCO groups and form urea bridges between the sPEG molecules. The process of crosslinking is relatively slow and the system requires at least 12 h for a complete crosslinking of a hydrogel layer of sPEG after coating a surface<sup>110</sup>.

Functionalisation of such repellent materials with special cell mediating signals allows control of adhesion of specific cell types while preventing that of others. Several *in vitro* experiments demonstrated successful prevention of protein adsorption when sPEG was used as a hydrogel layer on different biomedical substrates with simultaneous cell adhesion after

functionalisation with the ECM peptide sequence such as RGD<sup>113</sup> or YIGSR<sup>114</sup>, as well as the formation of a neuronal network by insect neurons through functionalisation with the lectin concanavalin A<sup>115</sup>.

## 2.5 Nerve regeneration after injuries

### 2.5.1 The nervous system

The nervous system is responsible for information transport from and to all parts of the body. It is classified into two components: the central nervous system (CNS) and the peripheral nervous system (PNS). The CNS includes the brain, spinal cord, optic and olfactory bulb and the auditory system. Here signals are interpreted and excitatory stimuli provided to the PNS. The PNS consists of the cranial nerves arising from the brain and the spinal nerves arising from the spinal cord. Additionally, sensory neurons and their processes which provide information about muscle and limb positions to the CNS, somatic motor neurons, which innervate skin, muscles, and joints and exteroceptors for touch, temperature and pain, belong to the PNS.

In the nervous systems, neurons are the basic structural and functional elements. They consist of a cell body (soma) and its extensions (axons and dendrites) and have the task to transmit electrical signals for information transport. Glial cells (Schwann cells in the PNS and oligodendrocytes in the CNS) surround the axons and support their functions. Several axons are bundled to form fascicles and several fascicles finally form the nerve cable<sup>116</sup>.

### 2.5.2. Injuries of the CNS and PNS

Injuries of the peripheral nerve or the CNS white-matter tracts are apparently followed by loss of motoric and sensory function and axonal degeneration, myelin sheath degradation and inflammatory and scar building reactions on the cellular level<sup>117-120</sup>.

PNS injuries are followed by degradation of destroyed axons and the myelin sheath. This process was first described by August Waller in 1850 and is therefore called “Wallerian degradation”<sup>120</sup>. Macrophages enter the lesion site and phagocytose cell debris together with monocytes. Often basement membranes which surround the axons and Schwann cells remain intact. Subsequently, Schwann cells at the distal nerve stump start to produce growth factors and neurotrophins which induce nerve sprouting at the proximal nerve stump towards the distal stump. At small gaps between distal and proximal stump, the growing sprouts reach the distal stump and the nerve is remyelinated by Schwann cells resulting in recovery of the lost function<sup>121</sup>. Figure 14 illustrates this process. With bigger injuries this self-healing process is not successful and surgical repair is required.

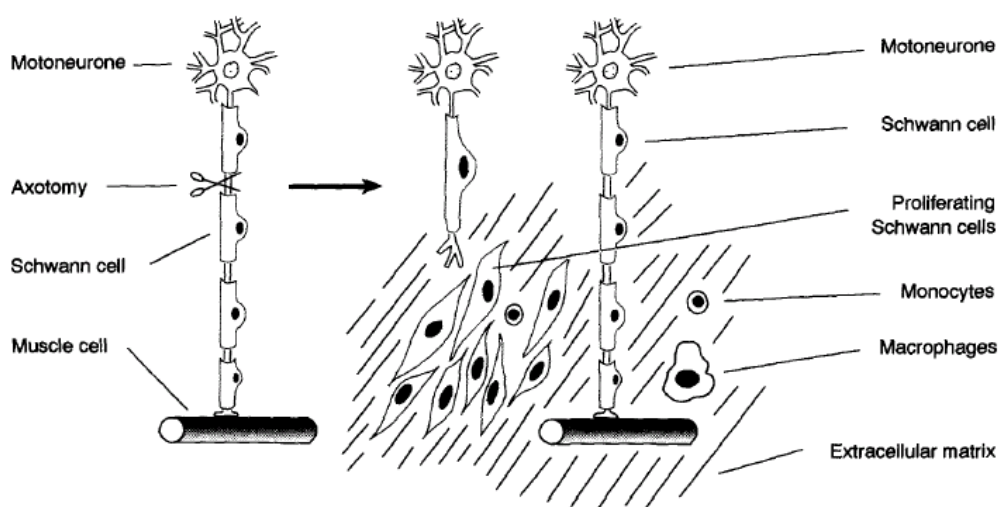


**Figure 14: Recovery process after nerve injury in the PNS.** After a nerve injury macrophages and monocytes remove myelin debris, while Schwann cells release neurotrophins and lead axons toward their synaptic targets, resulting in restored neuronal function. Drawing taken from literature<sup>122</sup>. Copyright (1994) with permission from Elsevier.

In contrast to the PNS, injuries of the central nervous system (CNS) do not regenerate due to several reasons. CNS injuries result in damages of the myelin sheath around the nerve fibres which is formed by oligodendrocytes. In myelin, several axonal-growth inhibitors are found which cause growth cone collapse and inhibit neurite outgrowth<sup>123, 124</sup>. Experiments in which the proteins themselves were targeted or the known receptor antagonised resulted in reduced inhibition effect of these proteins and enhanced axonal regeneration<sup>125</sup>. On the other hand, it was already reported that oligodendrocytes can produce growth factors which have trophic effects on nearby axons in the CNS<sup>126</sup> and support the regeneration.

Beside the problems caused by demyelination, the formation of a glial scar by activated astrocytes is the biggest issue in CNS regeneration. Astrocytes fulfil a great range of functions in the CNS. They provide for example nourishment for neurons and are responsible for synapse formation and ensheathment<sup>127, 128</sup>, axon guidance during development and secretion of growth factors and cytokines<sup>129</sup>. After injuries they primarily form the glia scar which protects the healthy tissue from infections and further physical damage but is also a barrier for regenerating axons<sup>130, 131</sup>. Additionally astrocytes express inhibiting molecules which prevent axonal growth and result in failure of regeneration<sup>117</sup>. However, it was found, that they also express growth-promoting molecules which make them interesting for nerve

regenerating studies<sup>79, 132</sup> and can support CNS axon regeneration<sup>132, 133</sup>. In any case, to date no treatment for regeneration of CNS injuries exists.

Very interesting cells of the CNS are olfactory ensheathing cells (OEC). They are very similar to SCs and permit axonal regeneration *in vivo*<sup>134, 135</sup>. OECs ensheath fascicles of unmyelinated primary olfactory axons and support their continuous regeneration from the PNS into the CNS during the whole life of a mammal<sup>136-138</sup>. This is a very rare ability and makes OECs promising candidates for CNS regeneration studies.

### 2.5.3 Nerve repair

Nerve repair is necessary to treat the loss of motoric and sensory function. It is effective, if remyelination of axons and neurite growth in both the PNS and CNS is supported and inflammatory and scar building reactions are overcome.

Nerve regeneration after injuries in the peripheral nervous system is an issue of the size of the lesion site. As mentioned above, very small lesions can regenerate by themselves due to self-healing processes of the body. Small lesions which do not regenerate autonomously can be treated by surgical reconnection of individual fascicles within the nerve cable. Figure 15 illustrates this.

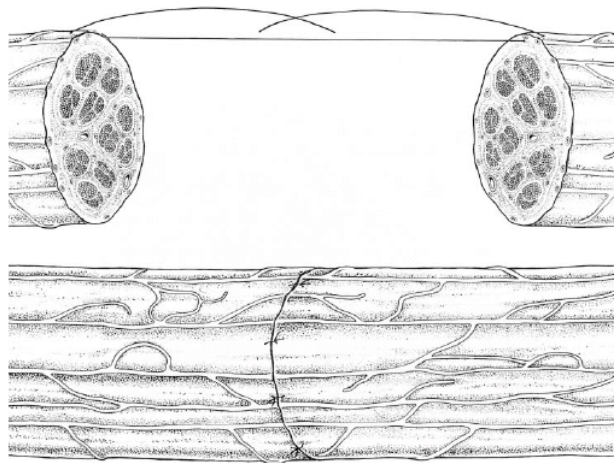


**Figure 15: Surgical reconnection.** Individual fascicles are sutured end-to-end within the nerve cable to achieve nerve recovery. Image taken from literature<sup>139</sup>. Copyright (2006) with permission from Elsevier.

However it became clear, that this method is unsuitable for bigger injuries (> 40 mm), which have to be treated by the use of natural or artificial grafts with guiding structures, implanted in the lesion site and help the axons to regenerate. The employment of nerve

autografts is state of the art today. They are taken from a healthy part of the patients' body, mainly from the *nervus seralis* and are implanted into the lesion site. This method has the advantage of few immunoreactions between the implant and the surrounding tissue but also raises a range of other problems such as multiple surgeries, neuroma pain and function loss at the donor site. Additionally, this material is limited. Allografts (same species, another individual) and xenografts (different species) have the advantage that the loss of sensation at the donor side of the patient is prevented and are normally available in larger amounts. However, rejection reactions happen quite often and therefore immune suppressive medication is required. The medication has to be carefully balanced as this treatment is not suitable for patients which suffer from low immunity<sup>116</sup>.

Artificial nerve grafts may help to overcome the problems occurring with natural grafts in the PNS and may be the only chance to achieve limited regeneration after injuries of the CNS as no natural treatment is known for these injuries yet. The artificial graft must be biocompatible, tolerated by the immune system and non-toxic. As usual in tissue engineering strategies, artificial nerve grafts have to mimic the natural occurring properties as good as possible. Thus, similar mechanical properties than in natural nerves, oriented structures for guiding regenerating axons and neurites and a cell friendly environment to support adhesion and proliferation of neurons and glia cells as well as vascularisation are required. Implants for the CNS should additionally bridge the lesion sites ignoring the glia scar.

Artificial nerve grafts commonly consist of a porous tube from non-degradable (e.g. silicone)<sup>140</sup> or degradable materials (e.g. chitosan<sup>141</sup> or poly(DL-lactide acid-*co*-glycolic acid)<sup>142</sup>). To induce directed axonal growth and cell migration oriented structures within the scaffolds are required. One possibility is the use of gels or sponges with longitudinal channels<sup>143, 144</sup>. An alternative approach applies oriented fibres within a matrix. This method, which is forced in this thesis takes advantage of the high surface to volume ratio of the fibres enabling a high amount of possible cell contacts and mimics the ECM. Material, porosity, and additional features such as incorporated cells, or the release of growth factors and antibodies binding inhibitory proteins, influence the success of such a scaffold<sup>116</sup>. Inclusion of natural peptides or proteins such as collagen<sup>140</sup> improved the regenerating properties. Figure 16 shows a degradable artificial nerve graft immediately after implantation (a) and after six month in a rat (b).

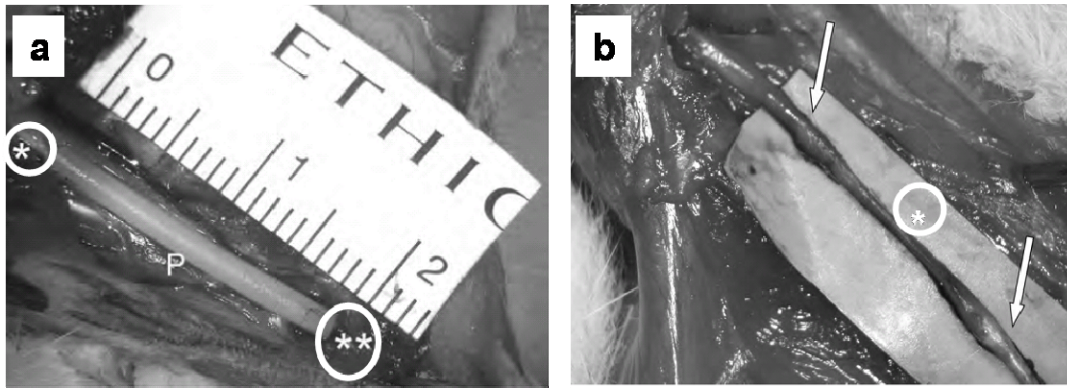


**Figure 16: Images of an artificial nerve conduit prepared of trimethylenecarbonate-co- $\epsilon$ -caprolactone, filled with Schwann cells and implanted into a rat. (a) Nerve graft photographed immediately after implantation with \* = proximal stump of the median nerve and \*\* = distal stump of the median nerve and P = nerve conduit. (b) Nerve graft after 6 months in the animal. In the midportion of the conduit (\*) a diameter change of the tissue demonstrated complete desorption. Vascular injections were present at the former insertion sites (arrows). Images taken from literature<sup>145</sup>. Copyright (2005) with permission from Rockwater, Inc.**

Cells from the nervous system such as Schwann cells were also included into the artificial nerve graft and demonstrated faster recovery than conduits without cells. It was assumed, that Schwann cells produce neurotrophic and growth factors which stimulate nerve regeneration<sup>145, 146</sup>. However, the implantation of cells is problematic: human Schwann cells are not easily available and often result in immunological rejection which requires the use of special drugs. Thus the development of a cell free conduit is desired.

Beside the choice of a biological supporting material, it is highly important that the artificial nerve graft guides neurites and axonal outgrowth. Oriented nanofibres fulfil important criteria for neurite guidance and aligned axon growth: (1) Their diameters are in the same magnitude as natural nerve fibres and it was already shown that the fibre diameter influences neurite outgrowth. (2) Due to their small size, they have a high surface to volume ratio and therefore offer multiple adhesion points for interactions with cells. And (3) nanofibre orientation was reported to play a significant role in cellular response and aligned fibres were highly efficient for axonal alignment and growth which were much better on aligned fibres than on random fibres<sup>146, 148</sup>. The method of electrospinning offers the possibility to produce aligned fibres in the nanometre range which fulfil the above mentioned

requirements. Thus, electrospinning can be a powerful tool for preparing scaffolds for nerve regeneration.

### 2.6 References

1. Watson, J.; Gonzalez, M.; Romero, A.; Kerns, J., Neuromas of the hand and upper extremity. *The Journal of Hand Surgery (American Volume)* **2010**, *35*, 499 - 510.
2. Dalton, P. D.; Mey, J., Neural interactions with materials. *Frontiers in Bioscience* **2009**, *14*, 769 - 795.
3. Oh, S. H.; Kim, J. H.; Song, K. S.; Jeon, B. H.; Yoon, J. H.; Seo, T. B.; Namgung, U.; Il Woo Lee, I. W.; Lee, J. H., Peripheral nerve regeneration within an asymmetrically porous PLGA/Pluronic F127 nerve guide conduit. *Biomaterials* **2008**, *29*, 1601 - 1609.
4. Ratner, B. D.; Hoffman, A. S.; Schoen, F. J.; Lemons, J. E., Biomaterials science: an interdisciplinarian endeavor. In *Biomaterials Science: An introduction to materials in medicine*, Ratner, B. D., Hoffman, A. S., Schoen, F. J., Lemons, J. E., Ed. Elsevier: San Diego, 2004; pp 1 - 9.
5. Ondarcuhu, T.; Joachim, C., Drawing a single nanofibre over hundreds of microns. *Europhys. Lett.* **1998**, *42*, (2), 215 - 220.
6. Feng, L.; Li, S.; Li, H.; Zhai, J.; Song, Y.; Liang, L.; Zhu, D., Super-hydrophobic surface of aligned polyacrylonitrile nanofibers. *Angewandte Chemie Int. Ed.* **2002**, *41*, (7), 1221 - 1223.
7. Martin, C. R., Membrane-based synthesis of nanomaterials. *Chemistry of Materials* **1996**, *8*, 1739 - 1746.
8. Ma, P. X.; Zhang, R., Synthetic nano-scale fibrous extracellular matrix. *Journal of Biomedical Materials Research* **1999**, *46*, 60 - 72.
9. Liu, G. J.; Ding, J.; Qiao, L. J.; Guo, A.; Dymov, B. P.; Gleeson, J. T.; Hashimoto, T.; Saijo, K., Polystyrene-block-poly (2-cinnamoyl ethyl methacrylate) nanofibers - preparation, characterization, and liquid crystalline properties. *Chemistry - A European Journal* **1999**, *5*, 2740 - 2749.
10. Whitesides, G. M.; Grzybowski, B., Self-assembly at all scales. *Science* **2002**, *295*, 2418 - 2421.
11. Taylor, G. I., The circulation produced in a drop by an electric field. *Proceedings of the Royal Society A* **1966**, *291*, 159 - 166.
12. Taylor, G. I., Disintegration of water drops in an electric field. *Proceedings of the Royal Society A* **1964**, *280*, 383 - 397.
13. Taylor, G. I., Electrically driven jets. *Proceedings of the Royal Society A* **1969**, *313*, 453 - 475.

14. Reneker, D. H.; Yarin, A. L.; Fong, H.; Koombhongse, S., Bending instability of electrically charged liquid jets of polymer solutions in electrospinning. *Journal of Applied Physics* **2000**, 87, 4531 - 4547.
15. Fridrikh, S. V.; Yu, J. H.; Brenner, M. P.; Rutledge, G. C., Controlling the fiber diameter during electrospinning. *Physical Review Letter* **2003**, 90, (14), 144502.
16. Deitzel, J. M.; Kleinmeyer, J.; Harris, D.; Tan, N. C. B., The effect of processing variables on the morphology of electrospun nanofibers and textiles. *Polymer* **2001**, 42, (1), 261 - 272.
17. Hohman, M. M.; Shin, M.; Rutledge, G.; Brenner, M. P., Electrospinning and electrically forced jets. I. stability theory. *Physics of Fluids* **2001**, (13), 2201 - 2220.
18. Hohman, M. M.; Shin, M.; Rutledge, G.; Brenner, M. P., Electrospinning and electrically forced jets. II. applications. *Physics of Fluids* **2001a**, 13, 2221 - 2236.
19. Rayleigh, L., *Phil Mag* **1882**, 14, 184.
20. Fong, H.; Chun, I.; Reneker, D. H., Beaded nanofibers formed during electrospinning. *Polymer* **1999a**, 40, (16), 4585 - 4592.
21. Shenoy, S. L.; Bates, W. D.; Frisch, H. L.; Wnek, G. E., Role of chain entanglements on fiber formation during electrospinning of polymer solutions: good solvent, non-specific polymer-polymer interaction limit. *Polymer* **2005**, 46, (10), 3372 - 3384.
22. Gupta, P.; Elkins, C.; Long, T. E.; Wilkes, G. L., Electrospinning of linear homopolymers of poly(methyl methacrylate): exploring relationships between fiber formation, viscosity, molecular weight and concentration in a good solvent. *Polymer* **2005**, 46, 4799 - 4810.
23. Lee, K. H.; Kim, H. Y.; Khil, M. S.; Ra, Y. M.; Lee, D. R., Characterisation of nano-structured poly( $\epsilon$ -caprolactone) nonwoven mats via electrospinning. *Polymer* **2003**, 44, (4), 1287 - 1294.
24. Liu, H. Q.; Hsieh, Y. L., Ultrafine fibrous cellulose membranes from electrospinning of cellulose acetate. *Journal of Polymer Science, Part B: Polymer Physics* **2002**, 40, 2119 - 2129.
25. Andraday, A. L., *Science and Technology of Polymer Nanofibers*. John Wiley & Sons: Hoboken, New Jersey, 2008; p 94.
26. Hsu, C.-M.; Shivkumar, S., Nano-sized beads and porous fiber constructs of poly( $\epsilon$ -caprolactone) produced by electrospinning. *Journal of Materials Science* **2004**, 39, (9), 3003 - 3013.
27. Megelski, S.; Stephens, J. S.; Chase, D. B.; Raboldt, J. F., Micro- and nanostructured surface morphology on electrospun polymer fibers. *Macromolecules* **2002**, 35, (22), 8456 - 8466.
28. Kim, B.; Park, H.; Lee, S.-H.; Sigmund, W. M., Poly(acrylic acid) nanofibers by electrospinning. *Material Letters* **2005**, 59, (7), 829 - 832.



29. Buchko, C. J.; Chen, L. C.; Shen, Y.; Martin, D. C., Processing and microstructural characterization of porous biocompatible protein polymer thin films. *Polymer* **1999**, 40, 7397 - 7407.
30. Kidoaki, S.; Kwon, I. K.; Matasuda, T., Structural features and mechanical properties of in situ-bonded meshes of segmented polyurethane electrospun from mixed solvents. *Journal of Biomedical Material Research Part B: Applied Biomaterials* **2006**, 76B, 219 - 229.
31. Tan, S.-H.; Inai, R.; Kotaki, M.; Ramakrishna, S., Systematic parameter study for ultra-fine fiber fabrication via electrospinning process. *Polymer* **2005**, 46, 6128 - 6134.
32. Ramakrishna, S.; Fujihara, K.; Teo, W.-E.; Lim, T.-C.; Ma, Z., *Electrospinning process, an introduction to electrospinning and nanofibers*. 1st ed.; World Scientific: Singapore, 2005; pp 96 - 98.
33. Pham, Q. P.; Sharma, U.; Mikos, A. G., Electrospinning of polymeric nanofibers for tissue engineering applications: a review. *Tissue Engineering* **2006**, 12, (5), 1197 -1211.
34. Huang, Z. M.; Zhang, Y. Z.; Kotaki, M.; Ramakrishna, S., A review on polymer nanofibers by electrospinning and their applications in nanocomposites. *Composites Science and Technology* **2003**, 63, (15), 2223 - 2253.
35. Li, D.; Xia, Y. N., Electrospinning of nanofibers: Reinventing the wheel? *Advanced Materials* **2004**, 16, (14), 1151 - 1170.
36. Inoguchi, H.; Kwon, I. K.; Inoue, E.; Takamizawa, K.; Maehara, Y.; Matsuda, T., Mechanical responses of a compliant electrospun poly(L-lactide-co-epsilon-caprolactone) small-diameter vascular graft. *Biomaterials* **2006**, 27, (8), 1470 - 1478.
37. Buttafoco, L.; Kolkman, N. G.; Engbers-Buijtenhuijs, P.; Poot, A. A.; Dijkstra, P. J.; Vermes, I.; Feijen, J., Electrospinning of collagen and elastin for tissue engineering applications. *Biomaterials* **2006**, 27, 724 - 734.
38. Dalton, P. D.; Klee, D.; Möller, M., Electrospinning with dual collection rings. *Polymer* **2005**, 46, (3), 611 - 614.
39. Li, D.; Wang, Y. L.; Xia, Y. N., Electrospinning of polymeric and ceramic nanofibers as uniaxially aligned arrays. *Nano Letters* **2003**, 3, (8), 1167 - 1171.
40. Rouhollah, J.; Morshed, M.; Ravadani, S. A. H., Fundamental parameters affecting electrospinning of PAN nanofibers as uniaxially aligned fibers. *Journal of Applied Polymer Science* **2006**, 101, (6), 4350 - 4357.
41. Sill, T. J.; von Recum, H. A., Electrospinning: applications in drug delivery and tissue engineering. *Biomaterials* **2008**, 29, 1989 - 2006.
42. Teo, W. E.; He, W.; Ramakrishna, S., Electrospun scaffold tailored for tissue-specific extracellular matrix. *Biotechnology Journal* **2006**, 1, 918 - 829.
43. Pan, H.; Jiang, H.; Chen, W., Interaction of dermal fibroblasts with electrospun composite polymer scaffolds prepared from dextran and poly lactide-co-glycolide. *Biomaterials* **2006**, 27, 3209 - 3220.

44. Min, B. M.; You, Y.; Kim, J. M.; Lee, S. J.; Park, W. H., Formation of nanostructured poly(lactic-co-glycolic acid)/chitin matrix and its cellular response to normal human keratinocytes and fibroblasts. *Carbohydrate Polymers* **2004**, *57*, 285 - 292.
45. Zhang, Y. Z.; Venugopal, J.; Huang, Z. M.; Lim, C. T.; Ramakrishna, S., Characterization of the surface biocompatibility of the electrospun PCL-collagen nanofibers using fibroblasts. *Biomacromolecules* **2005**, *6*, (5), 2583 - 2589.
46. Rho, K. S.; Jeong, L.; Lee, G.; Seo, B. M.; Park, Y. J.; Hong, S.-D.; Roh, S.; Cho, J. J.; Park, W. H.; Min, B.-M., Electrospinning of collagen nanofibers: effects on the behavior of normal human keratinocytes and earlystage wound healing. *Biomaterials* **2006**, *27*, 1452 - 1461.
47. Venugopal, J.; Ma, L. L.; Ramakrishna, S., Biocompatible nanofiber matrices for the engineering of a dermal substitute for skin regeneration. *Tissue Engineering* **2005**, *11*, 847 - 854.
48. Yoshimoto, H.; Shin, Y. M.; Terai, H.; Vacanti, J. P., A biodegradable nanofiber scaffold by electrospinning and its potential for bone tissue engineering. *Biomaterials* **2003**, *24*, 2077 - 2082.
49. Shin, M.; Yoshimoto, H.; Vacanti, J. P., In vivo bone tissue engineering using mesenchymal stem cells on a novel electrospun nanofibrous scaffold. *Tissue Engineering* **2004**, *10*, 33 - 41.
50. Wutticharoenmongkol, P.; Sanchavanakit, N.; Pavasant, P.; Supaphol, P., Preparation and characterization of novel bone scaffolds based on electrospun polycaprolactone fibers filled with nanoparticles. *Macromolecular Bioscience* **2006**, *6*, 70 - 77.
51. Kwon, I. K.; Matsuda, T., Co-electrospun nanofiber fabrics of poly(L-lactide-co-ε-caprolactone) with type I collagen or heparin. *Biomacromolecules* **2005**, *6*, 6096 - 2105.
52. Stitzel, J. D.; Pawlowski, K. J.; Wnek, G. E.; Simpson, D. G.; Bowlin, G. L., Arterial smooth muscle cell proliferation on a novel biomimicking, biodegradable vascular graft scaffold. *Journal of Biomaterials Applications* **2001**, *16*, 22 - 33.
53. Stitzel, J.; Liu, J.; Lee, S. J.; Komura, M.; Berry, J.; Soker, S.; Lim, G.; Van Dyke, M.; Czerw, R.; Yoo, J. J.; Atala, A., Controlled fabrication of a biological vascular substitute. *Biomaterials* **2006**, *27*, 1088 - 1094.
54. Shields, K. J.; Beckman, M. J.; Bowlin, G. L.; Wayne, J. S., Mechanical properties and cellular proliferation of electrospun collagen type II. *Tissue Engineering* **2004**, *10*, 1510 - 1517.
55. Matthews, J. A.; Boland, E. D.; Wnek, G. E.; Simpson, D. G.; Bowlin, G. L., Electrospinning of collagen type II: a feasibility study. *Journal of Bioactive and Compatible Polymers* **2003**, *18*, 125 - 134.
56. Shin, H. J.; Lee, C. H.; Cho, I. H.; Kim, Y.-J.; Lee, Y.-J.; Kim, I. A.; Park, K.-D.; Yui, N.; Shin, J.-W., Electrospun PLGA nanofiber scaffolds for articular cartilage reconstruction: mechanical stability, degradation and cellular responses under mechanical stimulation in vitro. *Journal of Biomaterials Science: Polymer Edition* **2006**, *17*, 103 - 119.

57. Li, W. J.; Danielson, K. G.; Alexander, P. G.; Tuan, R. S., Biological response of chondrocytes cultured in three-dimensional nanofibrous poly( $\epsilon$ -caprolactone) scaffolds. *Journal of Biomedical Materials Research* **2003**, 67A, 1105 - 1114.
58. Shin, M.; Ishii, O.; Sueda, T.; Vacanti, J. P., Contractile cardiac grafts using a novel nanofibrous mesh. *Biomaterials* **2004**, 25, 3717 - 3723.
59. Li, M.; Guo, Y.; Wei, Y.; MacDiarmid, A. G.; Lelkes, P. I., Electrospinning polyaniline-contained gelatin nanofibers for tissue engineering applications. *Biomaterials* **2006**, 27, 2705 - 2715.
60. Yang, F.; Murugan, R.; Wang, S.; Ramakrishna, S., Electrospinning of nano/micro scale poly(L-lactic acid) aligned fibers and their potential in neural tissue engineering. *Biomaterials* **2005**, 26, 2603 - 2610.
61. Yang, F.; Xu, C. Y.; Kotaki, M.; Wang, S.; Ramakrishna, S., Characterization of neural stem cells on electrospun poly(L-lactic acid) nanofibrous scaffold. *Journal of Biomaterials Science - Polymer Edition* **2004**, 15, 1483 - 1497.
62. Bini, T. B.; Gao, S.; Tan, T. C.; Wang, S.; Aymeric Lim, A.; Hai, L. B.; Ramakrishna, S., Electrospun poly(L-lactide-co-glycolide) biodegradable polymer nanofibre tubes for peripheral nerve regeneration. *Nanotechnology* **2004**, 15, 1459 - 1464.
63. Zhang, Y. Z.; Wang, X.; Feng, Y.; Li, J.; Lim, C. T.; Ramakrishna, S., Coaxial electrospinning of (fluorescein isothiocyanate-conjugated bovine serum albumin)-encapsulated poly( $\epsilon$ -caprolactone) nanofibers for sustained release. *Biomacromolecules* **2006**, 7, 1049 - 1057.
64. Jiang, H.; Hu, Y.; Li, Y.; Zhao, P.; Zhu, K.; Chen, W., A facile technique to prepare biodegradable coaxial electrospun nanofibers for controlled release of bioactive agents. *Journal of Controlled Release* **2005**, 108, 237 - 243.
65. Jiang, H.; Hu, Y.; Zhao, P.; Li, Y.; Zhu, K., Modulation of protein release from biodegradable core-shell structured fibers prepared by coaxial electrospinning. *Journal of Biomedical Materials Research Part B: Applied Biomaterials* **2006**, 79 B, 50 - 57.
66. Hubbell, J. A., Materials as morphogenetic guides in tissue engineering. *Current Opinion in Biotechnology* **2003**, 14, 551 - 558.
67. Gunatillake, P. A.; Adhikari, R., Biodegradable synthetic polymers for tissue engineering. *European Cells and Materials* **2003**, 5, 1 - 16.
68. Mo, X. M.; Xu, C. Y.; Kotaki, M.; Ramakrishna, S., Electrospun P(LLA-CL) nanofiber: a biomimetic extracellular matrix for smooth muscle cell and endothelial cell proliferation. *Biomaterials* **2004**, 25, 1883 - 1890.
69. Grafahrend, D.; Calvet, J. L.; Klinkhammer, K.; Salber, J.; Dalton, P. D.; Moller, M.; Klee, D., Control of protein adsorption on functionalized electrospun fibers. *Biotechnology and Bioengineering* **2008a**, 101, (3), 609 - 621.
70. Azzam, T.; Eisenberg, A., Monolayer-protected gold nanoparticles by the self-assembly of micellar poly(ethylene oxide)-*b*-poly( $\epsilon$ -caprolactone) block copolymer. *Langmuir* **2007**, 23, 2126 - 2132.

71. Bogdanov, B.; Vidts, A.; Van Den Bulcke, A.; Verbeeck, R.; Schacht, E., Synthesis and thermal properties of poly(ethylene glycol)-poly( $\epsilon$ -caprolactone) copolymers. *Polymer* **1998**, 39, 1631 - 1336.
72. Cowie, J. M. G., *Chemie und Physik der synthetischen Polymeren*. Vieweg Verlag: Braunschweig / Wiesbaden, 1997.
73. Hyun, H.; Kim, Y. H.; Song, I. B.; Lee, J. W.; Kim, M. S.; Khang, G.; Park, K.; Lee, H. B., *In vitro* and *in vivo* release of albumin using a biodegradable MPEG-PCL diblock copolymer as an in situ gel-forming carrier. *Biomacromolecules* **2007**, 8, 1093 - 1100.
74. Kim, M. S.; Seo, K. S. S.; Khang, G.; Cho, S. H.; Lee, H. B., Preparation of poly(ethylene glycol)-block-poly(caprolactone) copolymers and their applications as thermo-sensitive materials. *Journal of Biomedical Material Research Part A* **2004**, 70A, 154 - 158.
75. Ryner, M.; Stridsberg, K.; Albertsson, A.-C., Mechanism of ring-opening polymerization of 1,5-dioxepan-2-one and L-lactide with stannous 2-ethylhexanoate. A theoretical study. *Macromolecules* **2001**, 34, 3877 - 3881.
76. Meier, M. A. R.; Aerts, S. N. H.; Staal, B. B. P.; Rasa, M.; Schubert, U. S., PEO-*b*-PCL block copolymers: synthesis, detailed characterization, and selected micellar drug encapsulation behavior. *Molecular Rapid Communications* **2005**, 26, 1918 - 1924.
77. Akiyama, S. K.; LaFlamme, S. E., Bioadhesion and cell behavior. *Colloids and Surfaces B: Biointerfaces* **1994**, 2, 241 - 250.
78. Haralson, M. A.; Hassell, J. R., The extracellular matrix - an overview. In *Extracellular matrix - a practical approach*, Haralson, M. A.; Hassell, J. R., Eds. Oxford University Press: New York, USA, 1995.
79. Tom, V. J.; Doller, C. M.; Malouf, A. T.; Silver, J., Astrocyte-associated fibronectin is critical for axonal regeneration in adult white matter. *Journal of Neuroscience* **2004**, 24, (42), 9282 - 9290.
80. Spilker, M. H.; Yannas, I. V.; Kostyk, S. K.; Norregaard, T. V.; Hsu, H. P.; Spector, M., The effects of tubulation on healing and scar formation after transection of the adult rat spinal cord. *Restorative Neurology and Neuroscience* **2001**, 18, 23 - 38.
81. Liu, S.; Said, G.; Tadie, M., Regrowth of the rostral spinal axons into the caudal ventral roots through a collagen tube implanted into hemisected adult rat spinal cord. *Neurosurgery* **2001**, 49, 143 - 151.
82. Liu, R.-Y.; Snider, W. D., Different signaling pathways mediate regenerative versus developmental sensory axon growth. *Journal of Neuroscience* **2001**, 21, RC164(1-5).
83. Matthews, J. A.; Wnek, G. E.; Simpson, D. G.; Bowlin, G. L., Electrospinning of collagen nanofibers. *Biomacromolecules* **2002**, 3, (2), 232 - 238.
84. Lee, S. J.; Yoo, J. J.; Lim, G. L.; Atala, A.; Stitzel, J., *In vitro* evaluation of electrospun nanofiber scaffolds for vascular graft application. *Journal of Biomedical Materials Research Part A* **2007**, 83A, 999 - 1008.

85. Lee, S. J.; Liu, J.; Oh, S. H.; Soker, S.; Atala, A.; Yoo, J. J., Development of a composite vascular scaffolding system that withstands physiological vascular conditions. *Biomaterials* **2008**, 29, 2891 - 2898.
86. Yang, L.; Fitie, C. F. C.; van der Werf, K. O.; Bennink, M. L.; Dijkstra, P. J.; Feijen, J., Mechanical properties of single electrospun collagen type I fibers. *Biomaterials* **2008**, 29, (8), 955 - 962.
87. Zeugolis, D. I.; Khew, S. T.; Yew, E. S. Y.; Ekaputra, A. K.; Tong, Y. W.; Yung, L. Y. L.; Hutmacher, D. W.; Sheppard, C.; Raghunath, M., Electro-spinning of pure collagen nano-fibres - Just an expensive way to make gelatin? *Biomaterials* **2008**, 29, (15), 2293 - 2305.
88. Chen, Z. C. C.; Ekaputra, A. K.; Gauthaman, K.; Adaikan, P. G.; Yu, H.; Hutmacher, D. W., *In vitro* and *in vivo* analysis of co-electrospun scaffolds made of medical grade poly(epsilon-caprolactone) and porcine collagen. *Journal of Biomaterials Science - Polymer edition* **2008**, 19, (5), 693 - 707.
89. Schnell, E.; Klinkhammer, K.; Balzer, S.; Brook, G.; Klee, D.; Dalton, P.; Mey, J., Guidance of glial cell migration and axonal growth on electrospun nanofibers of poly-epsilon-caprolactone and a collagen/poly-epsilon-caprolactone blend. *Biomaterials* **2007**, 28, (19), 3012 - 3025.
90. Venugopal, J.; Zhang, Y. Z.; Ramakrishna, S., Fabrication of modified and functionalized polycaprolactone nanofibre scaffolds for vascular tissue engineering. *Nanotechnology* **2005**, 16, (10), 2138 - 2142.
91. Pankov, R.; Yamada, K. M., Fibronectin at a glance. *Journal of Cell Science* **2002**, 115, 3861 - 3863.
92. Venstrom, K. A.; Reichardt, L. F., Extracellular matrix 2: role of extracellular matrix molecules and their receptors in the nervous system. *FASEB Journal* **1993**, 7, 996 - 1003.
93. Zhang, Z.; Yoo, R.; Wells, M.; Beebe Jr., T. P.; Biran, R.; Tresco, P., Neurite outgrowth on well-characterized surfaces: preparation and characterization of chemically and spatially controlled fibronectin and RGD substrates with good bioactivity. *Biomaterials* **2005**, 26, 47 - 61.
94. Malinda, K. M.; Kleinman, H. K., The Laminins. *International Journal of Biochemistry and Cell Biology* **1996**, 28, 957 - 959.
95. Koh, H. S.; Yong, T.; Chan, C. K.; Ramakrishna, S., Enhancement of neurite outgrowth using nano-structured scaffolds coupled with laminin. *Biomaterials* **2008**, 29, (26), 3574 - 3582.
96. Patel, S.; Kurpinski, K.; Quigley, R.; Gao, H.; Hsiao, B. S.; Poo, M.-M.; Li, S., Bioactive nanofibers: synergistic effects of nanotopography and chemical signaling on cell guidance. *Nano Letters* **2007**, 7, (7), 2122 - 2128.
97. Schense, J. C.; Bloch, J.; Aebischer, P.; Hubbell, J. A., Enzymatic incorporation of bioactive peptides into fibrin matrices enhances neurite extension. *Nature Biotechnology* **2000**, 18, 415 - 419.

98. Horbett, T. A., The role of adsorbed proteins in tissue response to biomaterials. In *Biomaterials Science: An introduction to materials in medicine*, 2nd ed.; Ratner, B. D., Hoffman, A. S., Schoen, F. J., Lemons, J. E., Ed. Elsevier: San Diego, 2004; pp 237 - 240.
99. Johnson, R.; Harrison, D.; Tucci, M.; Tsao, A.; Lemos, M.; Puckett, A.; Hughes, J. L.; Benghuzzi, H., Fibrous capsule formation in response to ultrahigh molecular weight polyethylene treated with peptides that influence adhesion. *Biomed. Sci. Instrum.* **1997**, 34, 47 - 52.
100. Tang, L., Jennings, T. A., Eaton, J. W., Mast cells mediate acute inflammatory responses to implanted biomaterials. *PNAS* **1998**, 95, 8841 - 8846.
101. Harris, J. M., *Poly(ethylene glycol) Chemistry: Biotechnical and Biomedical Applications*. Plenum Press: New York, 1992.
102. Zhang, M.; Desai, T.; Ferrari, M., Proteins and cells on PEG immobilized silicon surfaces. *Biomaterials* **1998**, 19, 953 - 960.
103. Grafahrend, D.; Calvet, J. L.; Salber, J.; Dalton, P. D.; Moeller, M.; Klee, D., Biofunctionalized poly(ethylene glycol)-block-poly(epsilon-caprolactone) nanofibers for tissue engineering. *Journal of Materials Science-Materials in Medicine* **2008**, 19, (4), 1479 - 1484.
104. Chew, S. Y.; Mi, R.; Hoke, A.; Leong, K. W., The effect of the alignment of electrospun fibrous scaffolds on Schwann cell maturation. *Biomaterials* **2008**, 29, 653 - 661.
105. Pham, Q. P.; Sharma, U.; Mikos, A. G., Electrospun poly(epsilon-caprolactone) microfiber and multilayer nanofiber/microfiber scaffolds: characterization of scaffolds and measurement of cellular infiltration. *Biomacromolecules* **2006**, 7, 2796 - 2805.
106. Jeon, S. I.; Lee, J. H.; Andrade, J. D.; De Gennes, P. G., Protein - surface interactions in the presence of polyethylene oxide: I. Simplified theory. *Journal of Colloid and Interface Science* **1991**, 142, 149 - 158.
107. Irvine, D. J.; Mayes, A. M.; Griffith-Cima, L., Self-consistent field analysis of grafted star polymers. *Macromolecules* **1996**, 29, 6037 - 6043.
108. Irvine, D. J.; Mayes, A. M.; Satija, K. S.; Barker, G. J.; Sofia-Allgor, S. J.; Griffith, L. G., Comparison of tethered star and linear poly(ethylene oxide) for control of biomaterials surface properties. *Journal of Biomedical Materials Research* **1998**, 40, 498 - 509.
109. Sofia, S. J.; Premnath, V.; Merrill, E. W., Poly(ethylene oxide) grafted to silicon surfaces: grafting density and protein adsorption. *Macromolecules* **1998**, 31, 5059 - 5070.
110. Gasteier, P.; Reska, A.; Schulte, P.; Salber, J.; Offenhausser, A.; Moeller, M.; Groll, J., Surface grafting of PEO-based star-shaped molecules for bioanalytical and biomedical applications. *Macromolecular Bioscience* **2007**, 7, (8), 1010 - 1023.
111. Goetz, H.; Beginn, U.; Bartelink, C. F.; Grunbauer, H. J. M.; Möller, M., Preparation of isophorone diisocyanate terminated star polyethers. *Macromolecular Materials and Engineering* **2002**, 287, (4), 223 - 230.

112. Möller, M.; Mourran, C.; Spatz, J.; Rong, R. 2003, patent application no. DE 10203937A1.
113. Groll, J.; Fiedler, J.; Engelhard, E.; Ameringer, T.; Tugulu, S.; Klok, H. A.; Brenner, R. E.; Moeller, M., A novel star PEG-derived surface coating for specific cell adhesion. *Journal of Biomedical Materials Research Part A* **2005**, 74A, (4), 607 - 617.
114. Salber, J.; Gräter, S.; Harwardt, M.; Hofmann, M.; Klee, D.; Dujic, J.; Jinghuan, H.; Ding, J.; Kippenberger, S.; Bernd, A.; Groll, J.; Spatz, J. P.; Möller, M., Influence of different ECM mimetic peptide sequences embedded in a nonfouling environment on the specific adhesion of human-skin keratinocytes and fibroblasts on deformable substrates. *Small* **2007**, 3, 1023 - 1031.
115. Reska, A.; Gasteier, P.; Schulte, P.; Moeller, M.; Offenhäusser, A.; Groll, J., Ultrathin coatings with change in reactivity over time enable functional *in vitro* networks of insect neurons. *Advanced Materials* **2008**, 20, 2751 - 2755.
116. Schmidt, C. E.; Leach, J. B., Neural tissue engineering: strategies for repair and regeneration. *Annual Review of Biomedical Engineering* **2003**, 5, 293 - 347.
117. Fawcett, J. W.; Asher, R. A., The glial scar and central nervous system repair. *Brain Research Bulletin* **1999**, 49, (6), 377 - 391.
118. Pettigrew, D. B.; Shockley, K. P.; Crutcher, K. A., Disruption of spinal cord white-matter and sciatic nerve geometry inhibits axonal growth *in vitro* in the absence of glial scarring. *BMC Neuroscience* **2001**, 2, 8.
119. Schwab, M. E.; Bartholdi, D., Degeneration and regeneration of axons in the lesioned spinal cord. *Physiological Reviews* **1996**, 76, 319 - 370.
120. Evans, G. R. D., Peripheral nerve injury: a review and approach to tissue engineered constructs. *The anatomical records* **2001**, 263, 396 - 404.
121. Reichert, H., *Neurobiologie*. 2nd ed.; Georg Thieme Verlag: Stuttgart, 2000.
122. Bähr, M.; Bonhoeffer, F., Perspectives on axonal regeneration in the mammalian CNS. *Trends in Neuroscience* **1994**, 17 (11), 473 - 478.
123. Schwab, M. E.; Kapfhammer, J. P.; Bandtlow, C. E., Inhibitors of neurite growth. *Annual Review of Neuroscience* **1993**, 16, 565 - 595.
124. Woolf, C. J.; Bloechlinger, S., It takes more than two to Nogo. *Science* **2002**, 297, (16), 1132 - 1134.
125. Kastin, A. J., Targeting neurite growth inhibitors to induce CNS regeneration. *Current Pharmaceutical Design* **2005**, 11, 1247 - 1253.
126. Dai, X.; Lercher, L. D.; Clinton, P. M.; Du, Y.; Livingston, D. L.; Vieira, C.; Yang, L.; Shen, M. M.; Dreyfus, C. F., The trophic role of oligodendrocytes in the basal forebrain. *Journal of Neuroscience* **2003**, 23, 5846 - 5853.
127. Temburni, M. K.; Jacob, M. H., New functions for glia in the brain. *Proceedings of the National Academy of Sciences of the United States of America* **2001**, 98, (1), 3631.

128. Ullian, E. M.; Christopherson, K. S.; Barres, B. A., Role for glia in synaptogenesis. *Glia* **2004**, 47, (3), 209 - 216.
129. Kettenmann, H.; Ransom, B. R., *Neuroglia*. 2 nd ed.; Oxford University Press: Oxford, New York, 2005.
130. Busch, S. A.; Silver, J., The role of extracellular matrix in CNS regeneration. *Current opinion in neurobiology* **2007**, 1, (17), 120 - 127.
131. Klapka, N.; Müller, H. W., Collagen matrix in spinal cord injury. *Journal of Neurotrauma* **2006**, 23, 422 - 435.
132. Liberto, C. M.; Albrecht, P. J.; Herx, L. M.; Yong, V. W.; Levison, S. W., Pro-regenerative properties of cytokine-activated astrocytes. *Journal of Neurochemistry* **2004**, 89, 1092 - 1100.
133. Brook, G. A.; Lawrence, J. M.; Raisman, G., Columns of Schwann cells extruded into the CNS induce in-growth of astrocytes to form organized new glial pathways. *Glia* **2001**, 33, 118 - 130.
134. Bartolomei, J. C.; Greer, C. A., Olfactory ensheathing cells: bridging the gap in spinal cord injury. *Neurosurgery* **2000**, 47, (5), 1057 - 1069.
135. Raisman, G., Olfactory ensheathing cells - another miracle cure for spinal cord injury? *Nature Reviews of Neuroscience* **2001**, 2, (5), 369 - 375.
136. Barnett, S. C.; Chang, L., Olfactory ensheathing cells and CNS repair: going solo or in need of a friend? *Trends in Neurosciences* **2004**, 27, (1), 54 - 60.
137. Field, P.; Li, Y.; Raisman, G., Ensheathment of the olfactory nerves in the adult rat. *Journal of Neurocytology* **2003**, 32, 317 - 324.
138. Fraher, J. P., The ultrastructure of sheath cells in developing rat vomeronasal nerve. *Journal of Anatomy* **1982**, 134, 149 - 168.
139. Lundborg, G., A 25-year perspective of peripheral nerve surgery: evolving neuroscientific concepts and clinical significance. *The Journal of Hand Surgery* **2000**, 25A, 391 - 413.
140. Verdu, E.; Labrador, R. O.; Rodriguez, F. J.; Ceballos, D.; Fores, J.; Navarro, X., Alignment of collagen and laminin-containing gels improves nerve regeneration within silicone tubes. *Restorative Neurology and Neuroscience* **2002**, 20, (5), 169 -179.
141. Wang, X.; Hu, W.; Cao, Y.; Yao, J.; Wu, J.; Gu, X., Dog sciatic nerve regeneration across a 30-mm defect bridged by a chitosan/PGA artificial nerve graft. *Brain* **2005**, 128, 1897 - 1910.
142. Chang, C.-J.; Hsu, S.-H.; Lin, F.-T.; Chang, H.; Chang, C.-S., Low-intensity-ultrasound-accelerated nerve regeneration using cell-seeded poly (D,L-lactic acid-co-glycolic acid) conduits: an *in vivo* and *in vitro* study. *Journal of Biomedical Material Research Part B: Applied Biomaterials* **2005**, 75, 99 - 107.



143. Möllers, S.; Heschel, I.; Damink, L. H.; Schugner, F.; Deumens, R.; Muller, B.; Bozkurt, A.; Nava, J. G.; Noth, J.; Brook, G. A., Cytocompatibility of a novel, longitudinally microstructured collagen scaffold intended for the nerve tissue repair. *Tissue Engineering Part A* **2009**, 15, 461 - 472.
144. Yu, T. T.; Shoichet, M. S., Guided cell adhesion and outgrowth in peptide-modified channels for neural tissue engineering. *Biomaterials* **2005**, 26, 1507 - 1514.
145. Sinis, N.; Schaller, H.-E.; Schulte-Eversum, C.; Schlosshauer, B.; Doser, M.; Dietz, K.; Rösner, H.; Müller, H.-W.; M., H., Nerve regeneration across a 2-cm gap in the rat median nerve using a resorbable nerve conduit filled with Schwann cells. *Journal of Neurosurgery* **2005**, 103, 1067 - 1076.
146. Rutkowski, G. E.; Heath, C. A., Development of a bioartificial nerve graft. I. Design based on a reaction-diffusion model. *Biotechnology Progress* **2002**, 18, 362 - 372.
147. Corey, J. M.; Gertz, C. C.; Wang, B.-S.; Birrell, L. K.; Johnson, S. L.; Martin, D. C.; Feldman, E. L., The design of electrospun PLLA nanofiber scaffolds compatible with serum-free growth of primary motor and sensory neurons. *Acta Biomaterialia* **2008**, 4, 863 - 875.
148. Corey, J. M.; Lin, D. Y.; Mycek, K. B.; Chen, Q.; Samuel, S.; Feldman, E. L.; Martin, D. C., Aligned electrospun nanofibers specify the direction of dorsal root ganglia neurite growth. *Journal of Biomedical Materials Research Part A* **2007**, 83A, (3), 636 - 645.

# ELECTROSPINNING AND INVESTIGATION OF FIBRES OF POLY( $\epsilon$ -CAPROLACTONE)/COLLAGEN BLENDS

### 3.1 Introduction

The technique of electrospinning provides a fast, simple and inexpensive method of producing high-quality continuous fibres with nanoscale diameters. This makes them ideal candidates for the preparation of constructs for tissue engineering applications, especially because their diameters are similar to fibrils found in the extracellular matrix (ECM). Due to their small dimensions, these fibres have a high surface to volume ratio which enables multiple adhesion points for seeded cells. For the development of three dimensional implants it is advantageous if a higher number of small fibres can be introduced into tubes, for example for the preparation of nerve grafts, than few larger fibres to bring more guidance structure to the graft. Especially in neuronal experiments small fibre diameters influenced neurite outgrowth<sup>1-3</sup>. Different parameters including solution concentration, applied voltage, pump rate and collection configurations control the morphology of the electrospun fibres<sup>4</sup>. Depending on the collection configurations, such as single targets, parallel bars (gap method of alignment) or rotating drums either random or oriented fibres can be obtained<sup>5-7</sup>. Single targets result in nanofibrous mats with high fibre density. Here the fibres are mechanically stabilised by fusion and overlapping of each other. In contrast, dual collectors allow the production of oriented, separated fibres, offering the possibility to investigate interactions between a single cell and a single nanofibre. Only a few papers demonstrate the interactions between a cell and single fibres<sup>8-10</sup>, probably since the mechanical stabilisation of the electrospun mesh (and therefore increased fibre density) is an important prerequisite for cell culture studies where frequent media changes are required.

Many different natural and synthetic polymers have already been electrospun, including collagen<sup>6, 11</sup>, polylactides and poly( $\epsilon$ -caprolactone) (PCL)<sup>12, 13</sup>. PCL is a semi-crystalline, hydrophobic, biocompatible and biodegradable synthetic polymer. Degradation of PCL is a very slow process and occurs by ester hydrolysis<sup>14-16</sup>. Thus, PCL is chosen for biomedical applications which require long stability, for example in the field of tissue engineering. Electrospinning of PCL results in mechanically stable fibres. However they do not offer any biological signals improving cellular response. For this reason combinations of

two polymers were electrospun, often one synthetic polymer to obtain mechanical stability combined with a natural polymer to increase biological activity. Therefore PCL was combined with collagen to exploit the positive effect of biologically active collagen on cell behaviour, for example. Collagen activates integrin receptors at the surface of axons and glia and provides binding sites for cell adhesion<sup>17, 18</sup>. It can be degraded by special collagenases which cleave the native helix. Acid soluble collagen can be dissolved at pH 2-3 by acetic acid or hydrochloric acid<sup>19</sup>. Unfortunately collagen fibres have poor mechanical stability<sup>20</sup> and to the best of our knowledge, collagen has not been electrospun alone using the gap method of alignment before. Joining PCL and collagen should result in mechanically stable fibres with enhanced cell recognition properties. Different ways of combining both these materials have already been presented in the literature: (i) Core-shell fibres with PCL in the core and collagen as the shell were produced using co-axial electrospinning<sup>21</sup>, (ii) PCL fibres were coated with collagen after electrospinning<sup>22</sup> and (iii) PCL was blended with collagen type I and II before electrospinning to get directly functionalised fibres<sup>23, 24</sup>. In all these references, cell proliferation was increased compared to pure PCL fibres. However no investigations about the effects of oriented fibres were made in these studies, nor *in vitro* investigations with neuronal cells were prepared.

In recent publications unexpected degradation of collagen to gelatin during the electrospinning process was reported<sup>25, 26</sup> and the loss of collagen was described to be between 45 %<sup>25</sup> and 99 %<sup>26</sup>. However, several *in vitro* experiments have already confirmed the positive effect of collagen in fibres of PCL / collagen blends and cell proliferation was increased compared to pure PCL fibres<sup>9, 23, 24</sup>.

In this study, different PCL/collagen ratios were tested to find the blend which gives good quality suspended oriented fibres using the gap method of alignment with the highest possible amount of collagen<sup>5, 7</sup>. Additionally random fibres of these materials were produced. The quality of the electrospun fibres was judged by analysing scanning electron microscopy (SEM) images. X-ray photoelectron microscopy (XPS) and degradation tests were performed to estimate surface and bulk properties. "Diluted" electrospun fibres offer the possibility of investigating interactions between single fibres and single cells. The effect of fibre guidance on neurons is an interesting measure, particularly since oriented fibres could be used as artificial substrates for neural regeneration (e.g. reference 8) (see Chapter 5).

### 3.2 Materials and Methods

Unless otherwise stated, all chemicals were purchased from Sigma-Aldrich (Munich, Germany).

#### 3.2.1 Electrospinning

Poly( $\epsilon$ -caprolactone) (PCL) ( $M_w = 65000$  g/mol) was dissolved in chloroform/methanol (75/25 v/v). Blends of PCL and type I collagen from calf skin were prepared with different amounts of collagen (25, 50, 60 wt% collagen of total weight) by suspending the polymers in 1,1,1,3,3,3-hexafluoro-2-propanol overnight followed by a 2 h ultrasonic treatment. The blends were labelled “CPCL” followed by the amount of collagen, e.g. the blend with 25 wt% collagen is labelled “CPCL25”. Electrospinning was performed with concentrations of 3 to 9 wt%. The solution/suspension was filled in a 1 mL syringe with a stainless steel 20G flat tipped needle/spinneret (Hamilton, Bonaduz, Switzerland) and pumped with flow rates between 0.05 and 0.5 mL/h while voltages of 15 or 20 kV were applied. The distance between spinneret and target was 15 or 20 cm. Random fibres were collected on single targets while parallel fibres were collected suspended between dual collectors with a gap of 4 cm using the gap method for alignment<sup>5,7</sup>. These strategies typify the two main collection strategies for electrospun fibres in the literature<sup>27</sup>. Figure 1 shows a scheme of both electrospinning systems. Variation of the collection time between 10 s to 6 min offers the possibility to collect different densities of fibres. For scanning electron microscopy measurements fibres were either directly collected onto SEM stubs or the SEM stub was passed through the suspended oriented fibres.

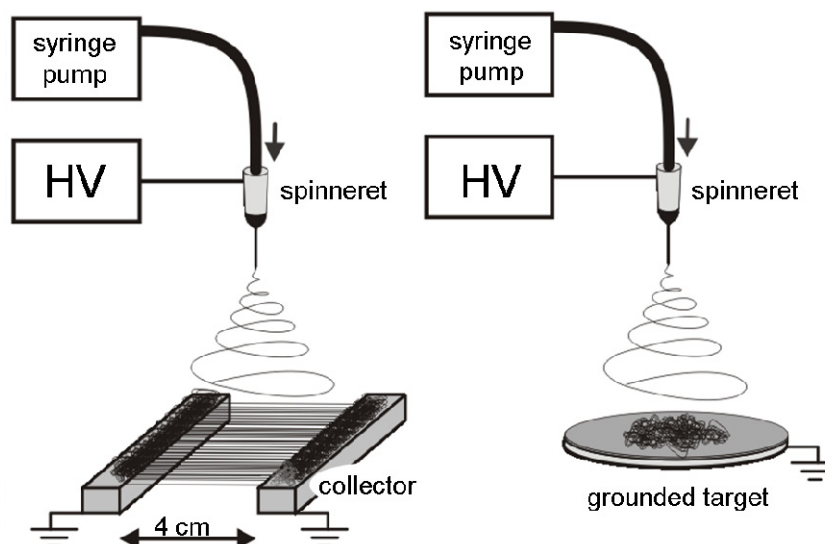


**Figure 1: Schematic of electrospinning system with a high voltage supply (HV), syringe pump, spinneret and grounded collector.** With these configurations, parallel fibres are collected suspended in air between two parallel bars (left) or random fibres are collected directly onto a grounded collector (right). Image reprinted from literature<sup>28</sup>. Copyright (2009) with permission from Mary Ann Liebert, Inc.

### 3.2.2 Fibre characterisation

#### *Scanning electron microscopy*

The electrospun fibres were visualised by scanning electron microscopy (SEM) (S360 Zeiss NTS, Oberkochen, Germany and Hitachi S3000 N, Hitachi High Technology Europe GmbH, Krefeld, Germany), using high tensions of 15 kV and working distances of 5 to 15 mm after sputtering with gold for 90 s (S150B, Edwards, Crawley, Great Britain). The SEM images were used to measure fibre diameters which are presented as the mean with standard deviation. The distances between the fibres were also determined with the help of SEM images.

#### *Infrared spectroscopy*

Small fibre mats of collagen, electrospun PCL and CPCL25 were investigated with infrared spectroscopy using the photo acoustic measuring cell (Photoacoustics Model 200, MTEC, Ames, Iowa, USA) in a FT-IR spectrometer (Nexus 470, Thermo Nicolet, Offenbach, Germany). The samples were kept in a helium atmosphere during measurement. The spectral resolution was  $8\text{ cm}^{-1}$  and the spectra were plotted using Omnic software (Omnic 6.1H, Thermo Nicolet, Offenbach, Germany).

### *Confocal raman microscopy*

Samples of oriented fibres of PCL and CPCL50 on glass cover slips (No. 1, diameter = 12 mm, Marienfeld, Germany) were analysed using Raman spectroscopy. Spectra were taken at the DWI e.V. at RWTH Aachen University, Aachen by Dr. Ahmed Mourran and at WITec GmbH, Ulm with an alpha300R confocal Raman microscope (WITec GmbH). The spectrum was recorded using a Peltier-cooled CCD detector.

#### Conditions:

- sample illumination: frequency doubled Nd:YAG laser with a maximum power of 50 mW at 532 nm excitation;
- grating: T1, 600 g/mm, BLZ = 500 nm;
- centre wavelength: 597.120 nm;
- spectral centre = 2049.935 rel. 1/cm;
- spectrometer operation mode: backscattering geometry

Images of the whole fibres were taken and complete Raman spectra at each image pixel were acquired afterwards (scan speed of 0.1 s per pixel) while achieving a diffraction-limited spatial resolution of  $\approx 360$  nm.

### *X-ray photoelectron spectroscopy*

Small fibre mats (2 x 8 mm) were examined by x-ray photoelectron spectroscopy (XPS) (Ultra Axis<sup>TM</sup> spectrometer, Kratos Analytical, Manchester, Great Britain) in an ultra-high vacuum ( $3 \times 10^{-9}$  mbar) to investigate the atomic composition of the surfaces of the different PCL/collagen blends. The samples were irradiated with monoenergetic Al K $\alpha$ <sub>1,2</sub> radiation (1486.6 eV) and the spectra were taken at a power of 144 W (12 kV x 12 mA). The charging was determined by the aliphatic carbon (C-C, C-H) at a binding energy of 285 eV (C 1s photoline). The spectral resolution - i.e. the Full Width of Half Maximum (FWHM) of the Ester carbon from PET - was better than 0.68 eV for the elemental spectra. The elemental concentration is given in atom%, but it should be considered that this method can detect all elements except hydrogen and helium and that therefore, the determination of the composition does not consider both these elements. Measurements were performed three times each. Data for atomic% were calculated from the peak areas of the spectrum.

### *Contact angle measurements*

Contact angles of random and oriented fibre samples of PCL and CPCL25 were estimated using a contact angle measuring system (G2 with DSA II software, Krüss GmbH, Hamburg, Germany). For oriented fibres contact angles were measured parallel and perpendicular to the fibre orientation. Fibres were collected in high densities on SEM stubs covered with aluminium foil. A small droplet of distilled water (5  $\mu$ l) was placed on the sample and 10 images from the droplet were taken automatically. Two contact angles per image (from the right and left side of the droplet) were calculated. Measurements were performed in triplicates.

### **3.2.3 Degradation of electrospun fibres**

Mats of random fibres of both PCL and CPCL25 were cut in pieces of approximately 8 mg and incubated in 1 ml phosphate buffered saline (PBS) at 37 °C under gentle shaking. The pH was controlled every second day and PBS was exchanged if the pH differed more than 0.2 from pH-value of 7.4. After defined time points the PBS was removed and 1 mL of distilled water was added to the sample. Incubation for 30 min under gentle shaking followed. This cleaning procedure was repeated once. Afterwards the samples were frozen in liquid nitrogen and freeze-dried for two days followed by half a day of drying at high vacuum. Samples were weighed again. For each time point four equal samples were investigated. Time points were: immediately, 1 d, 2 weeks, 1 month, 2 months, 3 months, 4 months, 6 months, 8 months, 10 months, and 1 yr after incubation. SEM images of random PCL and CPCL25 fibres incubated for one year were taken and compared with non-incubated samples.

## **3.3 Results**

### **3.3.1 Influence of polymer and electrospinning parameters on morphology of electrospun fibres**

PCL and blends of PCL with collagen type I in different amounts (25, 50 and 60 wt% corresponding to CPCL25, CPCL50 and CPCL60 respectively) were electrospun from solution. Two different collection configurations were used to achieve either random or parallel fibres (figure 1). Variations of solution concentration, collagen content and process parameters such as voltage, distance between spinneret and target and flow rate were optimised to determine conditions for high quality fibres. These should have a defect-free homogeneous appearance and a small fibre diameter distribution.

The *solution concentration* required for random and suspended, oriented fibres was determined for PCL and CPCL25. Figure 2 shows SEM images of CPCL25 fibres produced with different solution concentrations. Low solution concentrations of 3 and 5 wt% resulted in beaded fibres (figures 2a and b) and a suspended collection of oriented fibres could not be obtained. Increasing the concentration to 7 wt% improved the fibre quality and resulted in homogeneous continuous fibres when collected on a single collector (figure 2c). Collection of parallel fibres was also possible at this concentration (figure 2d).

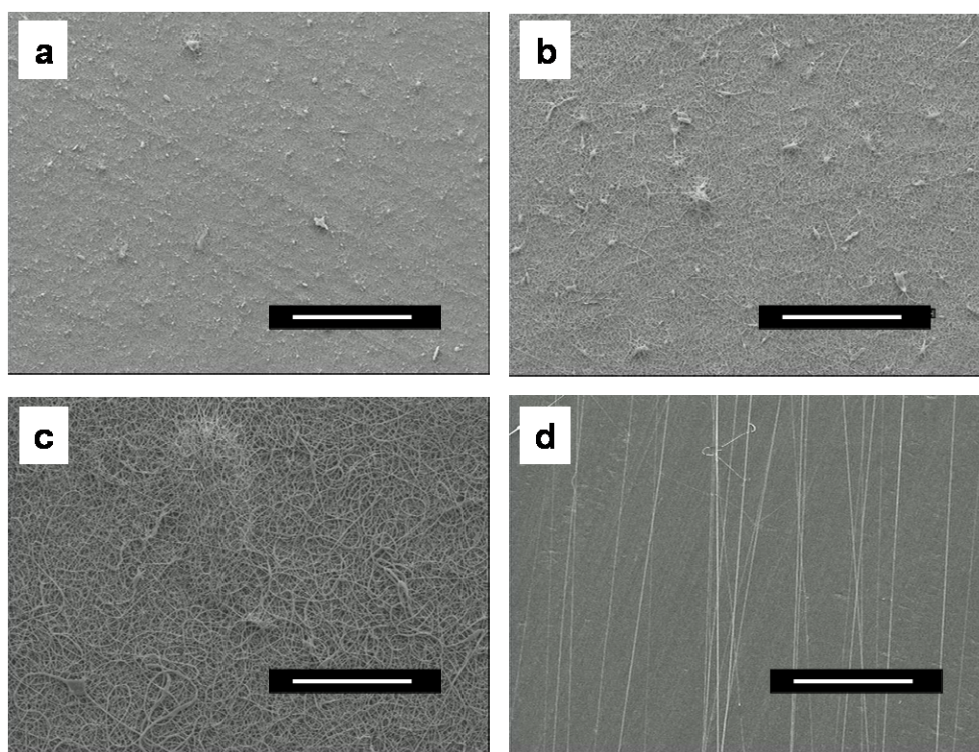


**Figure 2: SEM images of electrospun CPCL25 fibres produced with different solution concentrations showing different fibre qualities and orientations.** (a) 3 wt%, random fibres with beads; (b) 5 wt%, random fibres with beads; (c) 7 wt%, random fibres; (d) 7 wt%, parallel fibres. Scale bars = 100  $\mu\text{m}$ . Image reprinted from literature<sup>28</sup>. Copyright (2009) with permission from Mary Ann Liebert, Inc.

The influence of *voltage*, *distance between target and spinneret* and *flow rate* on fibre diameter and quality was investigated with PCL and all blends. Preliminary experiments showed that suspended oriented fibres were only obtained with intermediate flow rates. High flow rates resulted in jet instabilities which prevented electrospinning. Therefore a single flow



rate of 0.5 mL/h was used for electrospinning suspended fibres. The influence of the distance between target and spinneret was rather small as preliminary experiments showed. For oriented fibre collection, the distance had to be greater than 10 cm otherwise fibres fall down in the gap between the two parallel collection bars and were not held by them. Voltages between 15 and 25 kV were suitable for both random and oriented fibre collection.

Figure 3 shows SEM images of both random and oriented fibres of PCL and different collagen blends. Fibre quality decreased with increasing collagen content, especially for suspended fibres.

Electrospinning of **pure PCL** fibres resulted in fibre diameters between 0.30 and 0.80  $\mu\text{m}$  for random collection depending on electrospinning conditions. Suspended oriented fibres had similar diameters with 0.30 to 0.90  $\mu\text{m}$ . For both random and oriented collection, the best quality fibres were obtained with an applied voltage of 20 kV, a distance of 20 cm and a flow rate of 0.5 mL/h. Figure 3 shows random PCL fibres with diameters of  $0.43 \pm 0.25 \mu\text{m}$  (fig. 3a) and oriented PCL fibres with diameters of  $0.56 \pm 0.30 \mu\text{m}$  (fig. 3b).

PCL and collagen type I from calf skin were blended to obtain mechanically stable fibres with improved cell recognition properties. Blends with collagen contents of 25 to 60 % were tested for their ability to be electrospun in an oriented and random way.

Electrospinning of **CPCL25** resulted in good quality fibres for both random and oriented collection. Fibre diameters were 0.38 to 0.88  $\mu\text{m}$  for random fibres and 0.39 to 0.73  $\mu\text{m}$  for oriented fibres depending on electrospinning conditions. As with pure PCL, a voltage of 20 kV, a distance of 20 cm and a flow rate of 0.5 mL/h resulted in the best quality fibres. Figure 3 shows SEM images of these random (fig. 3c) and oriented (fig. 3d) fibres. The random fibres had diameters of  $0.74 \pm 0.18 \mu\text{m}$ , while oriented fibres had diameters of  $0.73 \pm 0.31 \mu\text{m}$ .

Electrospinning of the blend with 50 % collagen (**CPCL50**) resulted in a range of good quality random fibres independently from the electrospinning conditions. One example is shown in figure 3e. These fibres had diameters of  $0.90 \pm 0.38 \mu\text{m}$  and were electrospun with a voltage of 20 kV, a distance of 20 cm and a flow rate of 0.5 mL/h. Fibres with larger diameters of around 1.30  $\mu\text{m}$  were obtained with a flow rate of 0.3 mL/h, independent on the electrical field strength. The collection of oriented CPCL50 fibres was difficult. Often several fibres stuck together and formed large bundles while in other cases only very few fibres were collected. Electrospinning with a voltage of 25 kV, a flow rate of 0.5 mL/h and a distance

between spinneret and target of 20 cm resulted in well oriented, separate fibres, which are shown in figure 3f. Fibres have diameters of  $1.13 \pm 0.40 \mu\text{m}$ .

Fibres from the blend with a collagen content of 60 % (**CPCL60**) have larger diameters than from the other blends. They have diameters between 0.70 and 1.60  $\mu\text{m}$ . An example of moderate quality fibres is shown in figure 3g. These fibres were produced with a voltage of 15 kV, a distance of 20 cm and a flow rate of 0.3 mL/h. They had diameters of  $1.24 \pm 0.32 \mu\text{m}$ .

The problems occurring with suspended collection of CPCL50 fibres increased with blend CPCL60: only very few fibres could be collected or fibres fused together. The resulting oriented CPCL60 fibres have a broad diameter distribution from 1.20  $\mu\text{m}$  up to 2.30  $\mu\text{m}$ . Figure 3h shows an example of fused fibres. They have diameters of  $1.48 \pm 0.51 \mu\text{m}$  and were produced with a voltage of 20 kV, a distance of 20 cm and flow rate of 0.5 mL/h.

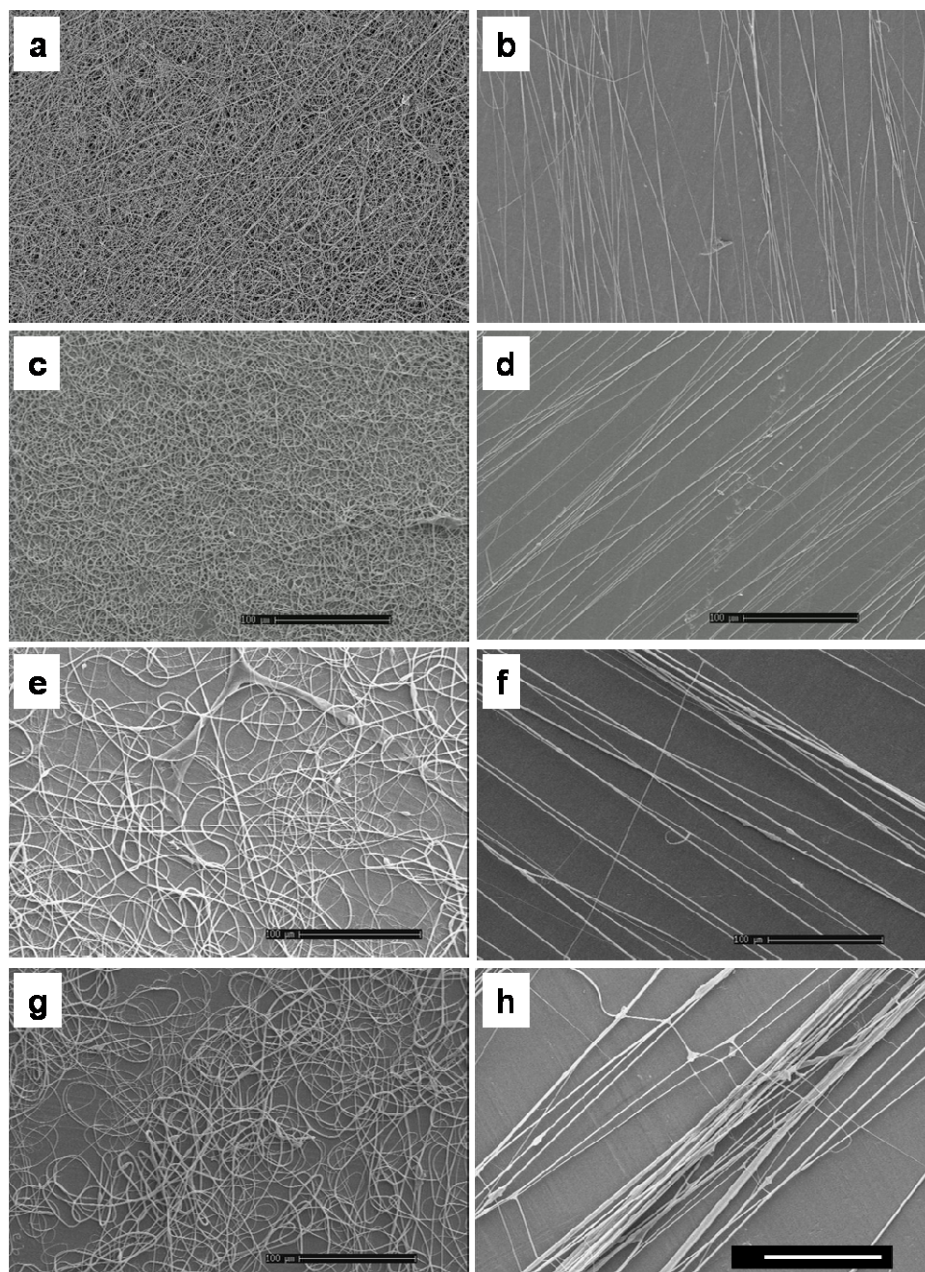


**Figure 3: SEM images of random and oriented fibres with different collagen content.** (a, b) PCL; (c, d) CPCL25; (e, f) CPCL50; (g, h) CPCL60 fibres. Images show fibres which were produced with those conditions that resulted in good quality fibres. These were for (a - e, h) a voltage of 20 kV, a distance between needle and target of 20 cm and a flow rate of 0.5 mL/h; (f) 25 kV, 20 cm, 0.5 mL/h; (g) 15 kV, 20 cm, 0.3 mL/h. Solution concentration was 9 wt% for all blends. Scale bar = 100  $\mu\text{m}$ .

Figure 4 compares the fibre diameters for different collagen content and spinning parameters. Figure 4a shows the diameter for random fibres and indicates an increase of the mean fibre diameter with increasing collagen content. For example, for condition “A” (20 kV,

20 cm) the fibre diameters increased from  $0.43 \pm 0.25 \mu\text{m}$  for pure PCL to  $1.59 \pm 0.46 \mu\text{m}$  for CPCL60. Exclusion to that is the fibre diameter of CPCL60 at condition “E” (25 kV, 20 cm). Here smaller fibres were achieved but the fibre quality was very low and a mixture of thick and small fibres was obtained. Figure 4b shows the data for oriented fibres. An increase of fibre diameter with increasing collagen content can be observed again. Here, the smallest PCL fibres have diameters of  $0.40 \pm 0.10 \mu\text{m}$  while CPCL60 fibres have diameters up to  $2.27 \pm 1.14 \mu\text{m}$ .

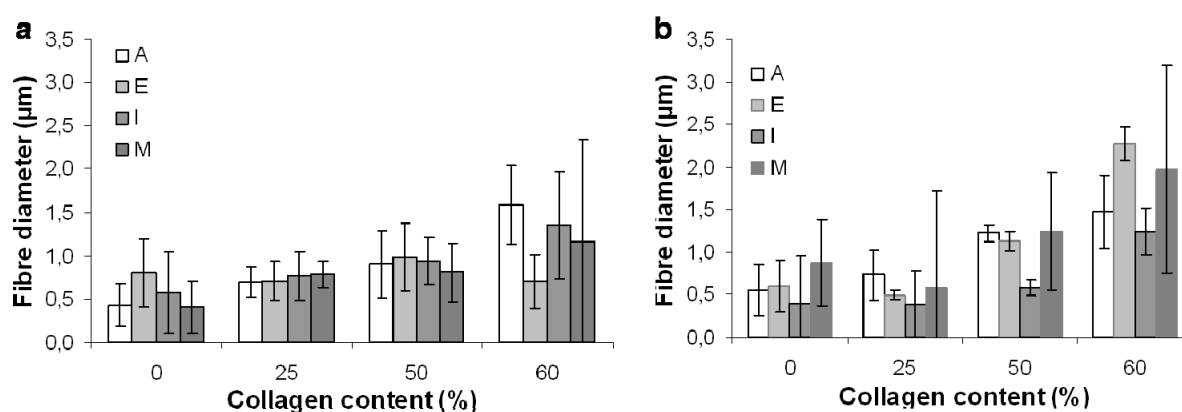


**Figure 4: Fibre diameters of PCL and PCL/collagen blend fibres.** The graphs demonstrate the dependence of fibre diameter on collagen content for both (a) random and (b) oriented fibres for different electrical field strengths (A: 20 kV, 20 cm, 0.5 mL/h; E: 25 kV, 20 cm, 0.5 mL/h; I: 15 kV, 20 cm, 0.5 mL/h; M: 20 kV, 15 cm, 0.5 mL/h).

Fibre density of suspended electrospun fibres depended on the collection time. For standard samples, fibres were collected between 45 s and 60 s resulting in diluted fibres with distances of 10 to 20 µm between them (figures 2d, 3b, 3d). It was also possible to shorten or prolong the collection time and collect fibres with different densities. Figure 5 shows these results with SEM images of electrospun PCL fibres collected for 10 sec (fig. 5a), 2 min (fig. 5b) and 6 min (fig. 5c). Higher collection times resulted in an increase of bead-building, a phenomenon which can be seen in figure 5c. Additionally higher densities were not desired, because this would result in fibre mat building which cannot be used for single fibre / cell investigation. The fibres were collected in densities from 40 fibres / mm up to 540 fibres / mm (fig. 5d).

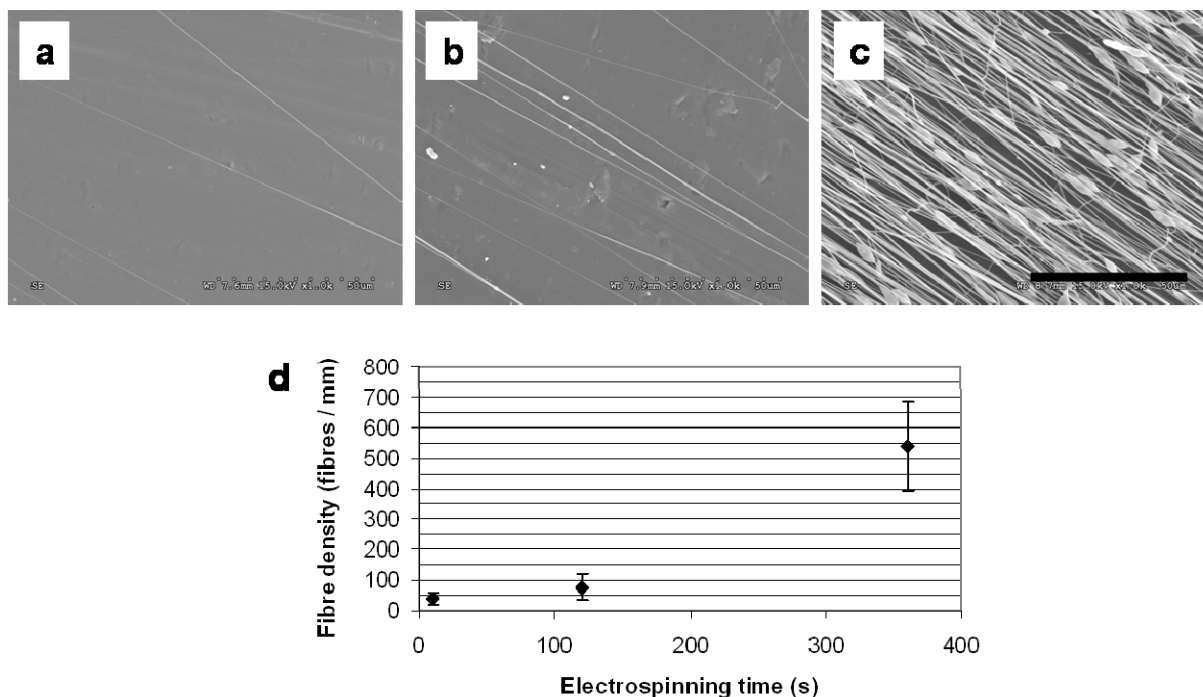


**Figure 5: Fibre density depending on collection time.** Electrospun fibres collected with increasing collection time (a) 10 sec; (b) 2 min and (c) 6 min resulted in an increase of fibre densities (d).

### 3.3.2 Surface and bulk characterisation of electrospun fibres

The electrospun fibres were characterised using a range of analysis methods including infrared spectroscopy, confocal raman spectroscopy, x-ray photoelectron spectroscopy and contact angle measurements.

#### *Infrared measurements on electrospun fibres*

The infrared spectra of PCL, collagen and CPCL25 were measured using the method of photo acoustics and are shown in figure 6. PCL fibres showed an ester band at 1727/1728  $\text{cm}^{-1}$ . Amide I (1651/1658  $\text{cm}^{-1}$ , C=O valence vibration) and amide II (1541  $\text{cm}^{-1}$ , N-H bending vibration) bands occurred in collagen. CPCL25 fibres demonstrated both amides and ester bonds, indicating that CPCL25 fibres contain both PCL and collagen.

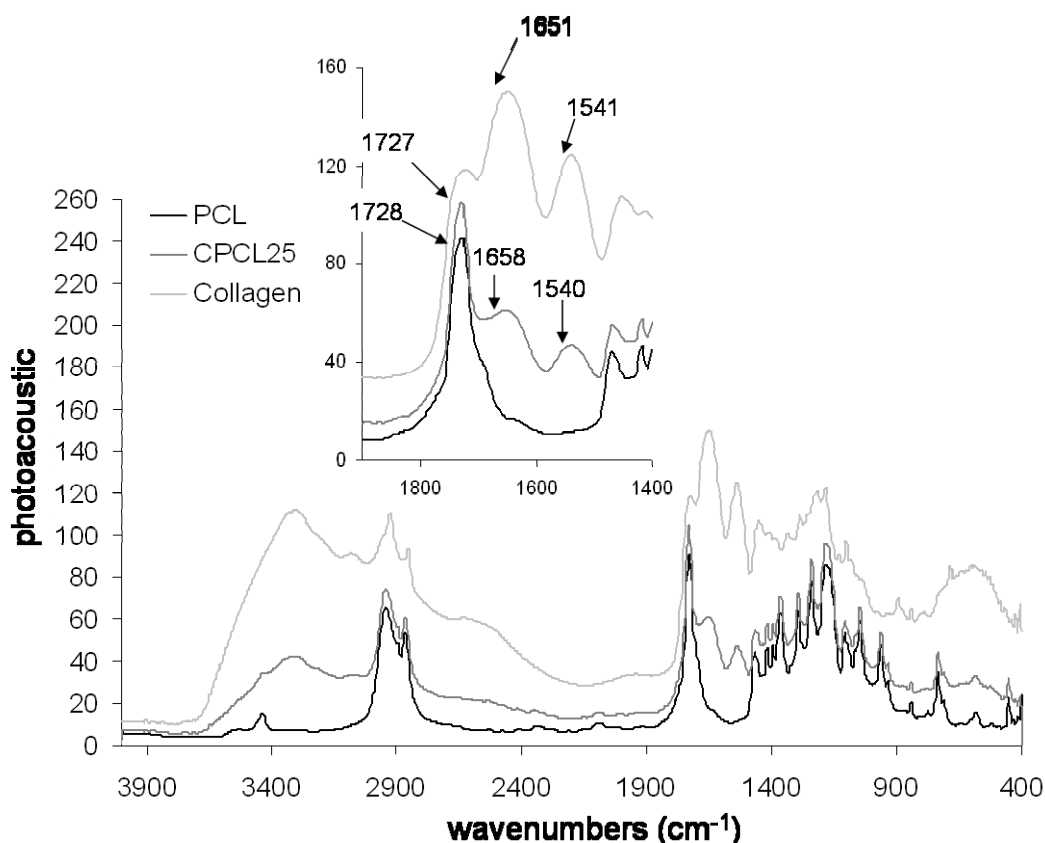


**Figure 6: Infrared spectrum of collagen, CPCL25 and PCL fibres.** The spectra of collagen and CPCL25 show amid I ( $1651/1658\text{ cm}^{-1}$ ) and amid II ( $1541/1540\text{ cm}^{-1}$ ) bands. The spectra of PCL and CPCL25 show an ester band at  $1728/1727\text{ cm}^{-1}$ . These bands indicate that CPCL25 fibres contain both PCL and collagen.

#### *Confocal raman microscopy of PCL and CPCL50 fibres*

PCL and CPCL50 fibres were investigated with confocal Raman microscopy. The first series of experiments was performed at the DWI. Figure 7 shows the results of these measurements. First an overview image of two analysed CPCL50 fibres was taken (fig. 7a) and then the intensity of the amide bond of collagen for these fibres was measured, shown in figure 7b. This image visualises the same area as figure 7a but the yellow dot in the upper left region demonstrated that collagen is only present in the bead-like part in the left fibre. In figure 7c the Raman spectra of a pure PCL (blue), of the right CPCL50 fibre in figure 7a (red) and of the CPCL50 fibre at the bead-like part in figure 7a (green) confirmed that collagen is only present at the bead-like part in the thicker fibre, visualised by the appearance of the amide bond in the green spectrum (arrow). The image of pure PCL fibres is not shown.

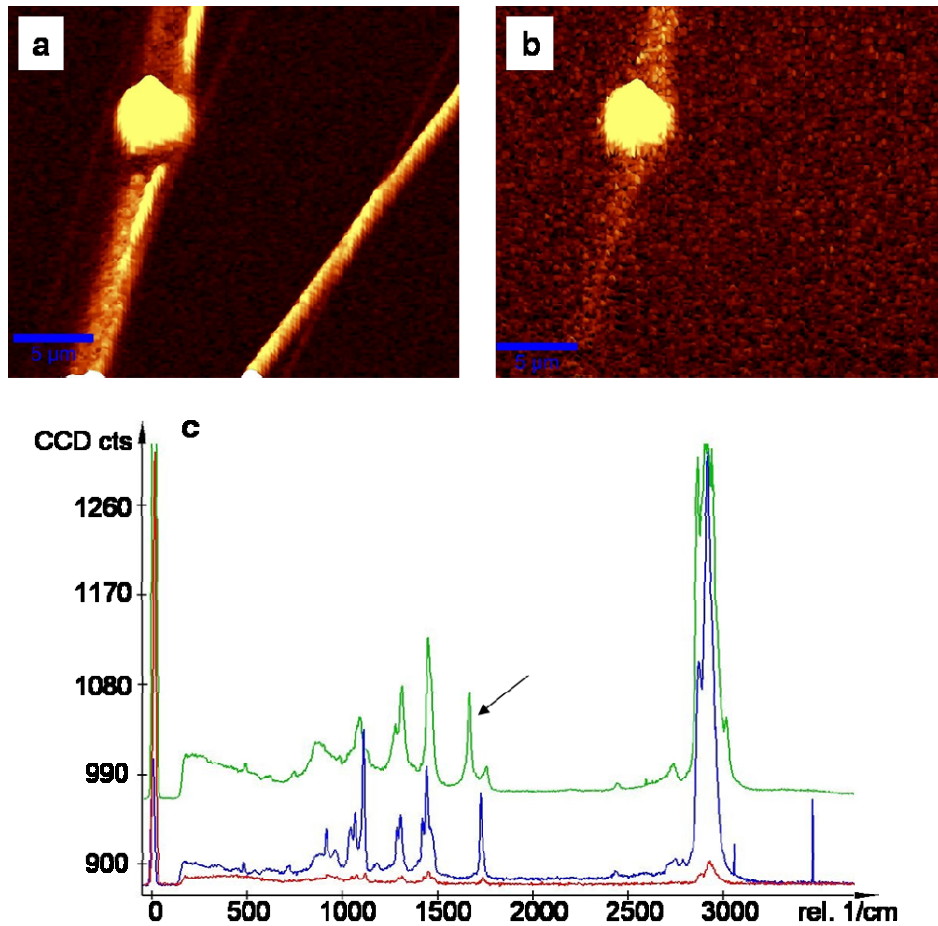


**Figure 7: Confocal Raman microscopy data from PCL and CPCL50 fibres.** (a) Overview image of two CPCL50 fibres; (b) Intensity of amide bond present in the same fibres than in (a); (c) Raman spectra of PCL fibres (blue), CPCL50 fibres (red) and CPCL50 fibre at the bead-like part in (a) (green). The arrow indicates the appearance of the amide bond.

In the second run of experiments, CPCL50 fibres were examined with a confocal Raman microscope at WITec GmbH. The results are shown in figure 8. Figure 8a gives an overview of the CPCL50 fibres which were analysed in detail. The blue frame encircles the fibre measured in figure 8b and the red frame the fibres in figure 8c. In figures 8b-e red colour indicates the presence of PCL and green the presence of collagen, identified by the appearance of the amide bond and indicated by the arrow in the spectrum in figure 8e. It became clear, that collagen is not present in the thin fibre from the blue frame (fig. 8b and d) but in both fibres from the red frame (the most left fibre in the blue frame in fig. 8a was not analysed) (8c and e). In the thicker fibre (right) PCL is surrounded by collagen which is at the fibre surface. In the thinner fibre (left) the fibre surface seems to be divided into one side existing of collagen and one side of PCL.

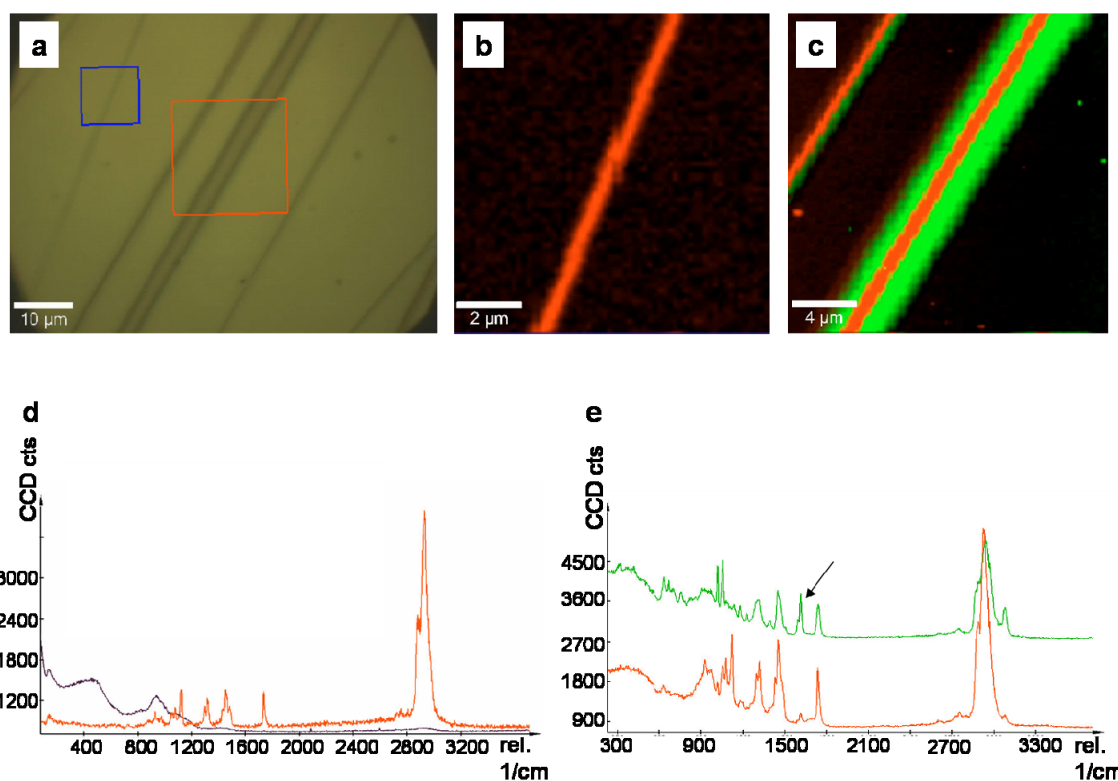


**Figure 8: Confocal Raman microscopy data from CPCL50 fibres.** (a) Overview image of CPCL50 fibres. The blue frames encircle the fibre that is analysed in (b), the red frame encircle the fibres analysed in (c). (d) Raman spectrum of the fibre in (b); (e) Raman spectrum of the fibres in (c). In (b)-(e) visualises red colour the presence of PCL and green colour the presence of collagen. The arrow in (e) indicates the appearance of the amide bond.

### *XPS of electrospun fibres*

Fibres of pure PCL, pure collagen and of the different blends were analysed by XPS. Table 1 presents the atomic concentrations of nitrogen, carbon and oxygen at the fibre surfaces of the different polymers. Fibres of pure PCL did not show any nitrogen at the surface as the chemical formula of PCL does not contain any nitrogen. The blends showed increasing amounts of nitrogen with increasing collagen content and in pure collagen fibres 9.9 % nitrogen was indicated. This means, the amount of collagen in a fibre blend can be calculated from the amount of nitrogen.



**Table 1: XPS data of electrospun fibres with different amounts of collagen.** The atomic concentrations of oxygen, nitrogen and carbon at the surface of electrospun fibres depend on the collagen content.

atomic conc %	PCL	CPCL25	CPCL50	CPCL60	Collagen
O	19.06	16.57	19.34	18.39	18.99
N	0.00	2.14	5.03	6.89	9.92
C	80.94	81.29	75.63	74.72	71.10

### *Contact angles of electrospun PCL and CPCL25 fibres*

Contact angles of water droplets on PCL and CPCL25 fibres were measured for both random and oriented fibres. With oriented fibres the contact angles were estimated along and perpendicular to the fibre orientation. Figure 9 shows images of water droplets on the different fibres for PCL. Images of oriented fibres are shown in figures 9 a (top view), b and c (both side views). The oriented fibres induced an elongation of the water droplet (fig. 9a) along the fibres. Therefore the droplet seems to have different shapes depending on the side of viewing. Figure 9b shows the side view of the droplet seen perpendicular to the fibre direction. The droplet has a flatten shape resulting in a smaller contact angle of  $124.1 \pm 3.8^\circ$  compared to the contact angle on random fibres. In figure 9c the viewing direction of the camera was parallel to the fibres. The droplet seems to narrow which resulted in a larger contact angle of  $128.9 \pm 3.2^\circ$ . Figures 9d (top view) and e (side view) show the water droplet on random PCL fibres. It had a round shape and the contact angle was estimated to be  $125.9 \pm 7.9^\circ$ .

Water droplets on random CPCL25 fibres showed the smallest contact angle of  $58.4 \pm 8.9^\circ$ . A large difference between the contact angles on oriented fibres investigated along ( $93.8 \pm 13.8^\circ$ ) and perpendicular to the fibre orientation ( $75.6 \pm 29.6^\circ$ ) was noticed. The high values for the standard deviations are probably due to the different fibre densities of the measured samples and sometimes the underlying hydrophobic aluminium foil influenced the measurement. However, the values for the contact angle perpendicular to the fibre direction were about  $20^\circ$  smaller than those measured in fibre direction within all measurements.

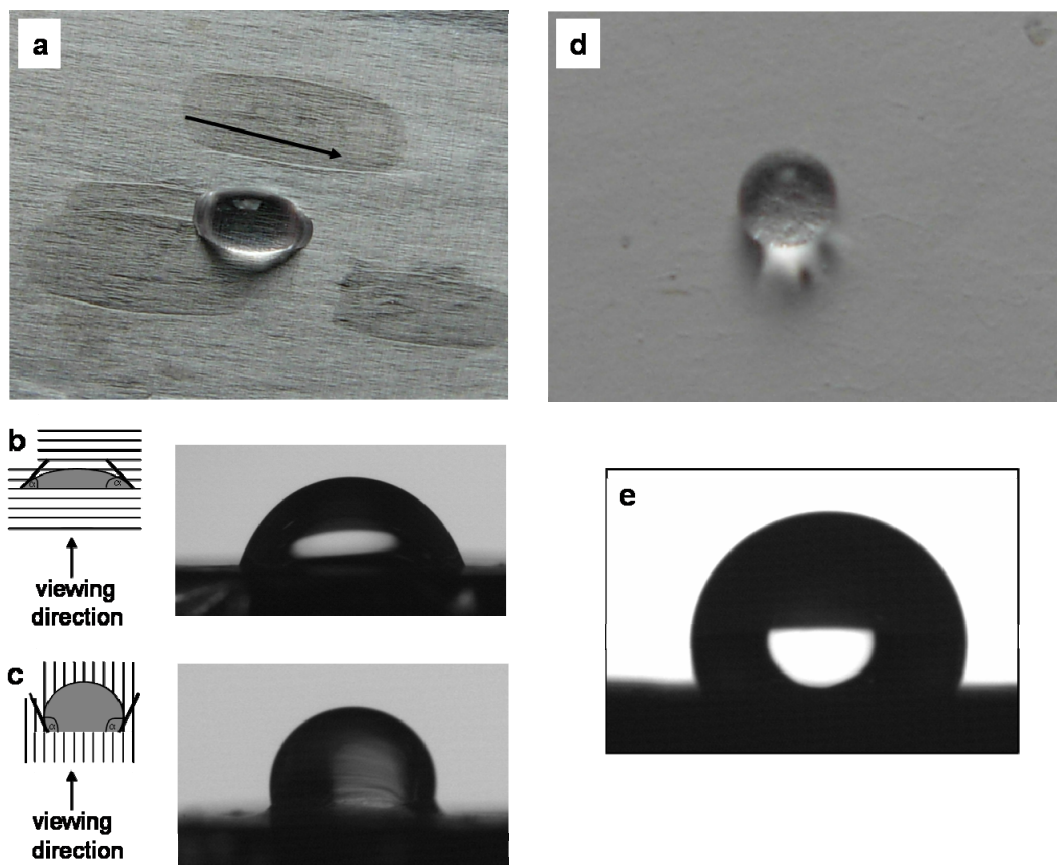


**Figure 9: Water droplets on PCL fibres.** The water droplet changes its shape depending on the orientation of fibres and was placed on (a – c) oriented and (d, e) random fibres. The top views demonstrate the elongated shape of the droplet on oriented fibres (a) while it remains round on random fibres (d). On oriented fibres contact angles were measured along and perpendicular to the fibre direction. The side views show a flattening of the droplet along the fibre orientation which results in smaller contact angles measured perpendicular to the fibre direction (b) and a compression of the droplet in the other direction resulting in higher contact angles measured parallel to the fibres (c). In contrast the droplet has a round shape on random fibres (e). The arrow in (a) indicates the fibre orientation.

### 3.3.3 Degradation of PCL and CPCL25 fibres

Fibre mats of random PCL and CPCL25 fibres were incubated in PBS to investigate the degradation of the samples. Figure 10 shows these results. PCL fibres lost between 0 and 3 % of weight within one year. No significant differences between the samples were noticed. In contrast, CPCL25 fibres lost 13 % of weight immediately after incubation. The weight loss increased up to 20 % within the first month and remained constant over the whole incubation time.

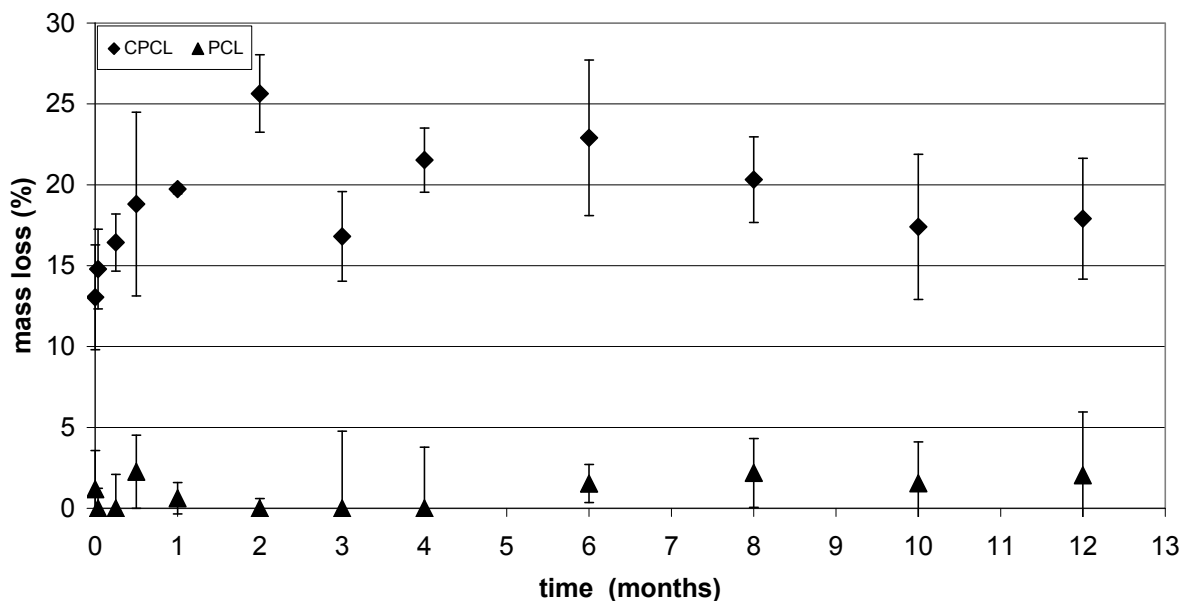


**Figure 10: Degradation of PCL and CPCL25 fibres over a period of one year.** PCL fibres lost less than 3 % of weight within one year. CPCL25 fibres lost more than 13 % of weight within the first hours of incubation and degraded around 18 % in one year.

In figure 11 SEM images of random fibres of CPCL25 (fig. 11a-c) and PCL (fig. 11d-f) after incubation in PBS for one year (fig. 11c, f) are compared with fibres which were not incubated (fig. 11a, d) and with those which were incubated only for a few minutes (fig. 8b, e). Non-incubated CPCL25 fibres (fig. 11a) had a smooth and clear surface. Incubation for a few minutes resulted in slight swelling of the fibres (fig. 11b). After one year in PBS buffer degradation of the fibre was observed. The surface was not smooth and fragments of fibres were found. In contrast no differences of the PCL fibres before (fig. 11d) and after a short incubation (fig. 11e) were noticed. Even after one year incubation left the fibre intact with only very few fragments on the surface (fig. 11f).

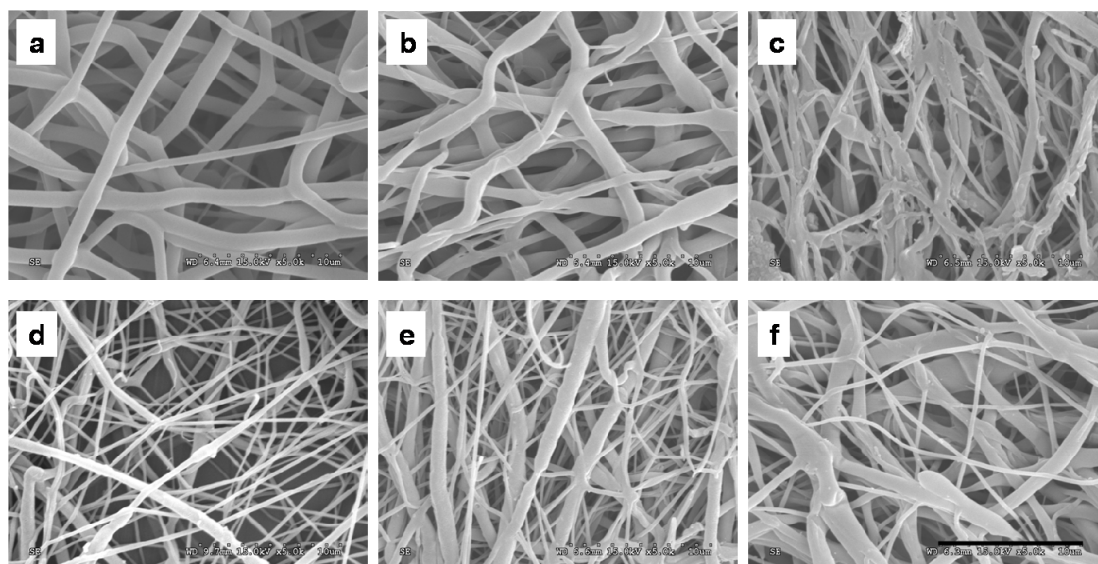


**Figure 11: SEM images of random CPCL25 and PCL fibres before and after incubation in PBS.** Electrospun fibres of (a – c) CPCL25 and of (d – f) PCL were investigated with SEM (a, d) before incubation, (b, e) immediately after incubation and (c, f) after one year of incubation. CPCL25 fibres showed differences in morphology with increasing incubation time, while PCL fibres did not. Scale bar = 100  $\mu\text{m}$ .

### 3.4 Discussion

Fibres of PCL and PCL/collagen blends were produced by electrospinning. The aim of this study was the optimising of electrospinning parameter in order to obtain homogeneous and bead-free nanofibres with diameters in the range of small diameter axons and ECM fibrils (0.5 – 5  $\mu\text{m}$ ). Fibres should also have an oriented structure and be collected by suspension in air. The collection of suspended fibres depends on solution and governing parameters (such as for other collection methods) and also on the fragility of the fibres and very thin or mechanically unstable fibres cannot be collected by the gap method of alignment. Therefore also random fibres were prepared and investigated. The most important factor for achieving high quality fibres was the collagen content in the blend. The best quality of suspended fibres (and of random fibres) were achieved without (pure PCL) (figure 3b) or with little collagen content (blend CPCL25, figure 3d). Here, fibres had diameters in the submicron range and showed very good alignment. With higher collagen content, the fibre quality decreased due to the poor mechanical stability of collagen<sup>20</sup> compared to PCL which forms stable fibres. Images of oriented fibres with higher collagen content often showed very few collected fibres or bundles of stuck fibres as could be seen in figure 3h for suspended CPCL60 fibres. These bundles may be formed when one fibre remained between the collecting bars and other fibres

fall down at the same position. Solvent residuals in the fibres may cause sticking that they tend to “fuse” together and form bundles<sup>29</sup>. Measurements of diameters of those bundles would not be representative and therefore the diameters given for oriented fibres of blend CPCL60 can only be seen as benchmarks. The observation of very few fibres may be a result from shorter collection times whereas fibres have not yet stuck together. Oriented fibres of PCL and CPCL25 did not show these effects as they are stable and single, in air suspended fibres can be collected next to each other.

These experiments show that it is very difficult to get suspended oriented fibres with higher collagen concentration. It is known from literature that even 100 % collagen can be electrospun to oriented fibres. However, in these cases rotating substrates such as coverslips were used<sup>30</sup>. This has the disadvantage that only fibre mats with a high density of fibres can be collected and further fixation of samples is necessary for cell experiments to prevent them from floating off during media changes. The gap method used in this study has only been described rarely in literature before<sup>5, 7, 31</sup>. We have shown that it is possible to collect different fibre densities of parallel fibres by simply varying the collection time (see figure 5). Additionally fibres can be picked up and deposited on various substrates.

Optimising the electrospinning conditions for one specific blend showed that the concentration of the electrospinning solution was the most important factor. Voltage, distance and flow rate had only comparatively small influences. A minimum concentration of 7 wt% was needed for the production of suspended parallel fibres, since lower concentrations resulted in beaded fibres (figure 2) as reported previously<sup>32</sup>. As the jet travels towards the collection plate, the surface tension may cause the formation of beads along the jet. Surface tension has the effect of decreasing the surface area of a fluid. High concentration of free solvent molecules results in a greater tendency of the solvent molecules to congregate and to adopt a spherical shape due to surface tension. In order to counteract this effect, higher concentrations and viscosities can be chosen. This increases interactions between solvent and polymer and the reduction of free solvent molecules. Thus less beads occur when the solution is stretched under the influence of charges<sup>33</sup>.

The surface properties of the electrospun fibres were investigated by IR, confocal Raman, XPS and contact angle measurements. Comparison of IR spectra showed that CPCL25 fibres combine significant peaks of both collagen and PCL fibres indicating that both materials are contained in CPCL25 fibres. XPS measurements confirmed the existence of collagen at the fibres surfaces. The measurements in this study demonstrated the

dependency of nitrogen content on collagen content in the fibre (table 1). Thus the theoretically adjusted PCL/collagen relation was confirmed experimentally. In contrast to IR and XPS measurements, which summarise the results of several fibres, confocal Raman microscopy can visualise single fibres. This method demonstrated that collagen is not homogeneous dispersed within the fibres. It appears preferentially in bead-like parts of thicker fibres (fig. 7b) and at the surface of thicker fibres (fig. 8c), while in thin fibres collagen seems to be present only occasionally. This effect may have several reasons. Firstly, collagen is not soluble in the electrospinning solvent HFP and thus electrospinning was performed with homogenous dispersions of PCL and collagen but not from “real” solutions. Therefore it might happen, that the elongating jet and thus the collected fibre occasionally does not contain collagen but PCL only. Secondly, it is assumed that PCL and collagen are not miscible and therefore domains of each polymer might occur inside the fibres. However, Raman measurements were performed with CPCL50 fibres while IR was done on CPCL25 fibres. Therefore the results can not be compared one to one with each other.

Contact angle measurements showed the high hydrophobicity of PCL fibres. The value for random PCL fibres was around  $126^\circ$ . This confirms data recently reported by Chen *et al.*<sup>24</sup> but is much higher than the reported values for solvent-cast films e.g.  $71^\circ$ <sup>14</sup>. Here, the surface morphology clearly influences wettability according to the theories of Cassie, Baxter and Wenzel<sup>34,35</sup>. The contact angles of oriented fibres confirm this observation. The values measured along fibre orientation is about  $3^\circ$  higher than the value for random fibres, while the contact angle perpendicular to the fibre direction is about  $2^\circ$  smaller. The water droplet placed on the fibre material changed its shape and stretched according to fibre direction. Capillary attractions possibly are the reason for this stretching, resulting in flattening of the droplet at the edges in fibre direction and lifting of the droplet perpendicular to fibre direction. Figures 9b and c illustrate these effects. Collagen is a very hydrophilic material and the inclusion of 25 wt% into the random fibres decreased the contact angle significantly to  $58^\circ$ . The contact angle measured parallel to the fibre direction is about  $93^\circ$ , while perpendicular to the fibre direction it is about  $75^\circ$ . The oriented fibres are not more hydrophobic than the random fibres according to the same chemical composition of random and oriented CPCL25 fibres and therefore material independent parameters affect the surface-water-interactions. As with PCL fibres, a stretching of the droplet on oriented fibres occurs and results in differences of the contact angles measured on random fibres and along and perpendicular to their orientation. These values for oriented CPCL25 fibres are much higher than for random fibres and in contrast to PCL fibres the difference between contact angles are larger too.

Additionally to capillary forces the different surface roughness of oriented and random fibres seems to play a role. Pores in random fibre mats have a round shape while the pores in mats of oriented fibres are elongated according to the fibres orientation. This also influences water-surface interactions and explains the differences in contact angles for oriented fibres along and perpendicular to the fibre direction. Similar effects were already described by Zhong *et al.* who noticed an increase of the contact angle for oriented collagen fibres compared to random collagen fibres of about  $15^\circ$ <sup>30</sup>. However, they did not mention in which direction the contact angle was measured.

Degradation tests showed that PCL fibres lose almost no weight at all (figure 10). The fibre surface which appears slightly fuzzy compared to the non-incubated fibres give hints about starting degradation process (figure 11). These results are similar to degradation assays of Bölgen *et al.* who observed very little molecular weight loss of PCL fibres after incubation in Ringer solution for 6 months<sup>14</sup>. PCL can be degraded by the water molecules attacking the ester bonds in the polymer chains, which results in shorter chains and decrease of molecular weight. It is possible that short chain fragments with carboxyl end groups become soluble in water and decrease the local pH value, resulting in catalysis of the degradation<sup>37,38</sup>. However, Kim *et al.* suggested that the diffusion length for degraded by-products is short for electrospun materials which limits the autocatalysis<sup>38</sup>. This may be an explanation of the slow degradation of PCL fibres.

In contrast, CPCL25 fibres lost weight very rapidly after incubation (figure 10), indicating that the weight loss of the CPCL25 fibres is due to degraded collagen. Collagen can be dissolved by acids such as acetic acid or degraded by special collagenases<sup>19</sup>. The fast weight loss indicates dissolution of the collagen instead of a slower degradation process. These results support the theory that collagen degrades to soluble gelatin during electrospinning mainly due to the use of fluoroalcohols (here 1,1,1,3,3,3-hexafluoro-2-propanol)<sup>25,26</sup>, as non electrospun solid collagen is not soluble in PBS. CPCL25 fibres contain 25 wt% of collagen. If it is assumed that only collagen degrades (and not the PCL) an average weight loss of 20 % of the total CPCL25 fibre mat indicated that around 20 % of the collagen did not degrade during the electrospinning and remains insoluble in the buffer solution.

Neither XPS, IR nor contact angle measurements could demonstrate that the effects observed with CPCL25 fibres were a result of collagen in the fibre and not of gelatine. However, degradation experiments indicated that some collagen remains stable during the

electrospinning process and this collagen offers the possibility for enhanced cell recognition properties of the blends in *in vitro* experiments, investigated in chapters 4 and 5.

### 3.5 Conclusion

In air suspended, oriented fibres of both PCL and PCL/collagen blends were produced from solution electrospinning using the gap method of alignment. Additionally random fibres of the same materials were electrospun. The collagen content in the blend influenced the quality of oriented fibres the most, while electrospinning parameters had less influence. The highest quality fibres were obtained from electrospinning PCL and a blend of PCL with 25 % collagen (CPCL25) at a solution concentration of 9 wt%. The existence of collagen at the fibre surface was shown by different surface analysis methods including XPS, IR and confocal raman spectroscopy. Contact angle measurements demonstrated differences in surface-water interactions along and perpendicular to the fibre orientation which might also influence cellular response in *in vitro* experiments.

### 3.6 References

1. Smeal, R. M.; Rabbitt, R.; Biran, R.; Tresco, P. A., Substrate curvature influences the direction of nerve outgrowth. *Annals of Biomedical Engineering* **2005**, 33, (3), 376 - 382.
2. Smeal, R. M.; Tresco, P. A., The influence of substrate curvature on neurite outgrowth is cell type dependent. *Experimental Neurology* **2008**, 213, (2), 281 - 292.
3. Yang, F.; Murugan, R.; Wang, S.; Ramakrishna, S., Electrospinning of nano/micro scale poly(L-lactic acid) aligned fibers and their potential in neural tissue engineering. *Biomaterials* **2005**, 26, 2603 - 2610.
4. Huang, Z. M.; Zhang, Y. Z.; Kotaki, M.; Ramakrishna, S., A review on polymer nanofibers by electrospinning and their applications in nanocomposites. *Composites Science and Technology* **2003**, 63, (15), 2223 - 2253.
5. Dalton, P. D.; Klee, D.; Möller, M., Electrospinning with dual collection rings. *Polymer* **2005**, 46, (3), 611 - 614.
6. Matthews, J. A.; Wnek, G. E.; Simpson, D. G.; Bowlin, G. L., Electrospinning of collagen nanofibers. *Biomacromolecules* **2002**, 3, (2), 232 - 238.
7. Li, D.; Wang, Y. L.; Xia, Y. N., Electrospinning of polymeric and ceramic nanofibers as uniaxially aligned arrays. *Nano Letters* **2003**, 3, (8), 1167 - 1171.
8. Schnell, E.; Klinkhammer, K.; Balzer, S.; Brook, G.; Klee, D.; Dalton, P.; Mey, J., Guidance of glial cell migration and axonal growth on electrospun nanofibers of poly- $\epsilon$ -caprolactone and a collagen/poly- $\epsilon$ -caprolactone blend. *Biomaterials* **2007**, 28, (19), 3012 - 3025.



9. Sun, T.; Norton, D.; McKean, R. J.; Haycock, J. W.; Ryan, A. J.; MacNeil, S., Development of a 3D cell culture system for investigating cell interactions with electrospun fibers. *Biotechnology And Bioengineering* **2007**, *97*, (5), 1318 - 1328.
10. Sun, T.; Norton, D.; Ryan, A. J.; MacNeil, S.; Haycock, J. W., Investigation of fibroblast and keratinocyte cell-scaffold interactions using a novel 3D cell culture system. *Journal of Materials Science-Materials in Medicine* **2007**, *18*, (2), 321 - 328.
11. Li, M. Y.; Mondrinos, M. J.; Gandhi, M. R.; Ko, F. K.; Weiss, A. S.; Lelkes, P. I., Electrospun protein fibers as matrices for tissue engineering. *Biomaterials* **2005**, *26*, (30), 5999 - 6008.
12. Inoguchi, H.; Kwon, I. K.; Inoue, E.; Takamizawa, K.; Maehara, Y.; Matsuda, T., Mechanical responses of a compliant electrospun poly(L-lactide-co-epsilon-caprolactone) small-diameter vascular graft. *Biomaterials* **2006**, *27*, (8), 1470 - 1478.
13. Xu, C. Y.; Inai, R.; Kotaki, M.; Ramakrishna, S., Electrospun nanofiber fabrication as synthetic extracellular matrix and its potential for vascular tissue engineering. *Tissue Engineering* **2004**, *10*, (7-8), 1160 - 1168.
14. Bölgen, N.; Menciloglu, Y. Z.; Acatay, K.; Vargel, I.; Piskin, E., *In vitro* and *in vivo* degradation of non-woven materials made of poly( $\epsilon$ -caprolactone) and nanofibers prepared by electrospinning under different conditions. *Journal of Biomaterials Science - Polymer Edition* **2005**, *16*, (12), 1537 - 1555.
15. Pitt, C. G.; Schinder, A., A biodegradable delivery system for levonorgestrel. In *Long-acting contraceptive systems*, Zatachini, G. L., Ed. Hapen and Rpw: Philadelphia, 1984; pp 63 - 84.
16. Sun, H.; Mei, L.; Song, C.; Cui, X.; Wang, P., The *in vivo* degradation, absorption and excretion of PCL-based implant. *Biomaterials* **2006**, *27*, 1735 - 1740.
17. Carbonetto, S., The extracellular-matrix of the nervous-system. *Trends In Neurosciences* **1984**, *7*, (10), 382 - 387.
18. Gelse, K.; Poschl, E.; Aigner, T., Collagens - structure, function, and biosynthesis. *Advanced Drug Delivery Reviews* **2003**, *55*, (12), 1531 - 1546.
19. Friess, W., Collagen - biomaterial for drug delivery. *European Journal of Pharmaceutics and Biopharmaceutics* **1998**, *45*, (2), 113 - 136.
20. Thomas, V.; Dean, D. R.; Jose, M. V.; Mathew, B.; Chowdhury, S.; Vohra, Y. K., Nanostructured biocomposite scaffolds based on collagen coelectrospun with nanohydroxyapatite. *Biomacromolecules* **2007**, *8*, (2), 631 - 637.
21. Zhang, Y. Z.; Venugopal, J.; Huang, Z. M.; Lim, C. T.; Ramakrishna, S., Characterization of the surface biocompatibility of the electrospun PCL-collagen nanofibers using fibroblasts. *Biomacromolecules* **2005**, *6*, (5), 2583 - 2589.
22. Venugopal, J.; Ma, L. L.; Yong, T.; Ramakrishna, S., *In vitro* study of smooth muscle cells on polycaprolactone and collagen nanofibrous matrices. *Cell Biology International* **2005**, *29*, (10), 861 - 867.

23. Venugopal, J.; Zhang, Y. Z.; Ramakrishna, S., Fabrication of modified and functionalized polycaprolactone nanofibre scaffolds for vascular tissue engineering. *Nanotechnology* **2005**, 16, (10), 2138 - 2142.
24. Chen, Z. C. C.; Ekaputra, A. K.; Gauthaman, K.; Adaikan, P. G.; Yu, H.; Hutmacher, D. W., *In vitro* and *in vivo* analysis of co-electrospun scaffolds made of medical grade poly(epsilon-caprolactone) and porcine collagen. *Journal of Biomaterials Science - Polymer edition* **2008**, 19, (5), 693 - 707.
25. Yang, L.; Fitie, C. F. C.; van der Werf, K. O.; Bennink, M. L.; Dijkstra, P. J.; Feijen, J., Mechanical properties of single electrospun collagen type I fibers. *Biomaterials* **2008**, 29, (8), 955 - 962.
26. Zeugolis, D. I.; Khew, S. T.; Yew, E. S. Y.; Ekaputra, A. K.; Tong, Y. W.; Yung, L. Y. L.; Hutmacher, D. W.; Sheppard, C.; Raghunath, M., Electro-spinning of pure collagen nano-fibres - Just an expensive way to make gelatin? *Biomaterials* **2008**, 29, (15), 2293 - 2305.
27. Li, D.; Xia, Y. N., Electrospinning of nanofibers: Reinventing the wheel? *Advanced Materials* **2004**, 16, (14), 1151 - 1170.
28. Klinkhammer, K., Seiler, N., Grafahrend, D., Gerado-Nava, J., Mey, J., Brook, G. A., Möller, M., Dalton, P. D., Klee, D. Deposition of electrospun fibers on reactive substrates for *in vitro* investigations. *Tissue Engineering Part C* **2009**, 15 (1), 77 - 85.
29. Hsu, C.-M.; Shivkumar, S., Nano-sized beads and porous fiber constructs of poly(epsilon-caprolactone) produced by electrospinning. *Journal of Materials Science* **2004**, 39, (9), 3003 - 3013.
30. Zhong, S. P.; Teo, W. E.; Zhu, X.; Beuerman, R. W.; Ramakrishna, S.; Yung, L. Y. L., An aligned nanofibrous collagen scaffold by electrospinning and its effects on *in vitro* fibroblast culture. *Journal of Biomedical Materials Research Part A* **2006**, 79A, (3), 456 - 463.
31. Kakade, M. V.; Givens, S.; Gardner, K.; Lee, K. H.; Chase, D. B.; Rabolt, J. F., Electric field induced orientation of polymer chains in macroscopically aligned electrospun polymer nanofibers. *Journal of The American Chemical Society* **2007**, 129, (10), 2777 - 2782.
32. Fong, H.; Reneker, D. H., Elastomeric nanofibers of styrene-butadiene-styrene triblock copolymer. *Journal of Polymer Science Part B-Polymer Physics* **1999**, 37, (24), 3488 - 3493.
33. Ramakrishna, S.; Fujihara, K.; Teo, W.-E.; Lim, T.-C.; Ma, Z., *Electrospinning process, an introduction to electrospinning and nanofibers*. 1st ed.; World Scientific: Singapore, 2005; pp 96 - 98.
34. Cassie, A. B. D.; Baxter, S., Wettability of porous surfaces. *Transaction Faraday Society* **1944**, 40, 546 - 551.
35. Wenzel, R. N., Resistance of solid surfaces to wetting by water. *Industrial and Engineering Chemistry* **1936**, 28, 988 - 994.

36. Li, S., McCarthy, S., Further investigations on the hydrolytic degradation of poly (D,L-lactide). *Biomaterials* **1999**, (20), 35 - 44.
37. Lu, L., Garcia, C. A., Mikos, A. G., *In vitro* degradation of thin poly(DL-lactic-co-glycolic acid) films. *Journal of Biomedical Materials Research* **1999**, 46, 236 - 244.
38. Kim, K., Yu, M., Zong, X., Chiu, J., Fang, D., Seo, Y.-S., Hsiao, B. S., Chu, B., Hadjiargyrou, M., Control of degradation rate and hydrophilicity in electrospun non-woven poly(D,L-lactide) nanofiber scaffolds for biomedical applications. *Biomaterials* **2003**, 24, 4977 - 4985.

### 2-DIMENSIONAL SUBSTRATES OF POLY( $\epsilon$ -CAPROLACTONE) AND POLY( $\epsilon$ -CAPROLACTONE)/COLLAGEN BLENDS FOR *IN VITRO* INVESTIGATIONS

#### 4.1 Introduction

Every year injuries of the peripheral nervous system occur thousand fold worldwide followed by serious complications with disconnection and loss of motor functions. The gold standard uses nerve autografts of the *nervus suralis*. However this includes sacrificing of healthy nerves and multiple surgeries. These insufficiencies could be avoided by the development of an artificial three dimensional (3D)-implant which combines mechanical strength with biological activities such as cell recognition, guidance of cell migration and neurite outgrowth.

Nanotechnology has attracted interest from numerous scientific areas, including tissue engineering (TE) and regenerative medicine. For example, nano-scale fibres exhibit a large surface to volume ratio, which offers multiple adhesion points for the attachment of cells. Such fibres have recently been investigated as TE scaffolds particularly by using a technique termed electrostatic spinning, or electrospinning. However, transforming such nanofibres into a medical device or research tool is often difficult<sup>1</sup>. The most common electrospinning configuration by far is the single collection system, with the resulting nanofibrous mat exhibiting a high fibre density. The fibre sheet is mechanically stabilised by fusion or overlapping between fibres. Dual collectors allow the production of oriented fibres and therefore the possibility of investigating interactions between a single cell and a single nanofibre. Such experiments were performed recently by a few research groups<sup>2-4</sup>.

Mechanical stabilisation of the electrospun fibres is an important technical prerequisite for cell culture studies where frequent media changes are required – studies of single electrospun fibres and cells are therefore still relatively limited in the literature. Several methods with specific limitations have been described where electrospun fibres were deposited on substrates for further cell experiments. Glue<sup>3</sup>, biocompatible adhesives<sup>5</sup> or disposable bandages<sup>6</sup> secure the fibres at the edge of the substrate. Complete attachment of the fibres in a one-step-procedure can be achieved by electrospinning onto collectors with adhesive coatings, for example with thin films of poly(ethylene terephthalate)<sup>7</sup>. Another

possibility is using initially chemically reactive layers of isocyanate-terminated 6-armed star-shaped poly(ethylene oxide)-*stat*-poly(propylene oxide) (sPEG). These sPEG coated substrates can chemically bind nanofibres before being transformed into a protein repellent surface by reaction of the isocyanate functionalities with water to form amino groups which form urea crosslinks with residual isocyanate groups<sup>8</sup>.

Materials used in biomedical applications should be biocompatible, non toxic and should not cause foreign body reactions. Optimising of surface chemistry, energy and topology of the implanted material can increase the body's acceptance. Endogenous proteins interact with the implanted biomaterial and adsorb to it according to their affinities to this surface. A transformation from an inert, foreign material to a biologically active and recognisable surface takes place. Cells respond to surfaces coated with proteins by specific receptors<sup>9</sup>. Protein adsorption on nanofibres has been investigated in detail very limited yet and was often neglected in cell adhesion studies. Only recently one study has investigated protein adsorption on nanofibres<sup>10</sup>, which is expected to play a key role in determining and triggering cell response to nanofibres.

In this chapter, a 2-dimensional *in vitro* system to test conditions needed for neurite guidance in nerve regeneration experiments with oriented fibres deposited onto functionalised substrates is presented. Two different materials, poly( $\epsilon$ -caprolactone) (PCL) and a blend of PCL with collagen type I from calf skin (CPCL25) were electrospun into both randomly and aligned single fibres and deposited on reactive sPEG substrates. Collagen activates integrin receptors at the surface of axons and glia and therefore offers binding sites for cell adhesion and migration<sup>11-13</sup>. The inclusion of collagen should therefore improve viability and cell attachment to the nanofibres compared to pure PCL fibres. Recent publications have indicated that collagen degrades to gelatin during the electrospinning process, especially when fluoroalcohols are used as solvent<sup>14, 15</sup>. The loss of collagen was described to be between 45 %<sup>14</sup> and 99 %<sup>15</sup>. However, the positive effect of including collagen has already been confirmed in several *in vitro* experiments with fibres of PCL/collagen blends, resulting in increased cell proliferation compared to pure PCL fibres<sup>2, 16, 17</sup>.

The fibres were deposited onto freshly sPEG coated substrates which promote fibre fixation and permit *in vitro* investigations with frequent media changes. After fibre deposition, the sPEG layer transformed into protein and cell repellent surface coatings. Additionally cell adhesive substrate surfaces were achieved by adding specific peptide sequences, e.g. repetitions of GRGDS, to the sPEG surface of the substrate prior to fibre deposition. Surface analysis of the differently modified substrates was performed including

the investigation of protein adsorption on the substrates as it is expected to play a key role in altering the biological interactions of the surface. *In vitro* experiments with cells from dorsal root ganglia allowed us to investigate the influence of biologically active extracellular matrix (ECM) molecules (PCL/collagen vs. PCL fibres) in combination with fibres orientation (aligned vs. random fibres) and underlying surface coating (sPEG vs. sPEG-RGD) on cell behaviour and neurite alignment.

## 4.2 Materials and Methods

### 4.2.1 Materials

Unless otherwise stated, all chemicals were purchased from Sigma-Aldrich (Germany). Toluene and tetrahydrofuran (THF) were dried by distillation over lithium aluminium hydride. Star shaped NCO-poly(ethylene oxide)-*stat*-poly(propylene oxide) (star-shaped poly ethers with a backbone of 80 % ethylene oxide and 20 % propylene oxide and isocyanate end groups,  $M_w = 12000$  g/mol) (sPEG) was synthesised in our laboratory from hydroxyl-terminated star polymer (DOW-chemicals, Terneusen, NL) by reaction with isophorone diisocyanate according to literature as described elsewhere<sup>18</sup>. All other chemicals were used as received.

### 4.2.2 Substrate Preparation

Reactive substrates were produced by surface modification of cover glass (No. 1, diameter = 12 mm, Marienfeld) with sPEG according to surface activation described elsewhere<sup>19</sup>. Briefly, the cover glasses were cleaned by ultrasonification with ethanol (KMF, Germany) and dried in a nitrogen stream. Then they were activated by UV-ozone-treatment for 12 min. Afterwards, the cover glasses were transferred into small glass holders and put into a glove box where they were aminosilanised with a solution of 0.3 mL of N-[3-(trimethoxysilyl)propyl] ethylene diamine (97 %) in 50 mL dry toluene for 2 h. After washing with dry toluene the cover glasses were stored in toluene in a nitrogen atmosphere. Prior to spin-coating a solution of 20 mg sPEG in 0.2 mL THF was prepared under nitrogen atmosphere. At normal atmosphere 1.8 mL of deionised water was added and crosslinking allowed for 5 min. Subsequently, the cover glasses were placed onto the spin-coater and covered with the filtered solution (0.2  $\mu$ m, Whatman). By acceleration within 5 s to 4000 rpm for 40 s, the sPEG layer was brought to the cover glasses. The prepared cover glasses are termed “sPEG-substrates” in this study. Silicon wafers were treated according to the same procedure with sPEG and these substrates are called “sPEG-sil”. Additionally, sPEG

substrates were surface functionalized with the cell adhesive peptide sequence GRGDS (H-Gly-Arg-Gly-Asp-Ser-OH) (Bachem, Switzerland). GRGDS was dissolved in deionised water (500 µg/mL) and mixed with the sPEG/THF solution. After crosslinking for 5 min this solution was spin-coated on the cover glass. These substrates are cited as 'GRGDS-sPEG-substrates'.

The glass holders used for aminosilanisation were cleaned with piranha solution (hydrogen peroxide: sulphuric acid = 1:2) for 1 h and then thoroughly washed with distilled water.

### 4.2.3 Electrospinning and fibre deposition

A 9 wt% solution of poly( $\epsilon$ -caprolactone) (PCL) ( $M_w = 65000$  g/mol) in chloroform/methanol (75/25 v/v) was prepared. For a 9 wt% solution of a blend of PCL with 25 wt% type I collagen from calf skin (CPCL25) the polymers were suspended in 1,1,1,3,3,3-hexafluoro-2-propanol overnight followed by a 2 h ultrasonic treatment. The solution/suspension was filled in a 1 mL syringe with a stainless steel 20 gauge flat tipped needle/spinneret (Hamilton, Bonaduz, Switzerland). Electrospinning was performed with a flow rate of 0.5 mL/h, a voltage of 20 kV and a distance of 20 cm between spinneret and target. Random fibres were collected on single targets while parallel fibres were collected suspended between dual collectors with a gap of 4 cm using the gap method for alignment<sup>1,20,21</sup>. A scheme of both electrospinning systems is shown in figure 1 in chapter 3. Depending on further experiments, fibres were deposited onto different substrates.

Electrospun fibres were deposited onto the sPEG-substrates 30 min after preparing the substrates ("sPEG-sub-fib"). The same procedure was applied to GRGDS-sPEG-substrates ("GRGDS-sPEG-sub-fib"). Figure 1 shows a scheme of the preparation of the substrate-fibre-system which is used in cell experiments: electrospun fibres of PCL or PCL/collagen were deposited onto differently modified cover glasses. Analytics of substrate and fibre surfaces and cell experiments were performed with these samples.

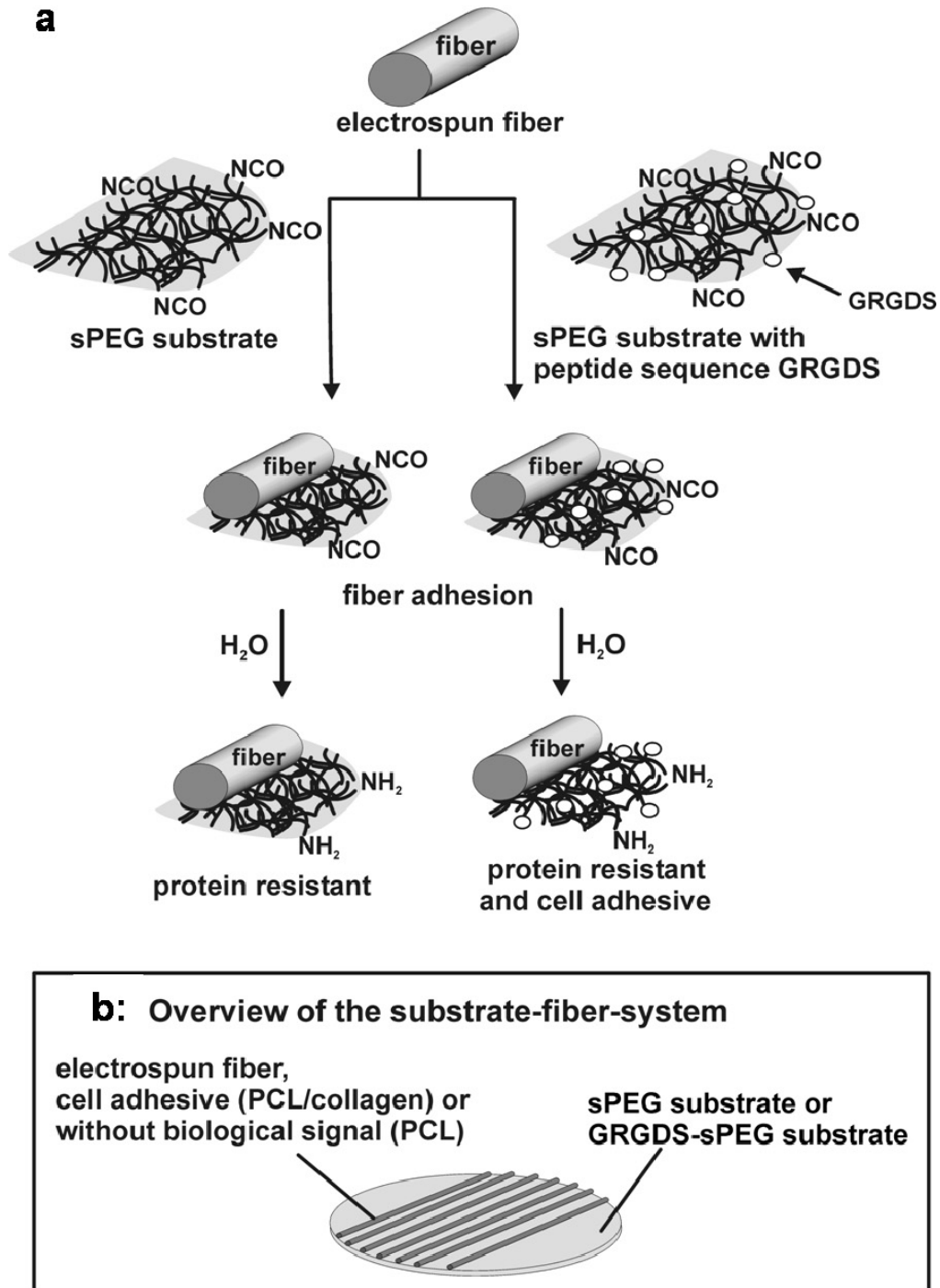


**Figure 1: Substrate-fibre-system used for surface characterisation and cell experiments.** (a) Chemical reactions for generating the substrates. (b) Overview of the substrate-fibre-systems of electrospun fibres and underlying substrates. Image reprinted from literature<sup>22</sup>. Copyright (2009) with permission from Mary Ann Liebert, Inc.



### 4.2.4 Reactive substrate characterisation

#### *Fibre characterisation*

The electrospun fibres were visualised by scanning electron microscopy (SEM) (S360 Zeiss NTS, Germany and Hitachi S3000 N), using 15 kV and working distances of 5 to 15 mm after sputtering with gold for 90 s (S150B, Edwards, Crawley, Great Britain). The SEM images were used to measure fibre diameters which are presented as the mean with standard deviation ( $n = 2$ , counting 90 fibres for random PCL and CPCL25 fibres; 57 fibres for parallel PCL fibres; 57 fibres for parallel CPCL25 fibres).

#### *Layer thickness determination by ellipsometry*

Ellipsometry was used to investigate the layer thickness of the coated surfaces. The layer thickness of each preparation step was determined with modified silicon wafers (see 4.2.2.) using three spots per sample with triplicate measurements per spot. Two samples with the same surface were investigated.

#### *Antibody staining*

Parallel PCL and CPCL25 fibres were placed onto sPEG coated cover glasses, pre-wetted in phosphate buffer saline (PBS) for 5 min and blocked for 1 h in PBS containing 10 % normal goat serum (NGS) and 1 % bovine serum albumin (BSA). Subsequently the substrates were incubated for 4.5 h at room temperature with the monoclonal anti-collagen type I antibody (Sigma C2456, ascites fluid, clone COL-1). This antibody has been reported to have no cross reactivity with other collagen types (i.e., II, III, IV, V, VI, VII, IX, X and XI) and does not react with the thermally denatured molecule. The antibody was diluted in antibody diluent (ABD) (PBS containing 10 % NGS and 2 % BSA; 1:100). The samples were washed three times with PBS followed by 1 h incubation with a fluorescent secondary antibody Alexa Fluor 488 nm (Molecular Probes) diluted in ABD (1:500) at room temperature in the dark. Negative controls were prepared by omitting primary antibodies. Afterwards, all samples were washed three times with PBS and then mounted upside-down onto microscope slides using Fluoroprep (bioMérieux). Epifluorescent microscopy was performed with a Zeiss Axioplan microscope. Images were taken with a constant exposure time of 50 s. Because the microscope gave a green background even without any samples, a background image was taken as blank with the same exposure time. This blank was then subtracted from the images of the samples using adobe photoshop software.

### *Protein adsorption*

Protein adsorption of sPEG coated silicon wafers with PCL and CPCL25 fibres were determined with fluorescently labelled bovine serum albumin (BSA) as previously described<sup>10</sup>. Briefly, the prepared sPEG-sil-fibs were incubated with rhodamine red labelled BSA diluted in PBS (50 µg/mL) for 20 min followed by three incubations in PBS for 20 min each. Afterwards the samples were incubated for 60 min in PBS and washed thoroughly with distilled water. The samples were kept in the dark during incubation and washing. The sPEG-sil-fibs were visualised with fluorescence microscopy (Axioplan 2 imaging, Zeiss, Germany) and images were taken with a constant exposure time of 1 s. Silicon wafers coated with GRGDS functionalised sPEG were also tested for protein adsorption.

### **4.2.5 Fibre adhesion in dependency on post-spincoating crosslinking time**

To investigate how long the sPEG surface is active after spincoating and crosslinking is lasting, electrospun PCL and CPCL random and oriented fibres were deposited onto sPEG-substrates after 30 min, 1 h, 2 h, 4 h, 8 h and 24 h after spincoating. sPEG-sub-fibs were then incubated in water for one hour followed by water exchange and incubation for 2 days. In a last step, 30 ml of water was floated over the sPEG-sub-fibs and then the samples were dried at 40 °C. Before water treatment and after each washing step the samples were investigated by light microscopy. sPEG-substrates were compared with pure glass surfaces by depositing random and oriented fibres directly onto untreated cover glass.

### **4.2.6 Cell culture experiments**

Cell experiments were performed in cooperation with Julia Bockelmann at the Institute of Biology II at RWTH Aachen University. Chicken embryos (day 10) were removed from the egg, decapitated and dissected in ice-cold PBS. The skin was removed with forceps to access the lumbar dorsal root ganglia (DRGs), closed forceps were inserted on both sides of the spinal cord and opened to cut off the limbs. Three to four DRGs from each side were transferred into a 15 mL centrifuge tube with ice-cold PBS. For dissociation of DRGs, the PBS buffer was removed and 1 mL 0.25 % Trypsin/EDTA (Invitrogen) was added for 5 – 8 min on ice, followed by 5 – 8 min at 37 °C. After washing with PBS, the tissue was triturated in 1 mL Dulbecco's modified Eagle medium (DMEM)/F12 + 10 % fetal calf serum (FCS). Then 10 mL of PBS was added and the suspension centrifuged at 130 g for 10 min. The supernatant was removed, and the cells were re-suspended in 1 mL medium and counted in a Thoma chamber.

Cells were cultivated at 37 °C and 5 % CO<sub>2</sub> on prepared sPEG- or GRGDS-sPEG-substrates with electrospun fibres in 24-well-plates under sterile conditions. SPEG-sub-fib and GRGDS-sPEG-sub-fib were sterilised with UV-light for 2 h, and cells seeded at a density of 2 x10<sup>4</sup>cells/500µl DMEM/F12 (1:1), containing 10 % FCS, and 2 % B27 supplement (GIBCO) per well. Nearly 20000 cells per well adhered and this number was stated as 100 % in the calculation of the proliferated cells.

After four days of incubation, the cells were fixed with 4 % paraformaldehyde and processed for immunocytochemical staining. The primary antibodies included anti-S100 to mark Schwann cells (1:200; polyclonal rabbit antibody; S2644 Sigma) and anti-NF 200 (1:500; neurofilament 200 kDa, monoclonal mouse antibody; N0142 Sigma) to stain neurons and axons. The antibodies were diluted in tris-buffered saline and Triton X (TBS-T), containing 1 % normal goat serum. Incubation was done over night at 4 °C. For secondary staining Alexa Fluor<sup>TM</sup> 488 goat-anti-mouse IgG (MoBiTec; A-11001) and Alex Fluor<sup>TM</sup> 546 goat-anti- rabbit IgG (MoBiTec; A-11010) were diluted 1:1000 in TBS-T and incubated for 1 h at room temperature. Cell nuclei were stained with 4',6'-diamidino-2-phenylindole (DAPI; 1:1000) for 5 min. Evaluation was done with an epifluorescence microscope (Zeiss Axiophot). To determine cell numbers, cells were counted from five randomly positioned pictures (area 0.15 mm<sup>2</sup>) from every cover glass. For every condition, experiments were repeated at least four times.

Measurement of neurite alignment was performed on fluorescence images with Image J software. The total length of every neurite was measured as well as the proportion of its length that was in direct contact with a fibre, which was unambiguously identified with a 40x objective. For every neurite, the ratio of its length in contact with an electrospun fibre to its total length was calculated. For every condition, at least 15 axons, all longer than 100 µm, were randomly selected and evaluated. Data are presented as means with standard error of mean and evaluated using ANOVA and Tukey-Kramer-test for multiple pairs (JMP 4.0 software, SAS Institute).

## 4.3 Results

### 4.3.1 Electrospinning

Electrospinning of PCL and a blend of PCL with 25 % collagen (CPCL25) with two different collection configurations was performed to achieve either random or parallel fibres (figure 1, chapter 3).

Figure 2 shows examples of PCL and CPCL25 random and parallel fibres which were used for all following experiments. Electrospinning of pure PCL at 9 wt% resulted in fibres with diameters of  $0.49 \pm 0.24 \mu\text{m}$  for random collection, which was similar to the diameter of parallel fibres ( $0.56 \pm 0.29 \mu\text{m}$ ) (fig. 2a and b). PCL and collagen type I from calf skin were blended to obtain mechanically stable fibres with improved cell recognition properties. The random CPCL25 fibres had diameters of  $0.74 \pm 0.18 \mu\text{m}$  (fig. 2c) while parallel fibres had diameters of  $0.73 \pm 0.31 \mu\text{m}$  (fig. 2d).

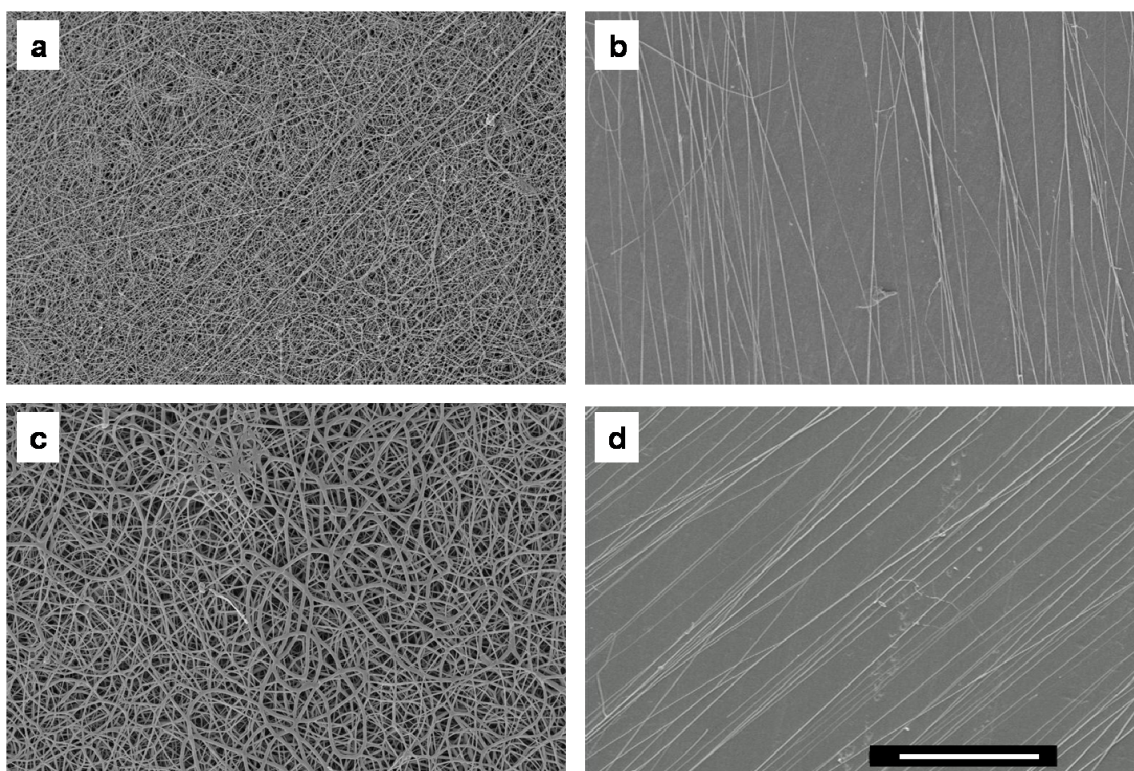


**Figure 2: SEM images of random and oriented fibres of PCL and of CPCL25 produced under optimum conditions for the achievement of good quality fibres.** (a, b) PCL fibres as well as (c, d) CPCL25 fibres were collected with a voltage of 20 kV, a distance between spinneret and target of 20 cm, a flow rate of 0.5 mL/h and a solution concentration of 9 wt%. Scale bar = 100  $\mu\text{m}$ . Image reprinted from literature<sup>22</sup>. Copyright (2009) with permission from Mary Ann Liebert, Inc.

### 4.3.2 Characterisation of *in vitro* substrates

Substrates were prepared by surface modification of silicon wafers or glass cover slips with a sPEG or a cell adhesive GRGDS-sPEG layer. The layer thickness of each step of the

surface modification of the sPEG-substrates was determined with coated silicon wafers. Activation of the silicon surface with UV light did not result in any significant increase of the SiO<sub>2</sub> layer thickness. The aminosilane layer was between 0.9 and 1.3 nm in thickness. With the sPEG coating a total film thickness of  $16.9 \pm 0.4$  nm was determined, meaning a thickness of the sPEG layer of  $15.7 \pm 0.4$  nm.

Electrospun fibres of PCL and CPCL25 were deposited onto the activated surfaces in a second step. Electrospinning directly onto unmodified cover glasses was also attempted. In this case, the random fibres adhered to the glass surface and were not readily washed off, probably due to residual solvent in the fibres that improved adhesion to the collector. In contrast, suspended arrays of parallel fibres which were placed onto unmodified cover glass immediately lifted off the substrate at first contact with water. It is likely that the residual solvent in the suspended fibres had evaporated before collection, thus preventing fibre adhesion. In contrast, parallel and random fibres deposited onto the sPEG layer adhered to this surface and were not washed off, irrespective of the method of collection. This effect was also observed if fibres were deposited onto reactive substrate surfaces 24 h after coating with sPEG.

Collagen was introduced into the fibre to improve cell attachment since it mediates cellular recognition via biochemical signals. The presence of collagen at the surface of the nanofibres was investigated using anti-collagen I antibody staining of both PCL and CPCL25 fibres. Figure 3 presents fluorescence images of stained CPCL25 (fig. 3a, b) and PCL (fig. 3c, d) fibres. The stained CPCL25 fibres (fig. 3a) showed more or less equally distributed green fluorescence indicating the presence of collagen, while no fluorescence was visible with the stained PCL fibres (fig. 3c), non-stained CPCL25 fibres did not auto-fluoresce and second antibody staining without the first antibody was also negative for both CPCL25 (fig. 3b) and PCL (fig. 3d) fibres.

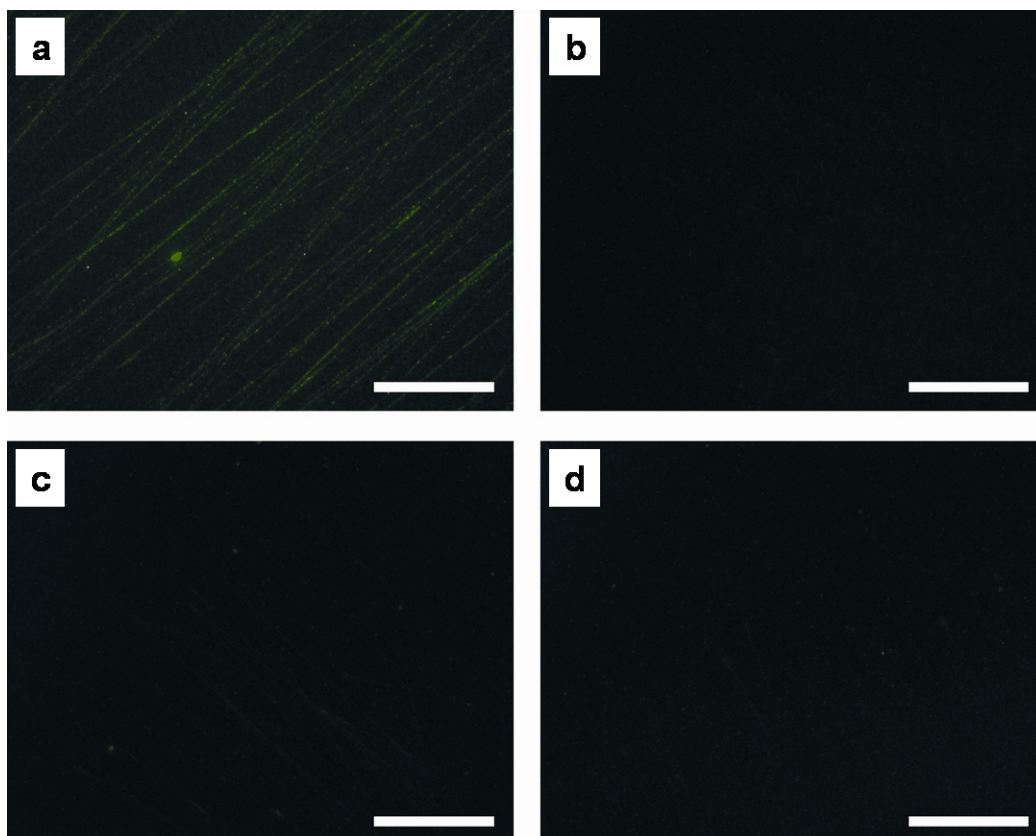


**Figure 3: Fluorescent images of fibres stained with collagen-I antibody.** (a) CPCL25 fibres and (b) PCL fibres stained with anti-collagen I antibody and secondary antibody. Negative controls of (c) CPCL25 and (d) PCL fibres were stained with secondary antibody only. Fluorescence was only observed with the CPCL25 fibres stained with the anti-collagen I antibody (a) demonstrating the presence of collagen at the fibre surface. Images were taken with the same exposure time of 50 s. Scale bars = 50  $\mu\text{m}$ . Image reprinted from literature<sup>22</sup>. Copyright (2009) with permission from Mary Ann Liebert, Inc.

Protein adsorption on biomaterials influences the response for *in vitro* and *in vivo* experiments. Therefore the protein adsorption of the sPEG-substrates with fibres was qualitatively determined by incubating the samples with the rhodamine red labelled model protein BSA. Figure 4 shows fluorescence images of the substrates. All fibres showed strong fluorescence indicating protein adsorption (fig. 4a, b and 4d, e), while the sPEG coated silicon wafer underneath, lacking the fluorescent dye, demonstrated the protein resistant properties of the sPEG coating. GRGDS-sPEG-substrates also did not show any fluorescence, while non-incubated controls with PCL and CPCL25 fibres did not auto-fluoresce (fig. 4c and f).

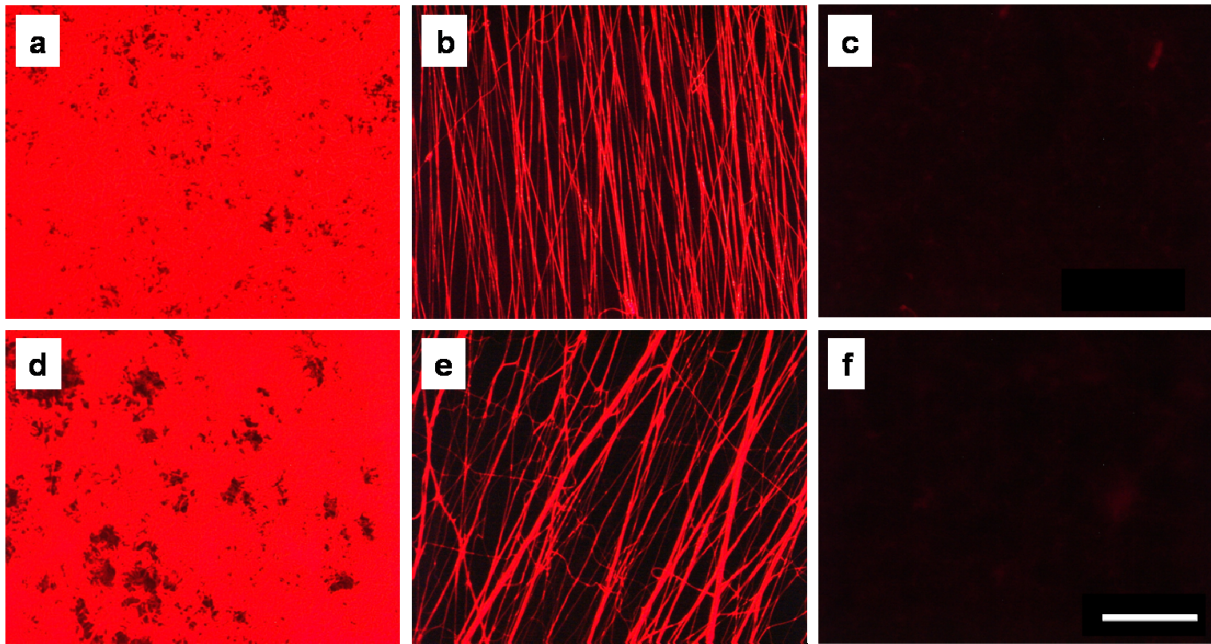


**Figure 4: Fluorescence images of random and parallel PCL and CPCL25 fibres, stained with rhodamine red labelled BSA on sPEG coated silica surfaces.** (a) Random and (b) oriented PCL fibres as well as (d) random and (e) oriented CPCL25 fibres showed red fluorescence due to BSA adsorption on their surfaces. Neither unstained PCL fibres (c) nor CPCL25 (f) fibres show autofluorescence. Images were taken with the same exposure time of 1 s. Scale bar = 100  $\mu\text{m}$ .

### 4.3.3 *In vitro* tests

*In vitro* experiments with the electrospun fibre/sPEG substrates were performed to test substrate durability, cell adhesion, survival and axonal guidance. sPEG-substrates were covered with PCL and CPCL25 fibres both in a random and in a parallel orientation. Additionally, parallel CPCL25 fibres were deposited on cell-adhesive GRGDS-sPEG-substrates were prepared. Dorsal root ganglia contain glial cells (Schwann cells, satellite cells) and sensory neurons of the peripheral nervous system. Dissociated dorsal root ganglia cells were placed on the substrates, and the influence of fibre orientation (random and parallel) and fibre material in combination with the effect of cell repellent (sPEG-substrate) or cell adhesive surface coatings (GRGDS-sPEG-substrate) on cell numbers and neurite alignment was investigated.

The substrates were robust during culture, in that way that fibres did not lift off during media exchanges and sequential washing for immunocytochemistry. In this respect, the reactive sPEG substrate was an excellent and simple method to adhere electrospun fibres. After 4 days incubation *in vitro* (DIV), DAPI-stained cells that adhered to the substrates were

counted. Due to proliferation of glial cells a more than 2-fold increase in cell numbers was counted on electrospun fibres after 4 DIV, without significant differences between materials (PCL vs. C/PCL) or orientation (random vs. parallel) of the electrospun fibres (figure 5). Cells did not adhere to or survive on the sPEG-substrates between the fibres or on sPEG-substrate without fibres. However, with GRGDS-sPEG-substrates, cells attached and proliferated on this surface, an observation previously seen and documented<sup>8</sup>.

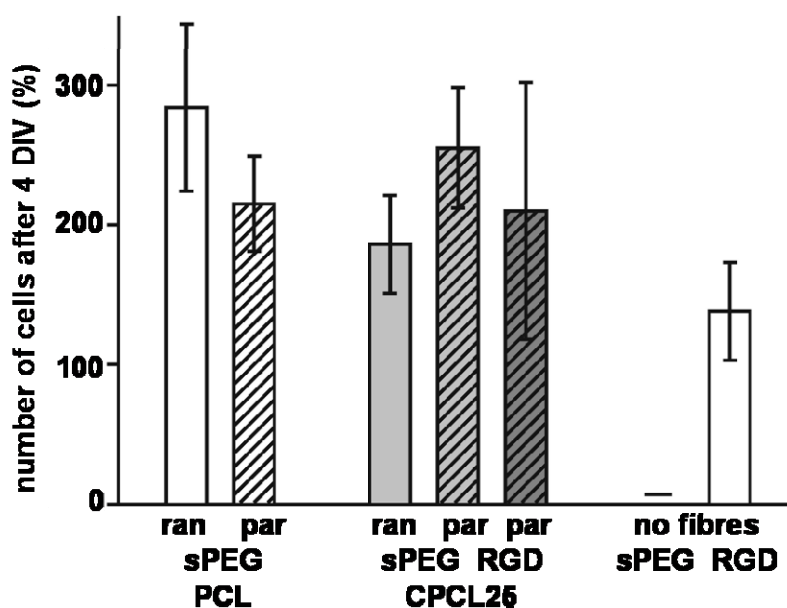


**Figure 5: Effect of electrospun nanofibres on peripheral nervous system cell survival/proliferation.** Cells from chick DRG were dissociated and seeded on randomly orientated (ran) or parallel oriented (par) nanofibres consisting of PCL or CPCL25. The numbers of viable cells after 4 DIV were counted and expressed as percentage of the initial population seeded on the fibres (n = 8 explants, error bars indicate standard error of the mean). The more than 2-fold increase of cell numbers indicates that both types of fibres, irrespective of orientation, supported survival and proliferation of DRG cells. Cells grew on sPEG-GRGD substrate (RGD) with or without fibres but not on pure sPEG substrates. Figure reprinted from literature<sup>22</sup>. Copyright (2009) with permission from Mary Ann Liebert, Inc.

Orientated nanofibres directed the growth of regenerating axons from DRG neurons *in vitro*. After 4 DIV growing sensory axons were fixed and stained immunocytochemically against 200 kD neurofilament protein. Immunostained axons in contact with random and oriented PCL and collagen/PCL fibres are shown in figure 6. On random fibres, axons mainly



did not follow the fibre orientation independently if they grew on PCL (fig. 6b) or on CPCL25 (fig. 6d) fibres. In contrast, a higher alignment of the axons according fibre orientation was observed on oriented fibres (fig. 6c, e).

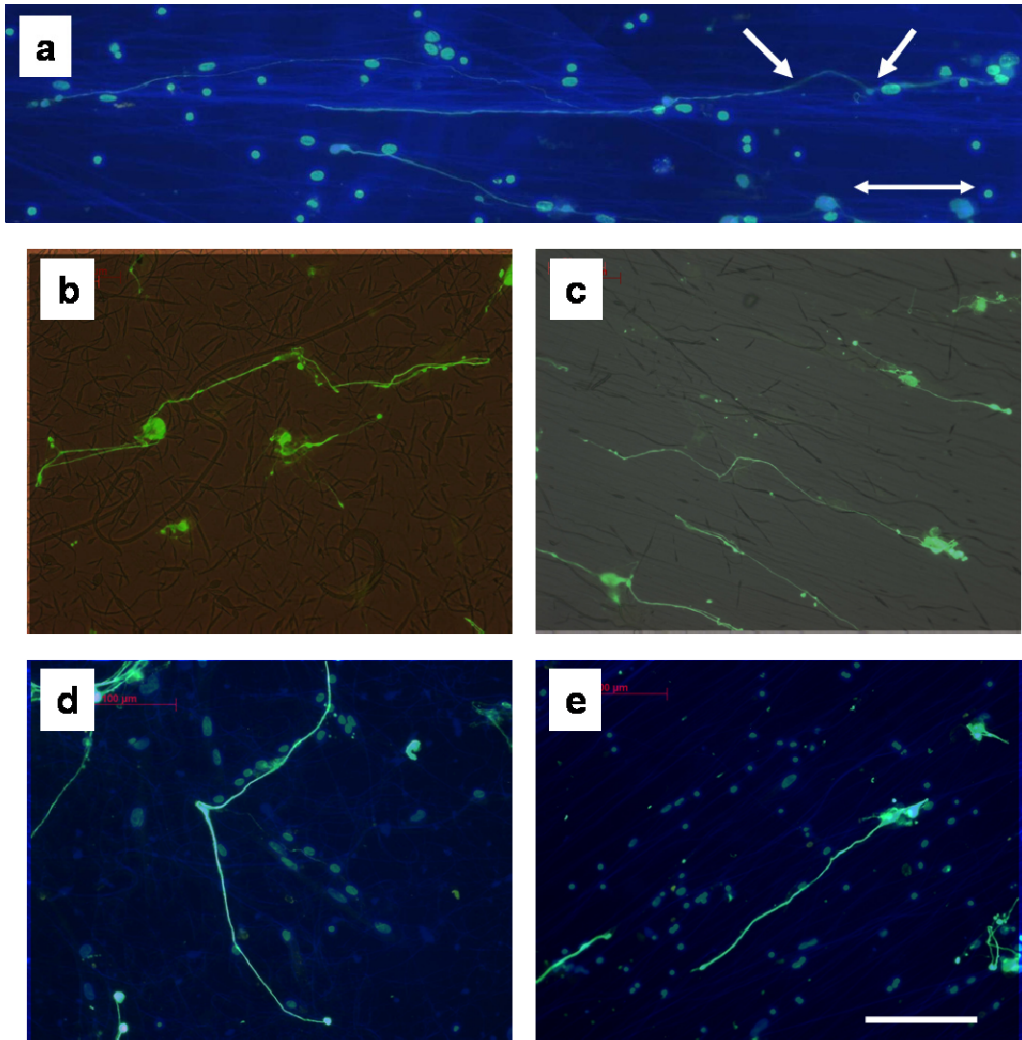


**Figure 6: Neurites from dissociated dorsal root ganglia (DRG) growing on random and oriented nanofibres from PCL and CPCL25.** (a) Immunostained (against 200 kD neurofilament protein) sensory axons in contact with parallel CPCL25 fibres. Nuclei of neurons and glia cells are visualised with DAPI, electrospun fibres are visible by their faint fluorescence. Double arrow indicates orientation of nanofibres while white arrows show where the axon is detached from electrospun fibres. (b) – (e) Neurites growing on random (b) and oriented PCL (c) and on random (d) and oriented (e) CPCL25 fibres. In case of PCL fibres, light microscopy was used to visualise the fibres while fibres containing collagen were slightly stained with DAPI. Neurites were stained against neurofilament and nuclei were visualised with DAPI. Scale bar = 100 μm. Image 6a reprinted from literature<sup>22</sup>. Copyright (2009) with permission from Mary Ann Liebert, Inc.

The lengths of axon sections that were either in direct contact with or that had detached from electrospun fibres were measured, and the percentage of neurite length in direct contact with nanofibres was calculated for every axon (figure 7). Contact guidance on orientated CPCL25 fibres was more pronounced (84 %) and significantly higher (t-test,  $p < 0.01$ ) than on PCL fibres (35 %), or on randomly orientated CPCL25 fibres (57 %). Similarly, when CPCL25 fibres were attached to sPEG-GRGDS surface, smaller stretches of neurites were in contact with the fibres (40 %).

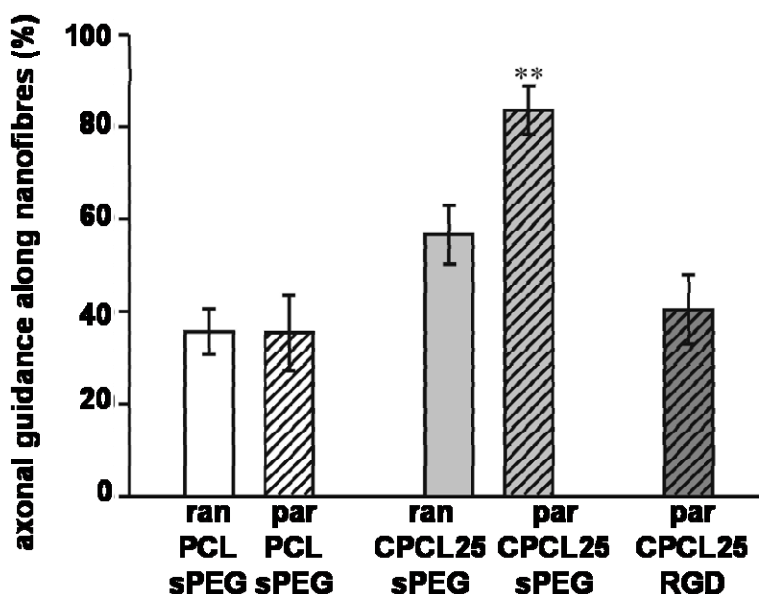


**Figure 7: Axon guidance along electrospun nanofibres on different substrates after 4 DIV.** Calculation of the percentage of lengths in direct contact with electrospun fibres for every neurite. Contact guidance on orientated CPCL25 fibres was most pronounced and significantly higher than on all other fibre materials and orientations when fibres were attached to integrin-binding sPEG-GRGDS (RGD) surface (\*\*  $p < 0.01$ ,  $n = 15$  axons/experiment, error bars indicate standard error of the mean). Image reprinted from literature<sup>22</sup>. Copyright (2009) with permission from Mary Ann Liebert, Inc.

Thus, PCL fibres exhibited a weaker ability to guide axonal growth than CPCL25 fibres and randomly collected CPCL25 fibres, where axons frequently encountered nanofibres perpendicular to their path, were less effective than parallel fibres. When the surface beneath the electrospun fibres was modified with GRGDS peptide, which competed for integrin binding on the cell surface, the guidance effect of CPCL25 fibres was reduced.

### 4.4 Discussion

This study aimed to develop a substrate for controlled cell / fibre interactions *in vitro*. The influence of fibre orientation, biological activity of the fibres as well as the influence of surface modification of the underlying coated cover glasses on cell behaviour was investigated. For this purpose electrospinning of high quality fibres of PCL and different PCL/collagen blends was performed according to fibre optimising in chapter 3. Fibres from both materials were homogeneous, bead-free and had a low diameter distribution and were collected randomly or suspended in air between two parallel targets. These fibres were deposited onto coated cover glasses and surface analysis of the fibres was conducted to investigate the presence of collagen at the fibre surface and the biological activity of the material. Finally *in vitro* experiments with dissociated cells from dorsal root ganglia (DRG) on the “dilute” electrospun fibre samples were performed.

#### 4.4.1 *In vitro* substrates

For sample preparation of the substrate-fibre-system, electrospun random and oriented PCL and CPCL25 fibres were deposited onto the coated cover glass. The reactions forming the protein resistant surface of the glass during preparation are shown in detail in figure 1. The isocyanate end groups of the sPEG molecules react with water to form amino groups and these react with residual isocyanate groups to form an urea-crosslinked sPEG nanolayer on the substrate. Thus, the initially chemically reactive layer transforms into an unreactive one. The sPEG layer thickness was determined by ellipsometry to be  $15.7 \pm 0.4$  nm. This thickness was described to prevent unspecific protein adsorption and should also prevent unspecific cell adhesion<sup>8</sup> due to the PEG backbone. Modification with GRGDS creates a cell adhesive but still protein resistant surface. (Bio)materials used in either *in vivo* and *in vitro* experiments typically come in contact with proteins as long as no special conditions are chosen. Within seconds proteins interact with the biomaterial and adsorb to its surface depending on the proteins' affinity to the biomaterial surface<sup>9</sup>. As cells interact with these adsorbed proteins, it is important to restrict protein adsorption on the desired material for the successful development of surface modified materials for *in vitro* systems and implants. The protein resistant properties of sPEG-coated substrates allow the investigation of the cellular response specifically on the fibres. In contrast, when oriented fibres were directly placed onto glass it is difficult to distinguish the influence of fibres on cells because the cells attach to the glass as well as to the fibres<sup>3</sup>. The protein resistant properties were confirmed by experiments with the model protein BSA. Both PCL and CPCL25 fibres showed protein adsorption; in contrast,

neither the underlying sPEG-substrates nor the cell-adhesive GRGDS-sPEG-substrates demonstrated protein adsorption (fig. 4). GRGDS was used in small amounts (500  $\mu\text{g}/\text{mL}$ ) and was randomly bound to the sPEG. Approximately 1.2 GRGDS molecules are bound to one star molecule, which has been shown to be enough for cell adhesion<sup>8</sup> but allows the formation of a protein resistant network upon crosslinking of the remaining sPEG arms.

The crosslinking process of the sPEG molecules is relatively slow. Fibres adhered to the coated surfaces even after 24 h post-spincoating indicating that the crosslinking process was not yet finished. Two different ways of how fibres are bound to the sPEG surface are imaginable. Firstly the reactive, not fully hardened sPEG layer serves as a kind of glue where fibres partly sink into the sticky, not-fully crosslinked hydrogel layer and are glued to the surface. Secondly, isocyanate endgroups of sPEG molecules additionally react with amine and hydroxyl groups at the fibre surfaces to form urea and urethane groups, respectively, and bind the fibres covalently to the substrate. Preliminary experiments were performed with electrospun polystyrene fibres, which do not have any functional groups for reaction with isocyanate groups via covalent binding (data not shown) and indicated that the first case plays a role in fibre adhesion. Similar observations were made with micro-contact printing on sPEG films. The stamps sunk into the coating if the printing was performed on freshly prepared films while after one hour of crosslinking, the layer was mechanically strong enough to enable standard micro-contact printing<sup>23</sup>. The nanofibres used here were significantly smaller in diameter than the stamps which allow them to adhere to a very thin wet hydrogel layer which probably remains even after 24 h of crosslinking. Both PCL and CPCL25 fibres can thus be readily bound to different targets without being washed off when coming in contact with water. These adherent fibres are strongly bound to the substrate surface and can readily be tested in cell cultures where frequent media changes are required.

No further fixation of the fibres as in other cell experiments<sup>3, 6, 7</sup> is required and even single cell/nanofibre investigations are possible. Only a few experiments have been reported using single cell interactions with individual fibres<sup>2-4</sup>, probably due to the difficulties of single fibre preparations for cell culture. The present investigation demonstrates a method using chemically reactive substrates that is extremely robust for the adhesion of electrospun fibres for *in vitro* investigations.

### 4.4.2 *In vitro* experiments with substrate-fibre-systems

Cell culture experiments with dissociated DRG demonstrated that the configuration of electrospun fibres on cell-repellent sPEG surfaces is well suited to investigate interactions between nanofibres, glia cells and growing axons.

Cell numbers (Schwann cells and neurons) counted after 4 DIV were not significantly different between the various types of electrospun fibres and confirmed biocompatibility of the substrates (fig. 5)<sup>2</sup>. Proteins adsorbed to both collagen containing and pure PCL fibres and played a role in cell adhesion.

Collagen was included to the fibres to provide cell activating signals<sup>11, 13</sup> and enhance the positive effects on cell behaviour. Recent publications have demonstrated the partial degradation of collagen to gelatin during electrospinning<sup>14, 15</sup>. In this study, the existence of collagen type-I immunoreactivity at the surface of CPCL25 fibres by antibody staining (fig. 3a) could be shown. Although the staining was weak, a clear difference between collagen containing CPCL25 fibres and pure PCL fibres was observed and at least some non-degraded collagen seems to be present at the fibre surface. Furthermore, collagen-mediated improvement of bioactivity (cell viability and attachment) of human coronary artery endothelial cells has already been demonstrated when using collagen functionalised poly(L-lactid acid)-*co*-PCL fibres<sup>24</sup> and also for collagen blended PCL fibres<sup>2, 16, 17</sup>.

In our experiments, stronger neurite alignment of dissociated DRG cells along CPCL25 fibres compared to pure PCL fibres indicated biochemical interactions between cell membranes and collagen contained in the fibres and showed the positive effect of collagen. Neurite alignment was significantly higher for parallel CPCL25 fibres on a sPEG-substrate compared with all other samples (fig. 6 and 7). This clearly demonstrates the synergistic effects of nanotopographic pattern and surface functionalisation for neurite guidance, which was already shown with DRG explants on poly(L-lactide) fibres<sup>6, 25</sup>.

The surface modification of the sPEG coating with GRGDS altered the axon guiding properties of the nanofibres, and more than half of the neurites grew without direct contact to oriented CPCL25 fibres. There is a competition between the fibre/substrate surface chemistry and the inherent topological guidance of the fibre<sup>26</sup>. These results demonstrated the need for a system in which surface material, fibre material and fibre orientation can be varied independently as cells react on the combination of all three parameters.

The results showed the potential of combining adhesive oriented fibres with anti-adhesive substrates or matrices. To translate this into *in vivo* guidance of neurons within tissue engineering devices, we hypothesise that the inclusion of adhesive fibres within a non-

adhesive matrix will be likely to assist the guidance of neurons, rather than the inclusion of adhesive fibres within adhesive matrices. However, for nerve regeneration not only neurite outgrowth is important but also other cell populations such as Schwann cells which myelinate axons in the peripheral nervous system and initiate neurite outgrowth and axon regeneration after injuries<sup>27,28</sup>. The surrounding matrix should for example support Schwann cell proliferation while preventing neurite outgrowth away from the fibres at the same time. With our fibre deposition system it is possible to collect fibres of different material or with different functionalities and deposit them next to each other on the same samples. The materials can be chosen in such a way that they support the different needs for nerve regeneration (e.g. regrowth of different fibre systems) additionally to the properties of the matrix. These requirements can be tested with our fibre-substrate-system in 2D. In a feasible 3D system fibres could be imbedded into a matrix which has the same properties as the substrate surface in 2D. The sPEG system offers an opportunity for this because not only thin surfaces can be prepared but also thick hydrogels<sup>29</sup> which may be functionalised in a similar manner. However, such predictions require *in vivo* validation to correlate the *in vitro* results with the *in vivo* performance. Further, the guidance might be enhanced by the use of collagen IV and other ECM molecules which support the regeneration of damaged peripheral nerve fibres<sup>30</sup>. An alternative would be to bind peptide sequences to the fibres, to specifically activate integrin receptors of regenerating neurites. The incorporation of recent technologies for functionalised, protein resistant fibres will be likely to provide greater insight into combinations which might be successful in guiding neurite outgrowth<sup>10</sup>. In such a scenario, surface chemistry of both fibre and substrate can be controlled independently and without non-specific protein adsorption.

### 4.5 Conclusion

An *in vitro* system was developed to test cellular interactions with biologically functionalised nanofibres, where the chemistry of fibres and the underlying substrate can be varied independently. The system was designed to comprise a chemically reactive coating of the substrate that transformed into a protein resistant sPEG or GRGDS-sPEG layer. Fibres adhered strongly to the surface due to the chemical reaction between sPEG molecules and functional groups at the fibres surface, allowing *in vitro* experiments with frequent media changes. Culture of dissociated DRGs demonstrated cell behaviour with regard to the competitive functionality of the fibre and substrate surfaces. The combination of aligned CPCL25 fibres on non-adhesive surfaces was most efficient in guiding neurite outgrowth. The

results demonstrate the benefit of having a system available in which different parameters can be varied independently to evaluate competitive parameters regarding cellular response on electrospun nanofibres.

### 4.6 References

1. Li, D.; Xia, Y. N., Electrospinning of nanofibers: Reinventing the wheel? *Advanced Materials* **2004**, 16, (14), 1151 - 1170.
2. Schnell, E.; Klinkhammer, K.; Balzer, S.; Brook, G.; Klee, D.; Dalton, P.; Mey, J., Guidance of glial cell migration and axonal growth on electrospun nanofibers of poly- $\epsilon$ -caprolactone and a collagen/poly- $\epsilon$ -caprolactone blend. *Biomaterials* **2007**, 28, (19), 3012 - 3025.
3. Sun, T.; Norton, D.; McKean, R. J.; Haycock, J. W.; Ryan, A. J.; MacNeil, S., Development of a 3D cell culture system for investigating cell interactions with electrospun fibers. *Biotechnology And Bioengineering* **2007**, 97, (5), 1318 - 1328.
4. Sun, T.; Norton, D.; Ryan, A. J.; MacNeil, S.; Haycock, J. W., Investigation of fibroblast and keratinocyte cell-scaffold interactions using a novel 3D cell culture system. *Journal of Materials Science-Materials in Medicine* **2007**, 18, (2), 321 - 328.
5. Grafahrend, D.; Calvet, J. L.; Salber, J.; Dalton, P. D.; Moeller, M.; Klee, D., Biofunctionalized poly(ethylene glycol)-block-poly(epsilon-caprolactone) nanofibers for tissue engineering. *Journal of Materials Science-Materials in Medicine* **2008**, 19, (4), 1479 - 1484.
6. Corey, J. M.; Lin, D. Y.; Mycek, K. B.; Chen, Q.; Samuel, S.; Feldman, E. L.; Martin, D. C., Aligned electrospun nanofibers specify the direction of dorsal root ganglia neurite growth. *Journal of Biomedical Materials Research Part A* **2007**, 83A, (3), 636 - 645.
7. Kim, G.; Park, J. H.; Park, S., Surface-treated and multilayered poly(epsilon-caprolactone) nanofiber webs exhibiting enhanced hydrophilicity. *Journal of Polymer Science Part B-Polymer Physics* **2007**, 45, (15), 2038 - 2045.
8. Groll, J.; Fiedler, J.; Engelhard, E.; Ameringer, T.; Tugulu, S.; Klok, H. A.; Brenner, R. E.; Moeller, M., A novel star PEG-derived surface coating for specific cell adhesion. *Journal of Biomedical Materials Research Part A* **2005**, 74A, (4), 607 - 617.
9. Horbett, T. A., The role of adsorbed proteins in tissue response to biomaterials. In *Biomaterials Science: An introduction to materials in medicine*, 2nd ed.; Ratner, B. D., Hoffman, A. S., Schoen, F. J., Lemons, J. E., Ed. Elsevier: San Diego, 2004; pp 237 - 240.
10. Grafahrend, D.; Calvet, J. L.; Klinkhammer, K.; Salber, J.; Dalton, P. D.; Moller, M.; Klee, D., Control of protein adsorption on functionalized electrospun fibers. *Biotechnology and Bioengineering* **2008a**, 101, (3), 609 - 621.
11. Carbonetto, S., The extracellular-matrix of the nervous-system. *Trends In Neurosciences* **1984**, 7, (10), 382 - 387.

12. Friess, W., Collagen - biomaterial for drug delivery. *European Journal of Pharmaceutics and Biopharmaceutics* **1998**, 45, (2), 113 - 136.
13. Gelse, K.; Poschl, E.; Aigner, T., Collagens - structure, function, and biosynthesis. *Advanced Drug Delivery Reviews* **2003**, 55, (12), 1531 - 1546.
14. Yang, L.; Fittie, C. F. C.; van der Werf, K. O.; Bennink, M. L.; Dijkstra, P. J.; Feijen, J., Mechanical properties of single electrospun collagen type I fibers. *Biomaterials* **2008**, 29, (8), 955 - 962.
15. Zeugolis, D. I.; Khew, S. T.; Yew, E. S. Y.; Ekaputra, A. K.; Tong, Y. W.; Yung, L. Y. L.; Hutmacher, D. W.; Sheppard, C.; Raghunath, M., Electro-spinning of pure collagen nano-fibres - Just an expensive way to make gelatin? *Biomaterials* **2008**, 29, (15), 2293 - 2305.
16. Chen, Z. C. C.; Ekaputra, A. K.; Gauthaman, K.; Adaikan, P. G.; Yu, H.; Hutmacher, D. W., *In vitro* and *in vivo* analysis of co-electrospun scaffolds made of medical grade poly(epsilon-caprolactone) and porcine collagen. *Journal of Biomaterials Science - Polymer edition* **2008**, 19, (5), 693 - 707.
17. Venugopal, J.; Zhang, Y. Z.; Ramakrishna, S., Fabrication of modified and functionalized polycaprolactone nanofibre scaffolds for vascular tissue engineering. *Nanotechnology* **2005**, 16, (10), 2138 - 2142.
18. Goetz, H.; Beginn, U.; Bartelink, C. F.; Grunbauer, H. J. M.; Möller, M., Preparation of isophorone diisocyanate terminated star polyethers. *Macromolecular Materials and Engineering* **2002**, 287, (4), 223 - 230.
19. Groll, J.; Ameringer, T.; Spatz, J. P.; Moeller, M., Ultrathin coatings from isocyanate-terminated star PEG prepolymers: layer formation and characterization. *Langmuir* **2005**, 21, 1991 - 1999.
20. Dalton, P. D.; Klee, D.; Möller, M., Electrospinning with dual collection rings. *Polymer* **2005**, 46, (3), 611 - 614.
21. Li, D.; Wang, Y. L.; Xia, Y. N., Electrospinning of polymeric and ceramic nanofibers as uniaxially aligned arrays. *Nano Letters* **2003**, 3, (8), 1167 - 1171.
22. Klinkhammer, K., Seiler, N., Grafahrend, D., Gerardo-Nava, J., Mey, M., Brook, G. A., Möller, M., Dalton, P. D., Klee, D. Deposition of electrospun fibers on reactive substrates for *in vitro* investigations. *Tissue Engineering Part C* **2009**, 15 (1), 77 - 85.
23. Gasteier, P.; Reska, A.; Schulte, P.; Salber, J.; Offenhausser, A.; Moeller, M.; Groll, J., Surface grafting of PEO-based star-shaped molecules for bioanalytical and biomedical applications. *Macromolecular Bioscience* **2007**, 7, (8), 1010 - 1023.
24. He, W.; Yong, T.; Teo, W. E.; Ma, Z. W.; Ramakrishna, S., Fabrication and endothelialization of collagen-blended biodegradable polymer nanofibers: Potential vascular graft for blood vessel tissue engineering. *Tissue Engineering* **2005**, 11, (9 - 10), 1574 - 1588.
25. Patel, S.; Kurpinski, K.; Quigley, R.; Gao, H.; Hsiao, B. S.; Poo, M.-M.; Li, S., Bioactive nanofibers: synergistic effects of nanotopography and chemical signaling on cell guidance. *Nano Letters* **2007**, 7, (7), 2122 - 2128.



26. Smeal, R. M.; Rabbitt, R.; Biran, R.; Tresco, P. A., Substrate curvature influences the direction of nerve outgrowth. *Annals of Biomedical Engineering* **2005**, 33, (3), 376 - 382.
27. Filbin, M. T., Qiu, J., Cai, D., Glial influences on axonal regeneration. In *Glial cell development - basic principles and clinical relevance.*, Jessen, K. R., Richardson, W. D, Ed. Oxford University Press: Oxford, 2001; pp 279-98.
28. Lisak, R. P.; Skundric, D.; Bealmear, B.; Ragheb, S., The role of cytokines in Schwann cell damage, protection, and repair. *Journal of Infectious Diseases* **1997**, 176, S173 - S179.
29. Dalton, P. D.; Hostert, C.; Albrecht, K.; Moeller, M.; Groll, J., Structure and properties of urea-crosslinked star poly[(ethylene oxide)-*ran*-(propylene oxide)] hydrogels. *Macromolecular Bioscience* **2008**, 8, (10), 923 - 931.
30. Jansen, K.; Meek, M. F.; van der Werff, J. F. A.; van Wachem, P. B.; van Luyn, M. J. A., Long-term regeneration of the rat sciatic nerve through a biodegradable poly(DL-lactide-epsilon-caprolactone) nerve guide: Tissue reactions with focus on collagen III/IV reformation. *Journal of Biomedical Materials Research Part A* **2004**, 69A, (2), 334 - 341.

### ***IN VITRO* INVESTIGATIONS ON ELECTROSPUN FIBRES OF POLY( $\epsilon$ -CAPROLACTONE) AND POLY( $\epsilon$ -CAPROLACTONE)/ COLLAGEN**

#### **5.1 Introduction**

Injuries of the nervous system cause loss of motoric and sensory function distal to the lesion site. Peripheral nervous system (PNS) injuries are followed by Wallerian degradation, firstly described by August Waller in 1850, during which destroyed axons and myelin sheath degrade<sup>1</sup>. Macrophages enter the lesion site and phagocytose cell debris. Often basement membranes which surround the axons and Schwann cells remain intact. Schwann cells at the distal nerve stump start to produce growth factors which induce nerve sprouting at the proximal nerve stump towards the distal stump. At small gaps between distal and proximal stump, the growing sprouts reach the distal stump and the nerve is remyelinated by Schwann cells resulting in recovery of the lost function<sup>2</sup>. Bigger injuries can be treated by the use of nerve autografts, mainly from the *nervus seralis*. Autografts cause few immunoreactions, which are a problem of allografts, but require multiple surgeries, often induce neuroma pain and patients loose function at the donor site. Biocompatible artificial implants can help to overcome these disadvantages.

Injuries of the central nervous system (CNS) do not result in regeneration due to several reasons. For example, only a small number of neuroepithelial cells remain mitotic active. Astrocytes are activated and migrate to the lesion site. Here, they build a glial scar to protect the healthy tissue from infections and further physical damage but the scar is also a barrier for regenerating axons<sup>3,4</sup>. Additionally astrocytes express increased chondroitin sulphate proteoglycans (CSPG) which inhibit axonal growth and result in failure of regeneration<sup>5</sup>. At present no treatment for regeneration of CNS injuries exists. Artificial implants may be used to overcome the glial scar and help to induce axonal regeneration.

Artificial nerve grafts must be biocompatible, tolerated by the immune system and must fulfil the mechanical requirements of the place of assignment. They commonly consist of a porous tube filled with a matrix material or longitudinally oriented fibres that leads axons in the desired direction. Tubes of both, non-degradable (e.g. silicone)<sup>6</sup> and degradable materials (e.g. chitosan<sup>7</sup> or poly(DL-lactide acid-*co*-glycolic acid)<sup>8</sup>) had been used to recover

injuries of the PNS *in vivo*. Inclusion of natural polymers such as collagen<sup>6</sup> improved the regenerating properties as well as the combination of the artificial nerve graft with Schwann cells<sup>8</sup>. However, human Schwann cells are not easily available and often cause immunological rejection, thus the development of the cell free conduit is desired. Most of all, an artificial nerve graft must have the right biological properties and must support adhesion and proliferation of several cell types important for neuronal regeneration and must guide neurites and axonal outgrowth.

Many different cell types play an important role in the nerve system. In the peripheral nervous system *neurons* generate and transmit messages. Glial cells, for instance *Schwann cells* (SC) myelinate axons and allow a fast signal transduction. As already mentioned, they express neurotrophic factors which induce regeneration after injuries. *Fibroblasts*, another non-neuronal cell type, have the function to produce extracellular matrix proteins such as collagen for supporting and anchoring cells. They also express basic fibroblast growth factors which play a physiological role in nerve regeneration<sup>9</sup>. In the central nervous system *oligodendrocytes* myelinate axons by wrapping around them and ensure fast information transfer. After injuries, oligodendrocytes express myelin associated proteins which have inhibiting effects on neurite outgrowth<sup>10,11</sup>. *Astrocytes* provide nourishment of neurons and form a matrix. After injuries they primarily form the glia scar, a molecular and physical barrier to regenerating neurons. Astrocytes provide both growth-promoting and growth-inhibiting molecules which make them interesting for nerve regenerating studies<sup>12</sup>. Other interesting cells are *olfactory ensheathing cells* (OEC). They belong to the CNS and are very similar to SCs. OECs ensheath fascicles of unmyelinated primary olfactory axons and support their continuous regeneration from the PNS into the CNS during the whole life of a mammal<sup>13-15</sup>. This is a very rare ability and makes OECs promising candidates for CNS regeneration studies. Investigation of the response of all the different cell types on an artificial nerve graft *in vitro* is very important to estimate *in vivo* reactions and offers the possibility to manipulate the implant in that way that desired cells adhere and grow on the implant while adhesion of undesired cells can be suppressed.

We developed 2-dimensional substrates consisting of oriented electrospun fibres of biocompatible poly( $\epsilon$ -caprolactone) (PCL) or a blend of PCL with 25 % collagen deposited on a cell repellent star shaped NCO-poly(ethylene oxide)-*stat*-poly(propylene oxide) (sPEG) hydrogel layer. Both materials PCL and collagen are biocompatible, provide good cell adhesion and served as substrates in several *in vitro* investigations<sup>16-18</sup>. Addition of collagen to PCL resulted in mechanically stable electrospun fibres with enhanced bioactivities and the

substrates with oriented fibres have already shown to serve as excellent guiding structures for dissociated cells from dorsal root ganglia *in vitro*<sup>19</sup>. This chapter summarises cell experiments with dorsal root ganglia, primary Schwann cells, fibroblasts, oligodendrocytes, olfactory ensheathing cells, astrocytes and U373 cells on 2D-substrates. Several cell studies were performed with these substrates to assess possible application of the electrospun fibres *in vivo* for the future development of a nerve graft with fibres as guiding structures. Results were mainly already published by Eva Schnell<sup>20, 21</sup>, Nadine Seiler<sup>22</sup> and José Gerardo-Nava<sup>23, 24</sup>.

## 5.2 Materials and Methods

### 5.2.1 Materials

Unless otherwise stated, all chemicals were purchased from Sigma-Aldrich (Germany).

### 5.2.2 Substrate Preparation

Reactive substrates were produced by surface modification of cover glass (No. 1, diameter = 12 mm, Marienfeld) with star shaped NCO-poly(ethylene oxide)-*stat*-poly(propylene oxide) (sPEG) and followed by deposition of electrospun nanofibres of either poly( $\epsilon$ -caprolactone) (PCL) or of a blend of PCL with 25 wt% collagen type I from calf skin (CPCL25) as already described in chapter 4.

### 5.2.3 Cell culture handling

#### *Surface treatments*

Cell culture flasks and cover glasses were coated with poly-L-Lysine (PLL, Sigma, P2636, 100  $\mu\text{g}/\text{mL}$ ) by preparing a 200  $\mu\text{g}/\text{mL}$  solution in sterile water (with penicillin/streptomycin, Invitrogen, #15140-122) and incubation over night at room temperature. Afterwards the fluid was removed and coated surfaces were washed twice with sterile water. They were stored at 4 °C. PLL-coated substrates served as controls. Sterilisation of the cover glasses coated with nanofibres was performed with 100 % ethanol and UV light for a minimum of 2 h. Then they were washed twice with phosphate buffered saline (PBS) solution.

*Cell culture conditions*

Cells were cultivated at 37 °C and 5 % CO<sub>2</sub> in 75 cm<sup>2</sup> PLL coated cell culture flasks (Cell Star) under sterile conditions and medium was changed every fourth day. Primary cells were treated special as described below.

*Thawing of cells*

Cells were frozen in 20 % DMSO/DMEM and stored at -80 °C. They were thawed quickly in a water bath at 37 °C and transferred to a 15-mL centrifuge tube containing 9 mL cell medium. Cells were centrifuged for 5 min at 200 g, the supernatant was removed and cells were resuspended in 1 mL cell medium. The cell suspension was given in a 75 cm<sup>2</sup> cell culture flask and incubated at 37 °C. On the next day, the medium was changed and cell debris removed.

*Cell expansion*

After confluent growth of the cells, the medium was removed and cells washed with 10 mL PBS to remove the fetal calf serum (FCS, Invitrogen) which inhibits trypsin reaction. The PBS was removed and cells incubated in 3 mL trypsin/EDTA (Sigma, #T4049) at 37 °C for 5 min to detach the cells from the flask. By adding 6 mL FCS containing DMEM (Gibco, #31966-047) the reaction was stopped and cells were transferred in 15-mL centrifuge vial and centrifuged at 800 rpm for 5 min. Before cells were resuspended in 1 mL cell medium, the supernatant was removed. For following cell experiments, cell number was determined. For further cultivation, 100 µl of the cell suspension was given in a cell culture flask with 12 mL cell medium.

*Cell counting*

An amount of 10 µl cell suspension was mixed with the same amount of trypan blue dye (Sigma, #T8154) which stains cell nuclei of dead cells. 10 µl of this mixture was transferred into a Thoma cell counting chamber and cells in five squares of the chamber were counted (=n). The following formula is used to calculate the cell concentration (=x) per µl cell suspension.

$$x = vzn \text{ [cells/}\mu\text{l]}$$

with v: volume coefficient (= 50)

z: dilution factor (= 2)

The dilution factor  $z$  is 2, because cell suspension and trypan blue were mixed 1:1. The volume coefficient is 50 due to a total volume of the Thoma cell counting chamber of  $1 \text{ mm}^3$  (extrapolated) and a volume of five counted squares of  $0.02 \text{ mm}^3$ . A cell density of  $5 \times 10^3$  cells /  $500 \text{ }\mu\text{l}$  was desired and the cell suspension was accordingly diluted with cell culture medium.

### 5.2.4 Preparation of DRG explants

Chicken embryos (day 10) were removed from the egg, decapitated and dissected in ice-cold PBS. The skin was removed with forceps to access the lumbar dorsal root ganglia (DRGs), closed forceps were inserted on both sides of the spinal cord and opened to cut off the limbs. Six to eight DRGs per embryo from L1-L4 were isolated and transferred into a 15 mL centrifuge tube with ice-cold PBS. Care must be taken to not squeeze and damage the tissue with the forceps. Two or three DRGs were deposited per cover glass and only  $100 \text{ }\mu\text{l}$  growth medium (DMEM-F12, 10 %FSC, 2 B27, Gibco) was immediately added because tissue tended to flow off the glass. After one day  $400 \text{ }\mu\text{l}$  growth medium was added and explants were cultured for 24 h, 4 and 7 d.

### 5.2.5 Primary cell cultures

Investigations with primary cell cultures have some advantages compared with cells from cell lines. Cell lines are immortal and proliferation can take place uncontrolled because they are often derived from tumours. This may result in genetic changes and the protein expression may have unknown patterns. In contrast tissue from primary cultures is taken directly from the living animal and therefore considered to be more reliable.

#### *Schwann cells*

Schwann cells were isolated from the sciatic nerves of perinatal rat pups according to a protocol published by Mey *et al.*<sup>25</sup>. A cell culture medium containing DMEM, 10 %FCS and  $2 \text{ }\mu\text{M}$  forskolin (Sigma, #F6886) was used.

#### *Fibroblasts*

The fibroblasts were preserved from the sciatic nerves of adult Lewis rats by the magnetic microbead separation and taken from the p75-negative fractions. The cell culture medium was DMEM-F12 with 10 % FCS and  $2 \text{ mL}/200 \text{ mL}$  Glutamax (2 mM, Invitrogen),  $200 \text{ }\mu\text{L}/200 \text{ mL}$  gentamycin (10 mg/mL) and  $200 \text{ }\mu\text{L}/200 \text{ mL}$  penicillin/streptomycin. The

fibroblasts were kindly donated by Dr. Gary Brook (Institute for Neuropathology, Medical Faculty at RWTH Aachen University).

#### *Olfactory entheating cells (OEC)*

In the laboratory of Dr. Gary Brook, the OECs were isolated from olfactory bulbs of rat and separated by magnetic affinity cell separation (MACS). Cultures were grown in Scotts medium containing DMEM, 2 mL/200 mL Glutamax, 4.4 mL/200 mL Sato-mix (ICN Biomedicals), 2 mL/200 mL progesterone (12.46 mg/20 mL ethanol absolute), 2 mL/200 mL selenium (7.4 mg/20 mL distilled water), 100 µL/200 mL gentamycin (10 mg/mL), 200 µL/200 mL insulin (10mg/mL), 1 mL/200 mL transferrin (20 mg/mL in HBSS), 8 µg/200 mL heregulin, 8 µg/200 mL bFGF, 1 µM forskolin, 0.25 % astrocyte conditioned medium (supernatant of U373 astrocyte cell line; Istituto Nazinale per la Ricerca sul Cancro c/o CBA, ICLC, Genova) and 10 % FCS.

#### *Astrocytes*

Astrocytes were prepared by Eric Kampmann and Sabien Neerven (both Institute for Biology II, RWTH Aachen University) from the cerebral cortex of perinatal rat pups (P1-2). After tissue preparation and dissociation, the astrocytes were freed from microglia by shaking on a horizontal rocker for 12 h and then expanded. This resulted in a 90 % pure culture of astrocytes still containing some microglia. Cells were cultured in medium of DMEM with 10 % FCS and 100 µL/500 mL penicillin/streptomycin. Staining with glial fibrillary acidic protein (GFAP) and S100 identified the astrocytes in culture immunohistochemically.

### **5.2.6 Cell lines**

#### *Oligodendrocytes*

The OLN-93 cell line was kindly provided by C. Richter-Landsberg (University of Oldenburg). It was isolated from brain glial cultures and derived from immature oligodendrocytes<sup>26</sup>. Cells were cultivated in DMEM containing 0.5 % FCS to induce differentiation of the cells to oligodendrocytes.

#### *U373 astrocytoma cell line*

Cells from the human U373 astrocytoma cell line were frozen in liquid nitrogen and thawed as previously described. They were kindly provided by Dr. Gary Brook. A cell culture

medium of DMEM/F12 (1:1, Gibco) containing 10 % FBS, 1 % glutamax (Gibco) and 1000 U penicillin/streptomycin was used<sup>23</sup>.

### 5.2.7 Immunocytochemistry

With immunocytochemistry proteins inside cells or tissue can be detected. Specific antibodies which bind to the protein of interest are used. A second antibody is linked to a fluorescent molecule on the one hand and can bind to the first antibody on the other hand resulting in fluorescent labelling of the protein to detect.

After the desired time of incubation, the cell medium was removed and cells were fixed with 4 % paraformaldehyde (PFA) for 30 min. Cells were washed twice with PBS and once with tris-buffered saline (0.1 M Tris/HCl (pH 7.8) + 0.8 % NaCl; TBS). To block unspecific binding sites cells were incubated with TBS containing 2 % normal goat serum (NGS, Sigma S-2007) and 0.4 % Triton X-100 (Serva) at room temperature for 30 min. The antibodies (table 1) were diluted in TBS with Triton X-100 (TBS-T), containing 1 % NGS. Incubation was for 2 h at room temperature. After washing twice with TBS the samples were incubated with the first antibody for 1 h (2 h for U373 cells) at room temperature. According to the primary antibody one or more secondary antibodies, Alexa Fluor<sup>TM</sup> 488 goat-anti-mouse IgG (MoBiTec; A-11001) and Alex Fluor<sup>TM</sup> 546 goat-anti-rabbit IgG (MoBiTec; A-11010) were chosen and diluted 1:500 in TBS-T. After washing again with TBS, cell nuclei were stained with 4',6'-diamidino-2-phenylindole (DAPI; 1:1000) for 5 min. Cover glasses were then washed twice with TBS, dried in air and mounted onto microscopic slides using Fluoroprep (BioMerieux S.A.) upside down. Evaluation was done with an epifluorescence microscope (Zeiss Axiophot) coupled to an online digital camera (Axiovision software). Confocal micrgraphs were taken with a Leica confocal microscope (20x objective or 40x objective oil immersion, 4x digital zoom, using 405 nm, 488 nm and 543 nm excitation and filter settings for DAPI, fluorescein and Cy3, sampling rate 200 Hz, Leica 200 software).



**Table 1: Primary antibodies used for immunocytochemical staining.**

Cell type / Localisation	Antibody	Protein	Species	Dilution
Schwann cells and astrocytes; cytoplasm and/or nucleus	S 100 (Sigma, S2644)	calcium binding protein	rabbit (polyclonal)	1:200
neurons; neuronal processes, peripheral nerves	NF 200 (Sigma, S0142)	neurofilaments, structural elements of neuronal axons and dendrites	mouse (monoclonal)	1:500; 1:1000 (U373)
fibroblasts, OEC, U373; cytoskeleton	Vimentin (clone V 9, Sigma, V 6330)	intermediate filament protein family	mouse (monoclonal)	1:1000; 1:5000 (U373)
astrocytes; cytoplasm, intermediate filaments of glial cells	GFAP (Sigma, G3893 or Dako)	glial fibrillary acidic protein	rabbit (polyclonal)	1:500 or 1:2500 (U373)
	(Mab360, Chemicon)		mouse (monoclonal)	1:500
oligodendrocytes, Schwann cells; myelin forming cells	CNPase	2', 3'-cyclic nucleotide 3'-phosphodiesterase	mouse (monoclonal)	1:1000

### 5.2.8 Cell numbers

Cell numbers of cells growing on the electrospun fibres were determined by counting DAPI stained cell nuclei after 1 and 7 DIV. Within a field of either 0.03 mm<sup>2</sup> or 0.39 mm<sup>2</sup> depending on cell density and objective used, counting was done six times. For each experiment two independent cultures were investigated. No cells were observed on sPEG coated substrates without any fibres.

### 5.2.9 Neurite outgrowth

Single images of DRG explants stained with neurofilament antiserum were used to determine neurite lengths. It was measured from the surface of the DRG to the tip of the neurite. Photoshop (version 6.0, Adobe) and Image J were employed for this measurement.

Additionally the orientation of the neurites in respect to the orientation of the fibres “orientation index” was determined. Two imaginary lines were deposited parallel to the fibres and two perpendicular to the fibres at the outer surface of the DRG and numbers of neurites crossing the lines were counted. The orientation index was defined as ratio of intersecting neurites parallel to the fibres to the number of all neurites passing all four lines.

### 5.2.10 Morphometric measurements

The different cell types were investigated with fluorescence microscopy after immunostaining with specific cell markers and DAPI. The longest process lengths of randomly chosen 100 cells were measured for every condition (time in culture; PCL and CPCL25 fibre). Process length was defined as the distance from the cell nucleus to the tip of the neurite/cell process. For U373 cells the 10 % longest processes of at least 50 randomly chosen cells were estimated. Because fibroblasts adhered poorly on PCL fibres here a lower cell number was investigated. Experiments were performed in triplicates.

### 5.2.11 Migration of cells

#### *Migration of cells escaping from DRG explant*

A region of 200  $\mu\text{m}$  width and length according the farthest cells radiating from the surface of the explant was photographed and all S-100 positive cells were counted. The distances of the 10 % of the cells that had migrated farthest were measured using Image J.

#### *Migration of U373 cells*

U373 astropheres were used to determine cellular migration. The astropheres were obtained by cultivating the cells in neural progenitor differentiation medium (NPDM) and placed on the different fibre types. After 2 DIV spheres were fixed with 4 % PFA and the distances of the 10 % farthest migrated DAPI-stained cells were measured parallel and perpendicular to the fibre orientation. This was repeated three times for each substrate type with a total of 12-15 spheres with a uniform diameter ( $272 \pm 10 \mu\text{m}$ ).

#### *Agarose drop assay*

The agarose drop assay was used to determine the distance of migration of all single cell cultures excluding U373 cells. A low melting agarose gel (0.6 %, melting point 70 °C; Sigma) was prepared in warm DMEM (Gibco) containing 10 % FCS and cooled down to 37 °C. Cells from two confluent T75 cell culture flasks were harvested, resuspended in 1 ml DMEM / 10 % FCS, and cell number was determined using a Thoma chamber. A final concentration of  $8 \times 10^7$  cells/mL was obtained by diluting in cell medium and the cell suspension was mixed with the gel solution (final concentration  $4 \times 10^7$  cells/mL, 0.3 % agarose). Three 1  $\mu\text{l}$  drops per slide were placed on the different substrates and four different slides per substrates type were used in parallel for one experiment. The sample was cooled for 10 min at 4 °C and then 500  $\mu\text{l}$  cell culture medium was added and samples were placed into

the incubator. Samples were analysed after 1 and 2 DIV and images were taken with inverse phase contrast light microscopy (Olympus CKX41, 10x objective) and Axiocam digital camera (Zeiss). Migrating cells were photographed on two opposite sides of the drop parallel to the oriented fibres. Cell numbers of migrating cells out of the drop and the distances of the 10 % farthest cells were determined (Image J).

### **5.2.12 Statistical analysis**

Data are presented as means with  $\pm$  standard error of the mean. Following ANOVA, means were compared with Tukey-Kramer-test for multiple comparisons (JMP 4.0 software, SAS Institute Inc.).

## **5.3 Results**

The purpose of this study was the investigations of electrospun oriented nanofibres as suitable substrates for neuronal cell growth and guidance structure. Therefore a multitude of different cells from dorsal root ganglia (DRG) explants, primary cultures and cell lines were placed on PCL and CPCL25 nanofibres deposited on sPEG coated cover glasses and firstly cell survival and proliferation were estimated. Cell numbers of the different cells were counted after 1 and 7 DIV. Figures 1 and 2 show these results. The values demonstrate the number of counted cells in comparison to initial seeded cells in %. Numbers of cells were quite different for the single cell types but cell numbers increased with time for all cells beside fibroblasts on CPCL25 fibres. Here no significant drop of cells was observed on CPCL25 fibres after 7 DIV compared to 1 DIV. Cell numbers of Schwann cells (SC) and fibroblasts (fib) were higher on CPCL25 fibres than on PCL fibres for both time points. However, the differences were not significant (fig. 1). With olfactory ensheathing cells, numbers of cells were significantly higher on PCL fibres after 1 DIV. After 7 DIV this relation was the opposite and now significantly more cells were counted on CPCL25 fibres (fig. 1).

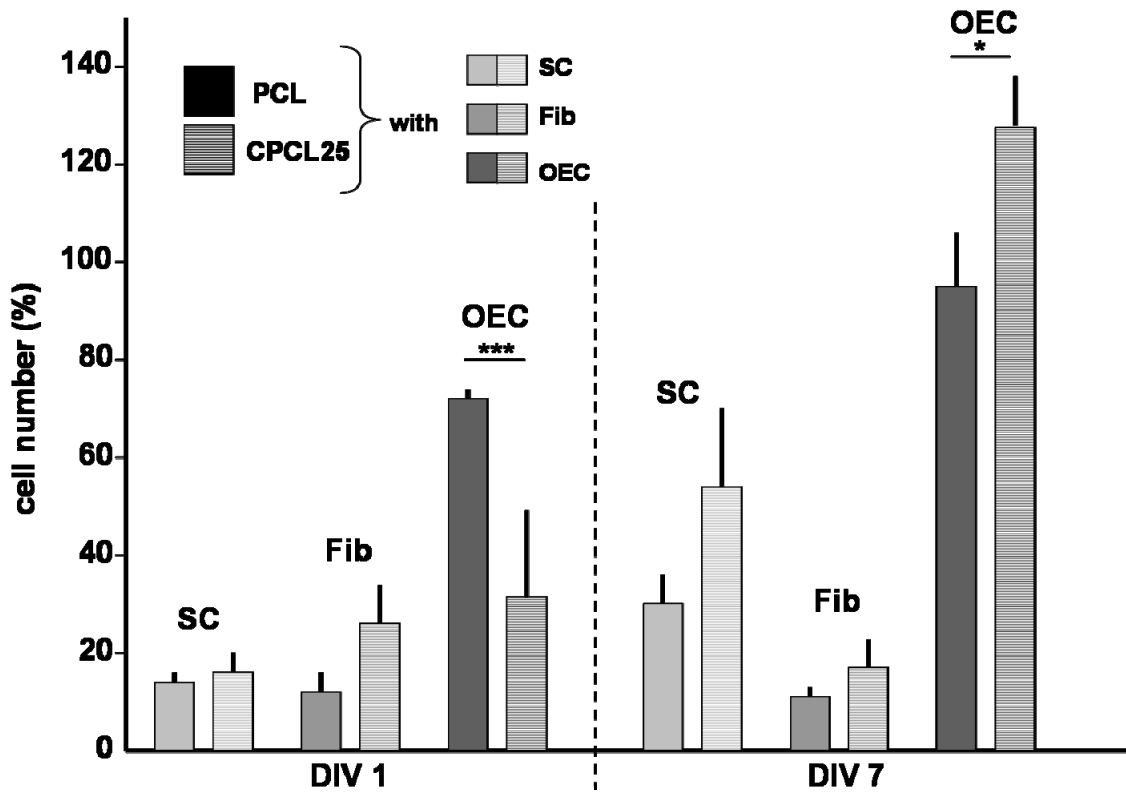
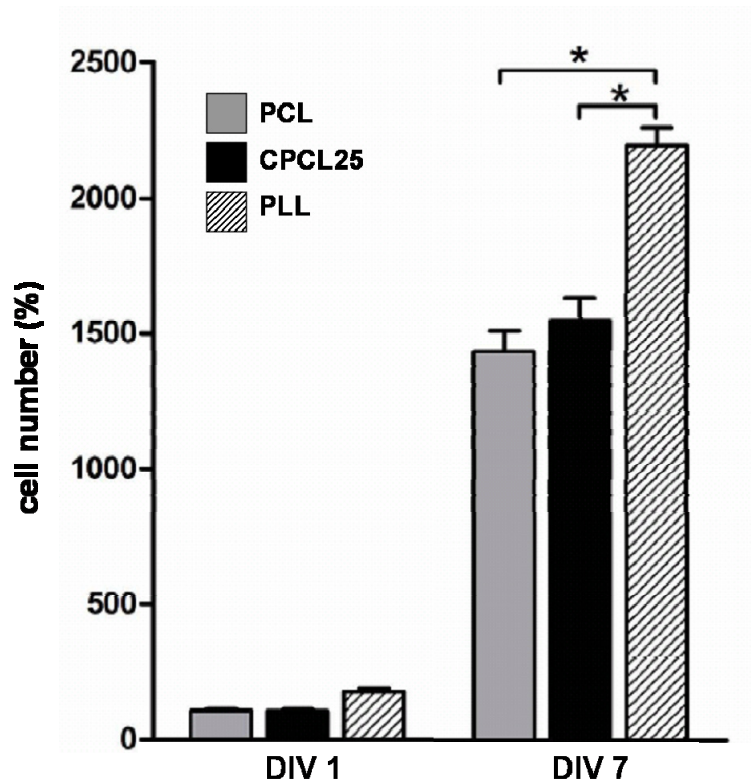


Figure 1: Cell survival/proliferation of Schwann cells (SC), fibroblasts (Fib) and olfactory ensheathing cells (OEC) after 1 and 7 DIV. (\* $P < 0.05$ , \*\*\* $P < 0.001$ )

Cell numbers of U373 cells were nearly the same on PCL and CPCL25 fibres. They increased significantly from 1 DIV to 7 DIV but were significantly less than on poly-L-lysine (PLL) coated cover glasses without fibres after 7 DIV (fig. 2).



**Figure 2: Cell survival/proliferation of U373 cells after 1 and 7 DIV. (\*P<0.05).** Data reproduced from reference<sup>23</sup> with permission of Future Medicine Ltd.

### 5.3.1 Effect of PCL and CPCL25 fibres on neurites and Schwann cells from DRG explants

DRG explants from chicks were used to estimate neurite outgrowth and Schwann cell migration on PCL and CPCL25 fibres. After a few hours of deposition on the fibre substrates, the explants adhered on the substrates and adopted a flattened appearance. Staining with an antibody against neurofilaments (NF200) showed a strong neuritic growth, seen in figure 3a, b on both PCL (fig. 3a) and CPCL25 (fig. 3b) fibres. On sPEG coated substrates without any fibres any explant adhered. Glial cells started to migrate out of the tissue. Neurites started to grow out within the first 24 h after incubation and were observed over a period of 7 days *in vitro* (DIV). Neurites grew mainly in direct contact with the oriented fibres and elongation was heightened along fibre orientation and not perpendicular to the fibre orientation. This was quantified by drawing imaginary lines parallel and perpendicular to the fibres (see fig. 3 b) and counting the number of neurites crossing the line perpendicular to the fibres and dividing this number by the number of neurites crossing all lines. This was called “orientation index” and the results are shown in figure 3c. An orientation index of 50 % means that an equal number of neurites grow along and perpendicular to the fibre orientation, visualised by the dashed line in figure 3c. After 1 DIV neurite outgrowth on PCL fibres was not in respect to

the fibre orientation. On CPCL25 fibres neurites mainly followed the oriented fibres and the orientation index was  $98.4 \pm 1.26\%$  (mean  $\pm$  standard error mean). This value remained after one week incubation while the orientation index increased on PCL fibres in favour of the fibre orientation.

A stronger fasciculation of axons emerging from the explants was observed on PCL fibres, which may indicate stronger interactions between axons instead of interactions between nanofibres and axons. The lengths of all neurites were measured to estimate the influence of nanofibres on axonal growth. Figure 3d shows the mean values of the 10% longest neurites. At all time points these neurites on PCL fibres (DIV 1:  $0.69 \pm 0.02$  mm; DIV 4:  $2.40 \pm 0.13$  mm; DIV 7:  $2.28 \pm 0.03$  mm) were significantly longer than those on CPCL25 fibres (DIV 1:  $0.39 \pm 0.01$  mm; DIV 4:  $1.25 \pm 0.03$  mm; DIV 7:  $1.61 \pm 0.04$  mm).

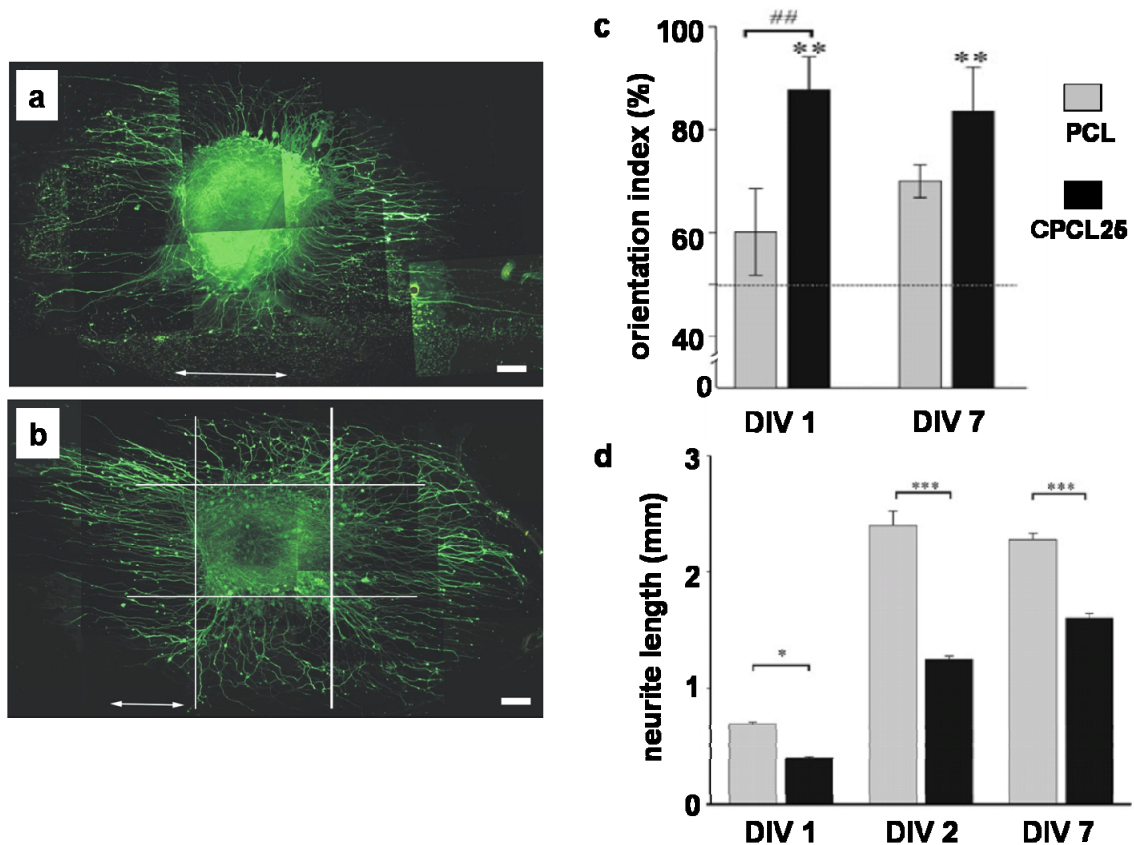


**Figure 3: Orientation of neurite outgrowth and neurite lengths from DRG explants.** (a, b) Neurofilament (NF200) staining of DRG explant on (a) PCL and (b) CPCL25 nanofibres, with additionally showing the square used for determining the orientation index; (c) orientation index of neurites along PCL and CPCL fibres after 1 and 7 DIV; (d) mean lengths of the 10% longest neurites per explant after 1, 2 and 7 DIV. Double arrow in (a, b) indicates fibre direction. Scale bar = 250  $\mu$ m. (n = 3-4 explants per condition, error bar = standard error of the mean; (c)

<sup>##</sup>P<0.01, \*P<0.05, \*\*P<0.01, significant differences from 50 %; (d) \*P<0.5, \*\*\*P<0.001) Data and images taken from literature<sup>21</sup>. Copyright (2007) with permission from Elsevier.

Schwann cells play an important role in guiding neurites and thus a positive effect of fibre material on Schwann cell physiology is desired which was tested with electrospun fibres. DAPI staining of cell nuclei showed that a large number of cells escaped from the DRG explant as seen in figure 4a. Double staining with S100 demonstrated that these cells were mainly Schwann cells (fig. 4b) and that they were in close contact with the nanofibres. The mean migration distance of the 10 % farthest migrated cells is shown in figure 4c. The migration distance was significantly higher on CPCL25 fibres (e.g. DIV 1:  $306.4 \pm 17.9 \mu\text{m}$ ; DIV 7:  $1.350 \pm 32.3 \mu\text{m}$ ) than on PCL fibres (e.g. DIV 1:  $254.5 \pm 9.1 \mu\text{m}$ ; DIV 7:  $791.2 \pm 13.0 \mu\text{m}$ ) at all time points. This indicates a faster migration on CPCL25 fibres.

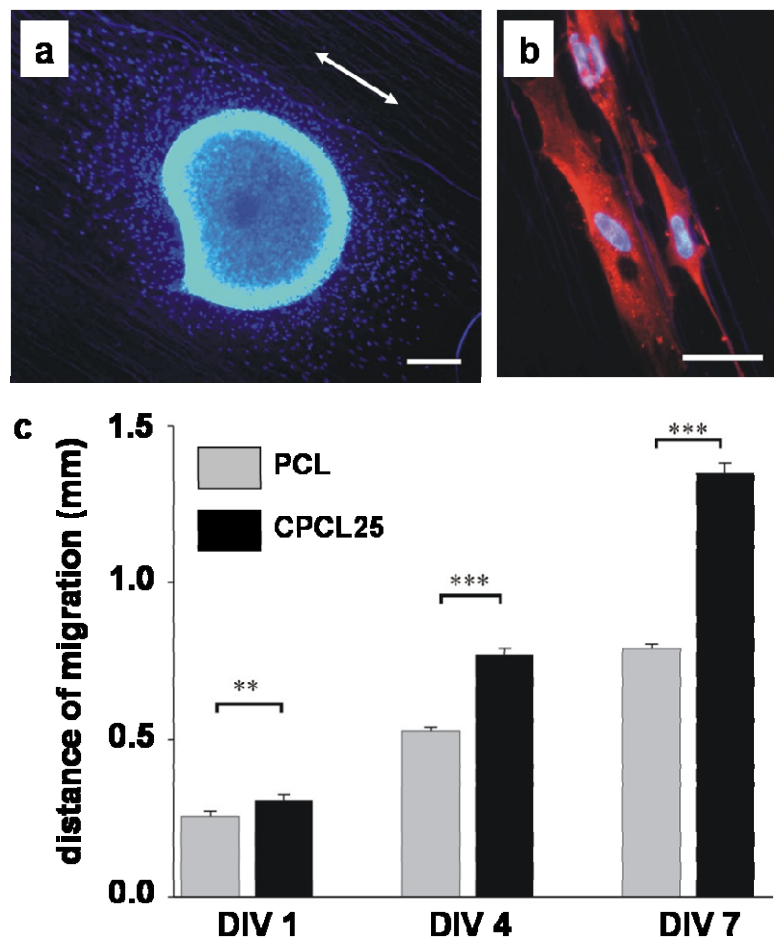


**Figure 4: Schwann cell migration from DRG explants.** (a) Overview of a DAPI-stained DRG explant on CPCL25 fibres after 4 DIV, scale bar =  $200 \mu\text{m}$ ; (b) detail from (a), S100 staining shows cytosol (red), DAPI staining shows cell nuclei (blue), scale bar =  $40 \mu\text{m}$ ; (c) distance of 10 % farthest migrated cells after 1, 4 and 7 DIV. Double arrow in (a) indicates fibre direction.

(n = 3-4 explants per condition, error bar = standard error of the mean, \*\*P<0.01, \*\*\*P<0.001).  
Data and images taken from literature<sup>21</sup>. Copyright (2007) with permission from Elsevier.

### 5.3.2 Effect of PCL and CPCL25 fibres on Schwann cells from primary culture

Schwann cells from the sciatic nerves of perinatal rat pups were placed on substrates with PCL and CPCL25 fibres and influence on morphology, process lengths and migration was investigated. Figures 5a and b present the morphology of Schwann cells on PCL (fig. 5a) and CPCL25 (fig. 5b) fibres. In both cases, cells were elongated and oriented parallel to the fibre orientation. Immunocytochemical staining with S100 allows the measurement of the cell processes from the surface of the cell nucleus (DAPI stained) to the tip of the process. Figure 5c shows these data. Process lengths were significantly longer with cells on CPCL25 fibres ( $33.4 \pm 1.3 \mu\text{m}$  vs.  $23.1 \pm 0.8 \mu\text{m}$ ) after 1 DIV and elongated even further after 7 DIV ( $52.3 \pm 1.5 \mu\text{m}$  on CPCL25 vs.  $41.5 \pm 1.5 \mu\text{m}$  on PCL). The measurement of the 10 % farthest migrated cells demonstrated additionally the positive effect of the included collagen on Schwann cells (fig. 5d). Cells migrated significantly further on collagen containing fibres and reached a distance of  $275.9 \pm 24.0 \mu\text{m}$  after 2 DIV on CPCL25 fibres but only  $141.0 \pm 43.7 \mu\text{m}$  on PCL fibres.



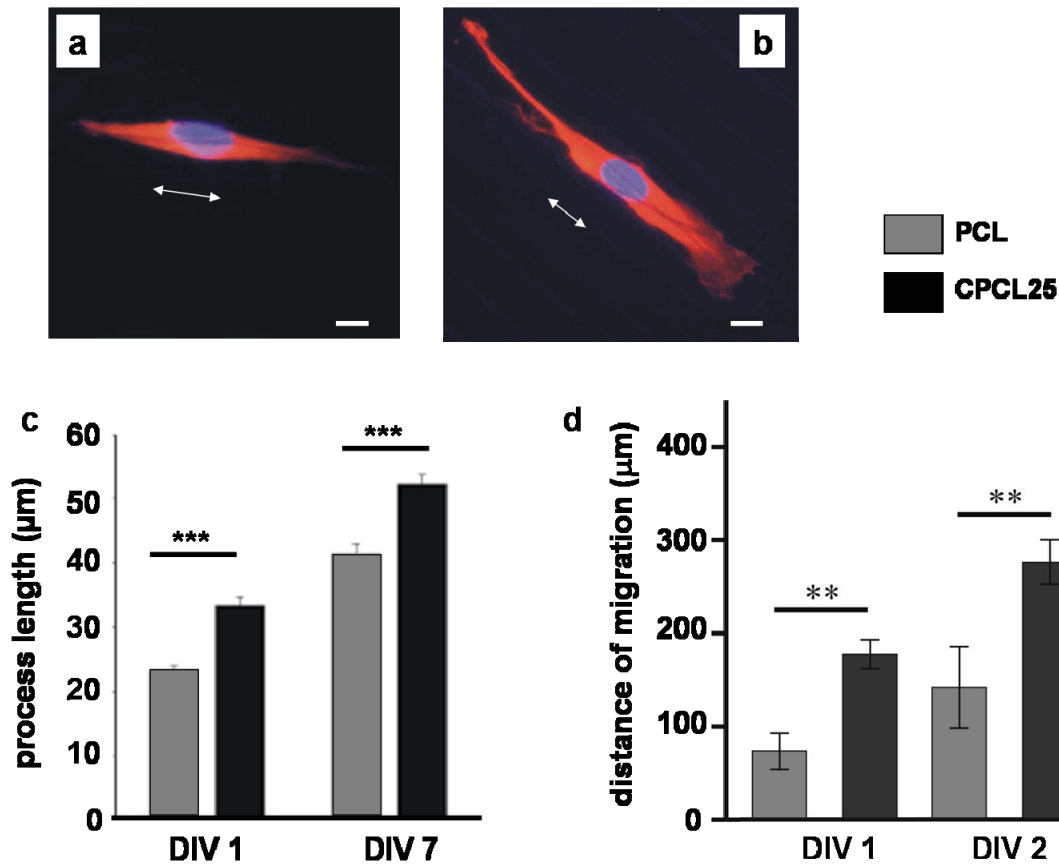


**Figure 5: Schwann cells in primary culture.** (a, b) S100 (red, cytosolic) and DAPI (blue, nuclei) staining of Schwann cell cultures on (a) PCL and (b) CPCL25; (c) process lengths of Schwann cells after 1 and 7 DIV,  $n = 300$  cells per condition; (d) migration distance of the 10 % farthest cells from the agarose drop after 1 and 2 DIV,  $n = 15$  pictures from 4 independent experiment. Scale bar = 20  $\mu\text{m}$ . Double arrow in (a, b) indicates fibre direction. (Error bar = standard error of the mean, \*\* $P < 0.01$ , \*\*\* $P < 0.001$ ). Data and images taken from literature<sup>21</sup>. Copyright (2007) with permission from Elsevier.

### 5.3.3 Effect of PCL and CPCL25 fibres on fibroblasts from primary culture

Fibroblasts secrete molecules of the extracellular matrix (ECM) which are important as growth substrates for neurons and glial cells. Therefore the influence of electrospun nanofibres was tested with rat fibroblasts. The morphology in dependence of fibre material is shown in figures 6a, b. While cells preferred to cluster and formed round cell agglomerates on PCL fibres (fig. 6a), CPCL25 fibres induced the elongation of the cellbody according the fibre orientation (fig. 6b). Process lengths from the surface of the nucleus to the tip of the process were measured and data are presented in figure 6c. Long processes along the CPCL25 nanofibres were formed (DIV1:  $77.7 \pm 9.2 \mu\text{m}$ , DIV 7:  $92.0 \pm 5.0 \mu\text{m}$ ) and were significantly longer than on PCL fibres.

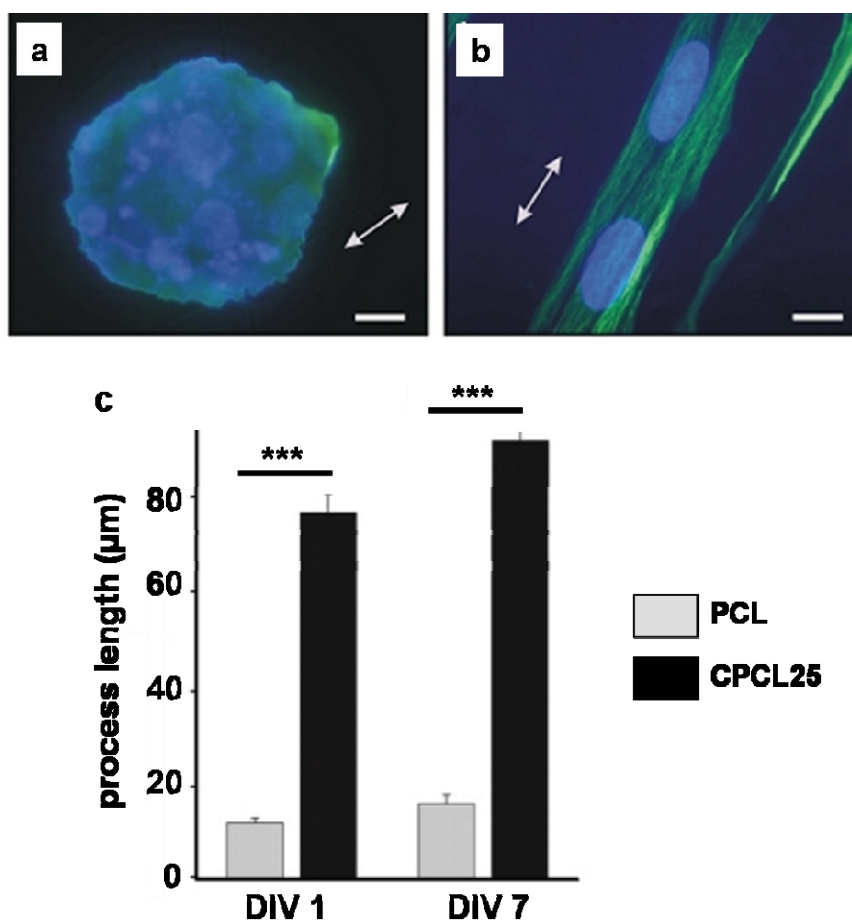


**Figure 6: Fibroblasts in primary culture.** (a, b) Vimentin (green, cytosolic) and DAPI (blue, nuclei) staining of cells cultured on (a) PCL and (b) CPCL25; (c) process lengths of fibroblasts after 1 and 7 DIV. Double arrows in (a, b) indicate fibre direction. Scale bar = 20 µm. (Error bar = standard error of the mean, n = 300 cells per condition, \*\*\*P<0.001) Data and images taken from literature<sup>21</sup>. Copyright (2007) with permission from Elsevier.

### 5.3.4 Effect of PCL and CPCL25 fibres on olfactory ensheathing cells from primary culture

Olfactory ensheathing cells appear in the olfactory bulb of the central nervous system (CNS) and fulfil many functions of Schwann cells. Axonal regeneration in olfactory bulb happens during the whole lifetime and therefore OECs have already been used in nerve grafts *in vivo*. The influence of PCL and CPCL25 fibres on morphology was tested with rat OECs. The effect of fibres on morphology is shown in figures 7a (PCL) and b (CPCL25). OEC extended processes which followed the direction of the fibres. This effect was significantly greater on CPCL25 fibres and the process lengths from the surface of the nucleus to the tip of the process were measured. Data are shown in figure 7c. While process lengths remained

nearly the same on PCL fibres ( $14.67 \pm 0.95 \mu\text{m}$ , 7 DIV) over time, process lengths increased from around  $18 \mu\text{m}$  to  $29 \mu\text{m}$  within seven days on CPCL25 fibres.

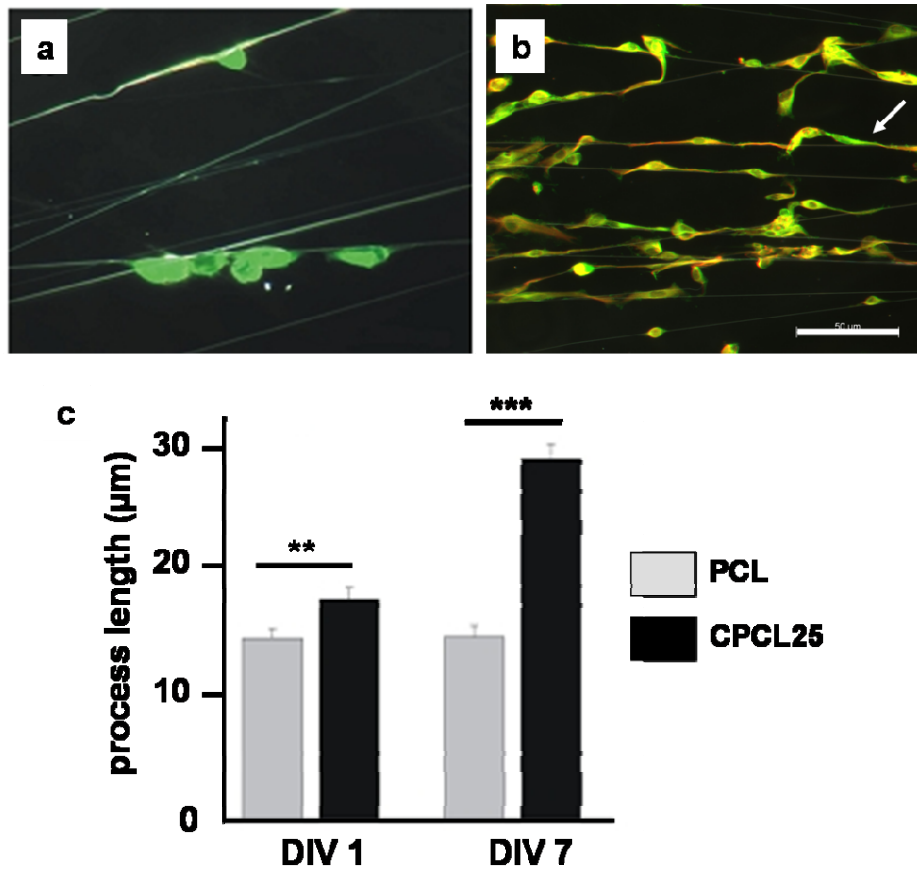


**Figure 7: Olfactory ensheathing cells (OEC) in primary culture.** Cells cultured on (a) PCL, stained with vimentin (green, cytosolic) and (b) CPCL25, stained with vimentin (red, cytosolic) and S100 (green); (c) process lengths of OECs after 1 and 7 DIV. Single arrow indicates an OEC process elongated along the fibre. Scale bar =  $20 \mu\text{m}$ . (Error bars = standard error of the mean,  $n = 300$  cells per condition,  $**P < 0.01$ ,  $***P < 0.001$ ) Data and images taken from literature<sup>21</sup>. Copyright (2007) with permission from Elsevier.

### 5.3.5 Effect of PCL and CPCL25 fibres on oligodendrocytes from a cell line

Experiments with oligodendrocytes, a glial cell type of the CNS, were performed in respect of the development of explants for the spinal cord. These cells produce myelin in the CNS. Cells of the OLN93 cell line were investigated. Figures 8a-c shows oligodendrocytes seeded on (a) PCL and (b) CPCL25 nanofibres and (c) on poly-D-lysine (PDL) coated surfaces without any fibres. Cell nuclei were round but elongation of the cellbodies according the fibre direction and process forming (fig. 8a and b) indicating a close contact of the cells to the fibres. Oligodendrocytes grew out of the agarose drop and migrated significantly further

on CPCL25 fibres compared to PCL fibres and reached a distance of about 615  $\mu\text{m}$  vs. a distance of  $194.6 \pm 30.1 \mu\text{m}$  (PCL) after 2 DIV. Figure 8d shows these results.

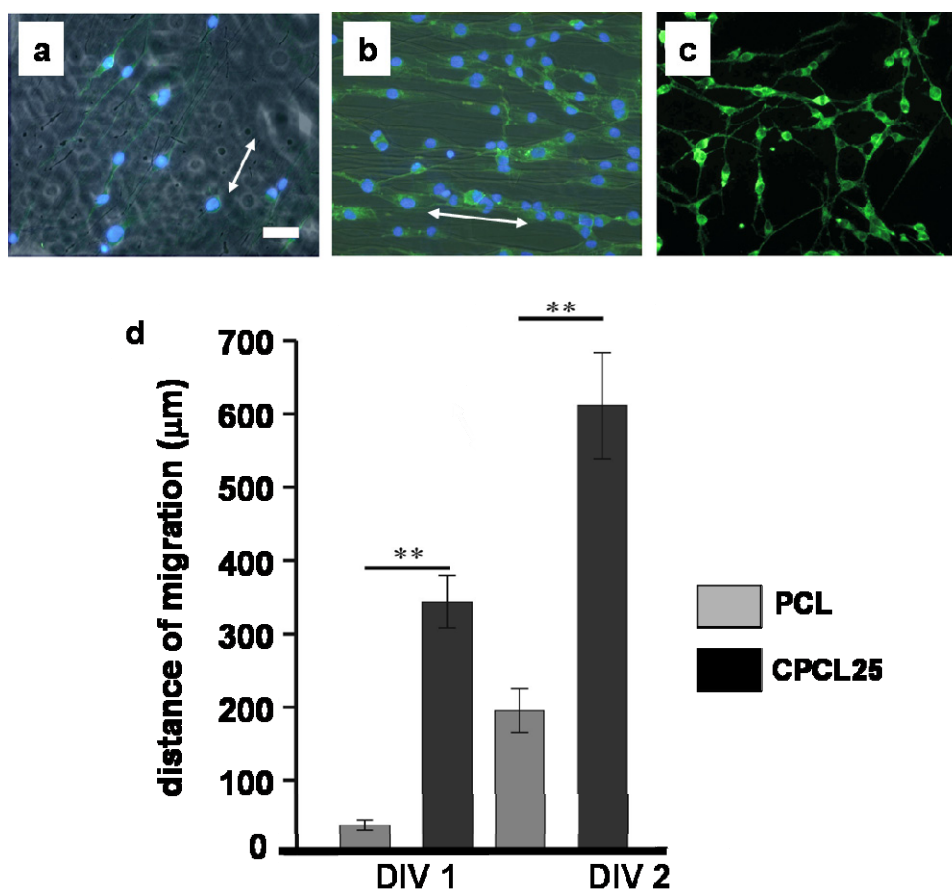


**Figure 8: Oligodendrocytes in primary culture.** (a-c) CNPase antibody (green) and DAPI (blue) staining of cells cultured on (a) PCL, (b) CPCL25 and (c) poly-D-lysine; (d) migration distance of the 10 % farthest cells from the agarose drop after 1 and 2 DIV. Double arrows in (a, b) indicate fibre direction. Scale bar = 50  $\mu\text{m}$ . (Error bars = standard error of the mean,  $n = 15$  pictures from 4 independent experiment,  $**P < 0.01$ )

### 5.3.6 Effect of PCL and CPCL25 fibres on astrocytes from primary culture

Astrocytes are also a cell type of the CNS and fulfill a variety of physiological functions for neuronal activity as for example synaptic functions, blood-brain barrier and reactions after injury. Astrocytes from perinatal rat pups were investigated regarding morphology and migration distance on PCL and CPCL25 fibres. Figures 9a-c show fluorescence images of the astrocytes on (a) PCL, (b) CPCL25 fibres and (c) on PDL coated substrates without fibres. Cell cultures were not pure as DAPI also stained cell nuclei of cells that did not express glial acidic fibrillary protein (GAFP). These images showed that astrocytes preferred to grow on CPCL25 fibres. This was confirmed by the agarose drop assay

to investigate the migration of the cells. From figure 9d it can be seen that astrocytes had migrated nearly twice as far on CPCL25 fibres ( $307.7 \pm 43.9 \mu\text{m}$ ) than on PCL fibres ( $132.2 \pm 23.1 \mu\text{m}$ ) after 2 DIV.

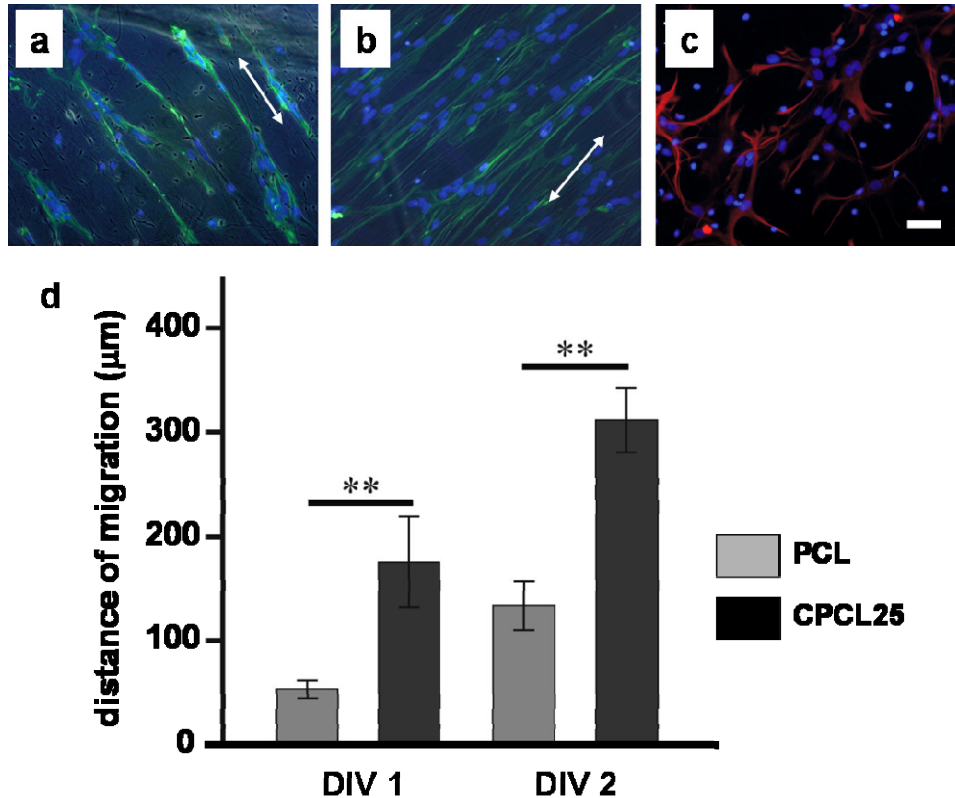


**Figure 9: Astrocytes in primary culture.** (a-c) GFAP (green in a, b and red in c) and DAPI (blue) staining of cells cultured on (a) PCL, (b) CPCL25 and (c) PDL; (d) migration distance of the 10 % farthest cells from the agarose drop after 1 and 2 DIV. Double arrows in (a, b) indicate fibre direction. Scale bar = 50  $\mu\text{m}$ . (Error bars = standard error of the mean,  $n = 15$  pictures from 4 independent experiment,  $**P < 0.01$ )

### 5.3.7 Effect of PCL and CPCL25 fibres on astrocytoma cell line U373 cells

Cells from the human cell line U373 were used to compare the differences between cells from animal and human. As done before, the influence of PCL and CPCL25 fibres on morphology, process lengths and migration was investigated. The results are summarised in figure 10. Figures 10a and b show fluorescence images of triple stained U373 cells confirming glial purity of the cell culture on (a) PCL and (b) CPCL25 fibres. Cells elongated along the fibres and long processes are formed. Due to the high proliferation rate (see fig. 2), process lengths were estimated after 1 DIV to avoid overlapping of cells and processes. Data are presented in figure 10c. Processes were around 142  $\mu\text{m}$  for both fibre materials. The

migration distance of U373 cells from the agarose drop was also the same for PCL and CPCL25 fibres. The 10 % farthest cells had migrated about 850  $\mu\text{m}$  (fig. 10d).

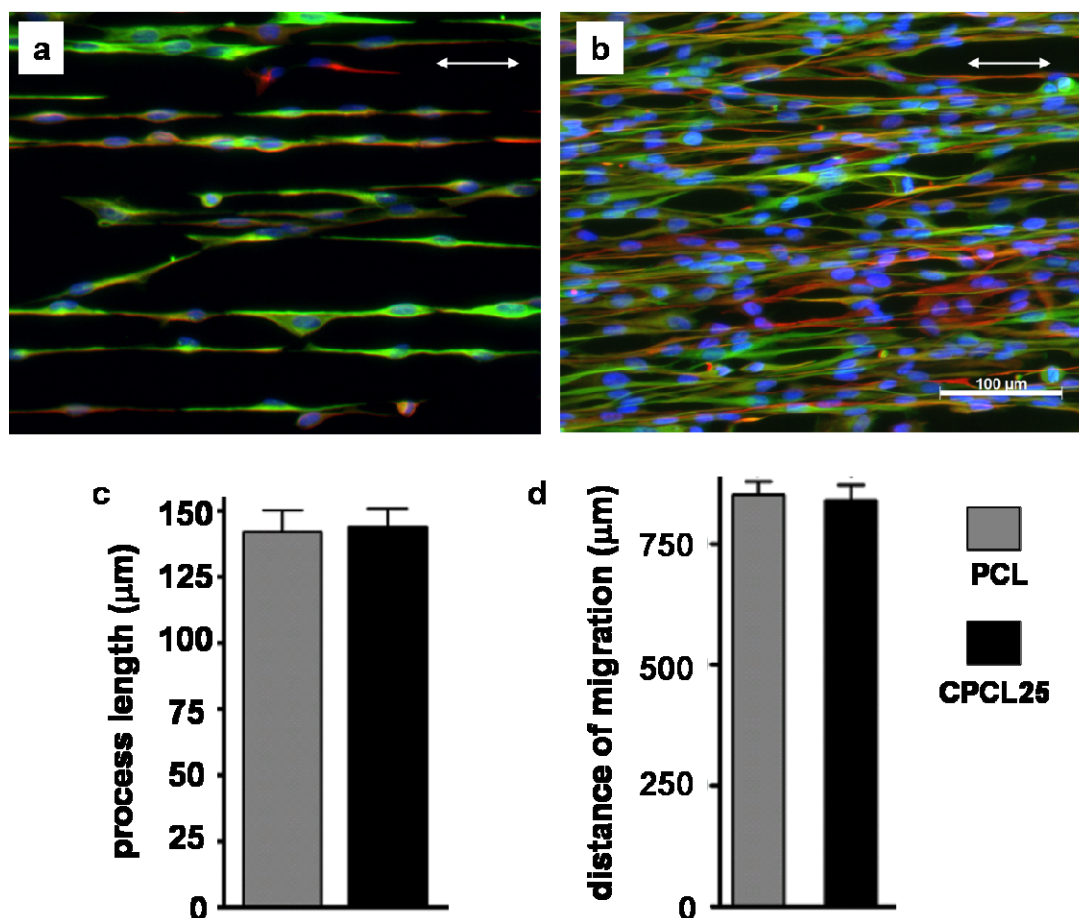


**Figure 10: U373 astrocytoma cells in culture.** (a, b) GFAP (green), vimentin (red) and DAPI (blue) staining of cells cultured on (a) PCL after 4 DIV and (b) CPCL25 after 7 DIV; (c) process lengths after 1 DIV; (d) migration distance of the 10 % farthest cells after 2 DIV. Double arrows in (a, b) indicate fibre direction. Scale bar = 100  $\mu\text{m}$ . (Error bars = standard error of the mean,  $n = 9$  astrospheres) Data reproduced from reference<sup>23</sup> with permission of Future Medicine Ltd.

## 5.5 Discussion

The development of an artificial nerve graft is of particular interest in multidisciplinary research. Injuries of the peripheral nerve or the CNS white-matter tracts are apparently followed by loss of motoric and sensory function and axonal degeneration, myelin sheath degradation, inflammatory and scar building reactions on the cellular level<sup>1, 5, 27, 28</sup>. Artificial implants must help to overcome these limitations and support re-myelination of axons and neurite growth in both the PNS and the CNS. In the CNS the implant should bridge

the lesion sites ignoring the glia scar. Therefore potential implants should take into account mechanical and functional properties of the possible application.

It is well known, that size, orientation and topography of an implanted substrate influence cell adhesion, proliferation, shape, growth and function<sup>29,30</sup>. Oriented nanofibres fulfil important criteria for neurite guidance and aligned axon growth: (1) Their diameters are in the same magnitude as naturally nerve fibres and it was already shown that the fibre diameter influences neurite outgrowth<sup>31-33</sup>. (2) Due to their small size, they have a high surface to volume ratio and offer therefore multiple adhesion points for interactions with cells. And (3) nanofibre orientation was reported to play a significant role in cellular response and aligned fibres were highly efficient for axonal alignment and growth which were much better on aligned fibres than on random fibres<sup>19,34,35</sup>. The electrospun highly aligned nanofibres used in our study fulfil these properties and were tested for their potential as guidance structure for the development of an artificial nerve graft. As materials pure PCL and a blend consisting of 25 % collagen and 75 % PCL (CPCL25) were chosen. PCL is a degradable, biocompatible synthetic polymer which was already used in several *in vitro* studies<sup>36,37</sup>. Collagen is in contrast a natural polymer occurring in the extracellular matrix and activates integrin receptors at the surface of axons and glia<sup>38,39</sup>. Fibres from both materials demonstrated their biocompatibility in our cell experiments and can serve as appropriate substrates for cell adhesion and proliferation (figs. 1 and 2).

### **5.5.1 Influence of nanofibres on morphology and migration of PNS cells**

The influence of PCL and CPCL25 fibres on cells derived from the PNS, neurons, Schwann cells and fibroblasts was evaluated in this study. The collagen in the nanofibres clearly affected morphology and migration of these cells compared with pure PCL fibres. Schwann cells (SC) migrating out from DRG explants elongated according to the fibre orientation (fig. 4b). Their migration was about twofold faster in the investigated time on CPCL25 fibres in comparison with PCL fibres (fig. 4c) and was much further than SC migration from single primary cultures (fig. 5d).

Neurites outgrowing from DRG explants grew significantly more in parallel with CPCL25 fibres (fig. 3c), but neurites were shorter on CPCL25 fibres. The longer neurites on pure PCL fibres appear to be a variance with results from SC migration but it is possible that neurite outgrowth on CPCL25 fibres was influenced, possibly retarded, by glia cell migration. Additionally, axons on PCL had fasciculate stronger which may have enhanced their

elongation rate and indicates that the mutual adhesion between neurites was stronger than between neurites and nanofibres.

On CPCL25 fibres neurites, Schwann cells and fibres were in close contact to each other and cell migration and neurite lengths were in the same range. The neurites grew on top of the Schwann cells but were also guided by the underlying fibres which indicate an indirect communication of guidance signals from the fibres via glial cells to neurites. Oriented SCs were already shown to guide axons from motor neurons<sup>40, 41</sup> while SCs preferentially migrate on axons<sup>42</sup> and express myelin associated glycoproteins (MAG) in the presence of axons<sup>43</sup>. Thus there seems to be mutual interactions between Schwann cells and neurites. On PCL fibres neurites elongation was faster than SC migration and neurites were guided by the fibres alone. Since there is no indication for specific interactions between PCL and axon guidance, the topology of the nanofibres must have a great effect. The electrospun fibres have diameters in the range of axons and might enhance SC migration and consequently might induce neurite response in *in vivo* regeneration. In cell-free implants SC migration from the host into the implant is of crucial importance since SCs provide neuropathic and chemopathic factors to attract macrophages and support neuronal survival<sup>44</sup>.

The easier migration of SCs on CPCL25 fibres suggests biochemical interactions between collagen at the fibre surface and cells. Such interaction is known to be mediated by the ECM glycoprotein fibronectin, which binds to integrin receptors on cell membranes and collagen I<sup>45</sup>. Integrins consist of two subunits,  $\alpha$  and  $\beta$ , and the  $\alpha$ -subunit is responsible for specific ligand binding. The integrin mediated cell adhesion results in building of focal adhesion points which also enabled cell migration.

Fibroblasts synthesise ECM molecules, such as collagen and fibronectin and in an ideal nerve graft, the biomaterial degrades by time and is replaced by ECM from the host. The strong effect of CPCL25 fibres on fibroblast morphology (fig. 6) may be a result of fibronectin secretion. Since the proliferation of human fibroblasts increased by inclusion of collagen in PCL/collagen fibres<sup>17</sup>, the presence of collagen in the electrospun fibres will be advantageous for ECM building in nerve grafts *in vivo*.

Thus, the inclusion of collagen in oriented fibres offers a highly efficient tool for attracting regeneration of cells of the PNS and should serve as a guidance structure in an artificial nerve graft.



### **5.5.2 Influence of nanofibres on morphology of olfactory ensheathing cells**

Olfactory ensheathing cells (OEC) play a specific role in investigations of nerve regeneration in the CNS. Although they belong to the CNS, they behave very similar to Schwann cells and permit axonal regeneration *in vivo*<sup>46,47</sup>. They myelinate axons and have a functional role in axonal growth, regeneration and guidance<sup>46</sup>. On CPCL25 fibres the cells showed an elongated shape and extended significantly longer processes which followed the fibre direction (fig. 7). Friede *et al.* found out that the myelin production is controlled by fibre diameter and when a critical axon diameter is reached, contact activates myelinating cells<sup>48</sup>. The diameters of the electrospun nanofibres are in the range of that of axons and it could be speculated that just the size of the nanofibre may enhance myelin production by contact of myelinating cells with the fibres when used in a nerve graft implant.

### **5.5.3 Influence of nanofibres on morphology and migration of CNS cells**

In contrast to the PNS, nerves cannot regenerate in the CNS spontaneously, mainly due to demyelination of axons, glial scar forming by activated astrocytes and an axon-growth inhibitory environment after CNS injuries.

CNS injuries result in damage of the myelin sheath around the nerve fibres which is formed by oligodendrocytes. Several axonal-growth inhibitors such as Nogo and MAG<sup>49</sup> were found in myelin. These proteins cause growth cone collapse and inhibit neurite outgrowth. Experiments in which the proteins themselves were targeted or the known receptor antagonised resulted in reduced inhibition effect of these proteins and enhanced axonal regeneration<sup>50</sup>. Our experiments showed that oligodendrocytes elongated according to the fibre direction and that especially the collagen containing fibres promoted adhesion and migration of these cells (fig. 8). These effects are important for re-myelinating of regenerating nerve fibres which is essential for functional recovery. Additionally, it was already reported that oligodendrocytes can produce growth factors which have trophic effects on nearby axons in the CNS<sup>51</sup>, supporting the regeneration.

Astrocytes fulfil a great range of functions in the CNS. They are for example responsible for synapse formation and ensheathment<sup>52,53</sup>, axon guidance during development and secretion of growth factors and cytokines<sup>54</sup>. After CNS lesion activated astrocytes form the glial scar and have been reported to have axon-growth promoting properties<sup>55</sup> which can support CNS axon regeneration<sup>55,56</sup>. Both, PCL and collagen were shown to reduce astrocytic activation<sup>57</sup>. In this study the electrospun fibres of PCL and CPCL25 promoted adherence and survival of astrocytes. The alignment of the fibres induced a shape shifting of astrocytes from

a round appearance to a highly oriented morphology and elongation along the fibre directions (fig. 9a, b and 10a-c). U373 cells migrated similar on both materials (fig. 10d) while migration of primary astrocytes was significantly enhanced by the collagen of CPCL25 fibres (fig. 9d). These differences might be explained by the different cell sources (rat vs. human and primary cell culture vs. cell line) showing that results clearly depend on the chosen *in vitro* experiments and conclusions on *in vivo* behaviour of cells must be considered with care. In any case, the collagen containing electrospun fibres offers a great chance for the development of an implant that promotes astrocyte survival, adherence and guidance and creating a suitable environment for regenerating axons. Additionally, suppressing astrocytic activation might result in reduced glial scar formation.

### 5.6 Conclusion

Electrospun fibres of PCL and a PCL/collagen blend with 25 % collagen were tested *in vitro* with a variety of cells from the peripheral and central nervous system. Fibres from both materials provided suitable substrates for cell survival and proliferation. The biological effects were significantly influenced by the presence of collagen. Neurites outgrowing from dorsal root ganglia grew parallel to fibre orientation and a close interaction between neurites, migrating glia and underlying nanofibres were observed. The collagen in the fibres induced great morphology changes by extension of significantly longer processes and longer migration distances of all cell types. Nerve grafts consisting of collagen containing oriented nanofibres may offer a great possibility for influencing nerve regeneration in *in vivo* applications.

### 5.7 References

1. Evans, G. R. D., Peripheral nerve injury: a review and approach to tissue engineered constructs. *The anatomical records* **2001**, 263, 396 - 404.
2. Reichert, H., *Neurobiologie*. 2nd ed.; Georg Thieme Verlag: Stuttgart, 2000.
3. Busch, S. A.; Silver, J., The role of extracellular matrix in CNS regeneration. *Current opinion in neurobiology* **2007**, 1, (17), 120 - 127.
4. Klapka, N.; Müller, H. W., Collagen matrix in spinal cord injury. *Journal of Neurotrauma* **2006**, 23, 422 - 435.
5. Fawcett, J. W.; Asher, R. A., The glial scar and central nervous system repair. *Brain Research Bulletin* **1999**, 49, (6), 377 - 391.

6. Verdu, E.; Labrador, R. O.; Rodriguez, F. J.; Ceballos, D.; Fores, J.; Navarro, X., Alignment of collagen and laminin-containing gels improves nerve regeneration within silicone tubes. *Restorative Neurology and Neuroscience* **2002**, 20, (5), 169 -179.
7. Wang, X.; Hu, W.; Cao, Y.; Yao, J.; Wu, J.; Gu, X., Dog sciatic nerve regeneration across a 30-mm defect bridged by a chitosan/PGA artificial nerve graft. *Brain* **2005**, 128, 1897 - 1910.
8. Chang, C.-J.; Hsu, S.-H.; Lin, F.-T.; Chang, H.; Chang, C.-S., Low-intensity-ultrasound-accelerated nerve regeneration using cell-seeded poly (D,L-lactic acid-co-glycolic acid) conduits: an *in vivo* and *in vitro* study. *Journal of Biomedical Material Research Part B: Applied Biomaterials* **2005**, 75, 99 - 107.
9. Grothe, C.; Meisinger, C.; Claus, P., *In vivo* expression and localization of the fibroblast growth factor system in the intact and lesioned rat peripheral nerve and spinal ganglia. *Journal of Comparative Neurology* **2001**, 434, (3), 342 - 357.
10. Schwab, M. E.; Kapfhammer, J. P.; Bandtlow, C. E., Inhibitors of neurite growth. *Annual Review of Neuroscience* **1993**, 16, 565 - 595.
11. Woolf, C. J.; Bloechlinger, S., It takes more than two to Nogo. *Science* **2002**, 297, (16), 1132 - 1134.
12. Tom, V. J.; Doller, C. M.; Malouf, A. T.; Silver, J., Astrocyte-associated fibronectin is critical for axonal regeneration in adult white matter. *Journal of Neuroscience* **2004**, 24, (42), 9282 - 9290.
13. Barnett, S. C.; Chang, L., Olfactory ensheathing cells and CNS repair: going solo or in need of a friend? *Trends in Neurosciences* **2004**, 27, (1), 54 - 60.
14. Field, P.; Li, Y.; Raisman, G., Ensheathment of the olfactory nerves in the adult rat. *Journal of Neurocytology* **2003**, 32, 317 - 324.
15. Fraher, J. P., The ultrastructure of sheath cells in developing rat vomeronasal nerve. *Journal of Anatomy* **1982**, 134, 149 - 168.
16. Chew, S. Y.; Mi, R.; Hoke, A.; Leong, K. W., The effect of the alignment of electrospun fibrous scaffolds on Schwann cell maturation. *Biomaterials* **2008**, 29, 653 - 661.
17. Venugopal, J.; Zhang, Y.; Ramakrishna, S., *In vitro* culture of human dermal fibroblasts on electrospun polycaprolactone collagen nanofibrous membrane. *Artificial Organs* **2006**, 30, 440 - 445.
18. Zhong, S. P.; Teo, W. E.; Zhu, X.; Beuerman, R. W.; Ramakrishna, S.; Yung, L. Y. L., An aligned nanofibrous collagen scaffold by electrospinning and its effects on *in vitro* fibroblast culture. *Journal of Biomedical Materials Research Part A* **2006**, 79A, (3), 456 - 463.
19. Klinkhammer, K.; Seiler, N.; Grafahrend, D.; Gerardo-Nava, J.; Mey, J.; Brook, G. A.; Möller, M.; Dalton, P. D.; Klee, D., Deposition of electrospun fibers on reactive substrates for *in vitro* investigations. *Tissue Engineering* **2009**, 15, (1), 77 - 85.

20. Schnell, E. Guidance of glial cell migration and axonal growth by electrospun nanofibers of poly- $\epsilon$ -caprolactone and a collagen/poly- $\epsilon$ -caprolactone blend. Diploma Thesis at RWTH Aachen, Aachen, 2006.
21. Schnell, E.; Klinkhammer, K.; Balzer, S.; Brook, G.; Klee, D.; Dalton, P.; Mey, J., Guidance of glial cell migration and axonal growth on electrospun nanofibers of poly- $\epsilon$ -caprolactone and a collagen/poly- $\epsilon$ -caprolactone blend. *Biomaterials* **2007**, 28, (19), 3012 - 3025.
22. Seiler, N. Elektrospun nanofibers as guidance structures for migration of Schwann cells and astrocytes. Diploma Thesis at RWTH Aachen, Aachen, 2007.
23. Gerardo-Nava, J.; Führmann, T.; Klinkhammer, K.; Seiler, N.; Mey, J.; Klee, D.; Möller, M.; Dalton, P. D.; Brook, G. A., Human cell interactions with oriented electrospun nanofibers *in vitro*. *Nanomedicine* **2009**, 4, (1), 11 - 30.
24. Gerardo-Nava, J. Doctoral Thesis at RWTH Aachen, Aachen, in preparation.
25. Mey, J.; Schrage, K.; Wessels, I.; Vollpracht-Crijns, I., Effects of inflammatory cytokines IL-1b, IL-6 and TNF $\alpha$  on the intracellular localization of retinoid receptors in Schwann cells. *Glia* **2007**, 55, 152 - 164.
26. Richter-Landsberg, C.; Heinrich, M., OLN-93: a new permanent oligodendroglia cell line derived from primary rat brain glial cultures. *Journal of Neuroscience Research* **1996**, 45, 161 - 173.
27. Pettigrew, D. B.; Shockley, K. P.; Crutcher, K. A., Disruption of spinal cord white-matter and sciatic nerve geometry inhibits axonal growth *in vitro* in the absence of glial scarring. *BMC Neuroscience* **2001**, 2, 8.
28. Schwab, M. E.; Bartholdi, D., Degeneration and regeneration of axons in the lesioned spinal cord. *Physiological Reviews* **1996**, 76, 319 - 370.
29. Dike, L. E.; Chen, C. S.; Mrksich, M.; Tien, J.; Whiteside, G. M.; Ingber, D. E., Geometric control of switching between growth, apoptosis, and differentiation during angiogenesis using micropatterned substrates. *In vitro Cellular and Developmental Biology-Animal* **1999**, 35, 441 - 448.
30. Singhvi, R.; Kumar, A.; Lopez, G. P.; Stephanopoulos, G. N.; Wang, D. I.; Whiteside, G. M.; Ingber, D. E., Engineering cell shape and function. *Science* **1994**, 264, 696 - 698.
31. Smeal, R. M.; Rabbitt, R.; Biran, R.; Tresco, P. A., Substrate curvature influences the direction of nerve outgrowth. *Annals of Biomedical Engineering* **2005**, 33, (3), 376 - 382.
32. Smeal, R. M.; Tresco, P. A., The influence of substrate curvature on neurite outgrowth is cell type dependent. *Experimental Neurology* **2008**, 213, (2), 281 - 292.
33. Yang, F.; Murugan, R.; Wang, S.; Ramakrishna, S., Electrospinning of nano/micro scale poly(L-lactic acid) aligned fibers and their potential in neural tissue engineering. *Biomaterials* **2005**, 26, 2603 - 2610.

34. Corey, J. M.; Gertz, C. C.; Wang, B.-S.; Birrell, L. K.; Johnson, S. L.; Martin, D. C.; Feldman, E. L., The design of electrospun PLLA nanofiber scaffolds compatible with serum-free growth of primary motor and sensory neurons. *Acta Biomaterialia* **2008**, 4, 863 - 875.
35. Corey, J. M.; Lin, D. Y.; Mycek, K. B.; Chen, Q.; Samuel, S.; Feldman, E. L.; Martin, D. C., Aligned electrospun nanofibers specify the direction of dorsal root ganglia neurite growth. *Journal of Biomedical Materials Research Part A* **2007**, 83A, (3), 636 - 645.
36. Johnson, J.; Nowicki, M. O.; Carol H. Lee, C. H.; Antonio Chiocca, E. A.; Viapiano, M. S.; Lawler, S. E.; Lannutti, J. L., Quantitative analysis of complex glioma cell migration on electrospun polycaprolactone using time-lapse microscopy. *Tissue Engineering, Part C* **2009**, 15, (4), 531 - 540.
37. Quynh P. Pham, Q. P.; Sharma, U.; Mikos, A. G., Electrospun poly( $\epsilon$ -caprolactone) microfiber and multilayer nanofiber/microfiber scaffolds: characterization of scaffolds and measurement of cellular infiltration. *Biomacromolecules* **2006**, 7, 2796 - 2805.
38. Tawil, J. N.; Houde, M.; Blacher, R.; Esch, F.; Reichardt, L. F.; Turner, D. C.; Carbonetto, S.,  $\alpha$ 1 $\beta$ 1 integrin heterodimer functions as a dual laminin/collagen receptor in neural cells. *Biochemistry* **1990**, 29, 6540 - 6544.
39. Turner, D. C.; Flier, L. A.; Carbonetto, S., Identification of a cell-surface protein involved in PC12 cell-substratum adhesion and neurite outgrowth on laminin and collagen. *Journal of Neuroscience* **1989**, 9, (9), 3287 - 3296.
40. Son, Y. J.; Thompson, W. J., Schwann cell processes guide regeneration of peripheral axons. *Neuron* **1995**, 14, 125 - 32.
41. Thompson, D. M.; Buettner, H. M., Neurite outgrowth is directed by Schwann cell alignment in the absence of other guidance cues. *Annals of Biomedical Engineering* **2006**, 34, 161 - 168.
42. Ide, C.; Tohyama, K.; Yokota, R.; Nitatori, T.; Onodera, S., Schwann cell basal lamina and nerve regeneration. *Brain Reseach* **1983**, 288, 61 - 75.
43. Nave, K.-A., *Myelin-specific genes and their mutations in the mouse*. 2 nd ed.; Oxford University Press: Oxford New York, 2001; pp 177 - 196.
44. Qiu, J.; Cai, D.; Filbin, M. T., A role for cAMP in regeneration during development and after injury. *Progress in Brain Research* **2002**, 137, 381 - 387.
45. Geiger, B.; Bershadsky, A.; Pankov, R.; Yamada, K. M., Transmembrane extracellular matrix - cytoskeleton crosstalk. *Nature Reviews Molecular Cell Biology* **2001**, 2, (11), 793 - 805.
46. Bartolomei, J. C.; Greer, C. A., Olfactory ensheathing cells: bridging the gap in spinal cord injury. *Neurosurgery* **2000**, 47, (5), 1057 - 1069.
47. Raisman, G., Olfactory ensheathing cells - another miracle cure for spinal cord injury? *Nature Reviews of Neuroscience* **2001**, 2, (5), 369 - 375.
48. Friede, R. L., Control of myelin formation by axon caliber. (With a model of the control mechanism). *The Journal of Comparative Neurology* **1972**, (144), 233 - 252.

49. Filbin, M. T., Qiu, J., Cai, D., Glial influences on axonal regeneration. In *Glial cell development - basic principles and clinical relevance.*, Jessen, K. R., Richardson, W. D., Ed. Oxford University Press: Oxford, 2001; pp 279 - 298.
50. Kastin, A. J., Targeting neurite growth inhibitors to induce CNS regeneration. *Current Pharmaceutical Design* **2005**, 11, 1247 - 1253.
51. Dai, X.; Lercher, L. D.; Clinton, P. M.; Du, Y.; Livingston, D. L.; Vieira, C.; Yang, L.; Shen, M. M.; Dreyfus, C. F., The trophic role of oligodendrocytes in the basal forebrain. *Journal of Neuroscience* **2003**, 23, 5846 - 5853.
52. Temburni, M. K.; Jacob, M. H., New functions for glia in the brain. *Proceedings of the National Academy of Sciences of the United States of America* **2001**, 98, (1), 3631.
53. Ullian, E. M.; Christopherson, K. S.; Barres, B. A., Role for glia in synaptogenesis. *Glia* **2004**, 47, (3), 209 - 216.
54. Kettenmann, H.; Ransom, B. R., *Neuroglia*. 2nd ed.; Oxford University Press: Oxford, New York, 2005.
55. Liberto, C. M.; Albrecht, P. J.; Herx, L. M.; Yong, V. W.; Levison, S. W., Pro-regenerative properties of cytokine-activated astrocytes. *Journal of Neurochemistry* **2004**, 89, 1092 - 1100.
56. Brook, G. A.; Lawrence, J. M.; Raisman, G., Columns of Schwann cells extruded into the CNS induce in-growth of astrocytes to form organized new glial pathways. *Glia* **2001**, 33, 118 - 130.
57. Wong, D. Y.; Hollister, S. J.; Krebsbach, P. H.; Nosrat, C., Poly( $\epsilon$ -caprolactone) and poly(L-lactic-co-glycolic acid) degradable polymer sponges attenuate astrocyte response and lesion growth in acute traumatic brain injury. *Tissue Engineering* **2007**, 13, (10), 2515 - 2523.

### **SYNTHESIS AND ELECTROSPINNING OF POLY(ETHYLENE OXIDE)-*b*-POLY( $\epsilon$ -CAPROLACTONE) BLOCK COPOLYMERS**

#### **6.1 Introduction**

Tissue engineering has evolved from biomaterials to produce cell/scaffold constructs that permit cellular organisation before scaffold degradation. It combines medical, mechanical, chemical and biological aspects and was defined, as “the recognition of biological tissue through the use of cells with the aid of supporting structures and / or biomolecules” by the European Commission in 2001<sup>1</sup>.

Polyesters from the poly( $\alpha$ -hydroxy) family are often used for tissue engineered scaffolds if bioresorbable and degradable materials are needed. Poly( $\epsilon$ -caprolactone) (PCL) is semi-crystalline and an ideal candidate for long-term applications due to its slow degradation rate. Neither PCL itself nor its degradation products are toxic and its biocompatibility was already proven by several biomedical applications<sup>2,3</sup>.

These applications require control of biomaterial-body interactions. Proteins adsorb on a biomaterial within seconds after contact of the material with body fluids, transforming the inert material surface to a biologically active one with all desired and undesired cellular reactions<sup>4</sup>. For better control of these reactions the masking of the biomaterial with a protein repellent surface is needed. Poly(ethylene oxide) (PEO) used as a thin hydrogel coating has been shown to prevent protein adsorption<sup>5,6</sup>, but also as part of electrospun nanofibres<sup>7</sup>. This polymer is hydrophilic, semi-crystalline and biocompatible. For controlled cell reactions, reactive end groups can be added, e.g. amino groups which allow further reactions with bioactive peptides.

Block copolymers, copolymers consisting of macromolecular blocks of different polymers, offer the opportunity to combine two (or more) polymers and profit from the properties of all partners. Type of polymer, block length, block ratio and structure define a broad range of properties including solubility and degradation rate but required monitored synthesis. Ring-opening polymerisation of cyclic esters such as  $\epsilon$ -caprolactone with alcohols demonstrated good control of molecular weights and high rates of yield. The synthesis of poly(ethylene oxide)-*block*-poly( $\epsilon$ -caprolactone) (PEO-*b*-PCL) copolymers can be performed in solution and from the melt. A PEO block with a certain block length serves as

macroinitiator, activated by a broad range of catalysts. Metallic catalysts as for example stannous II octoate<sup>8,9</sup> and zinc metal<sup>10</sup> as well as non-metallic activation with HCl\*diethyl ether<sup>11, 12, 13</sup>, were used resulting in PEO-*b*-PCL block copolymers with molecular weights from 1500 to 25000 Da. A four-armed PEO-*b*-PCL block copolymer was already synthesised using diethylzinc as catalyst starting from a PCL block as macroinitiator and ring-opening of ethylene oxide<sup>14</sup>. Linear PEO-*b*-PCL block copolymers have been widely applied in tissue engineered experiments as for example as drug-release-systems<sup>15, 16</sup> or as non-woven fibres for cell attachment<sup>7, 17</sup>. These fibres have diameters in the nanometre range and can easily be produced by the method of electrospinning. Here a polymer melt or solution is charged by a high voltage applied to the polymer. During the process a polymer jet is formed which moves towards a grounded target. Bending and stretching of the jet, due to repulsion forces, thins the jet during this way. Cooling or solution evaporation results in a solid fibre collected on the target. The fibre morphology is controlled by a range of parameters including molecular weight of the polymer, the solution concentration, applied voltage and flow rate with which the polymer (solution) is pushed<sup>18, 19</sup>. Depending on these parameters solid fibres, meshes of wet fibres or beads can occur.

Varying the collector setup enables the collection of non-wovens or mats of oriented fibres using a rotating role<sup>2, 20</sup>. Single oriented fibres can be obtained by applying parallel bars, referred to as the gap method of alignment<sup>21, 22</sup>.

In this study, several synthesis methods were used to yield PEO-*b*-PCL block copolymers with controlled block length and block length ratios. In dependency on the block length these polymers were electrospun to oriented fibres with the gap method of alignment. Single oriented fibres offer a great tool for investigating single cell / fibre interactions in tissue engineering. However the production of these fibres requires special demands on polymer material and electrospinning parameters which were investigated here. Polymers and fibres were analysed with a range of methods including nuclear magnetic resonance spectroscopy, gel permeation chromatography and scanning electron microscopy.

## 6.2 Materials and Methods

### 6.2.1 Chemicals

Unless otherwise stated, all chemicals were purchased from Sigma-Aldrich (Germany). Diethyl zinc was used as a 15 wt% solution in toluene. Star-NCO-poly(EO-*stat*-PO) (star-shaped poly ethers with a backbone of 80 % ethylene oxide and 20 % propylene oxide and isocyanate end groups, Mw = 12000 g/mol) (sPEG) was synthesised in our



laboratory from hydroxyl-terminated star polymer (DOW-chemicals, Terneusen, NL) by reaction with isophorone diisocyanate according to literature as described elsewhere<sup>23</sup>. It was stored in the glovebox and only the desired amounts were taken out just before using.

### 6.2.2 Drying procedures

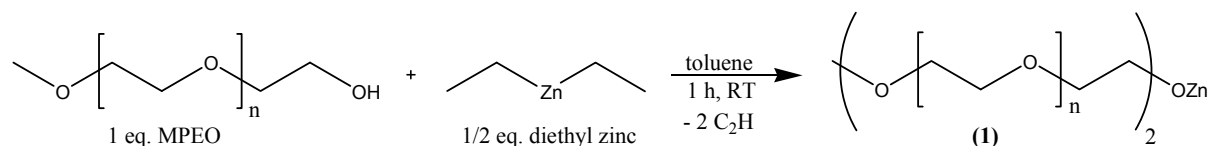
Toluene was dried by distillation over lithium aluminium hydride and stored under nitrogen and over molecular sieve (3Å) until further use. Dichloromethane (DCM) was dried by refluxing over calcium hydride for 5h at 50 °C and distillation under nitrogen afterwards.

$\epsilon$ -caprolactone ( $\epsilon$ -CL) was stirred in a nitrogen atmosphere over calcium hydride over night. For the condensation the distillation flask was heated to 70 °C while high vacuum was applied to the collection flask. The dried  $\epsilon$ -CL was stored under nitrogen at 4 °C until further use.

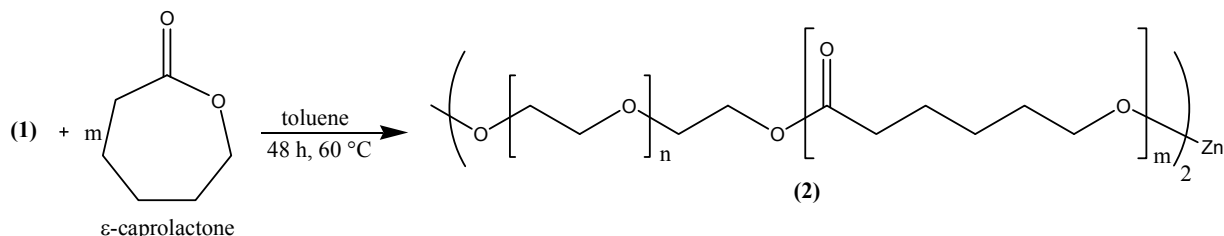
### 6.2.3 Synthesis in toluene with diethyl zinc as catalyst

Poly(ethylene oxide) mono methyl ether (MPEO, Mw = 550 and 5000 g/mol) as macroinitiator (1 eq.) was dried in a 250-mL three-neck-flask in 100 mL toluene using a Dean-Stark apparatus for 4 h at 150 °C in a nitrogen atmosphere and removing of about 40 mL toluene. After cooling-down to room temperature (RT) the Dean-Stark apparatus was replaced by a reflux condenser under nitrogen. Via a septum, ½ eq. diethyl zinc (Mw = 123.50 g/mol) was added and the solution stirred for 1h at RT. Then the solution was heated up to 60 °C and x eq.  $\epsilon$ -CL (Mw = 114.15 g/mol) were added. After 48 h the reaction was aborted by adding 0.2 mL of 0.1 M hydrochloric acid (HCl). The reaction product was concentrated by rotary evaporation, re-dissolved in a small amount of DCM and precipitated in ice-cold diethyl ether. Gel permeation chromatography (GPC) in tetrahydrofuran (THF) was used to estimate molecular weight and polydispersity. The GPC elugram is present in figure 5. The reaction scheme for this synthesis is presented in figure 1.

Initiation:



Propagation:



Termination:

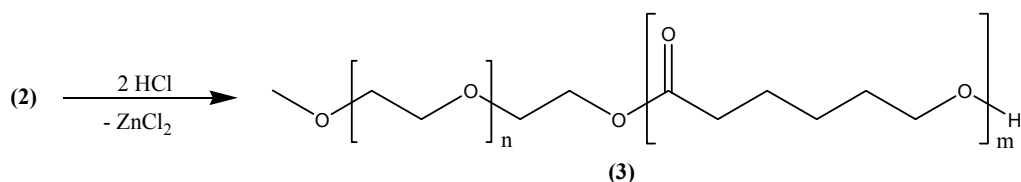


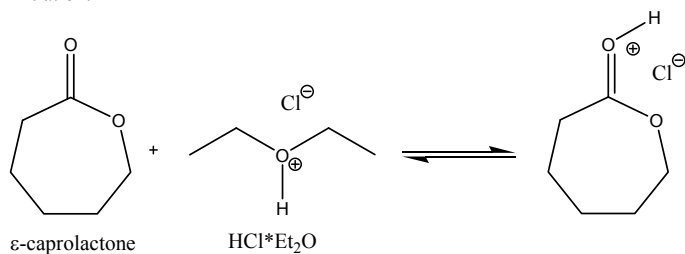
**Figure 1: Reaction scheme of the synthesis of MPEO-*b*-PCL block copolymer (3) with diethyl zinc as catalyst.** MeO-PEO was used as macroinitiator which was activated by diethyl zinc. Reaction with the monomer  $\epsilon$ -caprolactone resulted in the formation of an activated polymer. Termination with HCl resulted in the desired product.

#### 6.2.4 Synthesis in dichloromethane with HCl\*Et<sub>2</sub>O as catalyst

The synthesis with HCl\*Et<sub>2</sub>O as catalyst was performed according to the literature<sup>12, 13</sup>. One eq. alpha-amino-hydroxy poly(ethylene oxide) (Iris Biotech GmbH, Marktredwitz, Germany) (H<sub>2</sub>N-PEO, Mw = 3000 g/mol) was dried in a 250-mL three-neck-flask in 60 mL toluene using a Dean-Stark apparatus for 2h at 140 °C in a nitrogen atmosphere. By emptying the Dean-Stark apparatus several times, the toluene was then completely removed. After cooling-down to RT the Dean-Stark apparatus was replaced by a reflux condenser. Via a septum, 25 mL dry DCM and x eq. of  $\epsilon$ -CL were added. The reaction was started by addition of HCl\*Et<sub>2</sub>O (1 molar, 4 eq.). The solution was stirred under nitrogen while the reaction time was varied from 72 h to 3 weeks. The yellowish solution was precipitate in 300 mL ice-cold hexane, allowed to settle at -70 °C overnight and was then filtered resulting in a white powder. This powder was dissolved in DCM and precipitated again in 250 mL ice-cold diethyl ether. A white powder was filtered off and analysed by

NMR in deuterated chloroform ( $\text{CDCl}_3$ ) and GPC in THF. GPC elugrams are presented in figure 6, a NMR spectrum is shown in figure 4. The reaction scheme is shown in figure 2.

Initiation:



Propagation:

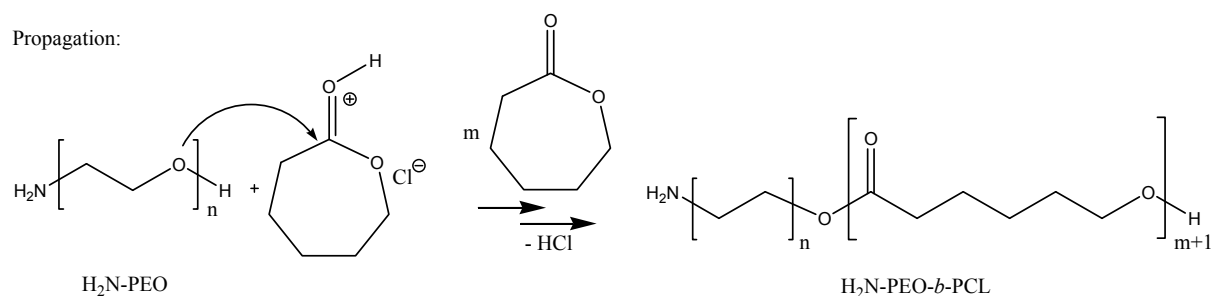


**Figure 2: Synthesis of  $\text{H}_2\text{N-PEO-}b\text{-PCL}$  block copolymer with HCl as catalyst.** Reaction of  $\epsilon$ -caprolactone with  $\text{HCl} \cdot \text{Et}_2\text{O}$  resulted in an activated monomer. The polymer was formed by reaction with the amino-functionalised poly(ethylene oxide).

### 6.2.5 Synthesis from melt with stannous II octoate as catalyst

The synthesis with stannous II octoate was performed according literature<sup>8</sup>. Poly(ethylene oxide) mono methyl ether (MPEO 10k,  $M_w = 10000$  g/mol; Biotech GmbH, Marktredwitz, Germany or MPEO 5k,  $M_w = 5000$  g/mol) (1 eq.) was filled in a tube and then  $x$  eq. of  $\epsilon$ -CL and two droplets of stannous II octoate ( $\text{Sn}(\text{Oct})_2$ ,  $M_w = 405.12$  g/mol) were added. Then the flask was evacuated for 45 min while it was cooled in an ice bath. Afterwards the flask was closed and stirred at  $120^\circ\text{C}$  for 22 h or 44 h. Then the flask was vented and the solid polymer was dissolved in a small amount of DCM. A white powder was received by precipitation in 800 mL ice-cold diethyl ether after filtering (raw product). After drying, the polymer was dissolved again in DCM and precipitated a second time in 500 mL ice-cold methanol. After filtration and drying a white powder was received.  $^1\text{H}$  and  $^{13}\text{C}$  NMR in  $\text{CDCl}_3$  and GPC in THF confirmed the polymerisation. A representative GPC elugram is presented in figure 7. The reaction scheme is presented in figure 3.

$^1\text{H}$  ( $\text{CDCl}_3$ ) NMR:  $\delta = 1.33\text{-}1.43$  (m,  $\text{OCCH}_2\text{CH}_2\text{CH}_2\text{CH}_2\text{CH}_2\text{OH}$ , PCL segment),  $1.60\text{-}1.71$  (m,  $\text{OCCH}_2\text{CH}_2\text{CH}_2\text{CH}_2\text{CH}_2\text{OH}$ , PCL segment),  $2.31$  (t,  $\text{OCCH}_2\text{CH}_2\text{CH}_2\text{CH}_2\text{CH}_2\text{OH}$ , PCL segment),  $3.65$  (s,  $\text{CH}_2\text{O}$ , PEO segment),  $4.06$  (t,  $\text{OCCH}_2\text{CH}_2\text{CH}_2\text{CH}_2\text{CH}_2\text{OH}$ , PCL segment) ppm. (polymer 10)

$^{13}\text{C}$  ( $\text{CDCl}_3$ ) NMR:  $\delta = 24.57$  ( $\text{OCCH}_2\text{CH}_2\text{CH}_2\text{CH}_2\text{CH}_2\text{OH}$ , PCL segment),  $25.53$  ( $\text{OCCH}_2\text{CH}_2\text{CH}_2\text{CH}_2\text{CH}_2\text{OH}$ , PCL segment),  $28.34$  ( $\text{OCCH}_2\text{CH}_2\text{CH}_2\text{CH}_2\text{CH}_2\text{OH}$ , PCL segment),  $34.11$  ( $\text{OCCH}_2\text{CH}_2\text{CH}_2\text{CH}_2\text{CH}_2\text{OH}$ , PCL segment),  $64.13$  ( $\text{OCCH}_2\text{CH}_2\text{CH}_2\text{CH}_2\text{CH}_2\text{OH}$ , PCL segment),  $70.56$  ( $\text{CH}_2\text{O}$ , PEO segment),  $173.51$  ( $\text{OCCH}_2\text{CH}_2\text{CH}_2\text{CH}_2\text{CH}_2\text{OH}$ , PCL segment) ppm. (polymer 10)

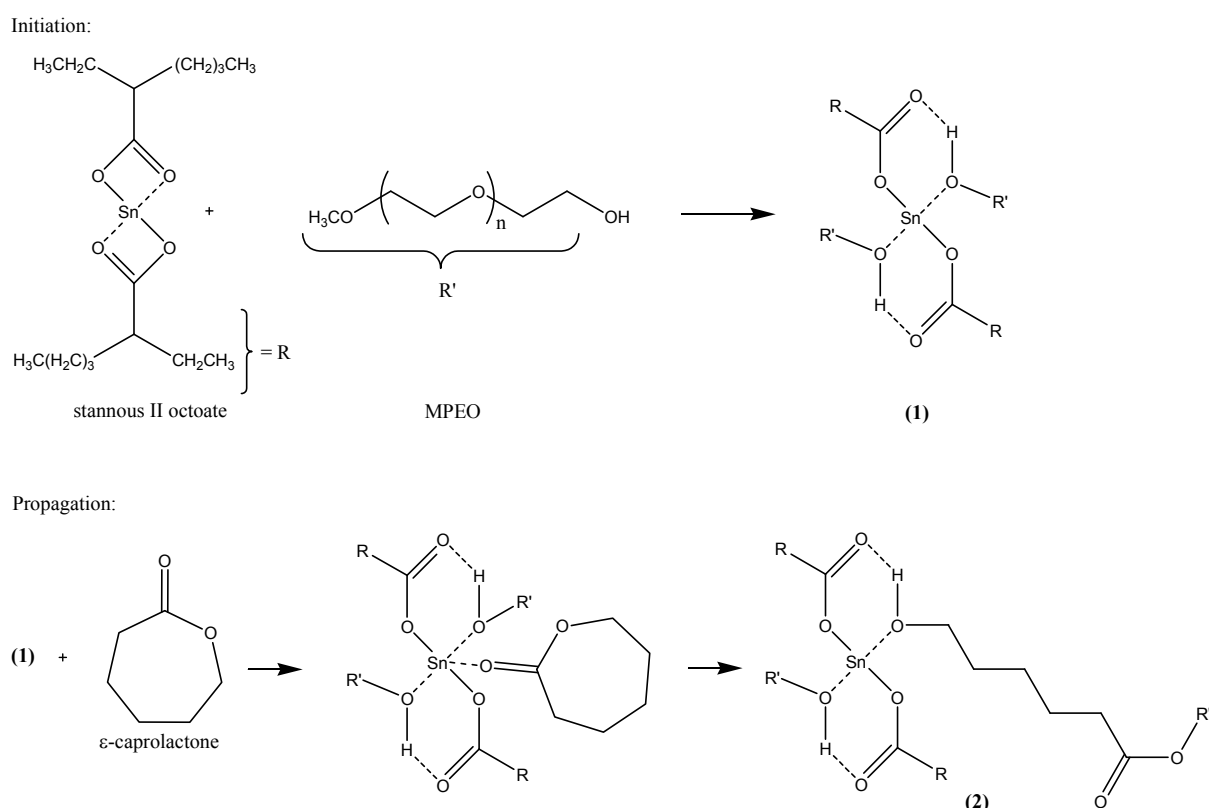


**Figure 3: Synthesis of MPEO-*b*-PCL block copolymer (2) with stannous II octoate as catalyst.** Reaction of the macroinitiator MPEO with the catalyst stannous II octoate resulted in the formation of an initiator complex (1). The polymer was obtained by further reaction with the monomer  $\epsilon$ -caprolactone.

## 6.2.6 Polymer characterisation

### Nuclear magnetic resonance (NMR)

For  $^1\text{H}$ - and  $^{13}\text{C}$  nuclear magnetic resonance spectroscopy, the polymers were dissolved in deuterated chloroform ( $\text{CDCl}_3$ ) (with 0.03 % (v/v) tetramethyl silane (TMS) as

internal standard) at a concentration of 80 mg/mL. The samples were measured in the Institute of Organic Chemistry at RWTH Aachen University with a Varian Mercury 300 ( $^{13}\text{C}$ : 75 MHz,  $^1\text{H}$ : 300 MHz) (Varian, Palo Alto, USA). The chemical shift is given in ppm and refers to TMS as internal standard. The spectra were described using the following abbreviation: s = singlet, d = duplet, t = triplet, q = quartet, m = multiplet. The software MestRec was used to analyse the spectra.

NMR data were used to estimate the molecular weight of the poly( $\epsilon$ -caprolactone) block ( $M_{\text{PCL}}$ ) in the synthesised block copolymers. The following abbreviations and calculations, according described before<sup>24</sup> were used:

- $M_{\text{PEO}}$  : Molecular weight of PEO block
- $M_X$  : Molecular weight of protection group in PEO block
- $M_{\text{EO}}$  : Molecular weight of ethylene oxide
- $n_{\text{CH}_2}\{\text{EO}\}$  : Number of H-atoms of  $\text{CH}_2$ -groups in ethylene oxide
- $I_{\text{PCL:OCH}_2}$  : Integral of all H-atoms of all  $\text{OCH}_2$ -groups of PCL ( $\delta \approx 4.1$ )
- $I_{\text{PEO:CH}_2}$  : Integral of all H-atoms of all  $\text{CH}_2$ -groups of PEO ( $\delta \approx 3.6$ )
- $n_{\text{OCH}_2}\{\epsilon\text{-CL}\}$  : Number of H-atoms of  $\text{OCH}_2$ -groups in  $\epsilon$ -caprolactone
- $M_{\epsilon\text{-CL}}$  : Molecular weight of  $\epsilon$ -CL

$$M_{\text{PCL}} = \frac{M_{\text{PEO}} - M_X}{M_{\text{EO}}} n_{\text{CH}_2}\{\text{EO}\} \frac{I_{\text{PCL:OCH}_2}}{I_{\text{PEO:CH}_2}} \frac{1}{n_{\text{OCH}_2}\{\epsilon\text{-CL}\}} M_{\epsilon\text{-CL}} \quad (\text{equation 1})$$

with  $n_{\text{CH}_2}\{\text{EO}\} = 4$  and  $n_{\text{OCH}_2}\{\epsilon\text{-CL}\} = 2$  and  $M_{\epsilon\text{-CL}} = 114.15$  g/mol and  $M_{\text{EO}} = 44.13$  g/mol follows:

$$M_{\text{PCL}} = 2(M_{\text{PEO}} - M_X) \frac{I_{\text{PCL:OCH}_2}}{I_{\text{PEO:CH}_2}} \frac{114.15}{44.13} \quad (\text{equation 2})$$

### *Gel permeation chromatography (GPC)*

The polymers were dissolved in THF (HPLC grade, destabilised, Carl Roth, Karlsruhe, Germany) with 0.25g/L 2,6-di-*tert*-butyl-4-methylphenol (BHT) at a concentration of 3-4 mg/mL. The samples were analysed at room temperature using a high-pressure liquid chromatography pump (HPLC pump, model 6420, ERC GmbH, Riemerling, Germany) and a refractive index detector (RI-230 I plus, Jasco GmbH Germany, Groß-Umstadt, Germany) at

a flow rate of 1.0 mL/min. One column with a length of 5 cm, a diameter of 8 mm and a nominal pore width of 50 Å was used as pre-column. Then four columns each with a length of 30 cm, and a diameter of 8 mm followed. They have nominal pore widths of 50, 100, 1000, and 10000 Å. All columns were loaded with MZ SDplus gel with a gel particles size of 5 µm. Conventional calibration was achieved using poly(methyl methacrylate) (PMMA) standards. The number-average molecular weight  $M_n$ , the weight-average molecular weight  $M_w$  and the polydispersity  $PDI=M_w/M_n$  were calculated by the program PSS WinGPC Unity. As PMMA was used as standard, the given molecular weights cannot be seen as absolute values and were not included.

### *Differential scanning calorimetry (DSC)*

Small polymer samples (7-8 mg) were analysed using a differential scanning calorimeter (DSC 7, Perkin Elmer with Thermal Analysis Controller TAC 7/DX, Perkin Elmer, Waltham, Massachusetts, USA) with the following temperature program: 0 °C (1 min); heating from 0 °C to 90 °C (10°C/min); 90 °C (1 min), cooling from 90 °C to -10 °C (10 °C/min); -10 °C (1 min); heating from -10 °C to 100 °C (10 °C/min).

### **6.2.7 Electrospinning of fibres**

For electrospinning, solutions of 10-40 wt% of the different block copolymers in chloroform/methanol (75/25 v/v) were prepared. The solution was filled in a 1 mL syringe with a stainless steel 20 gauge flat tipped needle (Hamilton, Bonaduz, Switzerland). Flow rates from 0.05 to 2.0 mL/h, voltages from 15 to 25 kV and distance between spinneret and target of 13 to 20 cm were used. Fibres from pure PCL were prepared by electrospinning a 9 wt% solution at 0.5 mL/h, 20 kV and 20 cm. These fibres served as reference. Random fibres were collected on single targets while parallel fibres were collected suspended between dual collectors with a gap of 2 or 4 cm. These strategies typify the two main collection strategies for electrospun fibres in the literature. A scheme of both electrospinning systems is shown in figure 1 in chapter 3. Depending on further experiments, fibres were deposited onto different substrates.

### **6.2.8 Fibre characterisation**

#### *Scanning electron microscopy (SEM)*

The electrospun fibres were visualised by scanning electron microscopy (SEM) (S360 Zeiss NTS, Germany and Hitachi S3000 N), using 15 kV and working distances of 5 to

15 mm after sputtering with gold for 90 s (S150B, Edwards, Crawley, Great Britain). The SEM images were used to measure fibre diameters which are presented as the mean with standard deviation.

### *Sample preparation for protein adsorption*

Silicon wafers were first cleaned in methanol with ultra sonic for four min and then dried with nitrogen. They were incubated in a solution of methanol with 2 % (v/v) 3-aminopropyl triethoxy silane for 2 min. The wafers were washed by placing them three times in distilled water for 2 min each. After drying in a nitrogen stream the wafers were kept at 4 °C before used on the following day. SPEG was dissolved in THF (100 mg/mL) and then distilled water was added (water/THF = 9:1) to end in a final concentration of 10 mg/mL. After crosslinking of the final solution for 5 min, the wafers were placed on the spin-coater and coated with the filtered solution (0.2 µm, Whatman). The wafers were accelerated within 5 s to 4000 rpm for 40 s. These coated silicon wafers were covered with electrospun fibres either by spinning directly onto the wafers for random fibres or by pushing the wafers through the suspended oriented fibres for oriented collection.

### *Protein adsorption*

Protein adsorption of the fibres was determined with fluorescently labeled bovine serum albumin (BSA) as previously described<sup>25</sup>. Briefly, the prepared substrates were incubated with rhodamine red labeled bovine serum albumin (BSA) diluted in phosphate buffer saline buffer (PBS) (50 µg/mL) for 20 min followed by three incubations in PBS for 20 min each. Afterwards the samples were incubated for 60 min in PBS and washed thoroughly with distilled water. The samples were kept in the dark during incubation and washing. The fibres were visualised with fluorescence microscopy (Axioplan 2 imaging, Zeiss, Germany) and images were taken with a constant exposure time of 1 and 20 s. Pure PCL fibres were used as reference.

### *X-ray photoelectron spectroscopy (XPS)*

Small fibre mats (2 x 8 mm) from different polymers were examined by x-ray photoelectron spectroscopy (XPS) (Ultra Axis<sup>TM</sup> spectrometer, Kratos Analytical, Manchester, Great Britain) to investigate the atomic composition at the fibre surfaces. The samples were irradiated with monoenergetic Al K $\alpha$ 1,2 radiation (1486.6 eV) and the spectra were taken at a power of 144 W (12 kV x 12 mA). The elemental concentration is given in

atom%, but it should be considered that this method can detect all elements except hydrogen and helium and that therefore, the determination of the composition does not consider both these elements.

### *Contact angle measurements*

The water-fibre interactions were investigated by measuring contact angles of random fibre samples of the different polymers using a contact angle measuring system (G2 with DSA II software, Krüss GmbH, Hamburg, Germany). Fibres were collected in high densities on SEM stubs covered with aluminium foil. A small droplet of distilled water (5  $\mu$ l) was placed on the sample and 10 images of the droplet were taken automatically. These images were used to calculate two contact angles (from the right and left side of the droplet). Two droplets were measured per fibre samples and three samples were measured per polymer. Pure PCL fibres served as reference.

## 6.3 Results

### 6.3.1 Synthesis of PEO-*b*-PCL block copolymers

Three different initiating systems were used to synthesise poly(ethylene oxide)-*block*-poly( $\epsilon$ -caprolactone) block copolymers (PEO-*b*-PCL) with different block lengths and block ratios. In every synthesis a poly(ethylene oxide) (PEO) block of a certain length was used as macroinitiator, while the PCL block was synthesised by ring-opening polymerisation of  $\epsilon$ -caprolactone. Table 1 summarises all synthesised polymers including their properties. Figure 4 shows exemplary a  $^1\text{H}$  NMR spectrum of polymer 10 (MPEO<sub>230</sub>-*b*-PCL<sub>580</sub>). The represented polymer has a methoxy functionalised PEO block and the protons from this group, indicated as proton 1 in the chemical structure seen in figure 4, have a chemical shift of 3.38 ppm. However, this peak cannot be seen because it is too small compared with the polymer referred peaks. It is the same with protons 3 and 9 which should appear at  $\delta = 4.22$  and 4.88 ppm respectively<sup>12</sup>. Due to this problem the NMR spectra of the different block copolymers look very similar although the PEO blocks had different functional endgroups. The peaks at  $\delta = 4.06$  ppm (t, 2H, CH<sub>2</sub>O, PCL) and at  $\delta = 3.65$  ppm (s, 4H, CH<sub>2</sub>O, PEO) were used to calculate the molecular weight of the synthesised PCL block according equation 2. Table 1 presents these data including polydispersity indices and summarises the reaction conditions.



**Table 1: Overview of synthesised PEO-*b*-PCL block copolymers** via different reaction ways and estimated molecular weights (Mn) and poly dispersity index (PDI).

Reaction No.	Polymer (theoretical) <sup>#, +</sup>	PEO : PCL	MW (PEO)*	Mn (PCL)* ( <sup>1</sup> H NMR)	Mn (PCL)* (theoretical)	PDI <sup>##</sup> (GPC)	Yield [%]	Reaction Solvent	Conditions	
									Catalyst	Time
1	MPEO <sub>10</sub> - <i>b</i> -PCL <sub>610</sub>	0.008	550	n.e.	69000	oligomers	n.e.	toluene	Et <sub>2</sub> Zn	68 h
2	MPEO <sub>110</sub> - <i>b</i> -PCL <sub>570</sub>	0.078	5000	n.e.	65000	oligomers	n.e.	toluene	Et <sub>2</sub> Zn	48 h
3	H <sub>2</sub> N-PEO <sub>70</sub> - <i>b</i> -PCL <sub>590</sub>	0.045	3000	26300	67000	1.49	10	DCM	HCl*Et <sub>2</sub> O	72 h
4	H <sub>2</sub> N-PEO <sub>70</sub> - <i>b</i> -PCL <sub>590</sub>	0.045	3000	40900	67000	1.56	63	DCM	HCl*Et <sub>2</sub> O	1 week
5	H <sub>2</sub> N-PEO <sub>70</sub> - <i>b</i> -PCL <sub>590</sub>	0.045	3000	45300	67000	1.23	50	DCM	HCl*Et <sub>2</sub> O	20 days
6	MPEO <sub>110</sub> - <i>b</i> -PCL <sub>530</sub>	0.083	5000	68500	60000	1.65 (n.e.)	76	-	Sn(Oct) <sub>2</sub>	44 h
7	MPEO <sub>230</sub> - <i>b</i> -PCL <sub>180</sub>	0.5	10000	24000	20000	1.77 (1.98)	44	-	Sn(Oct) <sub>2</sub>	22 h
8	MPEO <sub>230</sub> - <i>b</i> -PCL <sub>350</sub>	0.25	10000	47000	40000	1.77 (2.08)	76	-	Sn(Oct) <sub>2</sub>	22 h
9	MPEO <sub>230</sub> - <i>b</i> -PCL <sub>530</sub>	0.167	10000	66000	60000	1.84 (1.96)	90	-	Sn(Oct) <sub>2</sub>	22 h
10	MPEO <sub>230</sub> - <i>b</i> -PCL <sub>530</sub>	0.167	10000	66000	60000	1.91**	89	-	Sn(Oct) <sub>2</sub>	44 h

<sup>#</sup> MPEO: Mono methyl ether poly(ethylene oxide); H<sub>2</sub>N-PEO:  $\alpha$ -amino-hydroxy poly(ethylene oxide); + subscribed numbers present number of repeating units; \* in g/mol;

<sup>##</sup> values in brackets represent PDI of raw product; n.e.: not estimated; \*\* PDI of purified polymer was not estimated.

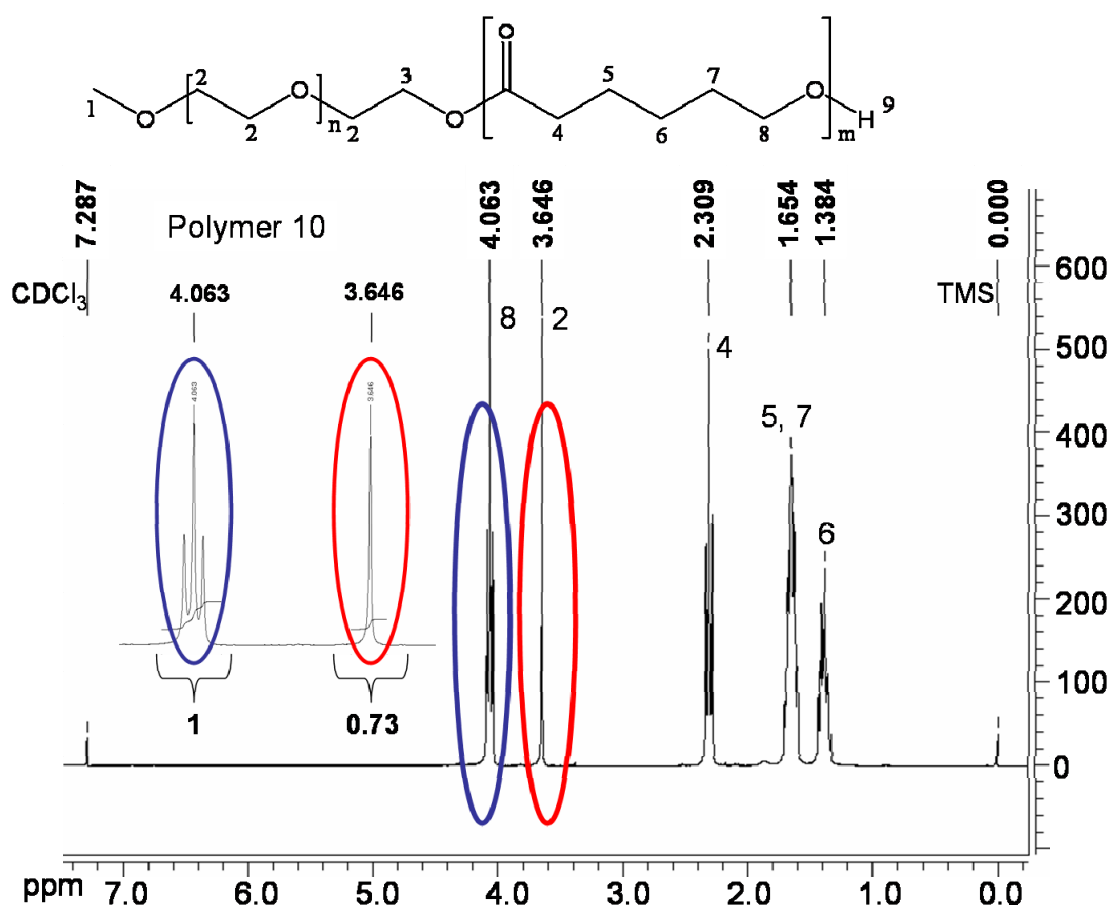


**Figure 4:** <sup>1</sup>H NMR spectrum of polymer 10 (MPEO<sub>230</sub>-b-PCL<sub>580</sub>). The peaks at 4.063 and 3.646 ppm were used for calculation of the molecular weight of the block copolymer.

#### *Synthesis in toluene with diethyl zinc as catalyst*

The first two syntheses of PEO-*b*-PCL block copolymers were performed in toluene with diethyl zinc (Et<sub>2</sub>Zn) as catalyst. Two different block copolymers, MPEO<sub>10</sub>-*b*-PCL<sub>610</sub> (polymer 1), and MPEO<sub>110</sub>-*b*-PCL<sub>570</sub> (polymer 2), should be synthesised. However, GPC analysis of the products showed the formation of oligomers and the desired block copolymers were not obtained in both cases. Figure 5 shows the GPC elugram of polymer 1. The molecular weights of the PCL blocks were not estimated because the values from NMR would only summarise the molecular weights of all oligomers.

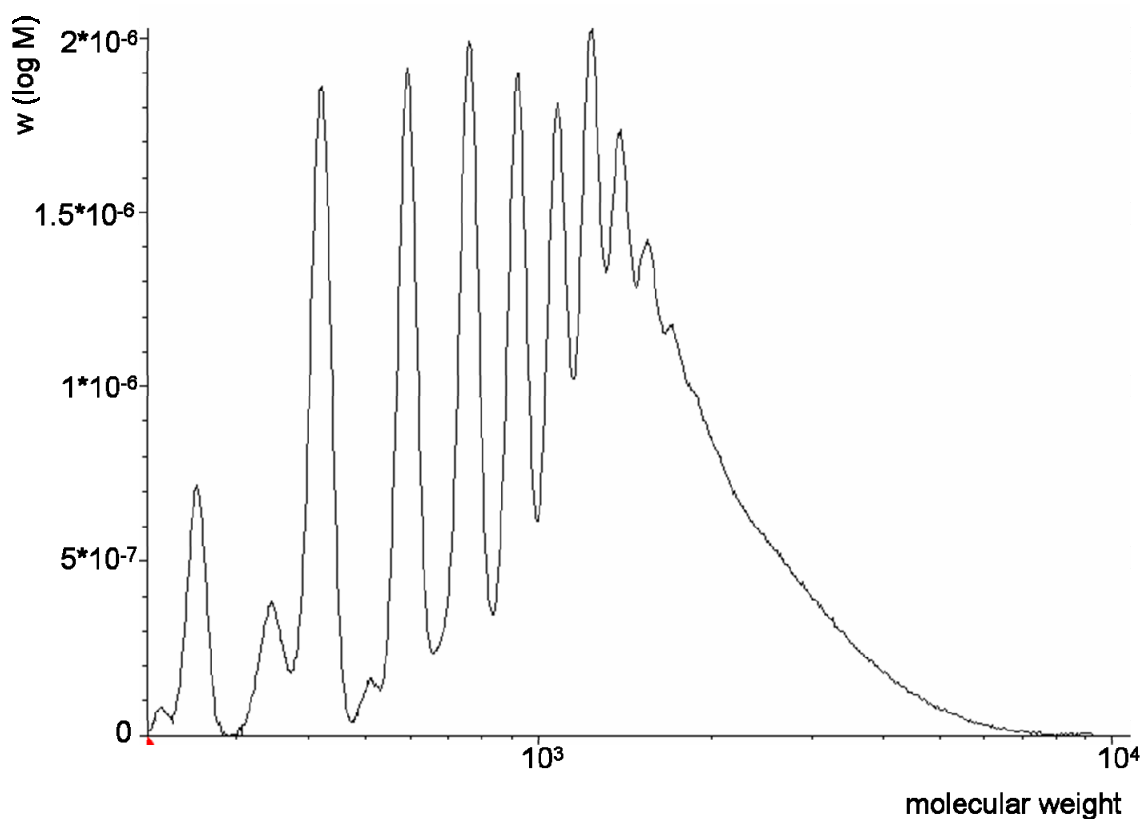


**Figure 5: GPC elugram of polymer 1 (MPEO<sub>10</sub>-*b*-PCL<sub>610</sub>) showing the formation of oligomers.**

*Synthesis in dichloromethane with HCl\*Et<sub>2</sub>O as catalyst*

An aminofunctionalised block copolymer of H<sub>2</sub>N-PEO<sub>70</sub>-*b*-PCL<sub>590</sub> was synthesised with another initiation method. The reaction in toluene with HCl\*diethyl ether (HCl\*Et<sub>2</sub>O) as catalyst was performed three times with increasing reaction times from 3 to 20 days. It turned out that this reaction was very slow: after three days reaction time only 10 % yield were obtained. After one week (polymer 5) the yield was 63 % which was higher than after a reaction time of 20 days (polymer 6) with a yield of 50 %. Additionally, the estimated molecular weight of the PCL block was 40900 g/mol respectively 45300 g/mol (table 1) and therefore much lower than desired. Figure 6 compares GPC spectra of polymer 4 (fig. 6a) and 5 (fig. 6b). The GPC elugram of polymer 4 shows the existence of a polymer with a broad molecular weight distribution. After nearly 3 week reaction time, the polydispersity became smaller as seen in the GPC elugram of polymer 5.

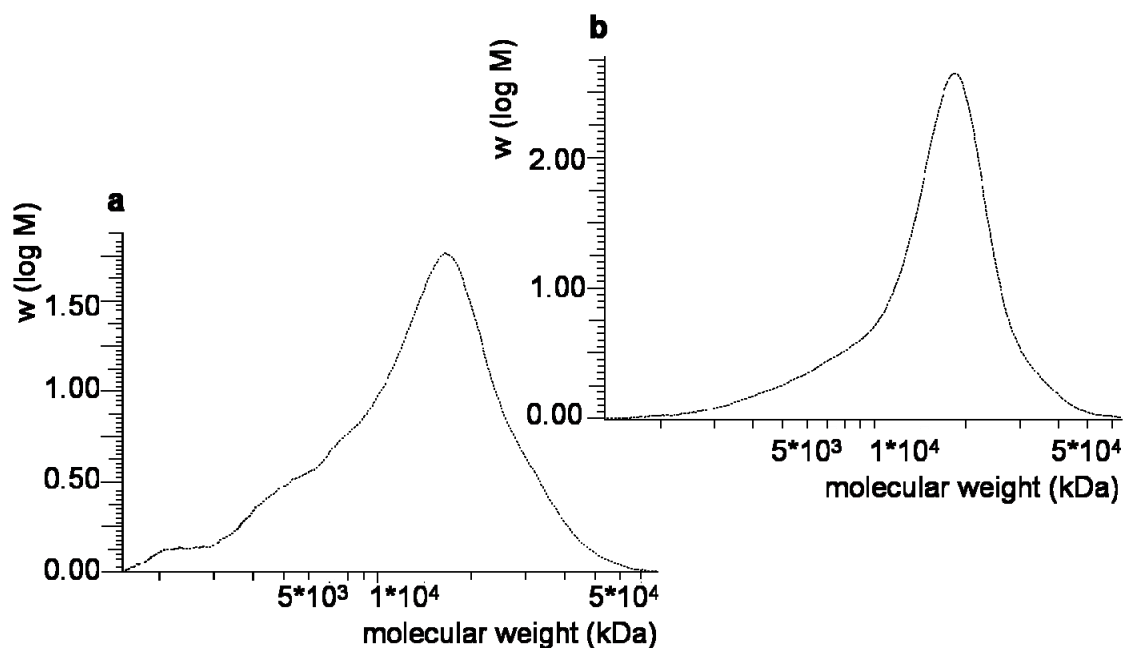


**Figure 6:** Elugram of (a) polymer 4 (MPEO<sub>90</sub>-*b*-PCL<sub>590</sub>, 1 week reaction time) and (b) polymer 5, (MPEO<sub>90</sub>-*b*-PCL<sub>590</sub>, 20 days reaction time). One week reaction time resulted in a polymer with a broad polydispersity. After 20 days of reaction a polymer with a narrow molecular weight distribution was achieved.

#### *Synthesis from melt with stannous II octoate as catalyst*

The third synthesis method was performed in the melt without any solvent using Sn(Oct)<sub>2</sub> as catalyst. Four block copolymers (MPEO<sub>110</sub>-*b*-PCL<sub>600</sub>, MPEO<sub>230</sub>-*b*-PCL<sub>210</sub>, MPEO<sub>230</sub>-*b*-PCL<sub>410</sub>, MPEO<sub>230</sub>-*b*-PCL<sub>580</sub>) were synthesised. The last mentioned block copolymer was synthesised twice with two reaction times of 22 (polymer 9) and 44 h (polymer 10). Table 1 compares the properties of these two polymers and demonstrated no significant influence of the reaction time. NMR (see figure 4) and GPC analysis demonstrated relatively good control of the synthesis. Figure 7 shows the GPC spectrum of polymer 10. The PDI was reduced by purification of the raw product and was between 1.77 and 1.91 for the purified polymers. With all polymers, the synthesised PCL block was about 10 % bigger than desired and yields were between 44 and 90 %.

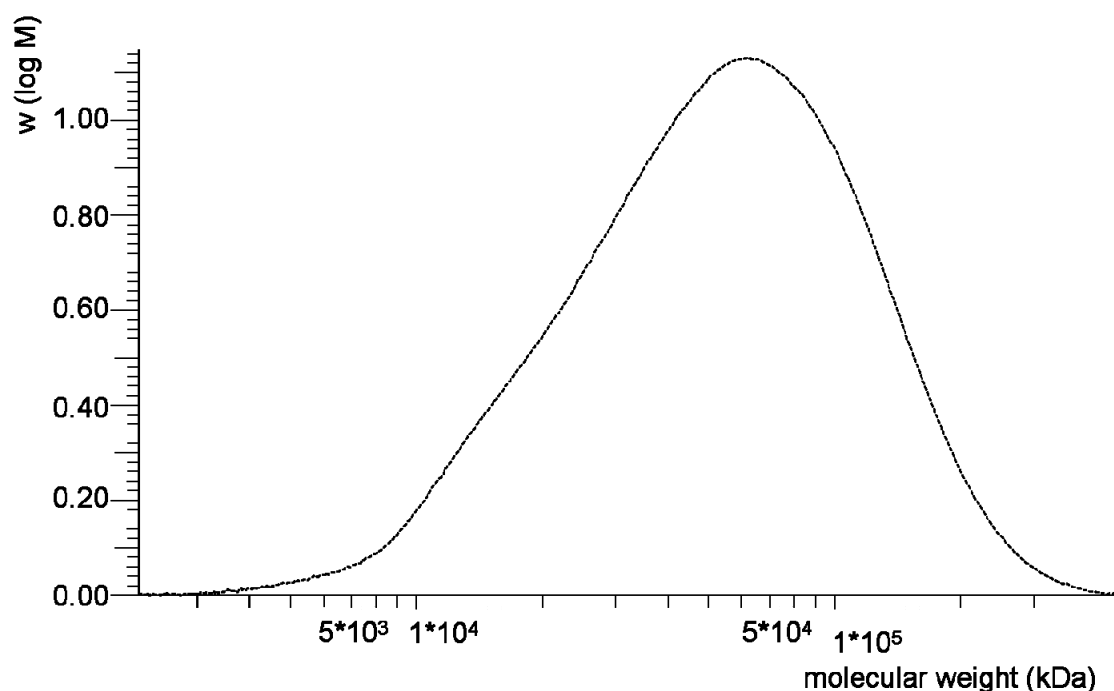


**Figure 7: Elugram of polymer 10.** A polymer with a broad dispersity was achieved.

### 6.3.2 Differential scanning calorimetry (DSC)

DSC was used to determine melting and crystallisation temperatures of the polymers. Figure 8 shows exemplary the DSC spectrum of polymer 9 (fig. 8a) and compares the cooling curves for polymer 6, 7, 8, 9, PCL and MPEO 10k (fig. 8b). Corresponding data are presented in table 2. The spectrum in figure 8a visualises two melting temperatures which correspond with the two heating periods of the measurement and one crystallisation temperature due to one cooling period. All polymers showed two melting points ranging from 59 °C to 68 °C and crystallisation temperatures between 21 °C (PCL) and 47 °C (MPEO 10k). The two copolymers with the highest PEO:PCL ratios (table 1), polymer 7 and 8 demonstrated the appearance of two crystallisation temperatures. Here, the first crystallisation temperature was around 40 °C while the second one was at 34 °C respectively 33 °C (table 2). The other block copolymers showed only one crystallisation temperature. They have a very long PCL block in comparison to the PEO block and overlapping of the peaks of PEO by the PCL peaks seems to occur.

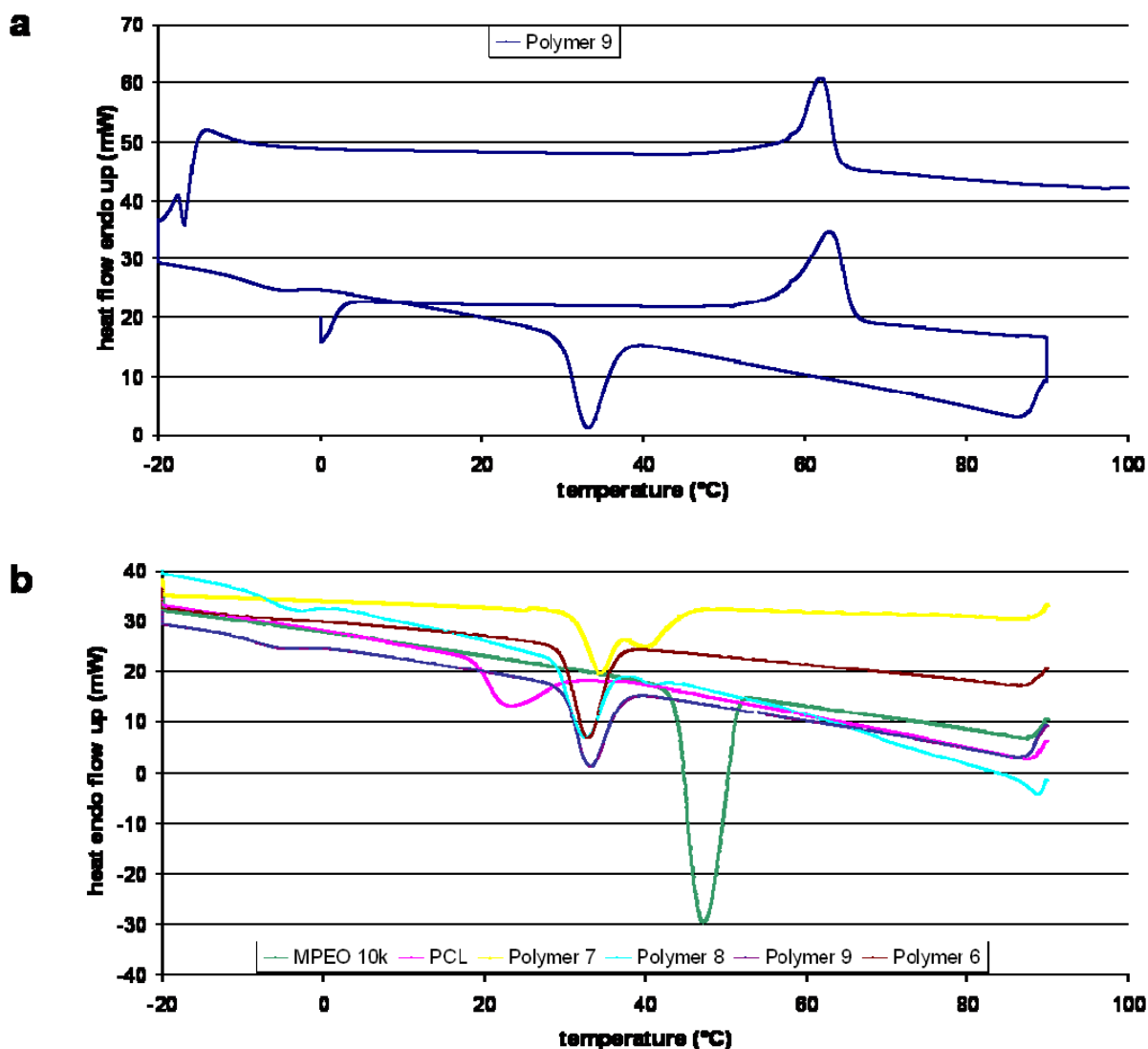


**Figure 8: DSC measurements of block copolymers.** (a) Complete spectrum of polymer 9 with two melting points and one crystallisation point. (b) Cooling curves of MePEO 10k, PCL, polymers 7, 8 and 9. Polymers 7 and 8 have two crystallisation points while the other polymers have only one. The appearance of two crystallisation points indicates that with short PCL blocks both, the PEO and the PCL block took part in the crystallisation process while the with long PCL blocks overlapping of the two peaks occurred.

**Table 2: Data from DSC measurements of the block copolymers** showing melting and crystallisation temperatures.

Reaction No.	Polymer	T <sub>m</sub> (1) (°C)	T <sub>m</sub> (2) (°C)	T <sub>c</sub> (1) (°C)	T <sub>c</sub> (2) (°C)
--	MPEO 5k	66.0	60.9	39.5	--
--	MPEO 10k	68.1	68.3	47.2	--
--	PCL	64.5	58.5	21.1	--
6	PEO <sub>110</sub> - <i>b</i> -PCL <sub>600</sub>	62.7	59.2	32.8	--
7	PEO <sub>230</sub> - <i>b</i> -PCL <sub>210</sub>	65.0	63.4	39.8	34.4
8	PEO <sub>230</sub> - <i>b</i> -PCL <sub>410</sub>	61.5	59.1	40.7	32.6
9	PEO <sub>230</sub> - <i>b</i> -PCL <sub>580</sub>	63.1	61.9	33.1	--

DSC data of polymers 1 to 5 were not measured due to the low quality of the polymers.

### 6.3.3 Electrospinning of PEO-*b*-PCL block copolymers

Electrospinning was used to produce fibres in the submicron range from the different synthesised polymers. The oriented collection of the fibres using the gap method of alignment was focused upon.

#### *Electrospinning of polymer 5*

H<sub>2</sub>N-PEO<sub>70</sub>-*b*-PCL<sub>400</sub> (polymer 5) was synthesised in toluene with HCl\*Et<sub>2</sub>O. Electrospinning was performed from 30 and 40 wt% solutions. These high concentrations were chosen, because fibre collection was not possible with lower concentrations. The products are shown in figure 9. Both solution concentrations resulted in beads with diameters from 1.8 - 4.2 µm (fig. 9a) and 3.6 - 6.9 µm (fig. 9b). The inclusion of 2 wt% high molecular weight PCL (Mw = 65000 g/mol) into a 20 wt% solution of polymer 5 ended in beads with diameters of 2.8 - 5.2 µm (fig. 9c). Fibres were not obtained with this polymer.

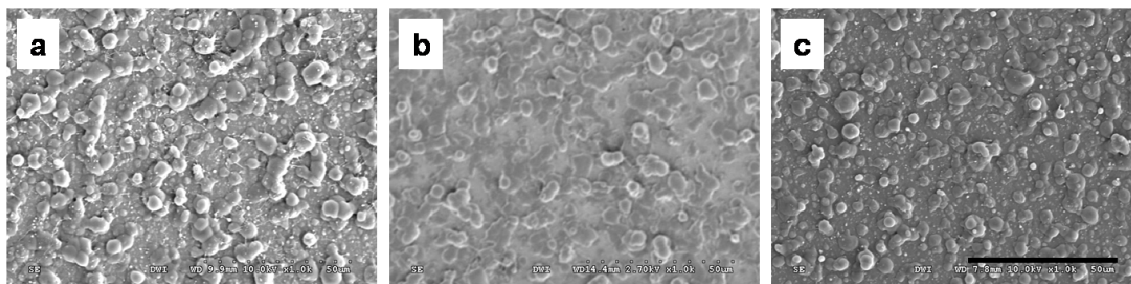


**Figure 9: SEM images of electrospinning products from polymer 5.** Beads were obtained with 20 kV, 20 cm and 0.5 mL/h at solution concentrations of (a) 30 wt%, (b) 40 wt% and (c) 20 wt% with 2 wt% high molecular weight PCL. Scale bar = 50  $\mu\text{m}$ .

### *Electrospinning of polymer 6*

MPEO<sub>110</sub>-*b*-PCL<sub>600</sub> (polymer 6) was synthesised in the melt with Sn(Oct)<sub>2</sub>. Electrospinning was performed from 10, 15 and 17 wt% solutions. Images of random and oriented fibres are shown in figures 10 and 11. Beaded fibres were obtained from random collection (fig. 10a, c). Increasing the concentration from 10 (fig 10a) to 15 (fig. 10c) wt% resulted in fibre diameters increase from  $0.16 \pm 0.05 \mu\text{m}$  to  $0.32 \pm 0.12 \mu\text{m}$ . The collection of oriented fibres from the 10 wt% solution was very difficult. Only one parameter set up with 20 kV, 20 cm and 1.0 mL/h resulted in oriented fibres of bad quality and diameters of  $0.53 \pm 0.21 \mu\text{m}$  (fig. 10b). Fibres electrospun from 15 wt% were much more homogenous and had diameters of  $0.33 \pm 0.10 \mu\text{m}$  (fig. 10d). Here, the flow rate has a significant influence for the production of oriented fibres: oriented fibre collection was only possible with 0.5 mL/h.



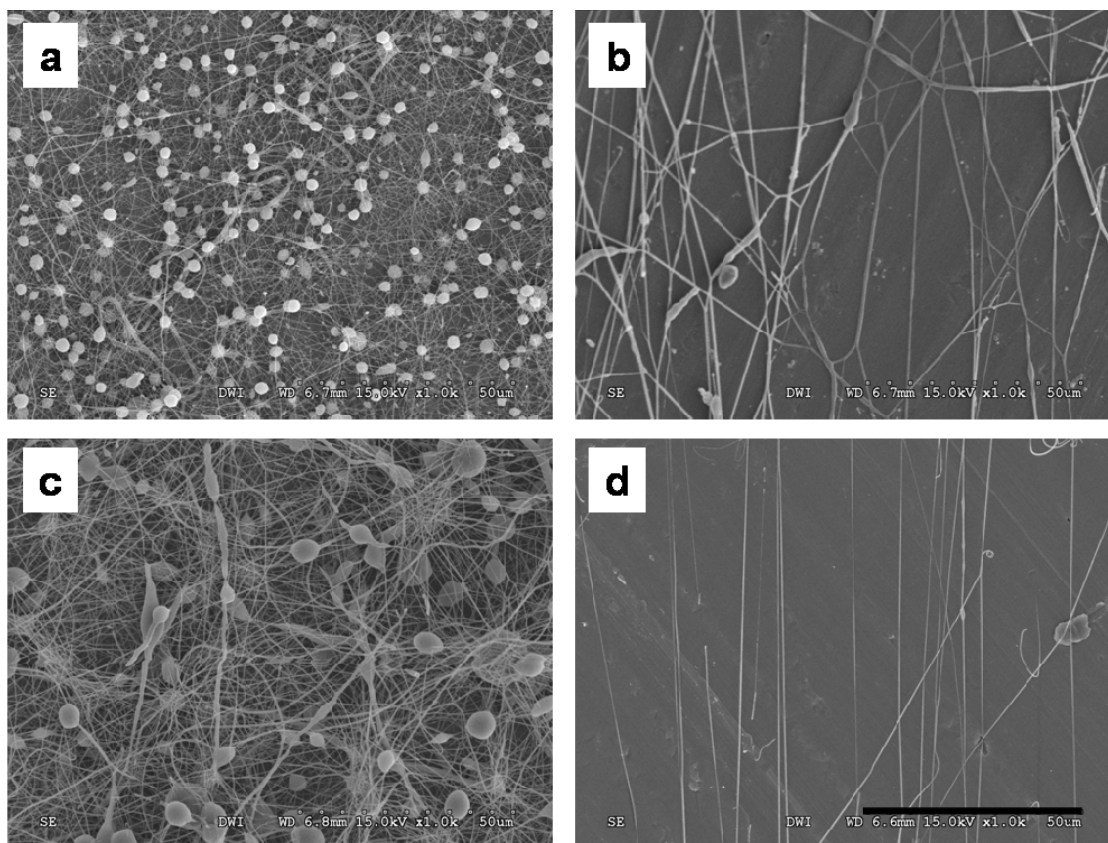


**Figure 10: SEM images of oriented and random fibres electrospun from polymer 6.** Fibres were electrospun with 20 kV, 20 cm and 0.5 mL/h, respectively 1 mL/h for (b), at a solution concentration of (a), (b) 10 wt% and (c), (d) 15 wt%. Although the random fibres have beads, the oriented fibres do not. The quality of the oriented fibres increases with higher solution concentration. Scale bar = 50  $\mu\text{m}$ .

Increasing the solution concentration up to 17 wt% enables the collection of oriented fibres also with other flow rates (0.3 – 2 mL/h) (figure 11). In contrast, the electrical field strength has only a small influence. Similar fibre qualities were received from both 15 and 17 wt% solutions with a distance of 15 cm and a flow rate of 0.5 mL/h independently from the applied voltage (fig. 11) Fibres with diameters around 0.35  $\mu\text{m}$  were obtained in all experiments.

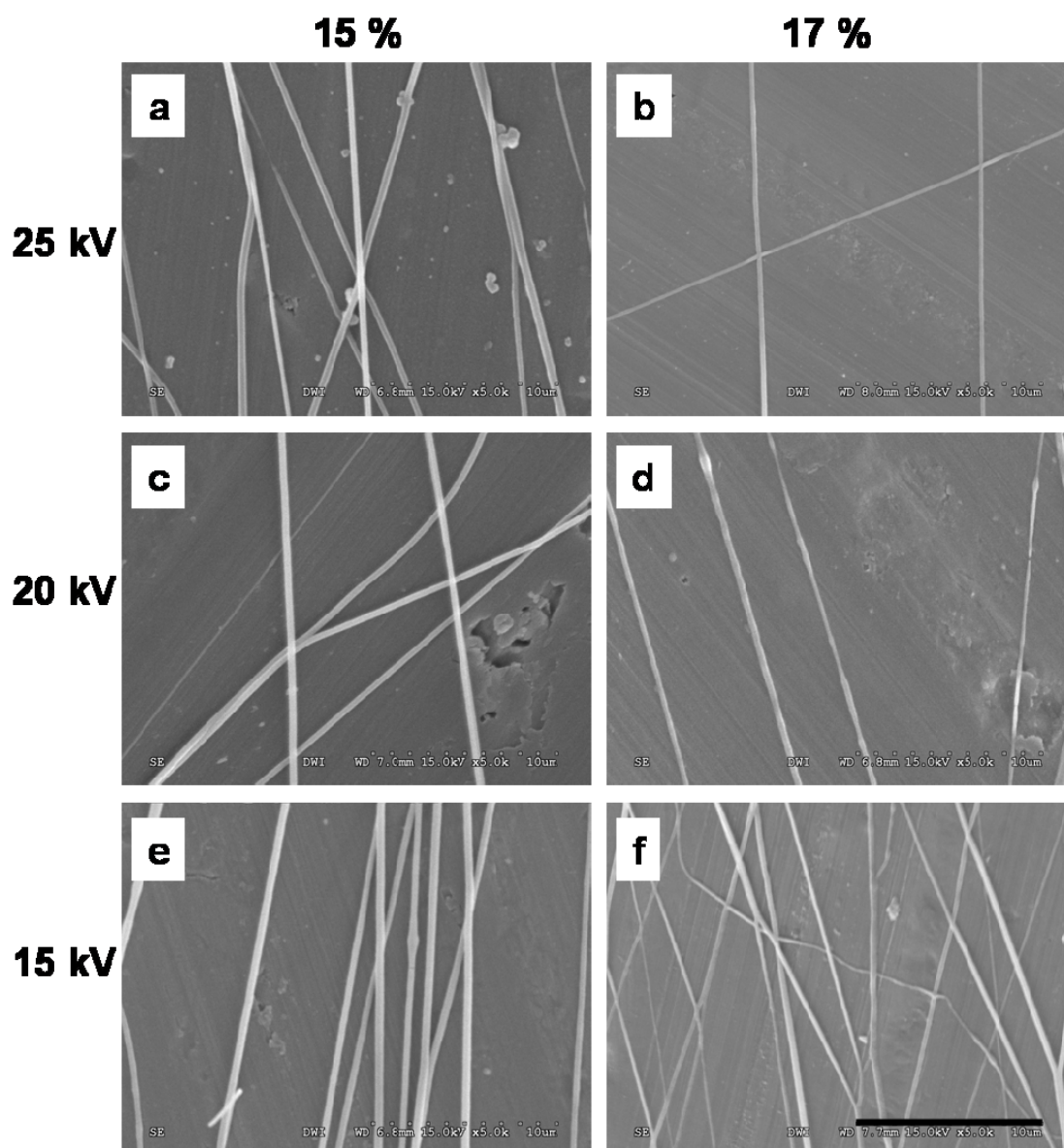


**Figure 11: SEM images of oriented fibres electrospun from polymer 6.** The fibres were electrospun with 15 cm and 0.5 mL/h at two different solution concentrations of (a), (c), (e) 15 wt% and (b), (d), (f) 17 wt% and with three different voltages of (a), (b) 25 kV, (c), (d) 20 kV and (e), (f) 15 kV. Scale bar = 10  $\mu\text{m}$ . All conditions resulted in similar oriented fibres with diameters of around 0.35  $\mu\text{m}$ .

### *Electrospinning of polymer 7*

Polymer 7 (MPEO<sub>230</sub>-*b*-PCL<sub>210</sub>) was electrospun from 15, 20 and 25 wt% solutions. The 15 wt% solution did not result in any electrospinning products. Electrospun fibres from a concentration of 20 wt% are shown in figure 12. Random fibres were collected from 20 kV, 20 cm and 0.8 mL/h (fig. 12a). These fibres were inhomogeneous and had diameters around 0.28  $\mu\text{m}$ . Oriented fibres were collected from 20 cm and 0.4 mL/h and different voltages.

With voltages of 20 kV (fig. 12b) and 25 kV (fig. 12c) networks of fibres occurred. Increasing the voltage up to 30 kV enhanced the parallelism of the fibres (fig. 12d). All fibres had diameters around 0.3  $\mu\text{m}$ .

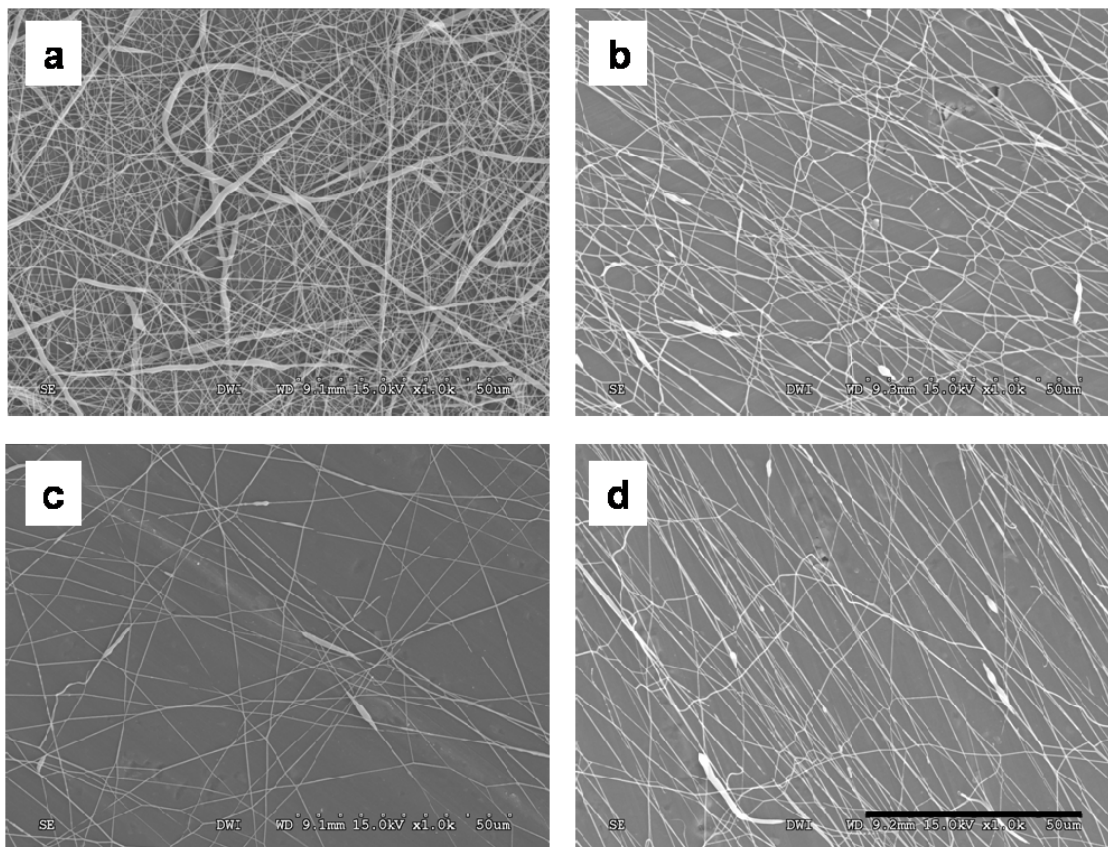


**Figure 12: SEM images of electrospun fibres of polymer 7 electrospun from a 20 wt% solution.** Fibres were obtained from 20 cm, 0.4 mL/h and (a) 20 kV, random, (b) 20 kV, oriented (c) 25 kV, (d) 30 kV. Random fibres showed a kind of slubs along the axis. The quality of the oriented fibres increased slightly with increasing voltages. Scale bar = 50  $\mu\text{m}$ .

Higher solution concentration of 25 wt% resulted in a better orientation of the fibres. Figure 13 compares these fibres electrospun from 20 kV and 15 cm at different flow rates. High flow rates of 0.8 and 0.6 mL/h resulted in molten interconnected fibres which had diameters of  $1.70 \pm 0.59 \mu\text{m}$  and  $3.60 \pm 1.45 \mu\text{m}$  respectively (fig. 13a, b). Only with a low flow rate of 0.4 mL/h high quality oriented fibres with diameters of  $0.50 \pm 0.19 \mu\text{m}$  (fig. 13c) occurred.

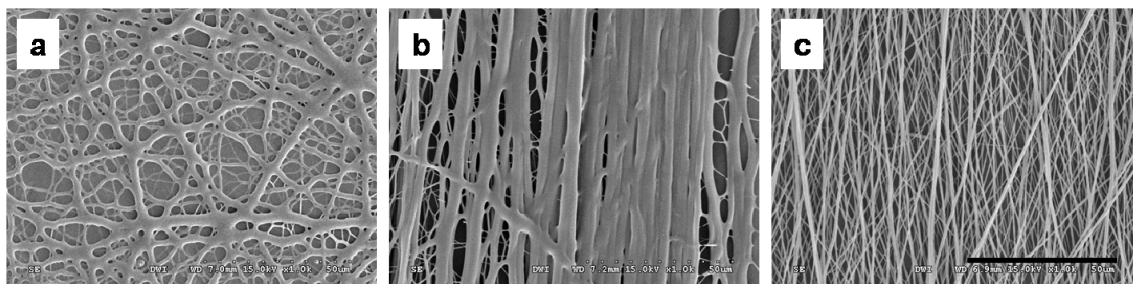


**Figure 13: SEM images of electrospun fibres of polymer 7 electrospun from a 25 wt% solution.** Fibres were obtained from 20 kV, 15 cm and (a) 0.8 mL/h, (b) 0.6 mL/h, (c) 0.4 mL/h. The fibre quality increases with decreasing flow rate. Scale bar = 50 µm.

When electrospun with 15 kV and 15 cm this tendency was partially reversed. Here fibres with relatively good quality were achieved with a flow rate of 0.8 mL/h ( $1.43 \pm 0.52 \mu\text{m}$ ) (fig. 14a). The best fibres with diameters of  $0.76 \pm 0.29 \mu\text{m}$  were obtained from a flow rate of 0.6 mL/h (fig. 14b), while lower flow rates resulted in a network of molten fibres with diameters of  $0.54 \pm 0.18 \mu\text{m}$  (fig. 14c).

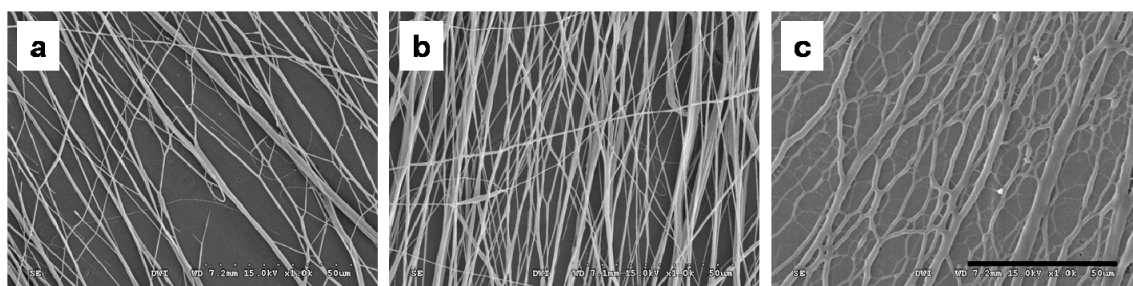


**Figure 14: SEM images of electrospun fibres of polymer 7 electrospun from a 25 wt% solution.** Fibres were obtained from 15 kV, 15 cm and (a) 0.8 mL/h, (b) 0.6 mL/h, (c) 0.4 mL/h. The fibre quality decreases with decreasing flow rate. Scale bar = 50 µm.

#### *Electrospinning of polymer 8*

Electrospinning of polymer 8 (MPEO<sub>230</sub>-*b*-PCL<sub>410</sub>) was performed with solution concentrations of 15, 17 and 20 wt%. With the 15 wt% solution hardly any fibres were obtained. Electrospinning from the 17 wt% solution resulted in high quality fibres with nearly all tested conditions. Figure 15 compares fibres electrospun with an electrical field strength of 1 kV/cm at 0.3 and 0.5 mL/h. With a flow rate of 0.3 mL/h highly oriented fibres were spun irrespective if 15 kV and 15 cm (fig. 15a) or if 20 kV and 20 cm (fig. 15b) were chosen. Increasing the flow rate to 0.5 mL/h resulted in a network of interconnected oriented fibres for

15 kV, 15 cm (fig. 15c) and in oriented fibres with a “bead on the string”-morphology for 20 kV, 20 cm (fig. 15d). All fibres have small diameters of around 0.28  $\mu\text{m}$ .

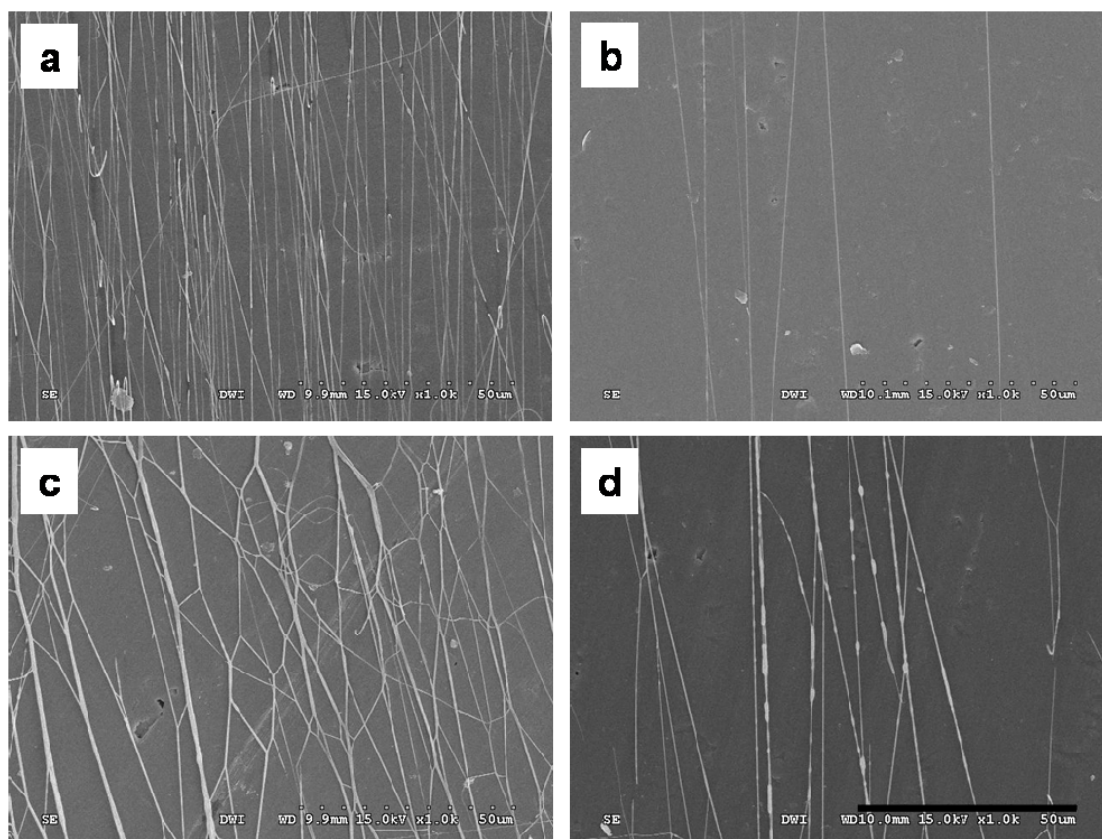


**Figure 15: SEM images of electrospun fibres of polymer 8 electrospun from a 17 wt% solution.** Fibres were obtained with electrical field strength of 1 kV/cm: (a) 15 kV, 15 cm, 0.3 mL/h, (b) 20 kV, 20 cm, 0.3 mL/h, (c) 15 kV, 15 cm, 0.5 mL/h, (d) 20 kV, 20 cm, 0.5 mL/h. The first two conditions resulted in high quality fibres. The third condition resulted in a network of oriented fibres and the fibres electrospun with the fourth condition have a “bead on the string”-morphology. Scale bar = 50  $\mu\text{m}$ .

Electrospinning with a concentration of 20 wt% resulted in very good oriented fibres on the one hand and on the other hand in many molten fibres depending on electrospinning conditions. Figure 16 compares fibres produced with 20 kV and 0.4 mL/h at two different distances between needle and target. A distance of 20 cm resulted in high quality fibres with small diameters of  $0.30 \pm 0.08 \mu\text{m}$  and a narrow diameter distribution (fig. 16a). Decreasing the distance to 15 cm led to a network of molten fibres with diameters of more than 2.7  $\mu\text{m}$  (fig. 16b).

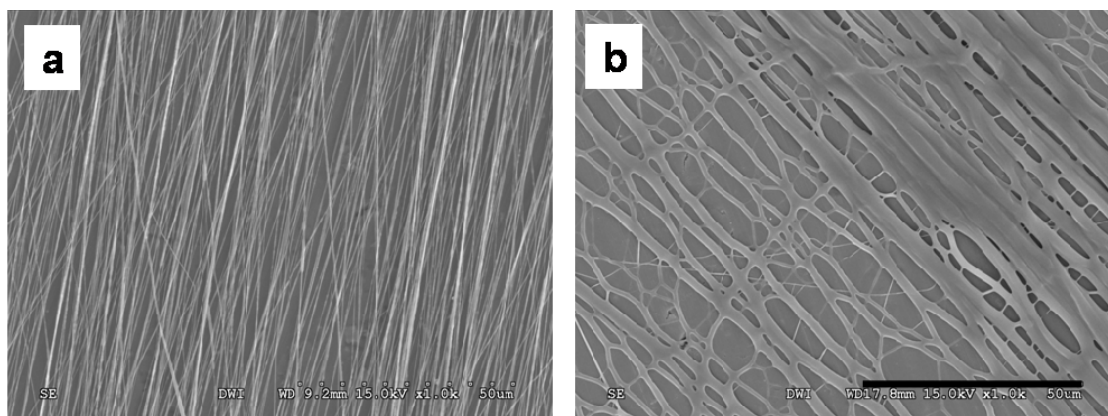


**Figure 16: SEM images of electrospun fibres of polymer 8 electrospun from a 20 wt% solution.** Fibres were obtained with 20 kV, 0.4 mL/h and (a) 20 cm or (b) 15 cm. A big distance between needle and target resulted in high quality oriented fibres, while with the smaller distance a network of molten fibres was obtained. Scale bar = 50  $\mu$ m.

Electrospinning with 15 kV and 20 cm demonstrated a dependency of the fibre quality on the flow rate (figure 17). While a high flow rate of 0.8 mL/h resulted in good quality fibres with diameters of  $0.55 \pm 0.20 \mu\text{m}$  (fig. 17a), molten fibres were observed with lower flow rates (fig. 17b, c).

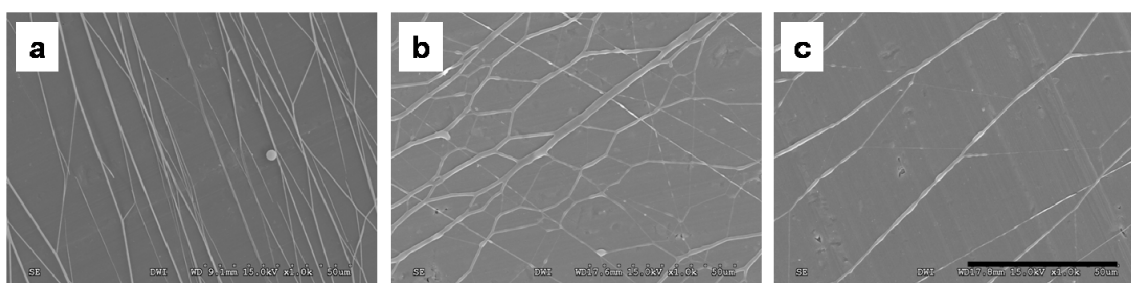


**Figure 17: SEM images of electrospun fibres of polymer 8 electrospun from a 20 wt% solution.** Fibres were obtained from 15 kV, 20 cm and (a) 0.8 mL/h, (b) 0.6 mL/h, (c) 0.4 mL/h. The fibre quality decreases with decreasing flow rate. Scale bar = 50  $\mu$ m.

### *Electrospinning of polymer 9*

Polymer 9 (MPEO<sub>230</sub>-*b*-PCL<sub>580</sub>) was electrospun from 10, 15, 17 and 20 wt% solutions. Electrospinning experiments with the raw product (precipitated only from diethyl ether) were compared with the purified polymer after the second precipitation in methanol. These results are presented in figure 18. Electrospinning from a 10 wt% solution resulted in random fibres with beads (fig. 18a) and an oriented fibre collection was impossible.

Increasing the concentration to 15 wt% resulted in homogeneous random fibres with diameters of  $0.50 \pm 0.23 \mu\text{m}$ , but still not in oriented fibres (fig. 18b). After purifying the polymer, oriented electrospinning was possible from a 15 wt% solution (fig. 18c) and fibres were well oriented and had small diameters of  $0.22 \pm 0.04 \mu\text{m}$ .

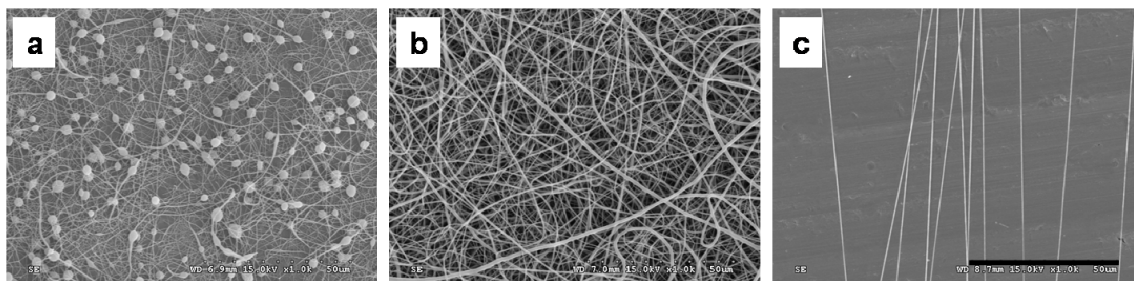


**Figure 18: SEM images of electrospun fibres of polymer 9.** (a) Raw product electrospun from a 10 wt% solution, (b) raw product electrospun from a 15 wt% solution, (c) purified polymer electrospun from a 15 wt% solution. Electrospinning was performed with 20 kV, 20 cm, 0.5 mL/h and resulted in beaded fibres for the 10 wt% solution. With the 15 wt% solution oriented fibres were only obtained after purifying the polymer, otherwise random fibres were got. Scale bar = 50  $\mu\text{m}$ .

With the purified polymer many high quality oriented fibres were obtained with 15, 17 and 20 wt% solutions from several conditions. Figure 19 shows SEM images of these fibres produced with 15 kV and 20 cm at different flow rates. All fibres were very homogeneous and had diameters around  $0.4 \pm 0.1 \mu\text{m}$ . The fibres produced from 17 %wt solutions show the highest parallelism hereby.

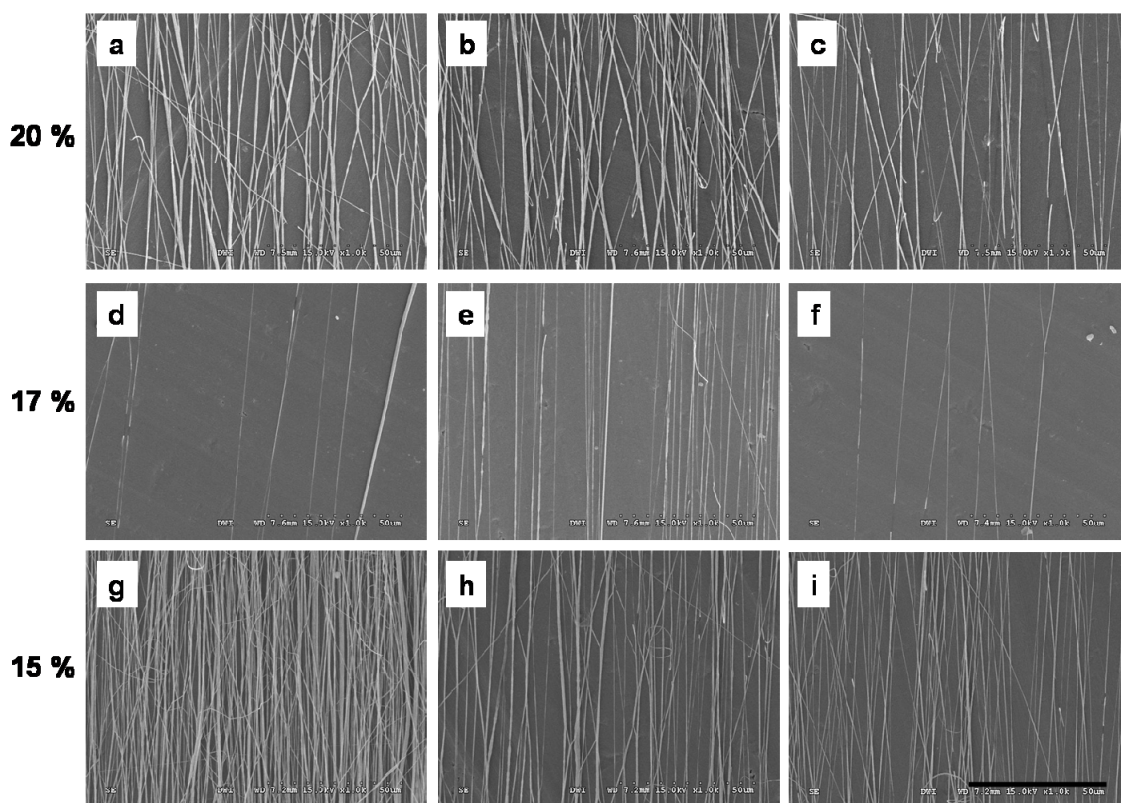


**Figure 19: SEM images of electrospun fibres of polymer 9 electrospun from different concentrations.** Fibres were obtained from 15 kV, 20 cm and (a), (g) 0.8 mL/h, (b), (h) 0.6 mL/h, (c), (i) 0.4 mL/h (d) 1.0 mL/h, (e), 0.5 mL/h, (f) 0.3 mL/h. The fibre quality mainly depends on solution concentration and with a concentration of 17 wt% the best orientated fibres were obtained. Scale bar = 50 µm.

Fibres were also produced from the same solution concentrations and flow rates but with 20 kV and 15 cm (figure 20). Here fibres electrospun from 20 wt% could be collected oriented but demonstrated interconnection between the single fibres (fig. 20a-c). Decreasing the solution concentration to 17 wt% reduces this effect (fig. 20d, e) and homogeneous fibres with diameters of  $0.34 \pm 0.09 \mu\text{m}$ , respectively  $0.38 \pm 0.05 \mu\text{m}$  occurred. Interconnected fibres were only noticed for fibres electrospun from 0.3 mL/h (fig. 20f). Decreasing the solution concentration resulted in a decrease of fibre orientation again (fig. 20g-i).



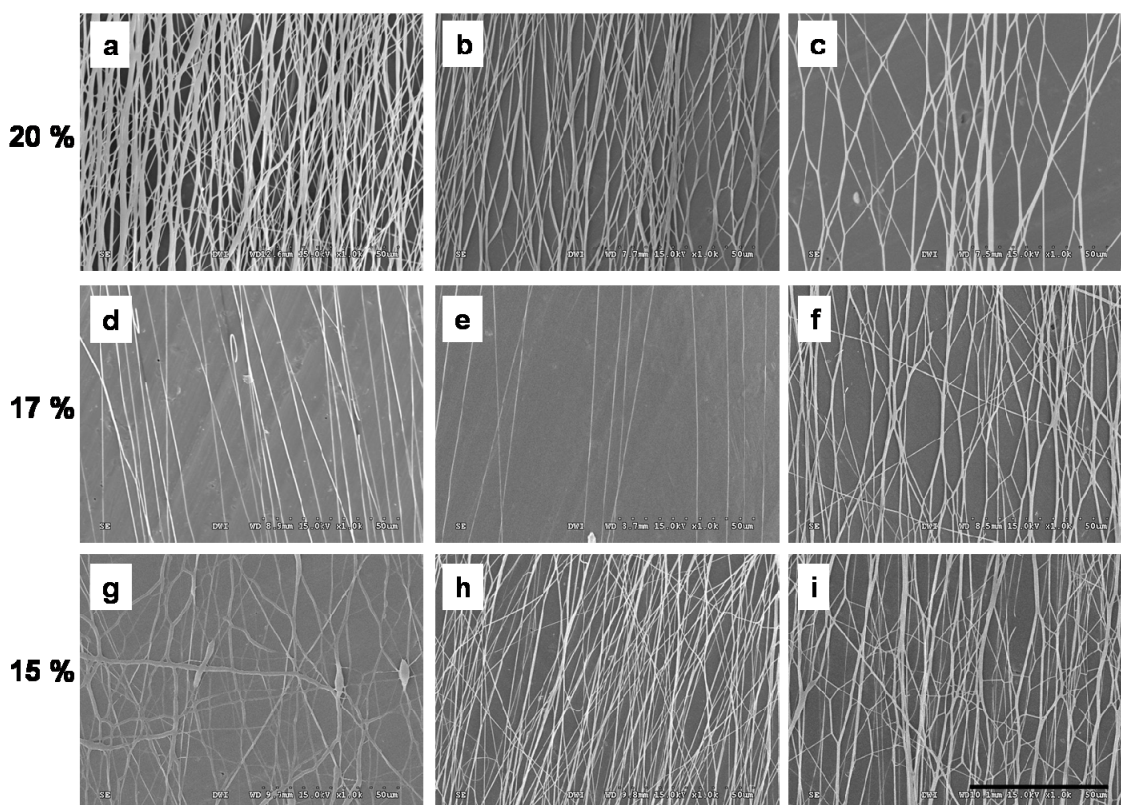


**Figure 20: SEM images of electrospun fibres of polymer 9 electrospun from different concentrations.** Fibres were obtained from 20 kV, 15 cm and (a), (g) 0.8 mL/h, (b), (h) 0.6 mL/h, (c), (i) 0.4 mL/h (d) 1.0 mL/h, (e), 0.5 mL/h, (f) 0.3 mL/h. The fibre quality mainly depends on the concentrations and with a solution concentration of 17 wt% the highest quality fibres were obtained. Scale bar = 50  $\mu$ m.

Polymer 10 was not electrospun because it had the same properties as polymer 9 and it was estimated that it behaves similar during electrospinning.

#### 6.3.4 Surface characterisation of electrospun fibres

For biomedical applications with guiding structures, high quality oriented fibres are required. These demands were obtained from polymers 6 – 9 and therefore fibres from these polymers only were surfaced analysed using protein adsorption assay, XPS and contact angle measurements.

Incubation of the fibres with rhodamine red conjugated BSA visualises their protein adsorption properties and the results are presented in Figure 21. Fluorescence images of the fibres were taken with 1 s (fig. 21a – e) and with 20 s (fig. 21f – j) exposure time. Higher exposure time resulted in stronger fluorescence. Fibres from polymer 7 showed the slightest protein adsorption with an exposure time of 1 s of all fibres (fig. 21a). With this exposure

time, polymers 6, 8 and 9 (fig. 21b-d) have a similar fluorescence which is lower than that of PCL fibres (fig. 21e). Images taken with an exposure time of 20 s present a comparable fluorescence of fibres of polymers 7 and 8 (fig. 21f, g). From polymer 9, over polymer 6 to PCL the fluorescence is increasing continuously (fig. 21h-j). Thus with a decreasing PEO:PCL ratio protein adsorption increased.

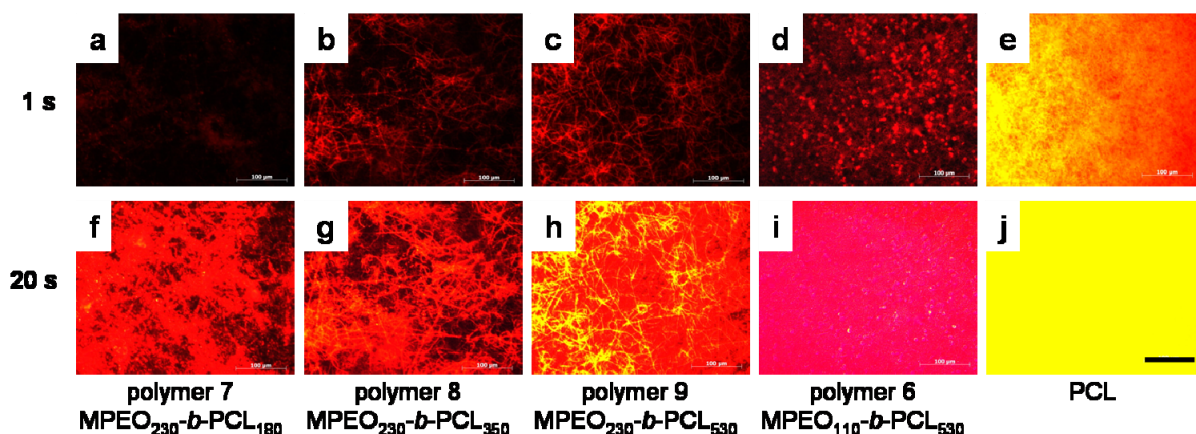


**Figure 21: Fluorescence images of electrospun fibres incubated with rhodamine red conjugated BSA.** (a – e) Images were taken with an exposure time of 1 s; (f – j) images with an exposure time of 20 s. Electrospun fibres adsorbed more BSA with decreasing PEO:PCL ratio. Scale bar = 100  $\mu$ m.

XPS was performed with polymers 6 – 9, PCL and MPEO 10kDa. The results are summarised in table 3 and were used to calculate the C/O ratios. They correlate with the PEO:PCL ratio calculated with the obtained Mn (PCL) (table 1) Comparison of the estimated C/O ratio (real) with the calculated C/O ratio (theor.) with the real Mn (PCL) (table 1) show that the estimated C/O values are slightly higher than the theoretical values but have the same tendency. The results indicate the existence of both block copolymers at the fibre surfaces.

**Table 3: XPS data from different polymers.** The C/O ratio increases with decreasing PEO:PCL ratio.

Atomic concentration (%)	MPEO 10kDa	Polymer 7	Polymer 8	Polymer 9	Polymer 6	PCL
O	26.85	23.63	22.47	21.49	18.5	19.06
C	73.15	76.37	77.53	78.51	79.35	80.94
Si	--	--	--	--	2.15	--
C/O	2.72	3.23	3.45	3.65	4.29	4.25
C/O (theor)*	2	2.65	2.78	2.84	2.92	3
PEO : PCL (real)	--	0.42	0.21	0.15	0.073	--

$$*C/O \text{ ratio was calculated according } C/O(\text{theor}) = \frac{6(M_{PCL} / 114.15) + 2(M_{PEO} / 44.13)}{2(M_{PCL} / 114.15) + (M_{PEO} / 44.13)}$$

Contact angles measurements were possible for PCL fibres ( $125.9 \pm 7.9^\circ$ ) and fibres of polymer 6 ( $93.2 \pm 4.7^\circ$ ) only. With all other polymers, the water droplet sunk within the fibres immediately after it was placed, preventing the measurement.

## 6.4 Discussion

### 6.4.1 Synthesis of PEO-*b*-PCL block copolymers

PEO-*b*-PCL block copolymers with different molecular weights and block lengths ratios were synthesised by ring-opening polymerisation (ROP) of  $\epsilon$ -caprolactone with a PEO block as macroinitiator using three different methods and initiating systems. The NMR spectrum of one block copolymer is shown in figure 4. The integral comparison of the peaks at 4.06 ppm (t, 2H,  $CH_2OH$ , PCL) and at 3.65 ppm (s, 4H,  $CH_2O$ , PEO) enables the calculation of the molecular weight of the synthesised PCL block according equation 2 from reference 24. Unfortunately, important end groups cannot be recognised in the spectra. Neither proton 3 which indicates a chemical reaction between the synthesised PCL block and the macroinitiator PEO, nor the protons from the functional group of the PEO block (proton 1 in polymer 10) are visible (fig. 4).

With diethyl zinc as catalyst, the reaction was not successful and only oligomers with different molecular weights were obtained (fig. 5), although this method was used for the synthesis of similar block copolymers before<sup>14, 26</sup>.

The second method of synthesis was performed using  $HCl \cdot Et_2O$  as monomer activator. The activated monomer polymerisation was described as a very powerful method to control ring-opening polymerisations as it can suppress undesired reactions such as back-

biting and disproportionation<sup>27</sup>. Additionally, syntheses performed with organometallic catalysts were described to sometimes cause problems due to incomplete removal of the metal from resultant polymers<sup>28</sup>, which can be a severe issue in tissue engineering applications. Thus ROP with HCl\*Et<sub>2</sub>O could be good alternative overcoming this controversy. However, experimental data showed that the synthesis was very slow and with shorter reaction times polymers with a broad polydispersity were obtained (fig. 6a). After a 20-day reaction, a polymer with a narrow polydispersity was achieved (fig. 6b). Kim *et al.* synthesised PCL blocks with Mn = 740 – 6000 Da and reported a good control of the molecular weights<sup>12, 29</sup>. However in this study, even after almost three weeks of reaction the resulting PCL block was much shorter than desired (table 1) indicating that this method seems not suitable for long block copolymers. Due to these results it was decided not to use this way of synthesis for further investigations with different block lengths and ratios.

The third type of synthesis was performed in the melt with Sn(Oct)<sub>2</sub> as catalyst. This ring-opening polymerisation has a coordination-insertion mechanism<sup>30</sup> and has quite often been used for the synthesis of PEO-*b*-PCL block copolymers in the past<sup>7-9, 31</sup>. However, those block copolymers had much smaller molecular weights (10000 – 30000 Da) than the ones required here. Five copolymers with different PEO and PCL block lengths and ratios were successfully synthesised. Experimental data demonstrated good control of molecular weights and even long PCL blocks with Mn = 77 kDa were obtained (in contrast to the synthesis with HCl\*Et<sub>2</sub>O) (table 1) which is much higher than commonly reported polymers (7000 – 25000 g/mol) in literature. The polymers had polydispersities between 1.77 and 1.96 (table 1) which were slightly higher than those reported in the literature.

The polymers 6 - 9 and additionally pure PCL (65 kDa) and the corresponding MPEOs (5 and 10 kDa) were analysed by DSC (table 2). PCL and PEO are both semi-crystalline and have similar glass transition and melting points of approximately -60 and 60 °C respectively. Because PEO and PCL are not miscible<sup>32</sup> two melting points, each corresponding to one component should occur. The investigated polymers had two melting points but these correspond with the two heating periods (fig. 8) as thermal treatment influences polymer crystallinity<sup>32</sup> and do not allow statements about miscibility of the two polymers. Comparing the data of the different polymers results also does not allow conclusion from melting and crystallisation points to PCL block length. Nevertheless, the two block copolymers with the highest PEO:PCL ratios (table 1), polymer 7 and 8 demonstrated the appearance of two crystallisation temperatures (fig. 8, table 2). This indicates that with short PCL blocks, both,

the PEO and the PCL block, took part in the crystallisation process while with long PCL blocks overlapping occurred.

The synthesis with  $\text{Sn}(\text{Oct})_2$  from the melt allowed the controlled polymerisation of a variety of different PEO-*b*-PCL block copolymers. Regardless the above mentioned problems with metallic-catalysed polymers in tissue applications, the so-prepared polymers had demonstrated their biocompatibility in several *in vitro* investigations, especially as electrospun non-woven fibre material for tissue engineering strategies<sup>7, 17</sup>.

### 6.4.2 Electrospinning of PEO-*b*-PCL block copolymers with different molecular weights

Electrospinning of polymers 5 - 9 was performed with a wide range of concentrations, flow rates and electrical field strength with the aim to produce oriented single fibres for application in tissue engineering, especially for guidance of nerve cells.

The two most important parameters for the possibility to electrospin polymers are the molecular weight and the concentration of the polymer solution prepared for electrospinning. The jet formation in the electrospinning process relies on the entanglement of the polymer chains. A stable jet is necessary for stable electrospinning and fibre formation and is a result of chain overlapping. Higher molecular weight as well as higher concentrations normally induce these effects. On the other hand, too high concentrations and molecular weights result in higher solution viscosities which can also prevent electrospinning<sup>33, 34</sup>.

Although polymer 5 has a molecular weight that was assumed to be high enough for obtaining electrospun nanofibres, only beads occurred even at high solution concentrations of 40 wt% (fig. 9). Obviously here another effect influences the spinnability too. Eventually residual ions from the activator,  $\text{HCl} \cdot \text{Et}_2\text{O}$ , were enclosed in the polymer and disturbed the electrospinning process. While small amounts of ions increase the conductivity of the electrospinning and normally result in higher quality of fibres, too high salt concentrations prevent electrospinning<sup>35</sup>.

Polymers 6 – 9 were produced from melt with  $\text{Sn}(\text{Oct})_2$  as catalyst. Although it was reported that small amounts of catalyst may remain in the polymer<sup>28</sup>, electrospinning of PEO-*b*-PCL block copolymers produced in this way was performed before and high quality random fibres were obtained<sup>7, 17</sup>. Five block copolymers with different block lengths and block length ratios were successfully electrospun into oriented suspended fibres in this study.

Polymer 6 consists of a PEO-block with a molecular weight of 5000 g/mol and a PCL-block of 68000 g/mol. With this polymer increasing solution concentration improved the quality of oriented collected fibres from a beaded to a bead-free, homogeneous morphology, but not that of random fibres (fig. 11). Further increasing of the solution concentration did not improve oriented fibre quality and variation of the applied voltage did not have any effect (fig. 11).

Polymers 7 - 9 were produced with a PEO block of 10000 g/mol and increasing PCL blocks from 20000 to 60000 g/mol in 20 kDa steps. With increasing molecular weights lower solution concentrations for obtaining fibres with a comparable quality were necessary. Polymer 7 had the lowest molecular weight of these polymers and here a high concentration of 25 wt% was necessary for good quality fibres (figs. 13, 14). With polymer 8 both 17 and 20 wt% solutions resulted in good fibres (figs. 15-17). Polymer 9 has the highest molecular weight and could be electrospun to high quality oriented fibres with the lowest concentration of 15 wt% (figs. 19, 20). The high molecular weight enables chain overlapping necessary for electrospinning with low solution concentrations.

Flow rate and applied voltages have influence on fibre morphology and diameter as well. The applied voltage induces the surface charge of the jet. Normally higher voltages increase instability and stretching of the jet<sup>36,37</sup> which results in smaller fibre diameter. In this study the influence of the applied voltage was noticed to be very small. With polymer 7 the best parallelism of the fibres was obtained with the highest voltage (fig. 12) but this was not significant. Anyhow, the effect of the voltage is described with some controversy in the literature and was stated to be much smaller than the concentration effect<sup>38</sup>. The flow rate ideally matches the removal rate of the polymer solution from the needle. Higher flow rates often result in larger fibre diameters and beads. The effect of the flow rate on the fibre diameter was observed with polymer 7: decreasing flow rates resulted in decreased fibre diameters (figs. 13, 14) but also influenced the fibre quality. Polymers 8 and 9 demonstrated relatively independency of the fibre quality on electrospinning parameters. Especially with polymer 9 highly oriented fibres from a broad range of conditions were achieved (figs. 19, 20). This confirms the finding that the molecular weight of a polymer has the biggest influence of its spinnability.

The ability to electrospin oriented fibres strongly depends on polymer purity. During synthesis the polymers were purified twice by precipitation from different solvents (see 6.2.5). The first precipitation in diethyl ether mainly removes impurities of unreacted

monomer and catalyst. Electrospinning from the raw product resulted in beaded fibres with a low solution concentration of 10 wt% and in high quality random with a concentration of 15 wt% (figs. 18a, b) but it was impossible to obtain oriented fibres. Precipitation in methanol also removes smaller PEO-*b*-PCL block copolymers indicated by a decreased PDI (table 1). This influenced the spinnability significantly and allowed the collection of oriented fibres (fig. 18c).

### 6.4.3 Surface characterisation of electrospun fibres

Surface properties of fibres electrospun from polymers 6 - 9 were analysed using protein adsorption, XPS and contact angle measurements. In all cases PCL fibres served as reference.

Protein adsorption is an important issue for tissue engineering applications. Within seconds proteins can adsorb on a biomaterial after contact with body fluid and transform an inert material into a biologically active one. This process relies on the protein affinity to the biomaterial and depends on topological and chemical properties of the material<sup>4</sup>. Cells respond to the protein layer and undesired reaction such as inflammation<sup>39</sup> and encapsulation<sup>40</sup> can occur. Poly(ethylene oxide) is capable to mask implants towards the host organism and electrospun fibres consisting of poly(ethylene oxide)-*block*-poly(D, L-lactide) copolymers has already shown their biocompatibility and protein resistant properties<sup>25</sup>. Similar to results from Grafahrend *et al.* the electrospun fibres in this study demonstrated dependency of protein adsorption on molecular weight and PEO:PCL ratio (fig. 21). All PEO containing fibres showed a reduced protein adsorption compared to pure PCL fibres. Comparison of polymers 6 and 9 show that the longer PEO block prevented protein adsorption more effectively. Increasing PEO:PCL ratios decreased the protein adsorption additionally. These results verify that both blocks appeared at the fibre surfaces.

This was also confirmed by XPS measurements which revealed an increasing C/O ratio with an decreasing PEO:PCL ratio (table 3). In pure PEO the C/O ratio is 2:1 while it is 6:2 in PCL and an increasing C/O ratio confirmed the existence of more PEO at the fibre surface. Contact angle measurements disclose the hydrophobic character of PCL fibres with a very high value of 126°. Even the polymer with the smallest PEO:PCL ratio (polymer 6) demonstrated strong hydrophilic properties by a much smaller contact angle. All other tested polymers were so hydrophilic, that contact angle measurements were impossible showing again the existence of PEO at the fibre surface.

The presented PEO-*b*-PCL block copolymers are amphiphilic due to the hydrophobic PCL-block and the hydrophilic PEO-block. Such polymers can spontaneously aggregate in selective solvents to form micelles which makes them interesting for drug delivery purposes<sup>14,31</sup>. Upon evaporation of the solvent during the electrospinning process, micelles break up and the hydrophilic PEO-block forms inclusions in a continuous matrix. The assignment of protic solvents such as methanol induces the appearance of the hydrophilic PEO-block at the fibre surface, also in combination with a non-polar solvent like chloroform. The exclusive use of chloroform would probably prevent this and would neglect the protein repellent properties<sup>25</sup>.

These results show the electrospun fibres of PEO-*b*-PCL block copolymers with a long PEO-block and a moderate PCL-block provide a good substrate for tissue engineering applications with minimised protein adsorption. However, for controlled biomaterial/body interactions biofunctionalisation of this inert material would be necessary. The coupling of cell specific peptide sequences, for example RGD, should evoke good cellular adhesion with simultaneously preventing undesired body reactions. Synthesis and electrospinning of an RGD-functionalised PEO-*b*-PCL block copolymer are described in chapter 7.

### 6.5 Conclusion

Amphiphilic PEO-*b*-PCL block copolymers were synthesised using three different methods. While solution polymerisation with diethyl zinc or HCl\*Et<sub>2</sub>O did not result in the desired products, the synthesis in the melt with stannous II octoate offered good control of polymers molecular weight and block lengths ratios. Five different polymers were synthesised in this way with molecular weights from 34000 to 76000 g/mol. DSC measurements indicated the immiscibility of both polymer blocks. Electrospinning of all polymers into oriented suspended fibres was successful and higher molecular weight polymers showed relatively independency of electrospinning parameters. Surface analysis of the electrospun fibres demonstrated a hydrophilic character and reduced protein adsorption properties which make the polymers suitable as implantable biomaterials with controlled material/body interactions.

### 6.6 References

1. The scientific committee on medicinal products and medical devices. *Opinion on The State of the Art concerning Tissue Engineering, SANCO/SCMPMD/2001/0006 Final*; European Commission: 2001.



2. Chew, S. Y.; Mi, R.; Hoke, A.; Leong, K. W., The effect of the alignment of electrospun fibrous scaffolds on Schwann cell maturation. *Biomaterials* **2008**, 29, 653 - 661.
3. Pham, Q. P.; Sharma, U.; Mikos, A. G., Electrospun poly( $\epsilon$ -caprolactone) microfiber and multilayer nanofiber/microfiber scaffolds: characterization of scaffolds and measurement of cellular infiltration. *Biomacromolecules* **2006**, 7, 2796 - 2805.
4. Horbett, T. A., The role of adsorbed proteins in tissue response to biomaterials. In *Biomaterials Science: An introduction to materials in medicine*, 2nd ed.; Ratner, B. D., Hoffman, A. S., Schoen, F. J., Lemons, J. E., Ed. Elsevier: San Diego, 2004; pp 237 - 240.
5. Sharma, S., Johnson, R.W., Desai, T.A., Evaluation of the stability of nonfouling ultrathin poly(ethylene glycol) films for silicon-based microdevices. *Langmuir* **2004**, 20, (2), 348 - 356.
6. Zhang, M.; Desai, T.; Ferrari, M., Proteins and cells on PEG immobilized silicon surfaces. *Biomaterials* **1998**, 19, 953 - 960.
7. Grafahrend, D.; Calvet, J. L.; Salber, J.; Dalton, P. D.; Moeller, M.; Klee, D., Biofunctionalized poly(ethylene glycol)-block-poly(epsilon-caprolactone) nanofibers for tissue engineering. *Journal of Materials Science-Materials in Medicine* **2008**, 19, (4), 1479 - 1484.
8. Azzam, T.; Eisenberg, A., Monolayer-protected gold nanoparticles by the self-assembly of micellar poly(ethylene oxide)-*b*-poly( $\epsilon$ -caprolactone) block copolymer. *Langmuir* **2007**, 23, 2126 - 2132.
9. Bogdanov, B.; Vidts, A.; Van Den Bulcke, A.; Verbeeck, R.; Schacht, E., Synthesis and thermal properties of poly(ethylene glycol)-poly( $\epsilon$ -caprolactone) copolymers. *Polymer* **1998**, 39, 1631 - 1336.
10. Huang, M.-H.; Li, S.; Coudane, J.; Vert, M., Synthesis and characterisation of block copolymers of  $\epsilon$ -caprolactone and DL-lactide initiated by ethylene glycol or poly(ethylene glycol). *Macromolecular Chemistry and Physics* **2003**, 204, 1994 - 2001.
11. Hyun, H.; Kim, Y. H.; Song, I. B.; Lee, J. W.; Kim, M. S.; Khang, G.; Park, K.; Lee, H. B., *In vitro* and *in vivo* release of albumin using a biodegradable MPEG-PCL diblock copolymer as an in situ gel-forming carrier. *Biomacromolecules* **2007**, 8, 1093 - 1100.
12. Kim, M. S.; Seo, K. S. S.; Khang, G.; Cho, S. H.; Lee, H. B., Preparation of poly(ethylene glycol)-block-poly(caprolactone) copolymers and their applications as thermo-sensitive materials. *Journal of Biomedical Material Research Part A* **2004**, 70A, 154 - 158.
13. Oh, J. M., Lee, S. H., Son, J. S., Khang, G., Kim, C. H., Chun, H. J., Min, B. H., Kim, J. H., Kim, M. S. Ring-opening polymerization of  $\epsilon$ -caprolactone by poly(propyleneglycol) in the presence of a monomer activator. *Polymer* **2009**, 50, 6019 - 6023.
14. Deng, M.; Chen, X.; Piao, L.; Zhang, X.; Dai, Z.; Jing, X., Synthesis of four-armed poly( $\epsilon$ -caprolactone)-*block*-poly(ethylene oxide) by diethylzinc as catalyst. *Journal of Polymer Science: Part A: Polymer Chemistry* **2004**, 42, 950 - 959.

15. Allen, C.; Han, J.; Yu, Y.; Maysinger, D.; Eisenberg, A., Polycaprolactone-*b*-poly(ethylene oxide) copolymer micelles as a delivery vehicle for dihydrotestosterone. *Journal of Controlled Release* **2000**, 63, 275 - 286.
16. Xiong, X.-B.; Mahmud, A.; Uludag, H.; Lavasanifar, A., Conjugation of arginine-glycine-aspartic acid peptides to poly(ethylene oxide)-*b*-poly( $\epsilon$ -caprolactone) micelles for enhanced intracellular drug delivery to metastatic tumor cells. *Biomacromolecules* **2007**, 8, 874 - 884.
17. Dalton, P. D.; Klinkhammer, K.; Salber, J.; Klee, D.; Möller, M., Direct *in vitro* electrospinning with polymer melts. *Biomacromolecules* **2006**, 7, (3), 686 - 690.
18. Huang, Z. M.; Zhang, Y. Z.; Kotaki, M.; Ramakrishna, S., A review on polymer nanofibers by electrospinning and their applications in nanocomposites. *Composites Science and Technology* **2003**, 63, (15), 2223 - 2253.
19. Pham, Q. P.; Sharma, U.; Mikos, A. G., Electrospinning of polymeric nanofibers for tissue engineering applications: a review. *Tissue Engineering* **2006**, 12, (5), 1197 -1211.
20. Matthews, J. A.; Wnek, G. E.; Simpson, D. G.; Bowlin, G. L., Electrospinning of collagen nanofibers. *Biomacromolecules* **2002**, 3, (2), 232 - 238.
21. Dalton, P. D.; Klee, D.; Möller, M., Electrospinning with dual collection rings. *Polymer* **2005**, 46, (3), 611 - 614.
22. Li, D.; Xia, Y. N., Electrospinning of nanofibers: Reinventing the wheel? *Advanced Materials* **2004**, 16, (14), 1151 - 1170.
23. Goetz, H.; Beginn, U.; Bartelink, C. F.; Grunbauer, H. J. M.; Möller, M., Preparation of isophorone diisocyanate terminated star polyethers. *Macromolecular Materials and Engineering* **2002**, 287, (4), 223 - 230.
24. Schreiber, T. Synthese von Polyethylenglycol-block-Polycaprolacton als Basis für elektrogesponnene Nanofasern. Diploma Thesis, RWTH Aachen, Aachen, 2006.
25. Grafahrend, D.; Calvet, J. L.; Klinkhammer, K.; Salber, J.; Dalton, P. D.; Moller, M.; Klee, D., Control of protein adsorption on functionalized electrospun fibers. *Biotechnology and Bioengineering* **2008a**, 101, (3), 609 - 621.
26. Hu, X.; Chen, X.; Xie, Z.; Liu, S.; Jing, X., Synthesis and characterisation of amphiphilic block copolymers with allyl side-groups. *Journal of Polymer Science: Part A: Polymer Chemistry* **2007**, 45, 5518 - 5528.
27. Kubisa, P.; Penczek, S., Cationic activated monomer polymerization of heterocyclic monomers. *Progress in Polymer Science* **1999**, 24, 1409 - 1437.
28. Pitt, C. G.; Schindler, A., *Capronor - a biodegradable delivery system for levonorgestrel*. Harper and Row Publishers: Philadelphia, USA, 1984; pp 48 - 63.
29. Kim, M. S.; Hyun, H.; Cho, Y. H.; Seo, K. S.; Jang, W. Y.; Kim, S. K.; Khang, G.; Lee, H. B., Preparation of methoxy poly(ethyleneglycol)-block-poly(caprolactone) via activated monomer mechanism and examination of micellar characterization. *Polymer Bulletin* **2005**, 55, 149 - 156.

30. Ryner, M.; Stridsberg, K.; Albertsson, A.-C., Mechanism of ring-opening polymerization of 1,5-dioxepan-2-one and L-lactide with stannous 2-ethylhexanoate. A theoretical study. *Macromolecules* **2001**, 34, 3877 - 3881.
31. Meier, M. A. R.; Aerts, S. N. H.; Staal, B. B. P.; Rasa, M.; Schubert, U. S., PEO-*b*-PCL block copolymers: synthesis, detailed characterization, and selected micellar drug encapsulation behavior. *Molecular Rapid Communications* **2005**, 26, 1918 - 1924.
32. Qiu, Z.; Ikehara, T.; Nishi, T., Miscibility and crystallization of poly(ethylene oxide) and poly( $\epsilon$ -caprolactone) blends. *Polymer* **2003**, 44, 3101 - 3106.
33. Gupta, P.; Elkins, C.; Long, T. E.; Wilkes, G. L., Electrospinning of linear homopolymers of poly(methyl methacrylate): exploring relationships between fiber formation, viscosity, molecular weight and concentration in a good solvent. *Polymer* **2005**, 46, 4799 - 4810.
34. Shenoy, S. L.; Bates, W. D.; Frisch, H. L.; Wnek, G. E., Role of chain entanglements on fiber formation during electrospinning of polymer solutions: good solvent, non-specific polymer-polymer interaction limit. *Polymer* **2005**, 46, (10), 3372 - 2284.
35. Kim, B.; Park, H.; Lee, S.-H.; Sigmund, W. M., Poly(acrylic acid) nanofibers by electrospinning. *Material Letters* **2005**, 59, (7), 829 - 832.
36. Buchko, C. J.; Chen, L. C.; Shen, Y.; Martin, D. C., Processing and microstructural characterization of porous biocompatible protein polymer thin films. *Polymer* **1999**, 40, 7397 - 7407.
37. Fridrikh, S. V.; Yu, J. H.; Brenner, M. P.; Rutledge, G. C., Controlling the fiber diameter during electrospinning. *Physical Review Letter* **2003**, 90, (14), 144502.
38. Kalayci, V. E.; Patra, P. K.; Buer, A.; Ugbohue, S. C.; Kim, Y. K.; Warner, S. B., Fundamental investigations on electrospun fibers. *Journal of Advanced Materials* **2004**, 36, (4), 43 - 47.
39. Tang, L., Jennings, T. A., Eaton, J. W., Mast cells mediate acute inflammatory responses to implanted biomaterials. *PNAS* **1998**, 95, 8841 - 8846.
40. Johnson, R.; Harrison, D.; Tucci, M.; Tsao, A.; Lemos, M.; Puckett, A.; Hughes, J. L.; Benghuzzi, H., Fibrous capsule formation in response to ultrahigh molecular weight polyethylene treated with peptides that influence adhesion. *Biomed. Sci. Instrum.* **1997**, 34, 47 - 52.

### **SYNTHESIS AND ELECTROSPINNING OF A GRGDS-FUNCTIONLISED POLY(ETHYLENE OXIDE)-*b*-POLY( $\epsilon$ -CAPROLACTONE) BLOCK COPOLYMER**

#### **7.1 Introduction**

In tissue engineering strategies scaffolds of biomaterials serve as constructs for cellular organisation in regenerative medicine. Depending on the application, non-degradable or degradable materials are necessary. In the later case, the scaffold degrades by time while cells express proteins which take over the structural functions more and more. The scaffold has to mimic mechanical and physical properties of the tissue to replace but also fulfil biological demands. For specific applications the artificial tissue should guide cell orientation such as muscle cells for the development of artificial blood vessels<sup>1</sup> or nerve cells in artificial nerve conduits<sup>2,3</sup>.

The method of electrospinning enables the production of fibres in the nanometre range, similar to fibrils in the extracellular matrix (ECM), by applying a high voltage to a polymer solution and collecting the resulting fibres on a grounded target. Details about the electrospinning process can be gained from literature<sup>4,5</sup>. Oriented fibres are obtained by collection on rotating drums<sup>6</sup> or with the gap method of alignment where low density suspended fibres are collected between two parallel bars<sup>7,8</sup>. The last kind of fibres offers investigations of single cell/fibre interactions for example of neuronal cells<sup>9</sup>. A great range of synthetic polymers have already been electrospun into oriented fibres including polystyrene, poly(L-lactic acid) (PLLA) and poly( $\epsilon$ -caprolactone) (PCL). Especially PCL is often used when slow degradation rates are desired and its biocompatibility has already been shown. While fibres of synthetic materials normally do not have any biological functionalities, combinations with natural proteins enhance cellular activation<sup>10,11</sup>. However, these fibres do normally not withstand protein adsorption, a process happening within seconds after an implant comes in contact with its host body, which can result in encapsulation of the implanted scaffold<sup>12</sup>. The application of protein resistant polymers such as poly(ethylene oxide) (PEO) can help to overcome this problem. PEO is able to mask a biomaterial and prevents it from unspecific body reactions. Combinations of PCL with PEO in terms of PEO-*b*-PCL block copolymer were successfully synthesised in a ring-opening polymerisation of  $\epsilon$ -

## **Synthesis and electrospinning of a GRGDS-functionalised PEO-*b*-PCL block copolymer**

caprolactone with PEO as macroinitiator and stannous II octoate as catalyst<sup>13</sup>. Electrospun fibres of this materials showed protein resistance (chapter 6) but also cell repellency<sup>14</sup>. For controlled cellular response of the inert material biological functionalisation is necessary. Cells bind to other cells or the ECM via integrin receptors which are, among others, specialised to the recognition of the peptide sequence RGD (R: arginine; G: glycine; D: aspartic acid). RGD is the cell binding domain in ECM proteins such as fibronectin and vitronectin<sup>15</sup>. Coupling of this peptide sequence to PEO-*b*-PCL block copolymer during its synthesis was already performed by Grafahrend *et al.*, who successfully electrospun random fibres of this polymer with cell attractive properties<sup>14</sup>.

In this study, a GRGDS-functionalised PEO-*b*-PCL block copolymer with a high molecular weight, necessary for electrospinning oriented fibres, was produced in a three-step synthesis. The polymer demonstrated minimised protein adsorption and the successful coupling of the peptide sequence for specific cell attractive properties was confirmed by colour reaction. Electrospinning experiments were performed for estimation the suitability of the application as tissue engineering scaffold for nerve regeneration.

## **7.2 Materials and Methods**

### **7.2.1 Chemicals**

All chemicals were purchased from Sigma-Aldrich (Germany) unless otherwise stated. Star-NCO-poly(EO-*stat*-PO) (star-shaped poly ethers with a backbone of 80 % ethylene oxide and 20 % propylene oxide and isocyanate end groups, Mw = 12000 g/mol) (sPEG) was synthesised in our laboratory from hydroxyl-terminated star polymer (DOW-chemicals, Terneusen, NL) by reaction with isophorone diisocyanate according to literature as described elsewhere<sup>16</sup>. It was stored in the glovebox and only the desired amounts were taken out just before using. Hydroxylamin was a 50 wt% solution in water.

### **7.2.2 Solutions**

#### MES-buffer:

0.213 g 2-(N-morpholino)ethanesulfonic acid (MES)

0.2937 g sodium chloride (NaCl)

10 mL distilled water

0.2 mL 2 N sodium hydroxide (NaOH)

pH = 6

### Ninhydrine/collidine spray-solution:

170 mL ethanol, p.a.  
57 mL acidic acid, 100 %, p.a.  
23 mL collidine (2,4,6-trimethylpyridine), p.a.  
0.28 g ninhydrine, p.a.

### Sakaguchi spray-solution:

solution 1: 8-hydroxyquinolin in acetone (0.1 %)  
solution 2: 0.2 mL brome  
100 mL 0.5 M NaOH

### Polymer solutions for ninhydrine/collidine and Sakaguchi-tests:

Boc-PEO-*b*-PCL, 3 mg/mL in dichloromethane (DCM)  
H<sub>2</sub>N-PEO-*b*-PCL, 3 mg/mL in DCM  
H<sub>2</sub>N-PEO-OH (M<sub>w</sub> = 10000 g/mol, Iris Biotech), 1 mg/mL in water  
MeO-PEO-OH (M<sub>w</sub> = 10000 g/mol, Iris Biotech), 1 mg/mL in water  
Peptide-PEO-*b*-PCL, 2 % in DCM  
GRGDS, 0.1 % in water

### **7.2.3 Synthesis of peptide-functionalised PEO-*b*-PCL block copolymer**

The synthesis of peptide-functionalised PEO-*b*-PCL block copolymer was performed in three steps based on a *tert*-butyloxycarbonyl mono-protected poly(ethylene oxide) polymer (Boc-PEO, M<sub>w</sub> = 10000 g/mol, Iris Biotech GmbH, Marktredwitz, Germany). In the first step Boc-PEG-*b*-PCL block copolymer was synthesised according a procedure already described in the literature<sup>17</sup>. Boc-PEG (0.5 g, 5\*10<sup>-5</sup> mol) was filled in a Schlenkflask and then 3 g of ε-CL (desired M<sub>w</sub> = 60000 g/mol) and three droplets of stannous II octoate (Sn(Oct)<sub>2</sub>) were added. Then the flask was evacuated for 35 min during cooling with an ice bath. Afterwards the flask was closed and stirred for 20 h at 120 °C. After the reaction, the flask was vented and the solid polymer was dissolved in a small amount of dichloromethane (DCM). A white powder was received by precipitation in 600 mL ice-cold diethyl ether after filtration. After drying, the polymer was dissolved again in DCM and precipitated in 600 mL ice-cold methanol. After filtration and drying a white powder with a yield of approximately 85 % was recieved. <sup>1</sup>H and <sup>13</sup>C NMR in deuterated chloroform (CDCl<sub>3</sub>) and GPC in tetrahydrofurane (THF) confirmed the polymerisation.

## Synthesis and electrospinning of a GRGDS-functionalised PEO-*b*-PCL block copolymer

The second step was the deprotection of the block copolymer to achieve an amine-functionalised block copolymer (H<sub>2</sub>N-PEO-*b*-PCL). For this purpose a solution consisting of 19 g para-toluene sulfonic acid (Mw = 172.2 g/mol), 20 ml DCM and 37.5 ml THF was prepared. An amount of 45.8 ml (16-fold excess per weight) of this solution was added to 2.87 g Boc-PEO-*b*-PCL block copolymer. The solution was stirred for 2 h at room temperature (RT), reduced by rotating evaporation and precipitated in 1.2 l of ice-cold (-20 °C) diethyl ether and filtered. The filtrate was washed three times with distilled water to remove excess deprotection reagent. The product was freeze-dried over night. A white powder with a yield of 51 % was obtained. Gel permeation chromatography (GPC) in THF and nuclear magnetic resonance (NMR) in CDCl<sub>3</sub> were applied to analyse the product. The same procedure was also performed with a 10-fold excess of deprotection solution. In additional experiments, the deprotected polymer was further purified using two different methods. Firstly the polymer was dissolved in a 50 fold excess of THF and dialysed in water at a ratio of 1:300 with a tube consisting of cellulose membrane (Mw = 12400 g/mol) for 24 h with one water exchange in between. Afterwards the content of the tube was filtered and the product freeze-dried over night. In an alternative experiment, the polymer was dissolved in a 3 fold excess in chloroform and shaken three times with the same volume of a NaHCO<sub>3</sub>-solution (1 M). The aqueous phase was shaken with the same volume of chloroform afterwards and the organic phases were combined. They were then washed three times with distilled water by thoroughly shaking. The organic phase was then separated and the volume reduced. This solution was precipitated in ice-cold methanol. The product was filtered and dried over night.

In the third step, functionalisation with the peptide sequence GRGDS (Gly-Arg-Gly-Asp-Ser, Mw = 490.5 g/mol Bachem) was performed. Three solutions were prepared first: 0.8 mg 1-ethyl-3-[3-dimethylaminopropyl]carbodiimide (EDC, Mw = 171.7 g/mol, Pierce Perbio Science) in 0.05 mL MES-buffer, 1.2 mg N-hydroxysuccinimide (NHS, Mw = 15.1g/mol, Pierce Perbio Science) in 0.05 mL MES-buffer and 11.6 mg GRGDS in 0.087 mL MES-buffer. An amount of 0.029 mL of the EDC- and the NHS-solutions each were added to the peptide solution. This mixture was stirred for 15 min at RT. Approximately 0.02 mL of 1 N NaOH-solution were used to get a basic peptide solution. This solution was then added to a pre-prepared solution of 0.5 g H<sub>2</sub>N-PEO-*b*-PCL in 4.38 mL THF and stirred for 20 h at RT. By addition of 7.08 µL HO-NH<sub>2</sub> the reaction was aborted. The light brownish solution was precipitated in ice-cold diethyl ether and the white product was filtered and washed three times with distilled water. Further purification was performed by dialysis of the

polymer: the polymer was filled in dialysis tube (cellulose membrane) and ion exchange was performed in water at a ratio of 1:300 for 24 h with one water exchange in between and slightly stirring. Afterwards the content of the tube was filtered and the product freeze-dried over night. A yield of 41 % of peptide-PEO-*b*-PCL was received. NMR and GPC were used to analyse the product.

$^1\text{H}$  ( $\text{CDCl}_3$ ) NMR (Boc-PEO-*b*-PCL):  $\delta = 1.33$ - $1.43$  (m,  $\text{OCCH}_2\text{CH}_2\text{CH}_2\text{CH}_2\text{CH}_2\text{OH}$ , PCL segment),  $1.60$ - $1.70$  (m,  $\text{OCCH}_2\text{CH}_2\text{CH}_2\text{CH}_2\text{CH}_2\text{OH}$ , PCL segment),  $2.31$  (t,  $\text{OCCH}_2\text{CH}_2\text{CH}_2\text{CH}_2\text{CH}_2\text{OH}$ , PCL segment),  $3.65$  (s,  $\text{CH}_2\text{O}$ , PEO segment),  $4.06$  (t,  $\text{OCCH}_2\text{CH}_2\text{CH}_2\text{CH}_2\text{CH}_2\text{OH}$ , PCL segment) ppm.

$^{13}\text{C}$  ( $\text{CDCl}_3$ ) NMR (Boc-PEO-*b*-PCL):  $\delta = 24.57$  ( $\text{OCCH}_2\text{CH}_2\text{CH}_2\text{CH}_2\text{CH}_2\text{OH}$ , PCL segment),  $25.52$  ( $\text{OCCH}_2\text{CH}_2\text{CH}_2\text{CH}_2\text{CH}_2\text{OH}$ , PCL segment),  $28.35$  ( $\text{OCCH}_2\text{CH}_2\text{CH}_2\text{CH}_2\text{CH}_2\text{OH}$ , PCL segment),  $34.11$  ( $\text{OCCH}_2\text{CH}_2\text{CH}_2\text{CH}_2\text{CH}_2\text{OH}$ , PCL segment),  $64.12$  ( $\text{OCCH}_2\text{CH}_2\text{CH}_2\text{CH}_2\text{CH}_2\text{OH}$ , PCL segment),  $70.56$  ( $\text{CH}_2\text{O}$ , PEO segment),  $173.50$  ( $\text{OCCH}_2\text{CH}_2\text{CH}_2\text{CH}_2\text{CH}_2\text{OH}$ , PCL segment) ppm.

### 7.2.4 Characterisation of polymer

#### *Nuclear magnetic resonance (NMR)*

For  $^1\text{H}$  and  $^{13}\text{C}$  nuclear magnetic resonance spectroscopy, the polymers were dissolved in deuterated chloroform ( $\text{CDCl}_3$ ) (with 0.03 % (v/v) tetramethyl silane (TMS) as internal standard) at a concentration of 80 mg/mL. The samples were measured in the Institute of Organic Chemistry at RWTH Aachen University with a Varian Mercury 300 ( $^{13}\text{C}$ : 75 MHz,  $^1\text{H}$ : 300 MHz) of the company Varian (Palo Alto, USA). The chemical shift is given in ppm and refers to TMS as internal standard. The spectra were described using the following abbreviation: s = singlet, d = duplet, t = triplet, q = quartet, m = multiplet. The software MestRec was used to analyse the spectra.

NMR data were used to estimate the molecular weight of the poly( $\epsilon$ -caprolactone) block ( $M_{\text{PCL}}$ ) in the synthesised block copolymer as described before (chapter 6).

#### *Gel permeation chromatography (GPC)*

The polymers were dissolved in THF (HPLC grade, destabilised, Carl Roth, Karlsruhe, Germany) with 0.25g/L 2,6-di-*tert*-butyl-4-methylphenol (BHT) at a concentration of 3-4 mg/mL. The samples were analysed at room temperature using a high-pressure liquid chromatography pump (HPLC pump, model 6420, ERC GmbH, Riemerling, Germany) and a



## Synthesis and electrospinning of a GRGDS-functionalised PEO-*b*-PCL block copolymer

refractive index detector (RI-230 I plus, Jasco GmbH Germany, Groß-Umstadt, Germany) at a flow rate of 1.0 mL/min. One column with a length of 5 cm, a diameter of 8 mm and a nominal pore width of 50 Å was used as pre-column. Then four columns each with a length of 30 cm, and a diameter of 8 mm followed. They have nominal pore widths of 50, 100, 1000, and 10000 Å. All columns were loaded with MZ SDplus gel with a gel particles size of 5 µm. Conventional calibration was achieved using poly(methyl methacrylate) (PMMA) standards. The number-average molecular weight  $M_n$ , the weight-average molecular weight  $M_w$  and the polydispersity  $PDI=M_w/M_n$  were calculated by the program PSS WinGPC Unity. As PMMA was used as standard, the given molecular weights cannot be seen as absolute values and were not included.

### *Amino group detection with ninhydrine*

Solutions of the different polymers and several references were prepared and dappled twice in thin lines on a thin-layer chromatography plate. The plate was dried for 10 min at 70 °C and then sprayed with the ninhydrine/collidine spray-solution until full wetting. After drying for 2 min at 70 °C, the development of coloured Ruhemanns' violet was observed.

### *Arginine detection with Sakaguchi reagent*

Solutions of the different polymers and several references were prepared and dappled twice in thin lines on filter paper. The paper was dried for 10 min at 70 °C and then sprayed with the first spray-solution until full wetting. After drying at RT, the second spray-solution was applied and again the paper was dried at RT. After approximately 15 min. the development of coloured complexes was observed

## **7.2.5 Electrospinning of fibres**

For electrospinning, solutions of 16.5 and 20 wt% of the polymers in chloroform/methanol (75/25 v/v) were prepared. The solution was filled in a 1 mL syringe with a stainless steel 20 gauge flat tipped needle (Hamilton, Bonaduz, Switzerland). Flow rates from 0.05 to 1.0 mL/h, voltages from 15 to 25 kV and distance between spinneret and target of 15 and 20 cm were used. Random fibres were collected on single targets while parallel fibres were collected suspended between dual collectors with a gap of 2 or 4 cm using the gap method for alignment.

### 7.2.6 Fibre characterisation

#### *Scanning electron microscopy (SEM)*

The electrospun fibres were visualised by scanning electron microscopy (SEM) (S360 Zeiss NTS, Germany and Hitachi S3000 N), using 15 kV and working distances of 5 to 15 mm after sputtering with gold for 90 s (S150B, Edwards, Crawley, Great Britain). The SEM images were used to measure fibre diameters which are presented as the mean with standard deviation.

#### *Sample preparation for protein adsorption*

Silicon wafers were first cleaned in methanol with ultra sonic for four min and then dried with nitrogen. They were incubated in a solution of methanol with 2 % (v/v) 3-aminopropyl triethoxy silane for 2 min. The wafers were washed by placing them three times in distilled water for 2 min each. After drying in a nitrogen stream the wafers were kept at 4 °C before using on the following day. SPEG was dissolved in THF (100 mg/mL) and then distilled water was added (water/THF = 9:1) to end in a final concentration of 10 mg/mL. After crosslinking of the final solution for 5 min, the wafers were placed on the spin-coater and coated with the filtered solution (0.2 µm, Whatman). The wafers were accelerated within 5 s to 4000 rpm for 40 s. These coated silicon wafers were covered with electrospun fibres either by spinning directly onto the wafers for random fibres or by pushing the wafers through the suspended oriented fibres for oriented collection.

#### *Protein adsorption*

Protein adsorption of the fibres was determined with fluorescently labeled bovine serum albumin (BSA) as previously described<sup>18</sup>. Briefly, the prepared substrates were incubated with rhodamine red labeled bovine serum albumin (BSA) diluted in phosphate buffer saline buffer (PBS) (50 µg/mL) for 20 min followed by three incubations in PBS for 20 min each. Afterwards the samples were incubated for 60 min in PBS and washed thoroughly with distilled water. The samples were kept in the dark during incubation and washing. The fibres were visualised with fluorescence microscopy (Axioplan 2 imaging, Zeiss, Germany) and images were taken with a constant exposure time of 1 s. PCL fibres were used as reference.

### 7.3 Results

#### 7.3.1 Synthesis of a GRGDS-functionalised PEO-*b*-PCL block copolymer

The synthesis of a GRGDS-functionalised PEO-*b*-PCL block copolymer was performed in three steps. First the block copolymer was synthesised by ring-opening polymerisation of  $\epsilon$ -caprolactone with a Boc-protected poly(ethylene oxide) (Boc-PEO) polymer as macroinitiator. The reaction scheme is shown in figure 1a. GPC was used to analyse the reaction. The elugram in figure 1b demonstrated the preparation of a polymer with a polydispersity of 1.67.

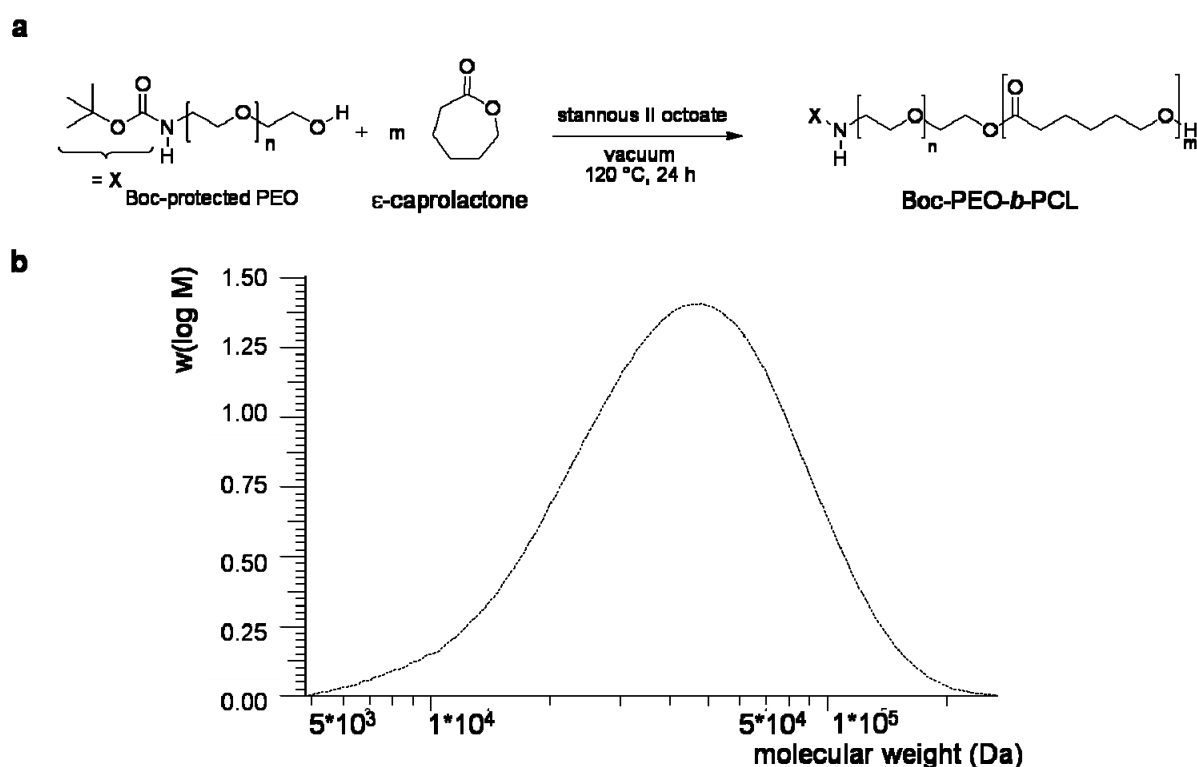


**Figure 1: First step of the synthesis showing the preparation of a Boc-protected PEO-*b*-PCL block copolymer. (a) Reaction scheme and (b) the corresponding elugram from GPC.**

NMR was additionally used to analyse the reaction product. The spectrum is presented in figure 2. Integrals from protons 3 and 9 were used to calculate the molecular weight. According to equation 1 and 2 in chapter 6 the PCL block had a molecular weight of 64000 g/mol. The amounts of protons 2, 4 and 10 in the block copolymer were too little to be visualised in the spectrum. The peak of protons 1 from the Boc protection group is also too small and was additionally overlaid from protons 7 and cannot be distinguished from these.

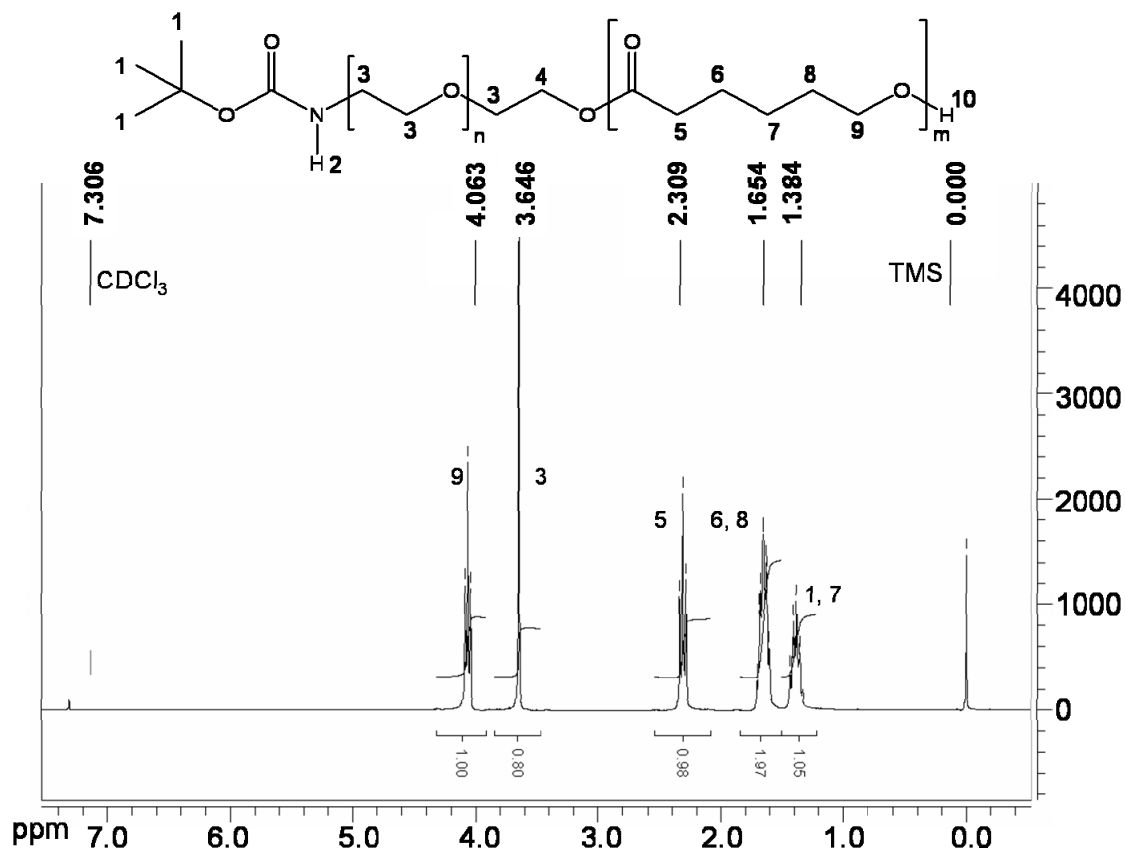


**Figure 2: NMR spectrum of Boc-protected PEO-*b*-PCL block copolymer.**

The deprotection of the amino group of the block copolymer was performed in the second step of the synthesis by using of *para*-toluene sulfonic acid (*p*-TSA). Figure 3a presents the reaction scheme. The employment of a 16-fold excess of *p*-TSA per weight resulted in a deprotected polymer with amino-functionality. The elugram in figure 3b from GPC demonstrated the formation of an inhomogeneous polymer and the polydispersity was calculated to be 1.51. A 10-fold excess of *p*-TSA deprotected the block copolymer only partially and the elugram presented a much smoother peak as seen in figure 3c. The polydispersity was also 1.51.

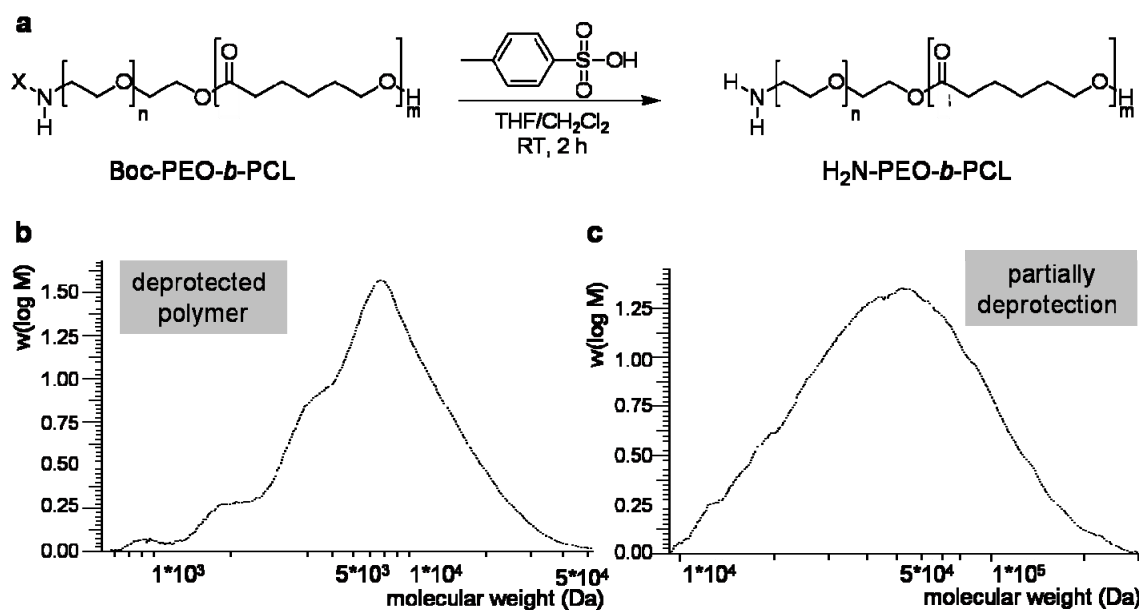


**Figure 3: Second step of the synthesis with deprotection of the amino-group.** (a) Reaction scheme, (b) the corresponding elugram from GPC of deprotected polymer with the application of 16-fold excess of *p*-TSA and (c) GPC elugram of the partially protected polymer prepared with a 10-fold excess of *p*-TSA.

In the last step of the synthesis the peptide sequence GRGDS was coupled to the amino-functionalised block copolymer using the well-known EDC/NHS system by formation of an amid-bond as shown in figure 4a. GPC displayed the existence of a shoulder in the elugram (figure 4b) and a polydispersity of 1.57.

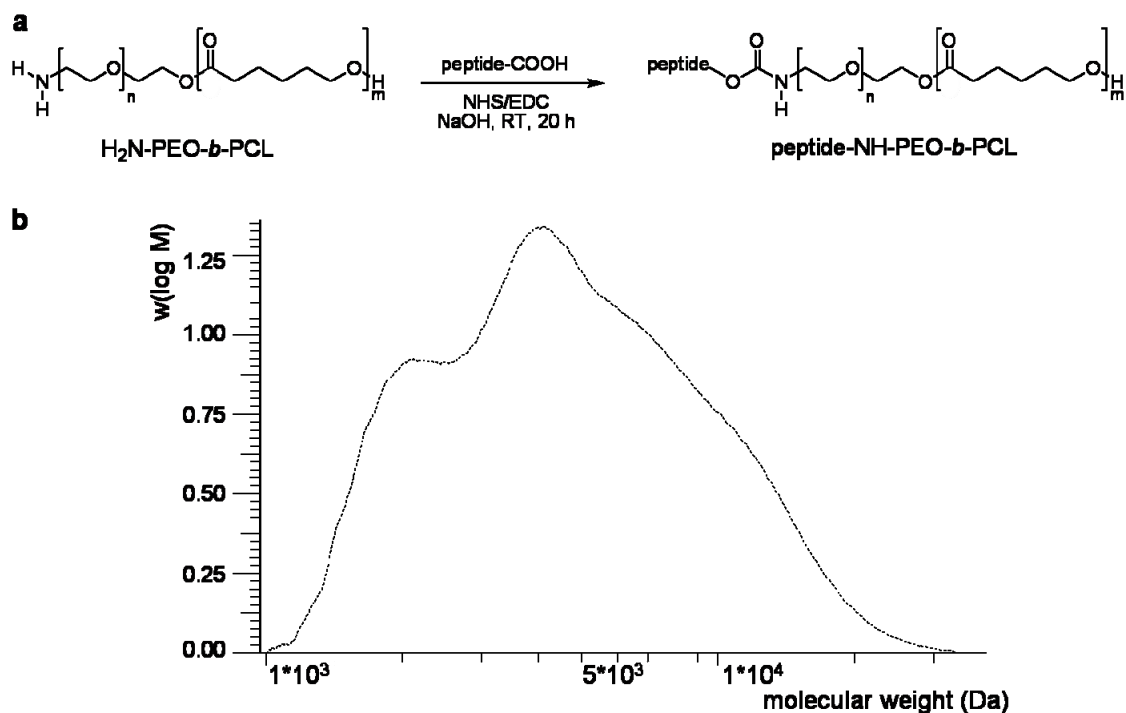


**Figure 4: Third step of the synthesis with peptide coupling to the amino-group.** (a) Reaction scheme and (b) the corresponding elugram from GPC.

NMR spectra from step 2 and 3 of the synthesis are not shown, because they do not differ from the spectrum shown in figure 2. The amount of amino protons in the deprotected polymer as well as protons from the peptide sequence were too little compared with the protons from the polymer blocks and thus did not appear in the spectrum. Therefore colour reactions were used to confirm the functionalisation steps of the synthesis. Amino groups were detected by their reaction with ninhydrin to the light coloured Ruhemann's violet. The reaction scheme and the thin layer chromatography plate are shown in figure 5. Here, the deprotected  $\text{H}_2\text{N-PEO-}b\text{-PCL}$  block copolymer (2) reacted with ninhydrin to a light violet coloured product (fig. 5b). The unprotected Boc-PEO- $b$ -PCL block copolymer (1) and a methoxy-functionalised PEO polymer (4) served as negative controls and did not show any colour reaction. The positive control of amino functionalised PEO polymer (3) presented the same reaction as the block copolymer (2) indicating the successful deprotection. The same test was performed with the Boc-PEO- $b$ -PCL block copolymer deprotected with a 10-fold excess of  $p$ -TSA. The absence of a colour reaction demonstrated that the amount of  $p$ -TSA was too small for the production of a detectable amount of amino groups.

## Synthesis and electrospinning of a GRGDS-functionalised PEO-*b*-PCL block copolymer

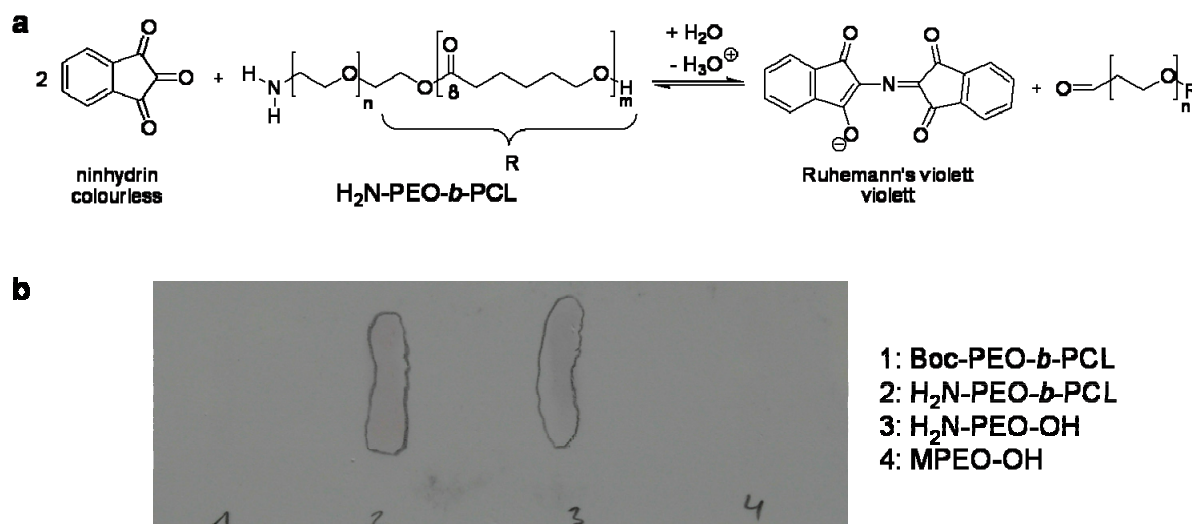


**Figure 5: Amino detection by reaction with ninhydrine.** (a) Reaction scheme and (b) thin layer chromatography plate with colour reaction of H<sub>2</sub>N-PEO-*b*-PCL block copolymer and several control polymers.

The peptide coupling of GRGDS to the amino functionalised block copolymer was confirmed by colour reaction with Sakaguchi reagent. Figure 6 shows the reaction scheme (fig. 6a) and a filter paper where different polymer solutions were applied to and treated with the reagent (fig. 6b). The amino acid arginine in the GRGDS peptide sequence reacted with Sakaguchi reagent to an orange dye complex. This effect could be noticed for the peptide functionalised block copolymer (4, 5) as well as for a diluted solution of the peptide alone (3) which served as positive control. Neither the methoxy-functionalised PEO polymer (1) nor the amino-functionalised block copolymer (2) showed a positive reaction with Sakaguchi reagent.

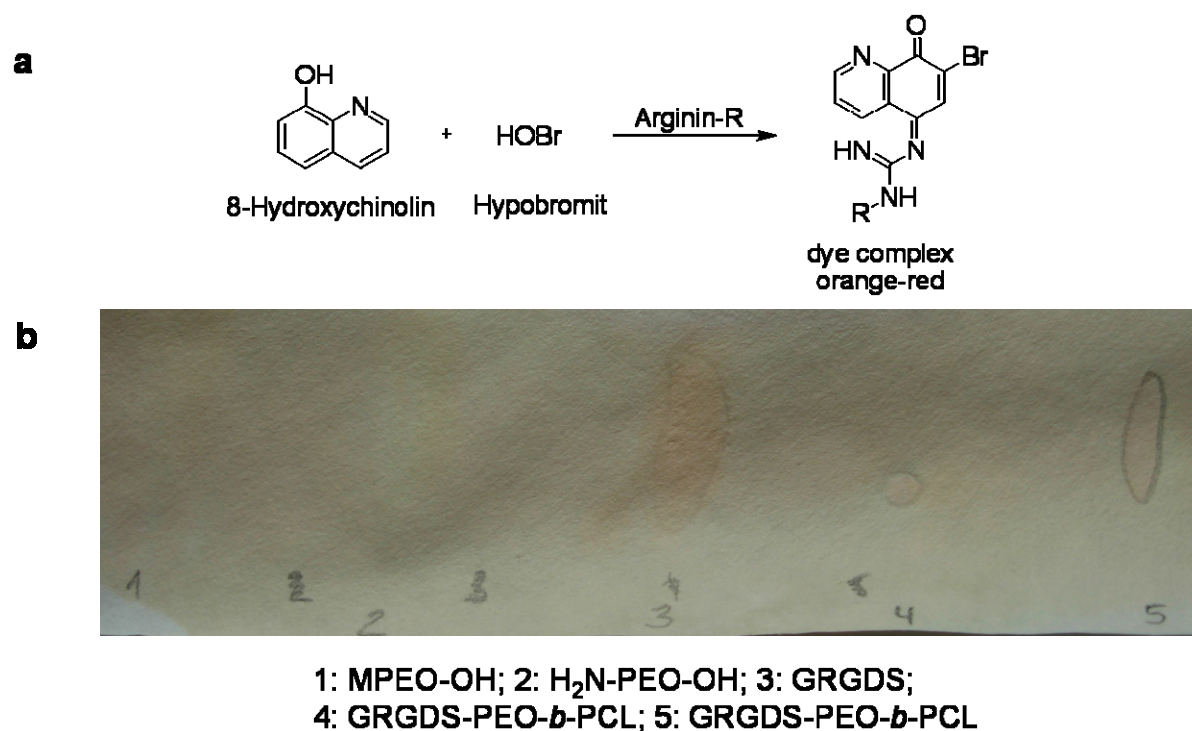


**Figure 6: Peptide detection by reaction with Sakaguchi reagent.** (a) Reaction scheme and (b) filter paper with colour reaction of GRGDS-PEO-*b*-PCL block copolymer and several controls.

### 7.3.2 Electrospinning of GRGDS-functionalised PEO-*b*-PCL block copolymer and fibre characterisation

Electrospinning of polymers from each synthesis step was performed to evaluate a dependency of spinnability and polymer functionalisation. Figure 7 shows images of these electrospinning products. The Boc-protected block copolymer could easily be electrospun to homogeneous oriented fibres with diameters of  $0.43 \pm 0.08 \mu\text{m}$  from a 16.5 wt% solution and using a voltage of 25 kV, a distance of 20 cm and a flow rate of 0.3 mL/h (fig. 7a). Other conditions (15 and 20 kV; 0.5 and 1.0 mL/h) resulted in similar fibres. Fibres with a similar quality and similar diameters were also achieved from the “partially deprotected“ Boc-PEO-*b*-PCL block copolymer. These fibres had diameters of  $0.44 \pm 0.10 \mu\text{m}$  and were produced from a 18 wt% solution with an applied voltage of 20 kV, a distance of 20 cm and a flow rate of 1 mL/h (fig. 7b). When the amount of deprotection reagent was increased to a 16-fold excess, it was impossible to obtain oriented fibres. Only random fibres connected by big polymer beads resulted from electrospinning of H<sub>2</sub>N-PEO-*b*-PCL. Figure 7c shows this product resulted from a 20 wt% solution. The additional purification steps (dialysis or shaking with NaHCO<sub>3</sub>) did not improve the quality of the electrospinning product. Peptide-coupling to this



## Synthesis and electrospinning of a GRGDS-functionalised PEO-*b*-PCL block copolymer

polymer prevented the electrospinning of fibres at all. Beads with diameters around 3  $\mu\text{m}$  were obtained from a 20 wt% solution (fig. 7d).

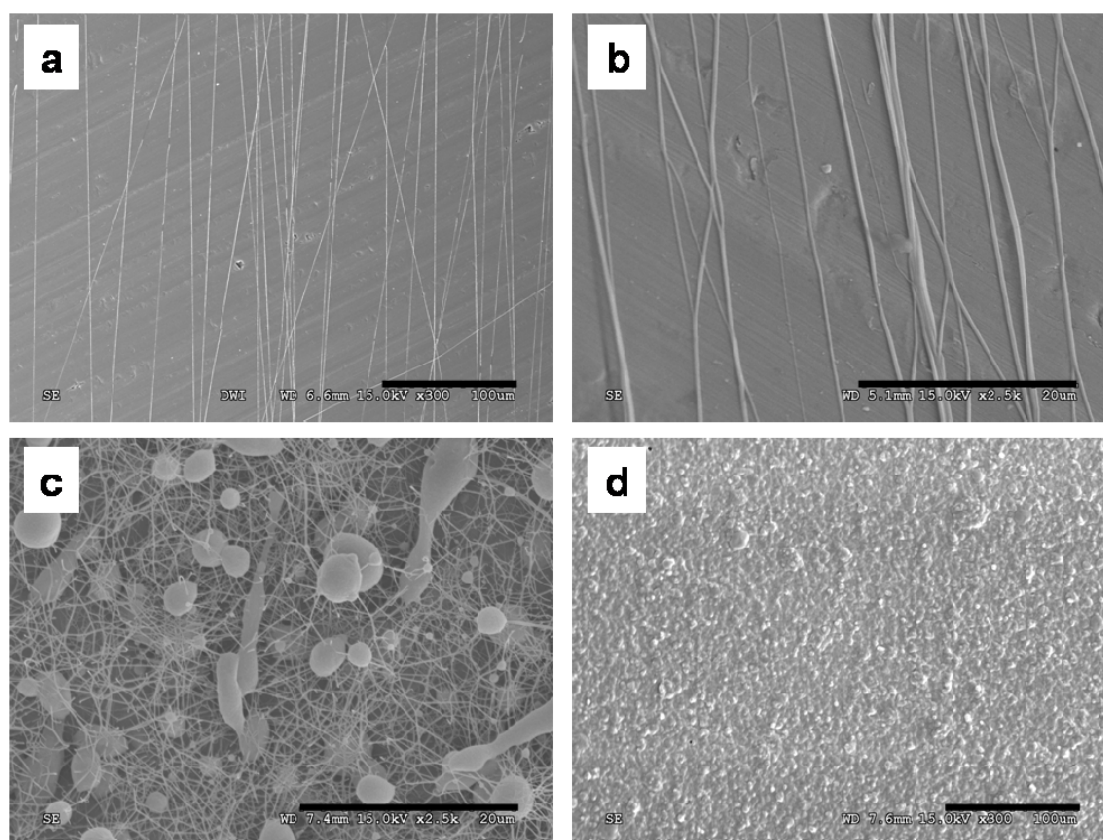


**Figure 7: Electrospinning products (a) Boc-PEO-*b*-PCL, (b) partially deprotected Boc-PEO-*b*-PCL, (c) H<sub>2</sub>N-PEO-*b*-PCL and (d) GRGDS-PEO-*b*-PCL block copolymers. Scale bars = 100  $\mu\text{m}$  (a, d) and 20  $\mu\text{m}$  (b, c).**

Electrospun fibres of Boc-PEO-*b*-PCL polymer were analysed regarding their protein adsorption properties by staining with rhodamine red conjugated bovine serum albumin. PCL fibres treated in the same manner served as control. Figure 8 shows that PCL fibres adsorbed a high value of proteins indicated by a strong red fluorescence. In contrast Boc-PEO-*b*-PCL fibres adsorbed very few proteins shown by slightly fluorescence of random fibres (fig. 8b).

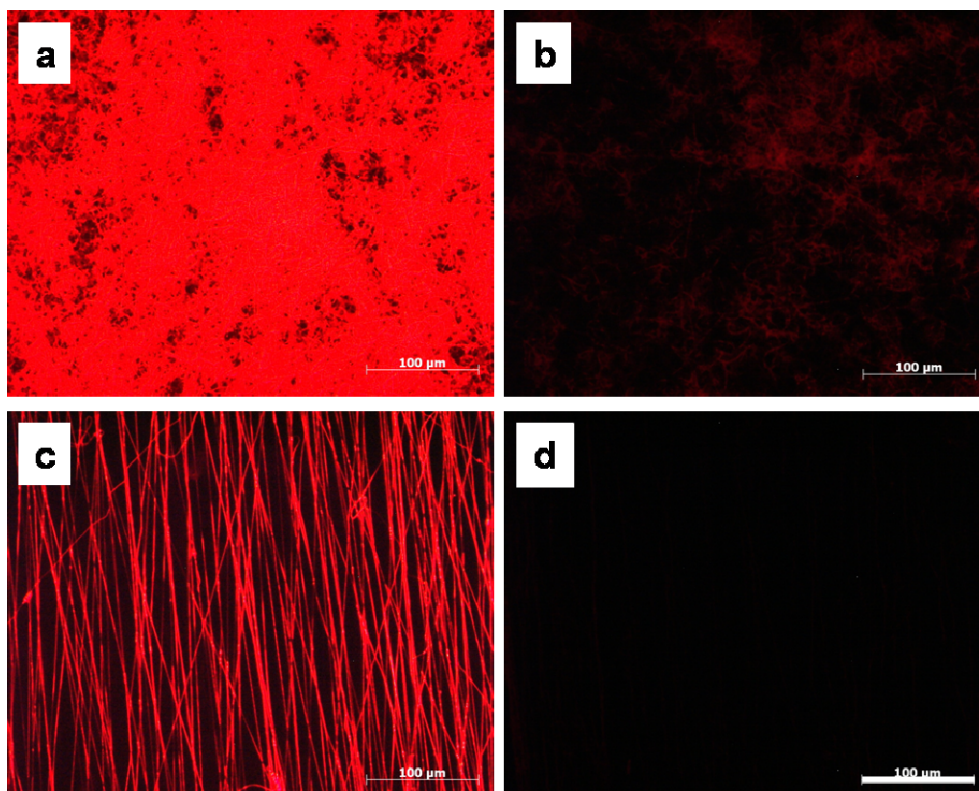


**Figure 8: Protein adsorption of (a, b) random and (c, d) oriented electrospun fibres of (a, c) PCL and (b, d) Boc-PEO-*b*-PCL block copolymer.** Fibres were stained with rhodamine red conjugated bovine serum albumin and images were taken with an exposure time of one second. Scale bar = 100 µm.

#### 7.4 Discussion

The subject of this study was the synthesis of a peptide functionalised PEO<sub>230</sub>-*b*-PCL<sub>560</sub> block copolymer and its electrospinning to oriented fibres. PEO-*b*-PCL block copolymers had demonstrated their useability in several tissue engineering strategies including drug delivery systems<sup>19,20</sup> and as non-woven fibres for cell attachment<sup>14,21</sup>. For tissue engineering application it is desired to design a biomaterial with specific body interactions. Due to the PEO block, these polymers can prevent cellular adhesion<sup>14</sup> and unspecific protein adsorption. Special biological properties, as for example cellular adhesion, can be brought to the block copolymer by functionalisation with cell adhesive peptide sequences such as GRGDS or naturally occurring ECM proteins such as fibronectin, collagen and laminin<sup>15</sup>.

The first step of the synthesis included ring-opening polymerisation of  $\epsilon$ -caprolactone with poly(ethylene oxide) as macroinitiator (fig. 1a). This synthesis using stannous II octoate

## **Synthesis and electrospinning of a GRGDS-functionalised PEO-*b*-PCL block copolymer**

as catalyst is well known in the literature<sup>13, 17</sup> and the preparation of high molecular weight PCL blocks was already performed successfully (chapter 6). The existence of the *tert*-butyloxycarbonyl (Boc) protection group did not affect the synthesis as GPC (fig. 1b) and NMR (fig. 2) analysis of the product showed. Good synthesis control was possible although the obtained molecular weight of the PCL block was about 4000 g/mol higher than desired. Electrospinning of this polymer resulted in highly oriented fibres with diameters in the nanometre range from several electrospinning conditions (fig. 7a).

In the second step of the synthesis, deprotection of the polymer was performed by usage of *p*-toluene sulfonic acid according to the method described by Brinkman *et al.* for protecting group removal in solid phase peptide synthesis<sup>22</sup>. This method is advantageous because it can be performed in DCM and THF, a solvent mixture suitable for both the deprotection reagent and the polymer. Additionally *p*-toluene sulfonic acid is less harmful than trifluoroacetic acid, the commonly used reagent for the removal of the boc protecting group<sup>23</sup>. This aspect is important in respect of a medical application of the produced fibres. The deprotection reagent was applied in a 16-fold volume per weight excess which is related to a 1200-fold molar excess. The successful formation of amino-groups was confirmed by colour reaction with ninhydrine (fig. 5). Obviously such high amounts were necessary as treating of Boc-PEO-*b*-PCL with a ten-fold volume per weight excess (900-fold molar excess) did not result in the formation of Ruhemann's violet. Unfortunately the high amount of deprotection reagent seems to cause degradation of the polymer, probably ester cleavage, indicated by the appearance of a shoulder in GPC spectrum of the deprotected polymer (fig. 3b). This effect was not estimated for the polymer deprotected with the smaller amount of *p*-TSA (fig. 3c) and influenced the spinnability of the polymer. While the partially deprotected polymer could be electrospun into oriented fibres (fig. 7b) this was not possible with the fully deprotected H<sub>2</sub>N-PEO-*b*-PCL block copolymer. Here only beaded fibres were obtained (fig. 7c) even with higher concentrations of the electrospinning solution. The electrospinning process was obviously disturbed by pollution with shorter block copolymers and residual salts from the deprotection step. This is similar to observations done before with polymers which were not purified (chapter 6). Further research is necessary to find a concentration of *p*-TSA that can generate amino-functionality but does not destroy the polymer backbone. Eventually another deprotection reagent would be useful.

The third step of the synthesis comprises the coupling of the peptide sequence GRGDS to the amino-functionalised block copolymer. This was performed using the well-known system of EDC and NHS (fig. 4a): the carboxyl group of the peptide sequence reacts with EDC to an unstable reactive *o*-acylisourea ester and by reaction with NHS a semi-stable amine-reactive NHS ester is build. By reaction with the amino group of the polymer a stable amid bond is formed (Pierce product data sheet). The coupling was confirmed by reaction of Sakaguchi reagent with the amine functionality of arginine forming a coloured complex (fig. 6). Electrospinning of this GRGDS-PEO-*b*-PCL block copolymer was not successful and beads instead of fibres were obtained (fig. 7c). Two important aspects can be used to explain the electrospinning results: Firstly, GPC showed the existence of an inhomogeneous polymer (fig. 4b) which is a result of the former deprotection step (fig. 3). Secondly, it is very likely that residual salt from the coupling step disturbed the electrospinning process additionally because it was performed in MES-buffer containing sodium hydroxide and sodium chloride. Small amounts of ions increase the conductivity of the electrospinning and normally result in higher quality of fibres but too high concentrations prevent electrospinning<sup>24</sup> as it seems to be the case here. Eventually a further purification step, additional to the dialysis, which removes residual salt as well as shorter polymer chains would help to overcome the problems with electrospinning.

Protein adsorption properties are an important issue for the development of biomaterials as unspecific adsorption can cause undesired body reactions such as inflammation and encapsulation<sup>25, 26</sup>. Investigations were performed with electrospun fibres of Boc-PEO-*b*-PCL block copolymers only because it was assumed that functionalisation with GRGDS did not cause an effect regarding these properties. The block copolymer prepared here showed hardly any protein adsorption (fig. 8b, d) which makes fibres from this material suitable for biomedical applications. The protein repellent properties make the GRGDS-functionalised block copolymer advantageous over blends of synthetic polymers with naturally proteins like PCL/collagen blends. They showed excellent biological activity<sup>10</sup> but cannot prevent the adsorption of proteins<sup>9</sup> in conjunction with unwanted body reactions such as encapsulation and inflammation.

### 7.5 Conclusion

A GRGDS-functionalised PEO<sub>226</sub>-*b*-PCL<sub>560</sub> block copolymer was successfully synthesised in three steps and the existence of the peptide sequence was confirmed by colour

reaction with Sagaguchi reagent. Due to its protein repellent properties this polymer is a suitable candidate for biomedical applications. Degradation of the polymer during synthesis and impurities prevented the electrospinning of the functionalised polymer to oriented fibres and further investigations to overcome these problems are necessary.

### 7.6 References

1. Xu, C. Y.; Inai, R.; Kotaki, M.; Ramakrishna, S., Aligned biodegradable nanofibrous structure: a potential scaffold for vessel engineering. *Biomaterials* **2004**, *25*, 877 - 886.
2. Bini, T. B.; Gao, S.; Tan, T. C.; Wang, S.; Aymeric Lim, A.; Hai, L. B.; Ramakrishna, S., Electrospun poly(L-lactide-*co*-glycolide) biodegradable polymer nanofibre tubes for peripheral nerve regeneration. *Nanotechnology* **2004**, *15*, 1459 - 1464.
3. Yu, T. T.; Shoichet, M. S., Guided cell adhesion and outgrowth in peptide-modified channels for neural tissue engineering. *Biomaterials* **2005**, *26*, 1507 - 1514.
4. Huang, Z. M.; Zhang, Y. Z.; Kotaki, M.; Ramakrishna, S., A review on polymer nanofibers by electrospinning and their applications in nanocomposites. *Composites Science and Technology* **2003**, *63*, (15), 2223 - 2253.
5. Li, D.; Xia, Y. N., Electrospinning of nanofibers: Reinventing the wheel? *Advanced Materials* **2004**, *16*, (14), 1151 - 1170.
6. Min, B. M.; Lee, G.; Kim, S. H.; Nam, Y. S.; Lee, T. S.; Park, W. H., Electrospinning of silk fibroin nanofibers and its effect on the adhesion and spreading of normal human keratinocytes and fibroblasts *in vitro*. *Biomaterials* **2004**, *25*, (7 - 8), 1289 - 1297.
7. Dalton, P. D.; Klee, D.; Möller, M., Electrospinning with dual collection rings. *Polymer* **2005**, *46*, (3), 611 - 614.
8. Li, D.; Wang, Y. L.; Xia, Y. N., Electrospinning of polymeric and ceramic nanofibers as uniaxially aligned arrays. *Nano Letters* **2003**, *3*, (8), 1167 - 1171.
9. Klinkhammer, K., Seiler, N., Grafahrend, D., Gerardo-Nava, J., Mey, J., Brook, G. A., Möller, M., Dalton, P. D. and Klee, D., Deposition of electrospun fibers on reactive substrates for *in vitro* investigations. *Tissue Engineering* **2009**, *15*, (1), 77 - 85.
10. Schnell, E.; Klinkhammer, K.; Balzer, S.; Brook, G.; Klee, D.; Dalton, P.; Mey, J., Guidance of glial cell migration and axonal growth on electrospun nanofibers of poly- $\epsilon$ -caprolactone and a collagen/poly- $\epsilon$ -caprolactone blend. *Biomaterials* **2007**, *28*, (19), 3012 - 3025.
11. Zhang, Y. Z.; Venugopal, J.; Huang, Z. M.; Lim, C. T.; Ramakrishna, S., Characterization of the surface biocompatibility of the electrospun PCL-collagen nanofibers using fibroblasts. *Biomacromolecules* **2005**, *6*, (5), 2583 - 2589.
12. Horbett, T. A., The role of adsorbed proteins in tissue response to biomaterials. In *Biomaterials Science: An introduction to materials in medicine*, 2nd ed.; Ratner, B. D., Hoffman, A. S., Schoen, F. J., Lemons, J. E., Ed. Elsevier: San Diego, 2004; pp 237 - 240.

13. Bogdanov, B.; Vidts, A.; Van Den Bulcke, A.; Verbeeck, R.; Schacht, E., Synthesis and thermal properties of poly(ethylene glycol)-poly( $\epsilon$ -caprolactone) copolymers. *Polymer* **1998**, 39, 1631 - 1336.
14. Grafahrend, D.; Calvet, J. L.; Salber, J.; Dalton, P. D.; Moeller, M.; Klee, D., Biofunctionalized poly(ethylene glycol)-block-poly(epsilon-caprolactone) nanofibers for tissue engineering. *Journal of Materials Science-Materials in Medicine* **2008**, 19, (4), 1479 - 1484.
15. Hersel, U., Dahmen, C., Kessler, H., RGD modified polymers: biomaterials for stimulated cell adhesion and beyond. *Biomaterials* **2003**, 24, 4385 - 4415.
16. Goetz, H.; Beginn, U.; Bartelink, C. F.; Grunbauer, H. J. M.; Möller, M., Preparation of isophorone diisocyanate terminated star polyethers. *Macromolecular Materials and Engineering* **2002**, 287, (4), 223 - 230.
17. Azzam, T.; Eisenberg, A., Monolayer-protected gold nanoparticles by the self-assembly of micellar poly(ethylene oxide)-*b*-poly( $\epsilon$ -caprolactone) block copolymer. *Langmuir* **2007**, 23, 2126 - 2132.
18. Grafahrend, D.; Calvet, J. L.; Klinkhammer, K.; Salber, J.; Dalton, P. D.; Moller, M.; Klee, D., Control of protein adsorption on functionalized electrospun fibers. *Biotechnology and Bioengineering* **2008a**, 101, (3), 609 - 621.
19. Allen, C.; Han, J.; Yu, Y.; Maysinger, D.; Eisenberg, A., Polycaprolactone-*b*-poly(ethylene oxide) copolymer micelles as a delivery vehicle for dihydrotestosterone. *Journal of Controlled Release* **2000**, 63, 275 - 286.
20. Xiong, X.-B.; Mahmud, A.; Uludag, H.; Lavasanifar, A., Conjugation of arginine-glycine-aspartic acid peptides to poly(ethylene oxide)-*b*-poly( $\epsilon$ -caprolactone) micelles for enhanced intracellular drug delivery to metastatic tumor cells. *Biomacromolecules* **2007**, 8, 874 - 884.
21. Dalton, P. D.; Klinkhammer, K.; Salber, J.; Klee, D.; Möller, M., Direct *in vitro* electrospinning with polymer melts. *Biomacromolecules* **2006**, 7, (3), 686 - 690.
22. Brinkman, H. R.; Landy Jr., J. J.; Paterson Jr., J. B.; Stone, P. J., The use of *p*-toluenesulfonic acid for removal of the N-t-butoxy-carbonyl protecting group in solid phase peptide synthesis. *Synthetic Communications* **1991**, 21, (3), 459 - 465.
23. Hanson, J. R., *Protecting groups in organic synthesis*. 1st ed.; Sheffield Academic Press: Sheffield, 1999; pp 82 - 83.
24. Kim, B.; Park, H.; Lee, S.-H.; Sigmund, W. M., Poly(acrylic acid) nanofibers by electrospinning. *Material Letters* **2005**, 59, (7), 829 - 832.
25. Johnson, R.; Harrison, D.; Tucci, M.; Tsao, A.; Lemos, M.; Puckett, A.; Hughes, J. L.; Benghuzzi, H., Fibrous capsule formation in response to ultrahigh molecular weight polyethylene treated with peptides that influence adhesion. *Biomed. Sci. Instrum.* **1997**, 34, 47 - 52.
26. Tang, L., Jennings, T. A., Eaton, J. W., Mast cells mediate acute inflammatory responses to implanted biomaterials. *PNAS* **1998**, 95, 8841 - 8846.

# FUNCTIONALISATION OF ELECTROSPUN FIBRES OF POLY( $\epsilon$ -CAPROLACTONE) AND STAR SHAPED NCO-POLY(ETHYLENE GLYCOL)-*STAT*-POLY(PROPYLENE GLYCOL) FOR NEURONAL CELL GUIDANCE

## 8.1 Introduction

Tissue engineering strategies are directed to restore physiological functions using artificial implants. Synthetic scaffolds are intended to repair the damage caused by injuries. This has a special importance in the case of the peripheral nervous system (PNS). *In vivo* cells are surrounded by a three-dimensional network of filaments, the extracellular matrix (ECM), which provides a growth permissive substrate for axonal regeneration. Biomaterials for nerve repair therefore have to mimic the properties of the ECM including its fibrillar structure and biochemical signals to the cells. Specifically, the ECM of lesioned peripheral nerves confers information to induce Schwann cell (SC) proliferation, migration and differentiation and to guide nerve fibres regeneration. After peripheral nerve injury, if proximal and distal nerve stumps remain in contact with each other, Schwann cells reorganise and align to form the axon growth promoting bands of Büngner<sup>1</sup>. Artificial substrates consisting of single fibres or bundles of fibres can serve as attractive guidance structures for oriented SC migration and neurite outgrowth<sup>1-3</sup>.

The method of electrospinning offers the possibility to produce microfibre scaffolds with diameters similar to that of ECM fibrils (0.5 - 5  $\mu\text{m}$ ) to act as cell adhesive substrates. With this technique, a high voltage is applied to a solution of (synthetic or natural) polymers generating a liquid jet. During its way to the grounded target the jet is continuously stretched due to electrostatic repulsion between surface charges whereas evaporation of the solvent leads to a solid fibre collected on the target<sup>4</sup>.

For the application as guidance structures in regenerating peripheral nerves, the prepared fibres were desired to be aligned in parallel, of homogeneous thickness and free of defects. Solution properties including polymer composition, molecular weight of the polymer, solution concentration and surface tension and polarity of the solvent predominantly influence the resulting fibres. However, governing parameter such as applied voltage, flow rate and distance between spinneret and target are also important<sup>5</sup>. Using different collector setups

result in different fibre arrangements. Two parallel bars (referred to as gap-method) allow the collection of oriented fibres which are suspended in air. This offers the possibility to deposit the fibres on various substrates such on chemically reactive hydrogel layers<sup>6</sup>.

In the development of a scaffold for nerve regeneration one must consider not only shape and mechanical strength of the implant but also biocompatibility of the material and its surface and bulk properties. Following implantation into the body, endogenous proteins immediately interact with the biomaterial according to their particular affinities to the material, and host cells respond to these adsorbed protein layers<sup>7</sup>. Nevertheless, unspecific protein adsorption is often undesired because it can cause problems such as acute and chronic inflammation<sup>8</sup> as well as fibrous encapsulation<sup>9</sup>. Protein resistant surfaces, mainly in the form of hydrogels and hydrogel coatings, should be hydrophilic, uncharged and flexible. Polyethylene glycol (PEG) fulfils these demands and is capable of masking the foreign nature of implants within the host organism. PEG is non-toxic and nonimmunogenic and has demonstrated its protein repellence in several studies<sup>10-12</sup>. Electrospun fibres consisting of poly(ethylene glycol)-*block*-poly(D,L-lactide) block copolymers have already shown their biocompatibility and protein resistance properties<sup>13</sup>. Star shaped NCO-poly(ethylene glycol)-*stat*-poly(propylene glycol), which is named “sPEG” in the following text instead of the chemical more correct description of “sP(EO-*stat*-PO)” allows the preparation of a dense polymer network by cross-linking of the arms via functional groups. This prevents unspecific proteins and has been shown to be superior to linear PEG-coatings<sup>14</sup>.

In contrast to undesired non-specific protein adsorption, specific protein- and cell-substrate interactions are required for successful integration and tissue repair. These special interactions can be triggered by surface functionalisation with special biological signals (e.g. ECM proteins, peptides or polysaccharides). Such biological signals showed the highest activity when immobilised on the scaffold, while proteins including collagen and laminin, are known to support cell adhesion via activation of integrin receptors<sup>15</sup>. Fibronectin (Fn) is an ECM glycoprotein and is known to play a role in neuronal migration and nerve regeneration after injury. Fibronectin and at least one of its receptors have been suggested to be important for nerve regeneration possibly by facilitating of Schwann cells<sup>16,17</sup>. The best-known peptide sequence of fibronectin is the amino acid sequence Arg-Gly-Asp (RGD) which additionally occurs in the ECM proteins collagen and laminin and is known to support cell adhesion by cells binding via integrin receptors<sup>15</sup>.

In this study, a method for the production of aligned biodegradable electrospun fibres based on a blend of PCL with functionalised sPEG was developed. The hydrophilic properties



of sPEG prevented unspecific protein adsorption while the covalent binding of the RGD peptide, used with flanking amino acids Gly and Ser (GRGDS) or with the fibronectin protein within the electrospinning solution resulted in favourable biological properties as revealed by *in vitro* assays using dorsal root ganglia explants.

## 8.2 Materials and Methods

### 8.2.1 Materials

Unless otherwise stated, all chemicals were purchased from Sigma-Aldrich (Munich, Germany). Toluene and tetrahydrofuran (THF) were dried by distillation over lithium aluminium hydride and stored in a nitrogen atmosphere. Acetone was dried statically over molecular sieve (3Å) for 3 days and then distilled in a nitrogen atmosphere. It was stored over molecular sieve and nitrogen. Star shaped NCO-poly(ethylene glycol)-*stat*-poly(propylene glycol) (with a backbone of 80 % ethylene oxide and 20 % propylene oxide and isocyanate end groups, Mw = 12000 g/mol) (sPEG) was synthesised in our laboratory from hydroxyl-terminated star polymer (DOW-chemicals, Terneuzen, NL) by reaction with isophorone diisocyanate according to details published elsewhere<sup>18</sup>. All other chemicals were used as received.

### 8.2.2 Solution preparation

Two different systems were chosen to determine electrospinning ability and cellular response on PCL/sPEG fibres. In the first part of experiments, fibres consisting of poly( $\epsilon$ -caprolactone) (PCL) (Mw = 65000 g/mol) with sPEG were produced. PCL was dissolved (17 wt%) in a mixture of dry dichloromethane (DCM) (p.a., crown capped) and dry acetone (1/1 v/v) or THF. Then a specific amount of sPEG (15 or 27 wt% of the solid fraction) dissolved in a third solvent (dimethyl sulfoxide (DMSO), N-methylpyrrolidone (NMP) or dimethylformamide (DMF)) was added. The volume of the third solvent containing sPEG was 5 % of the total solution. The mixture was stirred for 1 min. These blends were called “P-PEG” according to the combination of PCL and sPEG and the solution compositions are summarised in table 1.

**Table 1: Solution concentrations and polymer concentrations for the different PCL/sPEG blends consisting of PCL and sPEG.**

	Name	P-PEG1	P-PEG2	P-PEG3	P-PEG4	P-PEG5	P-PEG6	P-PEG7	P-PEG8
solvents	1. solvent	acetone	acetone	acetone	acetone	acetone	THF	THF	THF
	2. solvent	DCM	DCM	DCM	DCM	DCM	—	—	—
	3. solvent	DMSO	NMP	DMSO	NMP	DMF	DMSO	NMP	DMF
solutions which were mixed to prepare electrospinning solution	c(PCL-65k-solution) (wt%)	17	17	17	17	17	17	17	17
	c (sPEG-solution) (wt%)	57	57	54	54	54	54	54	54
<b>c(total electrospinning solution) (wt%)</b>		<b>23</b>	<b>23</b>	<b>26</b>	<b>26</b>	<b>26</b>	<b>26</b>	<b>26</b>	<b>26</b>
concentration of polymers in electrospun fibres	wt% (PCL-65k in fibre)	85	85	73	73	73	73	73	73
	wt% (sPEG in fibre)	15	15	27	27	27	27	27	27

In the second approach, different solutions were prepared first from three polymers resulting in eleven different mixtures: (1) a 15, 17 or 20 wt% solution of PCL in dry THF or in a mixture of dry DCM and dry acetone (1/1 v/v); (2) poly( $\epsilon$ -caprolactone)-diol (PCL-ol) ( $M_w = 2000$  g/mol) was dissolved with the same solvents resulting in solutions with 7.4 to 57.9 wt%; (3) sPEG was dissolved in THF resulting in a 50 % or 36 % (w/v) solution. To prepare the electrospinning solution with a total solution concentration of 15, 17 or 22 wt%, the PCL-ol solution was added to the sPEG solution, stirred for one min, followed by adding the PCL solution and stirring again one min. Finally, another solvent, N-methylpyrrolidone (NMP) or dimethyl formamide (DMF) (5 % of total solution (w/v)) was added as a fourth solvent and the mixture was stirred for another 30 sec. These blends were called “PPol-PEG” according to the combination of PCL, PCL-diol and sPEG. The solution compositions are summarised in table 2.

**Table 2: Solution concentrations and polymer concentrations for the different PCL/sPEG blends consisting of PCL, PCL diol and sPEG.**

	Name	PPol-PEG1	PPol-PEG2	PPol-PEG3	PPol-PEG4	PPol-PEG5	PPol-PEG6
solvents	1. solvent	acetone	acetone	acetone	acetone	THF	THF
	2. solvent	DCM	DCM	DCM	DCM	--	--
	3. solvent	THF	THF	THF	THF	THF	THF
	4. solvent	NMP	NMP	NMP	NMP	DMF	DMF
solutions which were mixed to prepare electro-spinning solution	c(solution 1, PCL-65k-solution) (wt%)	15	15	15	17	15	15
	c(solution 2, PCL-diol) (wt%)	40.2	53.1	57.9	50.6	28.3	35.6
	c(solution 3, sPEG) (wt%)	50	50	50	36	50	50
<b>c(total electrospinning solution) (wt%)</b>		<b>17</b>	<b>17</b>	<b>17</b>	<b>22</b>	<b>15</b>	<b>15</b>
concentration of polymers in electro-spun fibres	wt% (PCL-65k in fibre)	90	75	60	57.4	75	60
	wt% (PCL-diol in fibre)	3	8	13	13.1	8	13
	wt% (sPEG in fibre)	7	17	27	29.5	17	27
	Name	PPol-PEG7	PPol-PEG8	PPol-PEG9	PPol-PEG10	PPol-PEG11	
solvents	1. solvent	THF	THF	THF	THF	THF	
	2. solvent	--	--	--	--	--	
	3. solvent	THF	THF	THF	THF	THF	
	4. solvent	DMF	DMF	DMF	DMF	DMF	
solutions which were mixed to prepare electro-spinning solution	c(solution 1, PCL-65k-solution) (wt%)	15	20	20	20	20	
	c(solution 2, PCL-diol) (wt%)	40.2	7.4	16.7	24.8	31.8	
	c(solution 3, sPEG) (wt%)	50	50	50	50	50	
<b>c(total electrospinning solution) (wt%)</b>		<b>15</b>	<b>15</b>	<b>15</b>	<b>15</b>	<b>15</b>	
concentration of polymers in electro-spun fibres	wt% (PCL-65k in fibre)	44	90	75	59	44	
	wt% (PCL-diol in fibre)	19	3	8	14	19	
	wt% (sPEG in fibre)	37	7	17	27	37	

Table 3 gives details about the solution properties, calculated for a sPEG amount of 0.05 g each.

**Table 3: Solution composition for the different PPol-PEG mixtures.**

Name	PPol-PEG1	PPol-PEG2	PPol-PEG3	PPol-PEG4	PPol-PEG5	PPol-PEG6
m (sPEG) (g)	0.05	0.05	0.05	0.05	0.05	0.05
V (THF for sPEG) (mL)	0.1	0.1	0.1	0.14	0.1	0.1
m (PCL_65k) (g)	0.639	0.219	0.110	0.097	0.219	0.110
m (PCL-diol) (g)	0.025	0.025	0.025	0.022	0.025	0.025
m (PCL_65k-solution) (g)	4.262	1.461	0.735	0.571	1.461	0.734
m (PCL-diol-solution) (g)	0.062	0.047	0.043	0.044	0.088	0.070
V (4. solvent) (mL) (5 %)	0.224	0.083	0.046	0.038	0.085	0.048
Name	PPol-PEG7	PPol-PEG8	PPol-PEG9	PPol-PEG10	PPol-PEG11	
m (sPEG) (g)	0.05	0.05	0.05	0.05	0.05	
V (THF for sPEG) (mL)	0.1	0.1	0.1	0.1	0.1	
m (PCL_65k) (g)	0.060	0.639	0.219	0.110	0.060	
m (PCL-diol) (g)	0.025	0.025	0.025	0.025	0.025	
m (PCL_65k-solution) (g)	0.401	3.196	1.096	0.551	0.301	
m (PCL-diol-solution) (g)	0.062	0.338	0.150	0.101	0.079	
V (4. solvent) (mL) (5 %)	0.031	0.184	0.070	0.040	0.027	

For biologically functionalised fibres, the peptide sequence GRGDS (Bachem, Bubendorf, Switzerland; PPol-PEG3+RGD) or the ECM protein fibronectin (Biopur AG, Bubendorf, Switzerland, PPol-PEG4+Fn) was given to the NMP before this was added. The amount of GRGDS was one fifth of the amount of sPEG ( $n(\text{GRGDS}) = 1/5 n(\text{sPEG})$ ). Fibronectin was applied at a ratio of 1:250 (weight of fibronectin:weight of all polymer solids), which correlates to a ratio of sPEG to fibronectin of 2 : 1. Additionally a 9 wt% solution of PCL in methanol / chloroform (1/3 v/v) was prepared.

Fibres were termed “PCL/sPEG” when fibres containing PCL, PCL-diol and sPEG or PCL and sPEG were investigated without distinguishing between them (in contrast to pure PCL fibres). The solvent properties of the used solvents are summarised in table 4.

**Table 4: Properties of the solvents used in the electrospinning experiments.**

	Boiling point* (°C)	Vapour pressure* (20 °C, hPa)	Dielectric constant** (25 °C, Fm <sup>-1</sup> )	Surface tension# (Dyne / cm)
acetone	56	233	20.7	25
DCM	40	475	8.9	27
DMF	153	3.77	36.7	22
DMSO	189	0.56	46.7	43 <sup>+</sup>
NMP	202	0.32	36.7	41
THF	66	173	7.58	26

(\*www.merck.de, \*\*http://macro.lsu.edu/, #www.surface-tension.de, +www.bulkmsm.com)

### 8.2.3 Electrospinning

For electrospinning the solution was filled in a 1 mL syringe with a single-use blunt-end 21 gauge needle, (Hamilton, Bonaduz, Switzerland) and ejected with a defined flow rate. The needle was connected to a high voltage supply (Bertan, Spellman high voltage electronics corporation, Hauppauge, NY, USA) and a high voltage was applied to the polymer solution. Various voltages (10 – 25 kV), flow rates (0.5 - 2 mL/h) and working distances (5 - 25 cm) between needle and target were used. A scanning electron microscopy (SEM) stub (diameter = 14 mm) covered with aluminium foil was used for random fibres collection. Two parallel bars with a distance of 2 cm between them served as targets for oriented fibre collection. Pure PCL fibres served as controls and were produced by electrospinning with a voltage of 20 kV, a flow rate of 0.5 mL/h and a distance between needle and target of 20 cm.

### 8.2.4 Substrate preparation

Glass coverslips (No. 1, diameter: 12 mm, Marienfeld, Lauda-Königshofen, Germany) and silicon wafers were surfaced modified with a protein resistant sPEG-layer according substrate preparation 4.2.2. in chapter 4. Oriented fibres were deposited onto the substrates by drawing the substrate through the mat of suspended fibres. Random fibres were directly electrospun onto the reactive substrates.

### 8.2.5 Fibre characterisation

#### *Scanning electron microscopy (SEM)*

The electrospun fibres were visualised by scanning electron microscopy (SEM) (S360 Zeiss NTS, Oberkochen, Germany and Hitachi S3000 N, Hitachi High Technology Europe GmbH, Krefeld, Germany), using 15 kV and working distances of 5 to 15 mm after sputtering with gold for 90 s (S150B, Edwards, Crawley, Great Britain). The SEM images were used to

measure fibre diameters. For each preparation at least 30 fibers were measured and data are presented as mean +/- standard deviation. The same images were used to estimate the orientation distribution of the fibers.

### *Volume porosity*

The volume porosity of electrospun fibres were measured using SEM images. Here, the length of each fibre was measured and multiplied with the fibre diameter. To calculate the area which was covered by the fibres, these numbers were added together. This value was divided by the total area of the image and multiplied with 100 to get the volume porosity in percent. At least three images and 30 fibres per fiber material were used for the calculation. Data are presented as mean +/- standard deviation.

### *Contact angle measurements*

For contact angles measurements, fibres from the different materials (PCL and PPol-PEG3 and PPol-PEG4) were firstly collected as thick mats on aluminium surfaces with a diameter of 12 mm as substrates. Six samples per material were estimated using a contact angle measuring system (G2 with DSA II software, Krüss GmbH, Hamburg, Germany). A small droplet of distilled water (5 µl) was placed on the sample and 10 images from the droplet were taken automatically. Two contact angles per image (from the right and left side of the droplet) were calculated.

### *Protein adsorption*

Random PCL/sPEG fibres and fibres of PCL were collected onto sPEG coated silicon wafers. Four samples were prepared for each composition. Half of the samples were incubated in water for 5 days, washed with fresh distilled water afterwards and dried in a nitrogen stream. The second half remained untreated. Protein adsorption of the incubated and non-incubated fibres were determined using fluorochrom-labeled bovine serum albumin (BSA, Invitrogen, Karlsruhe, Germany) as previously described<sup>6, 13</sup>. Briefly, the various substrates were incubated for 20 min with rhodamine red labeled BSA (50 µg/mL) diluted in phosphate buffered saline buffer (PBS) followed by three washing steps (20 min each) in PBS. The samples were then incubated for 60 min in PBS and washed thoroughly with distilled water to remove not adsorbed proteins and dried with nitrogen. The samples were kept in the dark during incubation and washing. Protein adsorption was examined by fluorescence microscopy

(Axioplan 2 imaging, Zeiss, Germany), and images were taken with a constant exposure time of 20 s.

The same samples were additionally visualised with SEM to investigate the influence of water incubation on fibre morphology.

### *X-ray photoelectron spectroscopy*

Small fibre mats (2 x 8 mm) were examined by x-ray photoelectron spectroscopy (XPS) (Ultra Axis<sup>TM</sup> spectrometer, Kratos Analytical, Manchester, Great Britain) to investigate the atomic composition of the surfaces of the different PCL and PCL/sPEG fibres. Untreated samples and fibres which were incubated in water for five days and dried in a vacuum afterwards were investigated. The samples were irradiated with monoenergetic Al K $\alpha$ 1,2 radiation (1486.6 eV) and the spectra were taken at a power of 144 W (12 kV x 12 mA). The elemental concentration is given in atom%, but it should be stated that this method can detect all elements except hydrogen and helium and that therefore, the determination of the composition does not include these elements.

### **8.2.6 *In vitro* assays**

For *in vitro* cell experiments, orientated electrospun fibres were deposited onto glass coverslips which had been surface modified with a thin layer of sPEG hydrogel. To investigate migration of Schwann cells and regeneration of sensory axons on microfibres, explants of dorsal root ganglia (DRG) from chicks were placed on PPol-PEG3 fibres, GRGDS-functionalised PPol-PEG3 fibres, fibronectin-functionalised PPol-PEG4 fibres and PCL fibres. All substrates were sterilised with 70% ethanol for 10 min and washed three times (15 min each) with PBS before cell experiment application.

### *Dorsal root ganglia preparation and explants*

DRG were prepared from embryonic day 10 chick embryos as published previously<sup>2</sup>. Two to three DRG per cover slip were explanted onto the fibres. First 100  $\mu$ l cell culture medium (Dulbecco's modified Eagle Medium-DMEM, Gibco/Life Technologies), with 10 % fetal calf serum, 500  $\mu$ l fungizone and 2.5 mL penicillin/streptomycin were added to allow the tissue to adhere to the substrate. After a few hours in the incubator, an additional 400  $\mu$ l medium was given to ensure sufficient nutrition of the tissue. Explants were incubated for 4 days *in vitro* (DIV), then fixed 30 min with 4 % paraformaldehyde and stained immunocytochemically prior to microscopically analysis.

### *Neurite outgrowth*

Neurite outgrowth was measured using image J software on a montage of neurofilament stained images taken from DRG samples. Axon lengths were measured from the border of the DRG to the tips of the outgrowing neurites. For every explant the axons were separately evaluated on the two sides of the explant in parallel with the underlying microfibres. For each side, the 20 longest axons (if less: all axons) were measured.

### *Schwann cell migration*

The same DRGs were also used for Schwann cell migration measurements using S100/DAPI staining. Regions with a width of 50  $\mu\text{m}$  were selected on the two opposite sides of the explants, where nanofibres orientation was perpendicular to the edge of the explant, and cells were able to migrate in parallel to the fibre substrate. On these sides most cells migrated and the farthest migration distance was measured. The distance of the 10 farthest migrating cells of each side was determined using Image J software.

### *Immunohistochemistry*

Standard immunocytochemical staining procedures were used. The blocking solution was 2 % normal goat serum (G9023, Sigma) in tris buffered saline with 0.4 % Triton X 100 (Carl Roth, Karlsruhe, Germany). We used primary antibodies against S100 (polyclonal rabbit serum, S2644, Sigma; 1:100 dilution) to visualise Schwann cells, and against neurofilament (NF200; mouse monoclonal antibody, N0142, Sigma; 1:300-dilution) to mark neurons and axons. Samples were incubated with primary antibodies for 1 h at 37° C. As secondary antibodies Alexa Fluor™ 546 goat anti rabbit IgG (Molecular Probes, A-110106) and Alexa Fluor™ 488 goat anti mouse IgG (Molecular Probes, A-11001) were applied in dilution of 1:500, also for 1 h at 37° C. Cell nuclei were stained using 4',6-diamidino-2 phenylindole dihydrochloride (DAPI; 0,5 $\mu\text{g}/\text{ml}$ , Sigma), 5 min at room temperature. Results were evaluated using Zeiss Cell Observer Microscope coupled to MosaiX software and Zeiss Axiophot epifluorescence microscope (Carl Zeiss, Oberkochen, Germany) connected to on on-line digital camera (Spot Basic software).



### 8.3 Results

#### 8.3.1 Electrospinning

Electrospinning was performed with two solution systems (P-PEG and PPol-PEG) as described earlier. Figure 1 shows a schematic illustration of the electrospinning process, indicating the chemical reactions assumed to take place during fibres preparation.

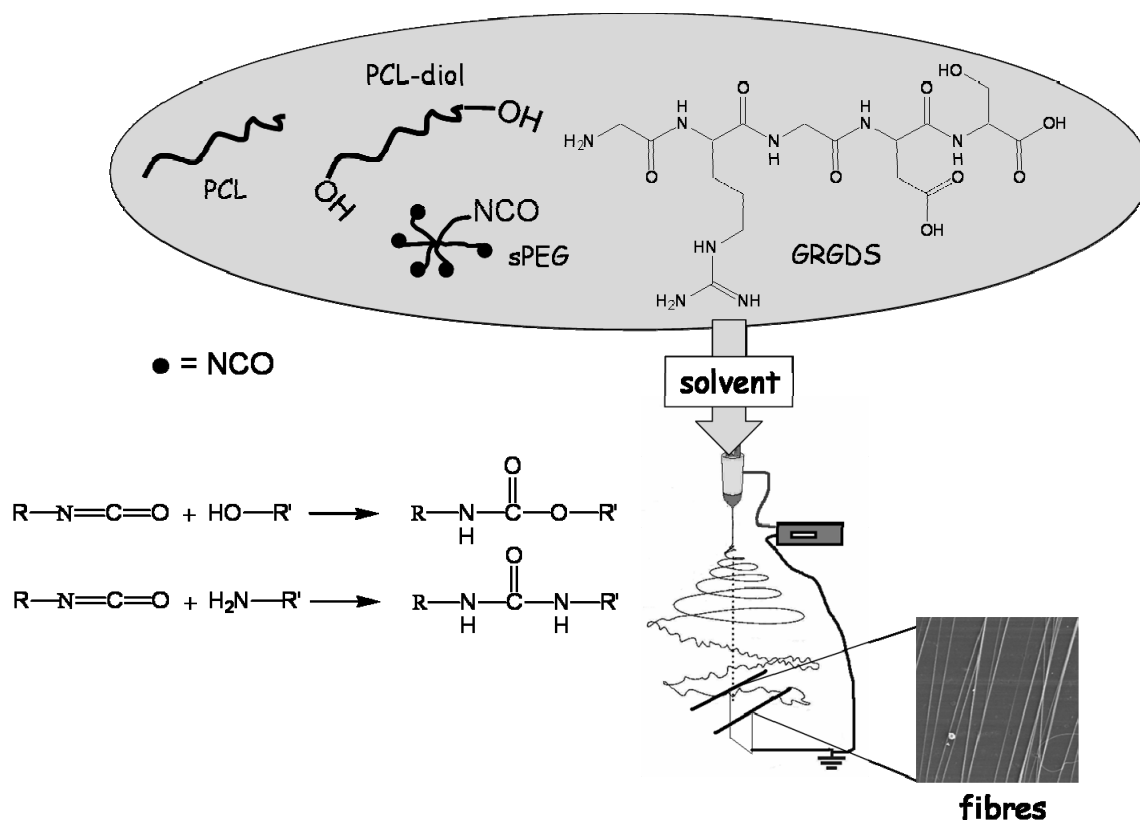


**Figure 1: Preparation of electrospinning solution and chemical reaction between components.** For the preparation of the electrospinning solution the different compounds PCL, PCL-diol, sPEG and RGD were mixed according tables 1 and 2 and dissolved in a solvent mixture. These solutions were electrospun to oriented fibres. Chemical reactions between isocyanate groups of the sPEG molecules and amine or hydroxyl groups of PCL and GRGDS form urethane and urea groups respectively and resulted in covalent binding between the molecules. Reprinted from reference 19, figure 1. With kind permission from Springer Science and Business Media.

Since high quality of electrospinning is necessary for the collection of parallel fibres, needed for the regeneration assays, much effort was expended in determining the optimal parameters for this purpose. The high quality fibres were indicated by alignment and suspension of fibres between the two parallel bars and a low variability of fibre diameter.

Variations of solvent mixtures, sPEG content and spinning parameters including voltage, flow rate and distance between needle and target were tested systematically. It was found that different process parameter had to be selected for the individual chemical compositions. In general, a voltage of 20 kV and a needle-target distance of 20 cm resulted in the best fibres.

In the first approach, fibres were produced by electrospinning from mixtures of high molecular weight PCL with different concentrations of sPEG (P-PEG). Different concentrations of sPEG (15 and 27 wt%) and different solvent compositions were used (see table 1). Figure 2 shows that blends of PCL with 15 wt% sPEG resulted in high quality fibres collected in an oriented manner independently which solvent was used (DMSO or NMP as third solvent). With both solvents orientated fibres with diameters of  $0.92 \pm 0.29 \mu\text{m}$  (DMSO, fig. 2a, P-PEG1) respectively  $0.64 \pm 0.11 \mu\text{m}$  (NMP, fig. 2b, P-PEG2) were obtained. Although electrospinning with DMSO tended to produce fibres with larger diameters, this effect was not statistically significant.

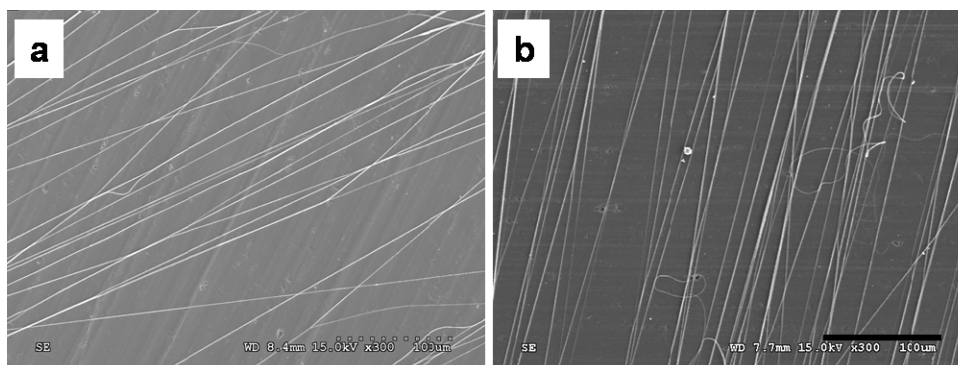


**Figure 2: Electrospun fibres produced with 15 wt% sPEG from different solvents.** (a) acetone/DCM + DMSO (P-PEG1) [20 kV, 20 cm, 1 mL/h] and (b) acetone/DCM + NMP (P-PEG2) [30 kV, 20 cm, 1 mL/h]. Scale bar = 100  $\mu\text{m}$ . Reprinted from reference 19, figure 2. With kind permission from Springer Science and Business Media.

Increasing the sPEG content up to 27 wt% in the blends with PCL affected the quality of the fibres. Figure 3 shows SEM images of electrospun fibres produced with 27 wt% sPEG from different solvent mixtures with acetone/DCM or THF. From electrospinning with the solvent system acetone/DCM/DMSO a fibre network of so-called “wet-fibres” occurred (fig. 3a, P-PEG3) irrespectively which electrospinning conditions were chosen. The use of NMP as third solvent resulted in thick, low quality oriented fibres with diameter of  $1.68 \pm$

0.87  $\mu\text{m}$  (fig. 3b, P-PEG4). When DMF was used as third solvent, oriented fibres with a better quality were obtained, but these fibres were very thick with diameters of  $2.36 \pm 0.82 \mu\text{m}$  (fig. 3c, P-PEG5). The fibres which were electrospun from acetone/DCM were compared with fibres electrospun from THF with the same additional solvents. Using DMSO resulted in evenly oriented fibres with very few beads and diameters of  $0.72 \pm 0.27 \mu\text{m}$  (fig. 3d, P-PEG6). With NMP as additional solvent, the fibre diameter of the oriented fibres was slightly increased to  $0.96 \pm 0.33 \mu\text{m}$  (fig. 3e, P-PEG7). With DMF the fibre collection was difficult and a low number of fibres with diameters of  $1.46 \pm 0.44 \mu\text{m}$  (fig. 3f, P-PEG8) occurred. P-PEG2 and P-PEG4 fibres were used for further investigations.

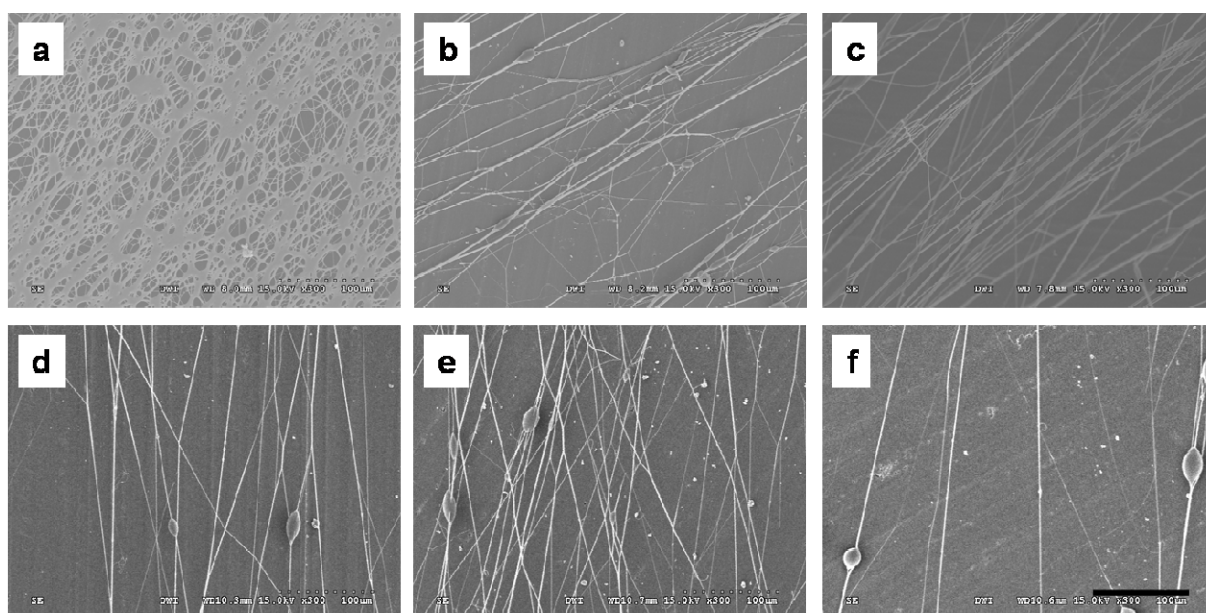


**Figure 3: Electrospun fibres with 27 wt% sPEG produced with different solvent systems.**

(a) acetone/DCM + DMSO (P-PEG3) [20 kV, 20 cm, 1.5 mL/h]; (b) acetone/DCM + NMP (P-PEG4) [20 kV, 20 cm, 3 mL/h]; (c) acetone/DCM + DMF (P-PEG5) [20 kV, 20 cm, 3 mL/h]; (d) THF + DMSO (P-PEG6) [20 kV, 18 cm, 1.5 mL/h]; (e) THF + NMP (P-PEG7) [20 kV, 18 cm, 1.5 mL/h]; (f) THF + DMF (P-PEG8) [20 kV, 18 cm, 3 mL/h]. Scale bar = 100  $\mu\text{m}$ . The values in brackets indicate the electrospinning conditions used for the fibre production.

In the second system, fibres were electrospun from solutions of PCL, PCL-ol and different amounts of sPEG with a variety of solvents (table 2). Figure 4 shows SEM images of fibres produced with different amounts of sPEG from acetone/DCM/NMP. With all sPEG concentrations good quality fibres with parallel orientation were easily obtained. Low sPEG concentrations of 7 wt% (PPol-PEG1) resulted in the deposition of smaller fibres ( $0.45 \pm 0.14$

$\mu\text{m}$ , fig. 4a) than concentrations of 17 wt% (PPol-PEG2) ( $0.66 \pm 0.21 \mu\text{m}$ , fig. 4b), 27 wt% (PPol-PEG3) ( $0.67 \pm 0.17 \mu\text{m}$ , fig. 4c), and 29.5 wt% (PPol-PEG4) ( $0.57 \pm 0.28 \mu\text{m}$ , fig. 3d).

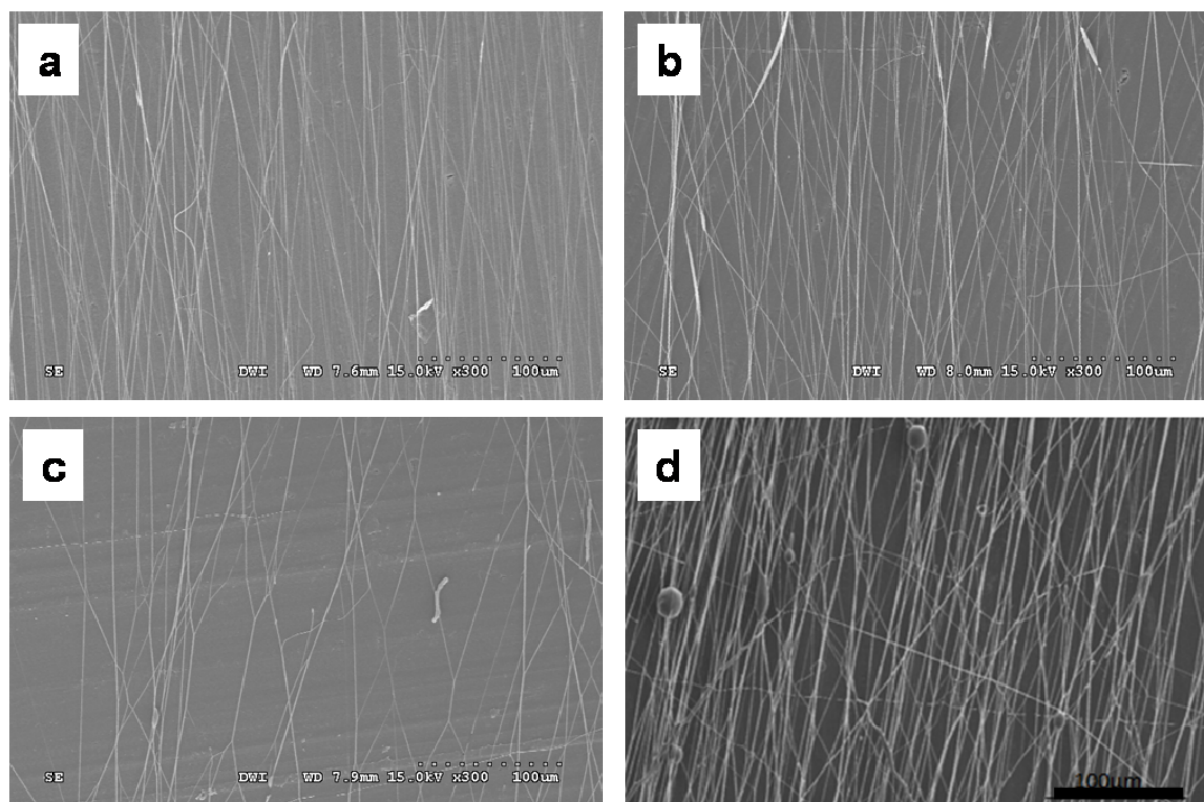


**Figure 4: Electrospun PPol-PEG fibres produced of PCL, PCL-ol and different amounts of sPEG in acetone/DCM/NMP.** (a) 7 wt % sPEG (PPol-PEG1) [25 kV, 20 cm, 0.5 mL/h]; (b) 17 wt% sPEG (PPol-PEG2) [25 kV, 20 cm, 1 mL/h]; (c) 27 wt % sPEG (PPol-PEG3) [20 kV, 20 cm, 0.5 mL/h]; (d) 29.5 wt% sPEG (PPol-PEG4) [20 kV, 20 cm, 1 mL/h]. Scale bars = 100  $\mu\text{m}$ . The values in brackets indicate the electrospinning conditions used for the fibre production. Reprinted from reference 19, figure 3. With kind permission from Springer Science and Business Media.

Increasing the sPEG concentration caused a slightly decrease of fibre quality, and concentrations above 37 wt% failed to generate any fibres. In a second run of experiments THF/DMF was used as solvent. Firstly an electrospinning concentration of 15 wt% was used. The PCL concentration was kept constant at 15 wt%, while sPEG and PCL-ol concentrations were varied. Fibres electrospun from these mixtures are presented in figure 5. A sPEG concentration of 17 wt% resulted in a fibre network, connected by beads (fig. 5a, PPol-PEG5). The collection of oriented fibres from this composition failed. Increasing the sPEG concentration to 27 wt% resulted in oriented fibres with a “bead on the string” morphology

(fig. 5b, PPol-PEG6). Further increasing of the sPEG concentration to 37 wt% prevented the collection of fibres and only beads were obtained (fig. 5c, PPol-PEG7).

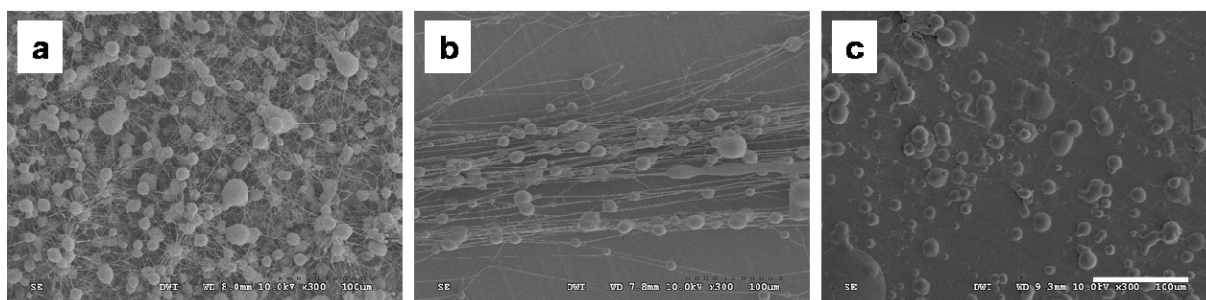


**Figure 5: Electrospun PPol-PEG fibres produced of PCL, PCL-ol and different amounts of sPEG in THF/DMF.** (a) 17 wt % sPEG (PPol-PEG5) [25 kV, 20 cm, 0.5 mL/h]; (b) 27 wt% sPEG (PPol-PEG6) [20 kV, 20 cm, 0.5 mL/h]; (c) 37 wt % sPEG (PPol-PEG7) [20 kV, 20 cm, 0.5 mL/h]. Fibres were produced with a PCL concentration of 15 wt%. Scale bar = 100  $\mu$ m.

Subsequently the PCL concentration was increased to 20 wt% while the concentration of the electrospinning solution was kept at 15 wt%. Results are shown in figure 6. Electrospinning of oriented fibres was not possible with these concentrations. Either very thick, inhomogeneous fibres (fig. 6a, PPol-PEG8 and fig. 6b, PPol-PEG9), beads (fig. 6c, PPol-PEG10) or a network of beaded fibres (fig. 6d, PPol-PEG11) was obtained. Following these results PPol-PEG3 fibres were used for further investigations including cell experiments, accompanied by PPol-PEG4 fibres.

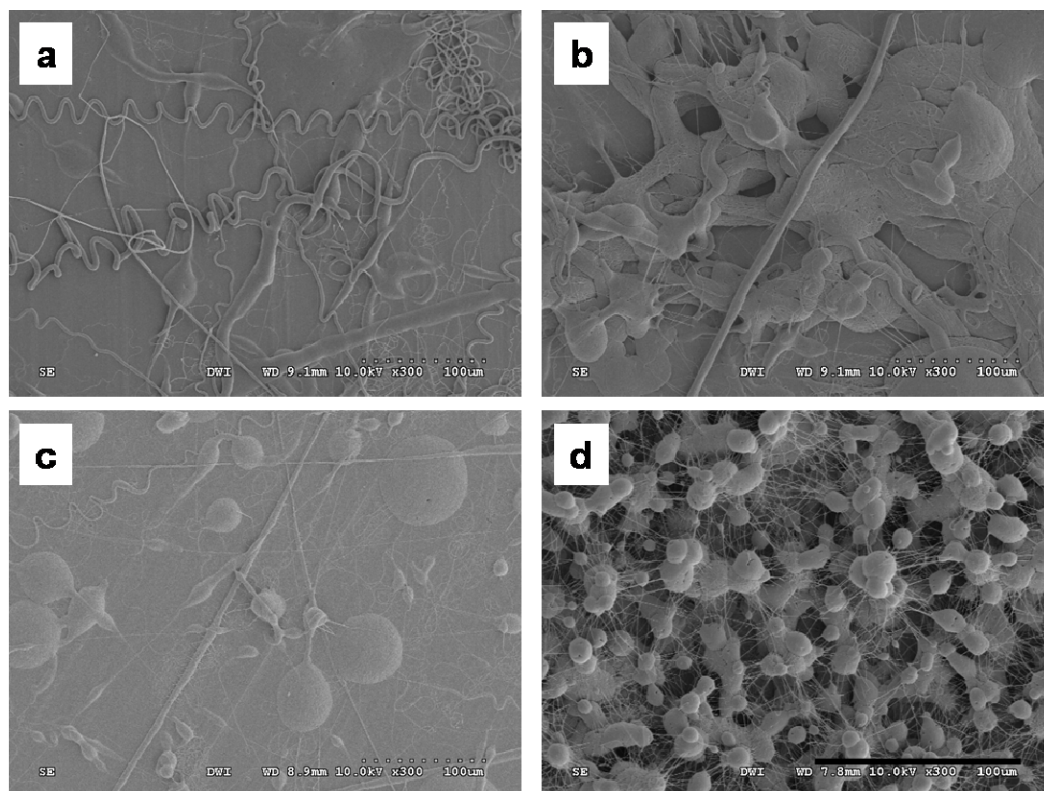


**Figure 6: Electrospun PPol-PEG fibres produced of PCL, PCL-ol and different amounts of sPEG in THF/DMF.** (a) 7 wt % sPEG (PPol-PEG8) [30 kV, 20 cm, 1 mL/h]; (b) 17 wt% sPEG (PPol-PEG9) [25 kV, 20 cm, 2 mL/h]; (c) 27 wt % sPEG (PPol-PEG10) [25 kV, 20 cm, 0.5 mL/h]; (d) 37 wt % sPEG (PPol-PEG11) [30 kV, 20 cm, 1 mL/h]. Fibres were produced with a PCL concentration of 20 wt%. Scale bar = 100  $\mu\text{m}$ . The values in brackets indicate the electrospinning conditions used for the fibre production.

To overcome the cell repellent properties of the sPEG containing fibres, GRGDS, a peptide sequence which is known to promote cellular adhesion (PPol-PEG3+RGD) fibres, or the whole ECM protein fibronectin (PPol-PEG4+Fn) were incorporated into the fibres and tested in *in vitro* assays. SEM was used to determine changes in fibre quality following the inclusion of bioactive molecules. Figures 7 and 8 show examples of such images. No difference in fibre quality could be observed in the presence (fig. 7a) or absence of GRGDS (fig. 7b), however the fibre diameter increased slightly ( $0.85 \pm 0.28 \mu\text{m}$ ) with inclusion of GRGDS. Occasional swelling of peptide-containing fibres was observed in *in vitro* experiments.

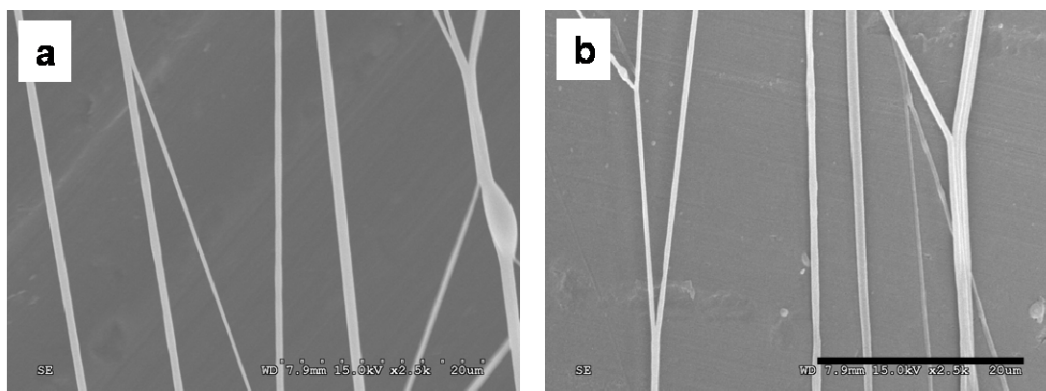


**Figure 7: SEM images of PPol-PEG3 fibres electrospun with (a) and without (b) the inclusion of GRGDS.** Fibres on both images were electrospun with 20 kV, 20 cm and 1 mL/h. Scale bar = 20  $\mu\text{m}$ . Reprinted from reference 19, figure 4. With kind permission from Springer Science and Buisness Media.

Similar results were achieved with PPol-PEG4 fibres. The fibre quality did not change visibly when fibronectin was incorporated (diameters of  $0.67 \pm 0.27 \mu\text{m}$ ; fig. 8a) compared to the fibres without the protein (fig. 8b) but occasional intersections between the fibres were noticed.

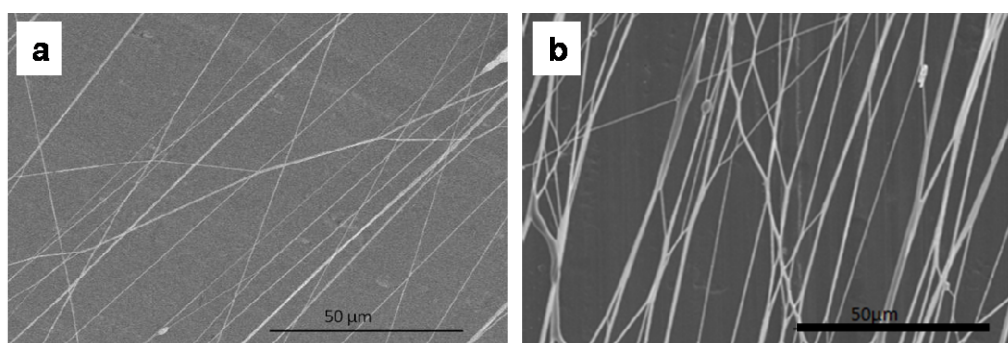


**Figure 8: SEM images of PPol-PEG4 fibres electrospun with (a) and without (b) the inclusion of fibronectin.** Inclusion of the protein fibronectin did not affect the fibre quality significantly. Scale bar = 50  $\mu\text{m}$ . Reprinted from reference 19, figure5. With kind permission from Springer Science and Buisness Media.

Table 5 gives information about the orientation distribution of the fibres and the volume porosity. The best parallel orientation of the fibres was achieved with biofunctionalised PPol-PEG+RGD and PPol-PEG+Fn fibres. Here the majority of the fibres (64 respectively 65 %) were parallel to each other or deviate maximum  $5^\circ$  from each other. PPol-PEG3 fibers had the worst orientation distribution with only 44 % of the fibres in a

deviation range of 5 ° and with PPol-PEG4 fibres 56 % of the fibres were in this range. The volume porosity is the area of a sample which is covered with fibres in comparison to the total sample area. As it can also be seen from the SEM images of the fibres, fibres were mainly clearly separated from each other and the volume porosity was calculated to be between around 6 % for the PPol-PEG4 and PPol-PEG4+Fn fibres and a bit higher for the PPol-PEG3 (12 %) and the PPol-PEG3+RGD (19 %) fibres.

**Table 5: Orientation distribution and volume porosity of various fibres.**

Name / Orientation distribution (%)		PPol-PEG3	PPol-PEG3+RGD	PPol-PEG4	PPol-PEG4+Fn
degree of deviation	0-4°	44	64	56	63
	5-10°	19	12	21	13
	11-15°	16	3	7	13
	16-20°	12	12	7	3
	>21°	9	9	9	8
volume porosity (%)		12.3 +/- 4.7	19.9 +/- 11.1	6.6 +/- 3.5	6.7 +/- 3.3

### 8.3.2 Fibre characterisation

Fibres were further characterised by contact angle determination, protein adsorption assays and XPS measurements. The contact angle of pure PCL fibres was 141.7 °. For PPol-PEG3 and PPol-PEG4 fibres the measurement of a contact angle was not possible because the water drop was fully adsorbed immediately after its deposition on the surface, demonstrating the hydrophilicity of these fibres. Protein adsorption was investigated because non-specific protein adsorption of the fibres may enhance adverse physiological reaction *in vivo*, and should therefore be avoided. Figure 9 presents results of protein adsorption tests with PCL and different PCL/sPEG fibres. All images were taken with the same exposure time of 20 s. Therefore a qualitative comparison between the samples based on the intensity of fluorescence was possible. PCL fibres showed the strongest protein adsorption (fig. 9a, b). It did not change after incubation in water. The fibres with 15 wt% sPEG (P-PEG2, fig. 9c, d) showed weaker protein adsorption than PCL fibres, and also did not change after incubation in water. The inclusion of 27 wt% sPEG (P-PEG4) in the fibres resulted in an even stronger reduction of protein adsorption (fig. 9e) compared to pure PCL fibres. After incubation in water, however the protein adsorption increased significantly (fig. 9f) and was comparable with the protein adsorption of fibres with 15 wt% sPEG. Fibres prepared with PCL-ol (PPol-PEG3) showed reduced protein adsorption comparable with P-PEG4 fibres. After incubation the protein adsorption did not change, indicating that the sPEG was still present at the fibre



surface. Because PPol-PEG4 fibres nearly contained the same polymer concentrations in the solid state (see table 2), protein adsorption assays were not performed with these fibres.

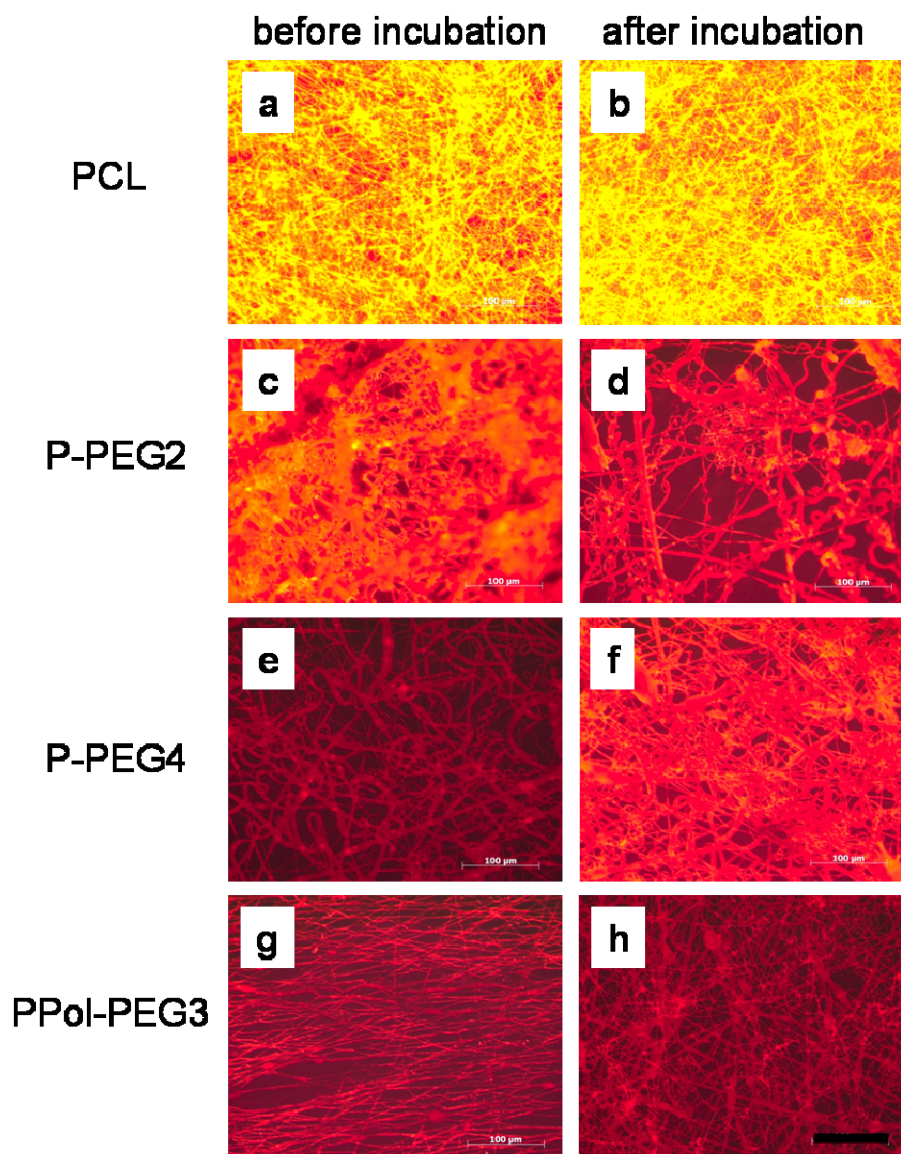


**Figure 9: Protein adsorption on fibre samples before and after incubation in water.** (a) PCL fibres before incubation; (b) PCL fibres after incubation; (c) P-PEG2 before incubation; (d) P-PEG2 after incubation; (e) P-PEG4 before incubation; (f) P-PEG4 after incubation; (g) PPol-PEG3 before incubation; (h) PPol-PEG3 after incubation. All images were taken with the same exposure time of 20 s. Scale bar = 100 µm. Reprinted from reference 19, figure 6. With kind permission from Springer Science and Business Media.

The same samples were investigated with SEM after the protein adsorption assay. Figure 10 shows SEM images of pure PCL fibres (fig. 10a, d), P-PEG4 fibres (fig. 10b, e) and

of PPol-PEG3 fibres (fig. 10c, f) before (fig. 10a-c) and after incubation in water (fig. 10d-f). Hardly any differences between the fibres could be noticed, neither for the sPEG containing fibres nor for the PCL fibres. All fibres showed a clear surface without any indices for swelling or degradation.

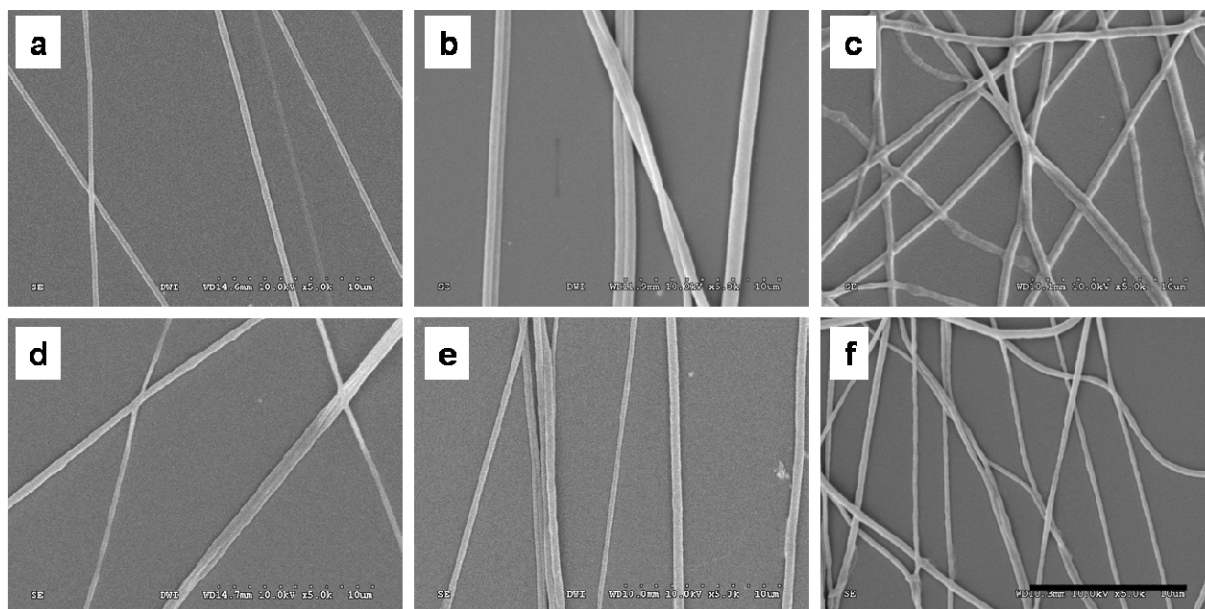


**Figure 10: SEM images of electrospun fibres before and after incubation.** Fibres of different materials (a, c) PCL, (b, e) P-PEG4 and (c, f) PPol-PEG3 were incubated 5 days in water and SEM images were taken of non-incubated (a-c) and incubated (d-f) fibres. Scale bar = 10  $\mu$ m.

XPS measurements of the fibres were performed to investigate surface compositions. Table 6 shows atomic concentration of oxygen, carbon, nitrogen and silicon of the fibre surfaces. Nitrogen, which may be used as an indicator for the existence of sPEG at the fibre surface, was measured in PPol-PEG3 fibres before and after incubation in water. Interestingly, the nitrogen content increased slightly from 0.5 % prior to water incubation to 0.9 % after incubation. We concluded that sPEG remained bound and may have been concentrated on the surface of the electrospun fibres. With PPol-PEG4 fibres similar results were observed. Based on the XPS data and comparative protein absorption, we highlight that the best blend of PCL/sPEG was achieved with the PPol-PEG3 and the PPol-PEG4 preparations. These types of fibres were therefore tested in bioassays.

**Table 6: XPS data showing atomic concentrations of elements from PCL and PCL/sPEG blends before and after incubation in water.** Nitrogen indicating the existence of sPEG in the fibres due to urethane groups was only observed with PPol-PEG3 and PPol-PEG4 fibres.

incubation	PCL	P-PEG2		P-PEG4		PPol-PEG3		PPol-PEG4
	before	before	after	before	after	before	after	before
O	19.0	20.1	26.0	21.4	23.8	21.2	25.0	17.8
C	80.2	79.9	71.5	78.1	73.3	77.1	72.6	81.8
N	0.0	0.0	0.0	0.0	0.0	0.5	0.9	0.3
Si	0.8	0.0	2.5	0.6	3.3	1.3	1.4	0.0

### 8.3.3 Cell experiments

In the context of the intended application of microfibres for peripheral nerve repair, two biological properties are considered to be the most important: (i) the ability to support Schwann cell migration, and (ii) the ability to guide axonal regeneration. Both properties were evaluated by placing dorsal root ganglia (DRG) explants onto fibres of various compositions. DRG were analysed with immunocytochemical staining after 4 day cultivation *in vitro* (DIV). S100 immunoreactive Schwann cells were found to have migrated from all explants. Axons from the sensory neurons within the explants had also grown out and were visualised using NF200 immunostaining (fig. 11). Schwann cell migration from the explants, as well as neurite outgrowth, was more pronounced on GRGDS containing PPol-PEG3 than on the other types of substrates (PCL fibres, PPol-PEG3 fibres without peptide). Axons grew in parallel to the GRGDS functionalised PPol-PEG3 (fig. 11a) fibres and on PCL (fig. 11b). In contrast, only few, very short axons were seen on PPol-PEG3 fibres without functionalisation (fig. 11c).

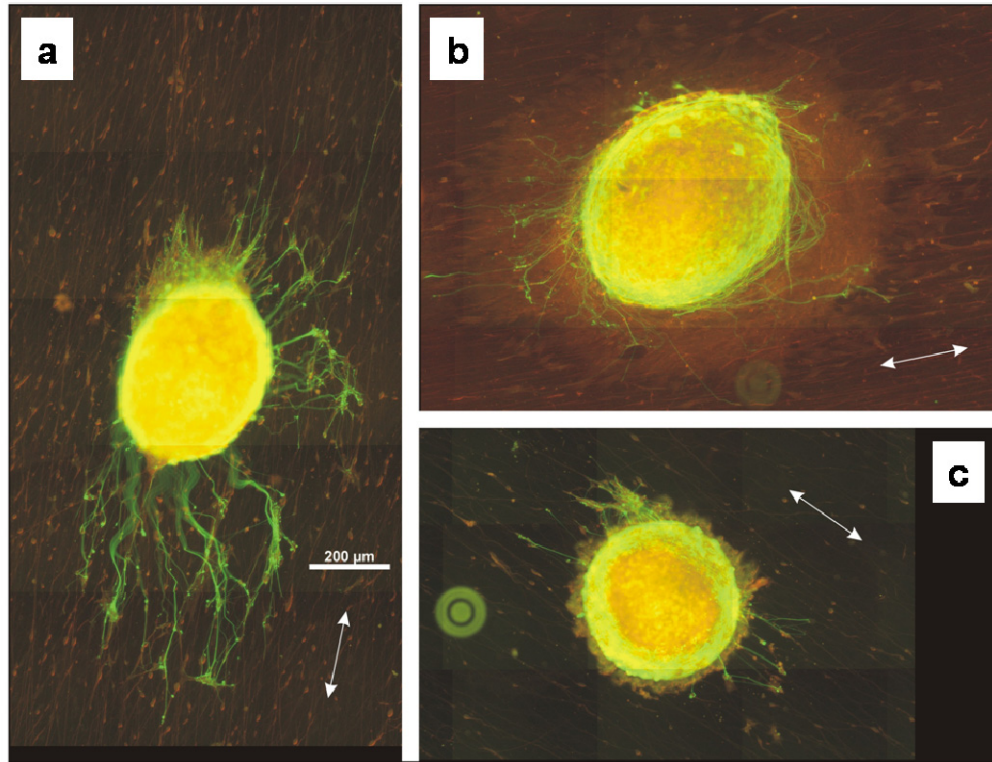


**Figure 11: Fluorescence images of DRG explants on different fibre material.** DRGs were explanted from E10 chick embryos and placed onto (a) PPol-PEG3+RGD, (b) PCL and (c) PPol-PEG3 fibres and incubated for 4 DIV. Outgrowing axons were stained with NF200 and were longest on RGD functionalised PPol-PEG3 fibres. The arrows indicate fibre orientation. Scale bar = 200  $\mu\text{m}$ . Reprinted from reference 19, figure 7. With kind permission from Springer Science and Business Media.

With PPol-PEG4 +Fn fibres neurites detached from the substrates and therefore an analysis of axonal growth was not possible here. However, Schwann cell migration did occur with these fibres (fig.12), and this was similar to the GRGDS containing fibres. Schwann cells did not grow in a preferred direction but spread equally around the explant. The reason for this might be the fact that the fibres were not very parallel but frequently intersected (fig. 8).

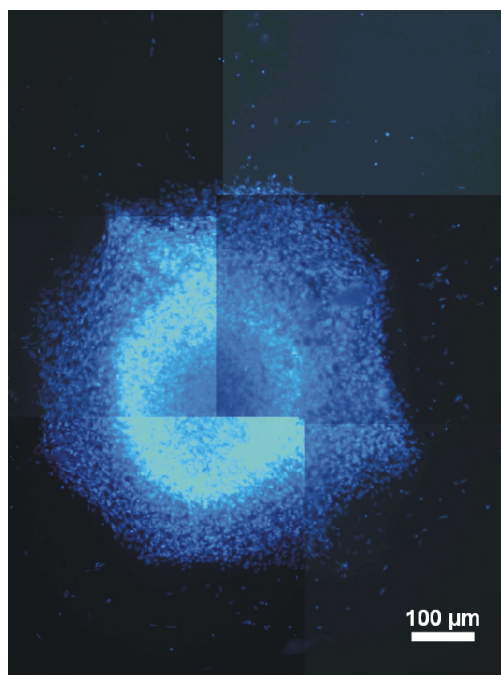


**Figure 12: Fluorescence image of DRG explant on PPol-PEG4+Fn fibres.** Nuclei of migrating cells were stained with DAPI. Scale bar = 100  $\mu\text{m}$ . Reprinted from reference 19, figure 8. With kind permission from Springer Science and Business Media.

Cell migration and neurite outgrowth were quantified in figure 13. Axonal growth was best on PPol-PEG3+RGD fibres, where the longest 10 % neurites reached a mean length of  $325 \pm 84 \mu\text{m}$  (mean  $\pm$  standard error of mean), while the 10 % longest neurites on PCL fibres had a length of  $230 \pm 34 \mu\text{m}$  and only  $140 \pm 30 \mu\text{m}$  on PPol-PEG3 fibres. To assess Schwann cell migration, the distances of the 20 cells that had migrated farthest from every explant was determined. Similar to the effect on axons, migration distances were largest on PPol-PEG3+RGD fibres ( $352 \pm 39 \mu\text{m}$ ), were slightly shorter on PPol-PEG4+Fn fibres ( $272 \pm 10 \mu\text{m}$ ) and on PCL fibres ( $290 \pm 16 \mu\text{m}$ ) and reached only half of this value on non-functionalised PPol-PEG3 fibres ( $168 \pm 5 \mu\text{m}$ ). With inspection after 4 DIV it appears that cell migration occurred within the same time frame as axonal growth. The results also show that functionalisation of PPol-PEG3 fibres with the GRGDS peptide substantially improved their biological properties.

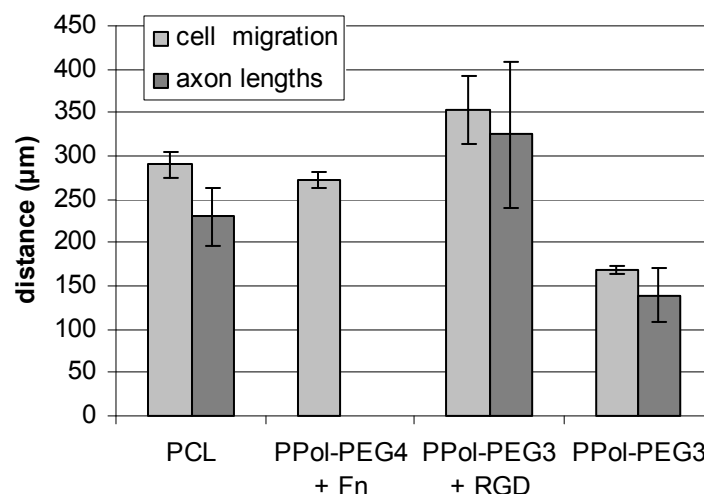


**Figure 13: Lengths of outgrowing axons and distance of Schwann cell migration different fibre materials.** Outgrowing cells migrated furthest on RGD functionalised fibres as well as axons grew along these fibres were the longest compared with the other fibre materials. The axons grew always shorter than the furthest cells migrated. t-test,  $p < 0.05$ , error bars = standard error of the mean. Reprinted from reference 19, figure 9. With kind permission from Springer Science and Business Media.

## 8.4 Discussion

### 8.4.1 Electrospinning and fibre characterisation

Fibres consisting of PCL and sPEG were produced by electrospinning, analysed and tested using *in vitro* assays in this study. It is already known that polyethylene glycol containing fibres<sup>13,20</sup> as well as surfaces covered with sPEG<sup>21</sup> prevent unspecific protein adsorption and cell adhesion. Here these properties of sPEG were exploited to produce electrospun fibres that can guide cell movement but are resistant to non-specific adsorption. Compared to the previously described approach, this process leads to functionalisable fibres in a simple manner and provide similar advantages of the minimised unspecific protein adsorption without the time consuming block copolymer synthesis. A more detailed comparison of these approaches is presented elsewhere<sup>22</sup>.

Since electrospun fibres cannot be generated using pure sPEG (due to its low molecular weight), PCL was added to the electrospinning solution. It is likely that a chemical reaction occurred between hydroxyl groups of PCL and the isocyanate groups of sPEG polymer, resulting in the formation of urethane groups and the building of a block copolymer. Although sPEG is, to a certain extent, soluble in aqueous solutions, the above reaction should

have prevented its diffusion into the cell culture-medium. In the hypothesised reaction, schematically shown in figure 1, both peptide- and protein functionalisation may occur by the formation of urea groups resulting from the reaction of amine groups of the peptide/protein with the isocyanate groups of sPEG.

Electrospinning of two different PCL/sPEG types was performed. The first type consisted of high molecular weight PCL, mixed with sPEG (P-PEG). The second type contains in addition low molecular weight PCL-diol (PPol-PEG). The higher amount of hydroxyl groups in this system offered more binding sites for reactions with isocyanate groups.

For electrospinning of the P-PEG system two base solvents were chosen consisting of acetone/DCM or THF and mixed with an additional solvent (DMSO, NMP or DMF). At the lower sPEG concentration of 15 wt% small oriented fibres could be produced from solutions based on acetone/DCM/NMP or acetone/DCM/DMSO (fig. 2a, b). Since protein adsorption (fig. 9) was not effectively prevented by this low sPEG concentration, a higher concentration of 27 wt% was investigated. While this resulted in a fibrous network when using DMSO-containing solvent (acetone/DCM/DMSO, fig. 3a), good quality fibres were generated using NMP-based (fig. 3b) or DMF-based (fig. 3c) solvent. Additionally, THF based electrospinning solutions were tested because pre-experiments with this solvent showed a reduced protein adsorption of fibres (results not shown). Here orientated fibres with a few beads were obtained irrespectively which additional solvent was used (fig. 3d-f). Although the different amounts of these additional solvents were small, their properties can significantly influence the electrospinning process.

The values for boiling point, vapour pressure and surface tension of the solvents have been presented in table 4. These properties and others influence the electrospinning process and the ability to obtain homogeneous fibres from a specific polymer/solvent composition. The *surface tension*  $\gamma$  is the opposite force to the coulomb repulsion and the balance between these two forces identify the curvature of the bending jet during instabilities. The surface tension together with the viscosity of the spinning solution is often the key factor if a specific polymer/solvent combination can be electrospun<sup>23</sup>. Normally small surface tensions are desired, because this requires smaller applied voltages. However, the surface tension of a solvent is changed by preparing a polymer solution in dependency on the concentration<sup>23</sup> and the nature of the polymer<sup>24</sup>.

The *dielectric constant*  $\epsilon$  measures how much electrical charge a solvent can hold. High electrical constants induce an even dispersion of the surface charge density on the jet which yields in higher quality fibres with smaller diameters<sup>25</sup>.

Another important factor is the *volatility* of the solvent. The evaporation of the solvent creates the solid fibre on the target. Ideally all solvent is evaporated during travelling from the needle to the target. Low boiling temperatures and high vapour pressures induce fast solvent evaporation and therefore were expected to result in high quality fibres. Slow evaporation of the solvent may prevent its complete removal during the electrospinning process, resulting in the deposition of “wet” fibres which may form meshes of fused fibres on the target<sup>26</sup>. However, too fast evaporation may result in drying of the polymer solution at the needle tip and causes blocking<sup>27</sup>.

The solvent properties of NMP and DMSO are very similar and differ from those of DMF which has a smaller boiling point and a seventh higher vapour pressure. Regarding these aspects, fibres produced from DMF should have the highest quality and differ from fibres from NMP and DMSO, while fibres from both these solvents should be similar. However fibres electrospun from NMP and DMF were very similar and differ from those of DMSO. These findings confirm former results<sup>25</sup> that for each polymer composition specific electrospinning conditions have to be evaluated empirically, and that knowing the polymer and solvent parameters is not enough to assess the ability of electrospinning. In contrast to the solvent mixture of acetone/DCM, electrospinning from THF resulted in oriented, but beaded fibres irrespectively from the added solvent (fig. 3d-f). Here eventually the lower dielectric constant of THF assists the building of beads due to an inhomogeneous surface charge density in the jet<sup>28</sup>.

Based on the data obtained from the P-PEG fibres, the best solvent combinations (acetone/DCM/NMP and THF/DMF) were used for the PPol-PEG fibres system. This system also included the additional step of using THF to pre-dissolve the sPEG. Electrospinning from acetone/DCM resulted in good oriented electrospun fibres (fig. 4). However, increasing the sPEG concentration above 30 wt% resulted in a solution that was too viscous and which could not be electrospun. Therefore, the mixtures with 27 and 29.5 wt% sPEG were chosen for further experiments to maximally exploit the protein repellent properties of the sPEG. Inclusion of the peptide sequence GRGDS or the protein fibronectin did not affect the ability to electrospin high quality fibers (fig. 7 and 8). The calculation of volume porosity confirmed the preparation of single fibers which were separated from each other. The area which was



covered with fibers was between 6 and 19 % for the different fibers materials (table 5). This high variation between the different samples may be the consequence of different fiber collection times during the electrospinning process. Higher collection times resulted in higher fiber densities.

When THF was used as a base solvent instead of acetone/DCM, the fibres quality changed significantly. First a PCL concentration of 15 wt% was tested. Here beaded fibres were obtained with sPEG concentrations of 17 and 27 wt% (fig. 5a, b). Increasing the concentration to 37 wt% resulted in the formation of beads (fig. 5c). This indicates that the solution viscosity<sup>28</sup> or the molecular weight<sup>29</sup> was too low. The concentrations of low molecular weight polymers sPEG and PCL-ol were probably too high in this solution to obtain chain overlapping necessary for fibre formation of fibres. To overcome this problem, the PCL concentration was raised to 20 wt% while the total concentration of the electrospinning solution was kept constant at 15 wt% (fig. 6). For low sPEG and PCL-diol concentrations the viscosity of the electrospinning concentration was too high and only batches of thick fibres occurred. As neither high nor low concentrations of the compounds resulted in high quality oriented fibres, it seems that the chosen polymers cannot be electrospun with a THF / DMF solvent mixture.

The electrospun fibres from both systems were analysed in several ways. The contact angles of PPol-PEG3 and PPol-PEG4 fibres could not be measured because the water droplet was fully adsorbed after its deposition on the fibres. This indicated that hydrophobic PCL had gathered inside the fibres while sPEG was at the surface, resulting in highly hydrophilic fibres.

PPol-PEG3 fibres were the only ones which showed reduced protein adsorption before and after incubation in water, in comparison with the PCL fibres. In P-PEG2 the sPEG content noticeably reduced protein adsorption compared to PCL fibres but this effect was not strong enough to fulfil the requirements of a protein repellent material. In P-PEG4 fibres, the protein repelling effect of sPEG appeared to be only partial because sPEG was washed out by incubation in water. With PPol-PEG3 fibres the protein adsorption was reduced most as visualised by fluorescence microscopy (fig. 9). This effect was stable during incubation with water. It is known from literature that PCL fibres degrade very slowly. Within six month incubation in Ringer solution only very little loss of molecular weight was observed<sup>30</sup>. Long-term degradation assays with electrospun poly(D,L-lactide-co-glycolide)/sPEG (PLGA/sPEG)

fibres showed only a minor accelerated degradation in comparison to pure PLGA fibres<sup>22</sup>. These results give an indication about the stability of the PCL/sPEG fibres that should be similar to pure PCL. As an additional indication, SEM images of the incubated fibres did not demonstrate structural changes of the fibres within the time of incubation (fig. 10). However, this conclusion has to be proved in *in vitro* experiments.

In XPS measurements only PPol-PEG3 and PPol-PEG4 fibres demonstrated nitrogen at their surfaces (table 6). Here, the nitrogen content was interpreted as an indicator for the existence of sPEG on the surface of the fibres due to the formation of urethane groups. Interestingly, the nitrogen content of PPol-PEG3 fibres increased slightly after incubation in water which might be the result of enrichment of sPEG molecules at the fibre surface in an aqueous environment due to the higher hydrophilicity of the sPEG chains compared with PCL polymer chains. Some fibres were contaminated with silicone which is a common impurity caused by grease from the environment in chemical laboratories.

The surface analysis of the different fibres showed that a high amount of sPEG in the electrospinning solution was necessary to overcome the protein adsorption effects of PCL. The PPol-PEG system seems to be more effective in binding sPEG to PCL, possibly due to the much higher amount of hydroxyl groups in this system. As PPol-PEG3 was the most successful in fulfilling the desired properties, *in vitro* experiments were performed to investigate cell-substrate interaction using these fibres, as well as parallel *in vitro* experiments using PPol-PEG4+Fn fibres.

### 8.4.2 Cell experiments

Cell experiments were performed on PCL, PPol-PEG3, PPol-PEG3+RGD and PPol-PEG4+Fn fibres. DRG explants were placed onto the fibres and incubated for 4 DIV. Measurements of the orientation distribution of these fibres demonstrated that only around 50 % of the PPol-PEG3 fibres and 63 % of the PPol-PEG4 fibres were exactly parallel to each other (table 5). This resulted in intersections of the electrospun fibres. When this occurred neurites were observed to switch between fibres (fig. 11). Neurites followed the fibres, irrespectively from their orientation which may result in the reduction of total speed of neurite growing in comparison with totally parallel aligned fibres. Thus, further research is required to increase the parallelism of the fibres.

Protein adsorption data suggested that PPol-PEG3 fibres might reduce inflammatory reactions or encapsulation *in vivo*<sup>8,9</sup>. In addition, preventing adhesion of proteins that inhibit axonal growth, e. g. components of central nervous system myelin<sup>31,32</sup> may be important for

axonal regeneration. Non-adhesive substrates, such as PEG containing microfibrils, might on the other hand not be well suited as substrates for glia cells and axons. The tests with DRG explants confirmed the expected properties of PPOI-PEG3 fibres: although DRG adhered to these substrates, only 20 % of the explants demonstrated cell migration and axonal outgrowth (fig. 11c). This property was overcome by incorporating of integrin activating bioactive molecules to the fibres, GRGDS peptide as well as fibronectin (fig. 11, 12). *In vitro* experiments with electrospun fibres of PEO-*b*-PCL demonstrated similar results as described before. These fibres showed cell repellent properties due to the hydrophilicity of the PEO block at the fibre surface. By functionalisation with the peptide sequence GRGDS this property was overcome and cells attached well to the fibres. However, in that study, human dermal fibroblasts were used on random fibres without investigating guidance properties of the fibres<sup>22</sup>. Therefore a direct comparison of the results in both studies is not possible, due to the use of different cell types and different fibre orientation.

Stimulation of Schwann cell proliferation supports neurite outgrowth and axon regeneration after injuries<sup>33,34</sup>. Therefore a bridging substrate for peripheral nerve repair should possess properties that encourage the growth promoting physiology of Schwann cells. Other groups have included peptide sequences from laminin<sup>35,36</sup> or growth factors<sup>37</sup> into biomaterial to achieve this effect. In this study it is shown that the isocyanate groups of the sPEG offer the possibility to insert such functionalities into electrospun fibres without overcoming their protein repellence. The inclusion of an ECM derived peptide, GRGDS, or the whole protein, fibronectin, to the PCL/sPEG fibres stimulated axon growth and Schwann cell migration. These two methods of biofunctionalisation offer specific advantages. Peptide sequences are small molecules which are relatively easy to handle. They are often more easily solubilised than proteins and are more resistant to hydrolysis and temperature induced degradation. On the other hand, proteins mimic the natural state of the ECM more closely than peptides. They are often involved in a wide range of cellular processes and offer several binding sites for a number of cell types. Fibronectin has two major heparin-binding sites, a collagen-binding domain and more than one binding sites for integrin receptors for cell attachment. In addition to the well-known RGD sequence, a second, distinct region that acts synergistically with RGD has been identified. Both are important for cell adhesion and migration that is mediated by integrin receptors. The alternatively spliced IIIICS segment acts independently from the both former mentioned sequences and contains another cell adhesive region. It is primarily recognised by cells of neural crest origin<sup>17,38</sup>. Surfaces patterned with

fibronectin or its binding-domain peptide RGD have been shown to enhance neuronal outgrowth in comparison to controls lacking such molecules<sup>39</sup>.

Although the cellular response towards the PPol-PEG3+RGD and PPol-PEG4+Fn fibres did not induce Schwann cell migration to a significantly larger extent than simple PCL fibres, the first two mentioned fibre types possess two main advantages over pure PCL. They minimise unspecific protein adsorption, and they can be further modified by the incorporation of other molecules with specific biofunctionalities. Other examples of fibre functionalisation has been the generation of blended PCL/collagen fibres<sup>2</sup> or poly(L-lactide) fibres functionalised with basic fibroblast growth factor<sup>37</sup>. Such approaches demonstrated greater cell migration and axonal outgrowth, than observed in the present investigation (using GRGDS- or fibronectin-functionalised fibres), however previous publications did not address the possible problems associated with unspecific protein adsorption.

The beneficial effects of biofunctionalisation of the PCL/sPEG fibres might be improved by increasing the concentration of such bioactive molecules. In this study GRGDS was bound to approximately 20 % of the sPEG molecules. Groll and colleagues demonstrated with GRGDS functionalised sPEG surfaces that the binding of 0.5 – 1 GRGDS molecule per sPEG molecule is very effective for adhesion of SaOS cells (human epithelial-like osteosarcome cells)<sup>21</sup>. Future studies will have to show whether increasing the GRGDS concentration enhances the biological activity of functionalised PPol-PEG fibres with respect to neuronal cells. Fibronectin was added with a ratio of sPEG to Fn to be 2 to 1. In comparison with the molecular weight of fibronectin ( $\approx$  400 kDa), the active sequences such as RGD and its synergistic region were included in a very small amount. Higher protein concentrations have to be tested in the future and comparisons with a range of different RGD concentrations and other peptides and the potency of this approach should be assessed further.

Another important step will be the development of three dimensional scaffolds that incorporate biofunctionalised fibres. Simple nerve conduits consisting of hollow tubes have already implanted several hundreds patients with peripheral nerve injuries<sup>40</sup>. With this approach a length of about 30 mm is the longest gap that can be bridged. However, animal experiments indicate that regeneration can be improved when nerve conduits contain longitudinal guiding structures<sup>41, 42</sup>. Some investigations have already incorporated electrospun fibres or similar filaments in a 3D configuration in nerve conduits<sup>43-45</sup>. Therefore, we anticipate that artificial nerve implants that can substitute autologous nerve transplantation will have to combine topographical cues, such as electrospun fibres in a 3D matrix, with molecular signals, such as integrin activating peptides.

### 8.5 Conclusion

The electrospinning technique was used to produce oriented microfibrils of PCL/sPEG that could be functionalised with bioactive peptides from the extracellular matrix. A preparation consisting of 27 wt% sPEG, PCL and PCL-diol electrospun from acetone/DCM/NMP/THF (PPol-PEG3) minimised protein adsorption and resulted in the presence of sPEG at the surface of aligned fibres. In experiments with dorsal root ganglia explants, non-functionalised PPol-PEG3 fibres supported little cellular migration and axonal outgrowth. However, functionalisation of PPol-PEG3 with the peptide sequence GRGDS strongly increased these cellular interactions. Experiments with fibronectin containing fibres showed an advantage over PPol-PEG3 only with respect to Schwann cell migration. Thus, the PPol-PEG3+RGD fibres demonstrated their usefulness for promoting functional repair by supporting more specific cell-substrate interaction than would be expected if non-protein repellent materials had been chosen as the substrate.

### 8.6 Acknowledgment

We thank Marie Pradella for help with evaluating the cell experiments. Kristin Michael and Bernd Hoffmann kindly allowed us to use their equipment for making composite photographs of DRG explants. This work was supported by a grant from the Interdisciplinary Centre for Clinical Research "BIOMAT." within the faculty of Medicine at Aachen University (RWTH) (TV B111), the DFG-Graduiertenkolleg 1035 "Biointerface" and a Marie-Curie EST grant from the EU (EURON).

### 8.7 References

1. Lietz, M., Dreesmann, L., Hoss, M., Oberhoffner, S., Schlosshauer, B., Neuro tissue engineering of glial nerve guides and the impact of different cell types. *Biomaterials* **2006**, 27, 1425 - 1436.
2. Schnell, E.; Klinkhammer, K.; Balzer, S.; Brook, G.; Klee, D.; Dalton, P.; Mey, J., Guidance of glial cell migration and axonal growth on electrospun nanofibers of poly- $\epsilon$ -caprolactone and a collagen/poly- $\epsilon$ -caprolactone blend. *Biomaterials* **2007**, 28, (19), 3012 - 3025.
3. Smeal, R. M.; Rabbitt, R.; Biran, R.; Tresco, P. A., Substrate curvature influences the direction of nerve outgrowth. *Annals of Biomedical Engineering* **2005**, 33, (3), 376 - 382.
4. Li, D.; Xia, Y. N., Electrospinning of nanofibers: Reinventing the wheel? *Advanced Materials* **2004**, 16, (14), 1151 - 1170.

5. Huang, Z. M.; Zhang, Y. Z.; Kotaki, M.; Ramakrishna, S., A review on polymer nanofibers by electrospinning and their applications in nanocomposites. *Composites Science and Technology* **2003**, 63, (15), 2223 - 2253.
6. Klinkhammer, K., Seiler, N., Grafahrend, D., Gerardo-Nava, J., Mey, J., Brook, G. A., Möller, M., Dalton, P. D. and Klee, D., Deposition of electrospun fibers on reactive substrates for in vitro investigations. *Tissue Engineering* **2009**, 15, (1), 77 - 85.
7. Horbett, T. A., The role of adsorbed proteins in tissue response to biomaterials. In *Biomaterials Science: An introduction to materials in medicine*, 2nd ed.; Ratner, B. D., Hoffman, A. S., Schoen, F. J., Lemons, J. E., Ed. Elsevier: San Diego, 2004; pp 237 - 240.
8. Tang, L., Jennings, T. A., Eaton, J. W., Mast cells mediate acute inflammatory responses to implanted biomaterials. *PNAS* **1998**, 95, 8841 - 8846.
9. Johnson, R.; Harrison, D.; Tucci, M.; Tsao, A.; Lemos, M.; Puckett, A.; Hughes, J. L.; Benghuzzi, H., Fibrous capsule formation in response to ultrahigh molecular weight polyethylene treated with peptides that influence adhesion. *Biomed. Sci. Instrum.* **1997**, 34, 47 - 52.
10. Harris, J. M., *Poly(ethylene glycol) Chemistry: Biotechnical and Biomedical Applications*. Plenum Press: New York, 1992.
11. Jeon, S. I.; Lee, J. H.; Andrade, J. D.; De Gennes, P. G., Protein - surface interactions in the presence of polyethylene oxide: I. Simplified theory. *Journal of Colloid and Interface Science* **1991**, 142, 149 - 158.
12. Sharma, S., Johnson, R.W., Desai, T.A., Evaluation of the stability of nonfouling ultrathin poly(ethylene glycol) films for silicon-based microdevices. *Langmuir* **2004**, 20, (2), 348 - 356.
13. Grafahrend, D.; Calvet, J. L.; Klinkhammer, K.; Salber, J.; Dalton, P. D.; Moller, M.; Klee, D., Control of protein adsorption on functionalized electrospun fibers. *Biotechnology and Bioengineering* **2008a**, 101, (3), 609 - 621.
14. Gasteier, P.; Reska, A.; Schulte, P.; Salber, J.; Offenhausser, A.; Moeller, M.; Groll, J., Surface grafting of PEO-based star-shaped molecules for bioanalytical and biomedical applications. *Macromolecular Bioscience* **2007**, 7, (8), 1010 - 1023.
15. Hersel, U., Dahmen, C., Kessler, H., RGD modified polymers: biomaterials for stimulated cell adhesion and beyond. *Biomaterials* **2003**, 24, 4385 - 4415.
16. Venstrom, K. A.; Reichardt, L. F., Extracellular matrix 2: role of extracellular matrix molecules and their receptors in the nervous system. *FASEB Journal* **1993**, 7, 996 - 1003.
17. Akiyama, S. K.; LaFlamme, S. E., Bioadhesion and cell behavior. *Colloids and Surfaces B: Biointerfaces* **1994**, 2, 241 - 250.

18. Goetz, H.; Beginn, U.; Bartelink, C. F.; Grunbauer, H. J. M.; Möller, M., Preparation of isophorone diisocyanate terminated star polyethers. *Macromolecular Materials and Engineering* **2002**, 287, (4), 223 - 230.
19. Klinkhammer, K. Bockelmann, J., Simitzis, C., Brook, G. A., Grafahrend, D., Groll, J., Möller, M., Mey, J., Klee, D. Functionalization of electrospun fibers of poly( $\epsilon$ -caprolactone) with star shaped NCO-poly(ethylene glycol)-stat-poly(propylene glycol) for neuronal cell guidance. *Journal of Material Science: Materials in Medicine* **2010**, 21, 2637 - 2651.
20. Grafahrend, D.; Calvet, J. L.; Salber, J.; Dalton, P. D.; Moeller, M.; Klee, D., Biofunctionalized poly(ethylene glycol)-block-poly(epsilon-caprolactone) nanofibers for tissue engineering. *Journal of Materials Science-Materials in Medicine* **2008**, 19, (4), 1479 - 1484.
21. Groll, J.; Fiedler, J.; Engelhard, E.; Ameringer, T.; Tugulu, S.; Klok, H. A.; Brenner, R. E.; Moeller, M., A novel star PEG-derived surface coating for specific cell adhesion. *Journal of Biomedical Materials Research Part A* **2005**, 74A, (4), 607 - 617.
22. Grafahrend, D.; Heffels, K.-H., Beer, M. V., Gasteier, P.; Möller, Boehm, G., Dalton, P. D.; Groll, J., Degradable polyester scaffolds with controlled surface chemistry combining minimal protein adsorption with specific bioactivation. *Nature Materials* **2011**, 10, 67 - 73.
23. Deitzel, J. M.; Kleinmeyer, J.; Harris, D.; Tan, N. C. B., The effect of processing variables on the morphology of electrospun nanofibers and textiles. *Polymer* **2001**, 42, (1), 261 - 272.
24. Lee, K. H.; Kim, H. Y.; Khil, M. S.; Ra, Y. M.; Lee, D. R., Characterisation of nano-structured poly( $\epsilon$ -caprolactone) nonwoven mats via electrospinning. *Polymer* **2003**, 44, (4), 1287 - 1294.
25. Andradý, A. L., *Science and Technology of Polymer Nanofibers*. John Wiley & Sons: Hoboken, New Jersey, 2008; p 94.
26. Hsu, C.-M.; Shivkumar, S., Nano-sized beads and porous fiber constructs of poly( $\epsilon$ -caprolactone) produced by electrospinning. *Journal of Materials Science* **2004**, 39, (9), 3003 - 3013.
27. Megelski, S.; Stephens, J. S.; Chase, D. B.; Raboldt, J. F., Micro- and nanostructured surface morphology on electrospun polymer fibers. *Macromolecules* **2002**, 35, (22), 8456 - 8466.
28. Fong, H.; Chun, I.; Reneker, D. H., Beaded nanofibers formed during electrospinning. *Polymer* **1999a**, 40, (16), 4585 - 4592.
29. Shenoy, S. L.; Bates, W. D.; Frisch, H. L.; Wnek, G. E., Role of chain entanglements on fiber formation during electrospinning of polymer solutions: good solvent, non-specific polymer-polymer interaction limit. *Polymer* **2005**, 46, (10), 3372 - 2284.

30. Bölgen, N.; Menciloglu, Y. Z.; Acatay, K.; Vargel, I.; Piskin, E., *In vitro* and *in vivo* degradation of non-woven materials made of poly( $\epsilon$ -caprolactone) and nanofibers prepared by electrospinning under different conditions. *Journal of Biomaterials Science - Polymer Edition* **2005**, 16, (12), 1537 - 1555.
31. Park, J. B.; Yiu, G.; Kaneko, S.; Wang, J.; Chang, J.; He, Z., A TNF receptor family member, TROY, is a coreceptor with Nogo receptor in mediating the inhibitory activity of myelin inhibitors. *Neuron* **2005**, 45, 345 - 351.
32. Vyas, A. A.; Blixt, O.; Paulson, J. C.; Schnaar, R. L., Potent glycan inhibitors of myelin-associated glycoprotein enhance axon outgrowth *in vitro*. *Journal of Biological Chemistry* **2005**, 280, (16), 16305 - 16310.
33. Filbin, M. T., Qiu, J., Cai, D., Glial influences on axonal regeneration. In *Glial cell development - basic principles and clinical relevance.*, Jessen, K. R., Richardson, W. D., Ed. Oxford University Press: Oxford, 2001; pp 279-298.
34. Lisak, R. P.; Skundric, D.; Bealmear, B.; Ragheb, S., The role of cytokines in Schwann cell damage, protection, and repair. *Journal of Infectious Diseases* **1997**, 176, S173 - S179.
35. Schense, J. C.; Bloch, J.; Aebischer, P.; Hubbell, J. A., Enzymatic incorporation of bioactive peptides into fibrin matrices enhances neurite extension. *Nature Biotechnology* **2000**, 18, 415 - 419.
36. Tong, Y. W.; Shoichet, M. S., Enhancing the neuronal interaction on fluoropolymer surfaces with mixed peptides or spacer group linkers. *Biomaterials* **2001**, 22, 1029 - 1034.
37. Patel, S.; Kurpinski, K.; Quigley, R.; Gao, H.; Hsiao, B. S.; Poo, M.-M.; Li, S., Bioactive nanofibers: synergistic effects of nanotopography and chemical signaling on cell guidance. *Nano Letters* **2007**, 7, (7), 2122 - 2128.
38. Pankov, R.; Yamada, K. M., Fibronectin at a glance. *Journal of Cell Science* **2002**, 115, 3861 - 3863.
39. Zhang, Z.; Yoo, R.; Wells, M.; Beebe Jr., T. P.; Biran, R.; Tresco, P., Neurite outgrowth on well-characterized surfaces: preparation and characterization of chemically and spatially controlled fibronectin and RGD substrates with good bioactivity. *Biomaterials* **2005**, 26, 47 - 61.
40. Schlosshauer, B.; Dreesmann, L.; Schaller, H.-E.; Sinis, N., Synthetic nerve guide implants in humans: a comprehensive survey. *Neurosurgery* **2006**, 59, 740 - 747.
41. Möllers, S.; Heschel, I.; Damink, L. H.; Schugner, F.; Deumens, R.; Müller, B.; Bozkurt, A.; Nava, J. G.; Noth, J.; Brook, G. A., Cytocompatibility of a novel, longitudinally microstructured collagen scaffold intended for the nerve tissue repair. *Tissue Engineering Part A* **2009**, 15, 461 - 472.



42. Yu, T. T.; Shoichet, M. S., Guided cell adhesion and outgrowth in peptide-modified channels for neural tissue engineering. *Biomaterials* **2005**, 26, 1507 - 1514.
43. Kim, Y. T.; Haftel, V. K.; Kumar, S.; Bellamkonda, R. V., The role of aligned polymer fiber-based constructs in the bridging of long peripheral nerve gaps. *Biomaterials* **2008**, 29, 3117 - 3127.
44. Lundborg, G.; Dahlin, L.; Dohi, D.; Kanje, M.; Terada, N., A new type of “bioartificial“ nerve graft for bridging extended defects in nerves. *Journal of Hand Surgery (British and European Volume)* **1997**, 22B, 299 - 303.
45. Matsumoto, K.; Ohnishi, K.; Kiyotani, T.; Sekine, T.; Ueda, H.; Nakamura, T.; Endo, Y.; Shimizu, Y., Peripheral nerve regeneration across an 80-mm gap bridged by a polyglycolic acid (PGA)-collagen tube filled with laminin-coated collagen fibers: a histological and electrophysical evaluation of regenerated nerves. *Brain research* **2000**, 868, 315 - 328.

## Curriculum Vitae

### Persönliche Daten

Name	<b>Klinkhammer (geb. Feil)</b>
Vorname	<b>Kristina</b>
Geburtstag	31.01.1980
Geburtsort	Herdecke
Staatsangehörigkeit	deutsch

### Qualifikationen

Mai 1999	Allgemeine Hochschulreife
1999 – 2005	Studium der Chemie an der RWTH Aachen
Okt. 2004 – März 2005	Diplomarbeit bei Prof. Möller am Lehrstuhl für Textil- und Makromolekulare Chemie der RWTH Aachen, Thema „ <i>Melt electrospinning of scaffolds for tissue engineering</i> “
März 2005	Diplom
Juli 2005 – Mai 2009	Promotion bei Prof. Möller am Lehrstuhl für Textil- und Makromolekulare Chemie der RWTH Aachen

### Berufstätigkeit

Juli 2002	Studentische Hilfskraft an der RWTH Aachen
April 2005 – Juni 2005	Wissenschaftliche Hilfskraft am DWI e. V. an der RWTH Aachen
Juli 2005 – Mai 2009	Wissenschaftliche Mitarbeiterin am Universitätsklinikum an der RWTH Aachen und seit Juli 2008 am DWI e. V. an der RWTH Aachen
seit Juni 2009	Wissenschaftliche Mitarbeiterin am Forschungsinstitut für Textil- und Bekleidung der Hochschule Niederrhein in Mönchengladbach

---

## List of publications

Parts of this thesis are published, submitted to be published, or were presented at conferences:

### Publications

Bockelmann, J.; Klinkhammer, K.; von Holst, A.; Seiler, N.; Faissner, A.; Brook, G.A.; Klee, D.; Mey, J., Functionalization of electrospun poly( $\epsilon$ -caprolactone) fibers with the extracellular matrix-derived peptide GRGDS improves guidance of Schwann cell migration and axonal growth. *Tissue Engineering Part A* **2011**, 17, (3-4), 475 - 468.

Klinkhammer, K.; Bockelmann, J.; Simitzis, Ch.; Brook, G. A.; Grafahrend, D.; Groll, J.; Möller, M.; Mey, J.; Klee, D, Functionalization of electrospun fibers of poly( $\epsilon$ -caprolactone) with star shaped NCO-poly(ethylene glycol)-*stat*-poly(propylene glycol) for neuronal cell guidance. *Journal of Materials Science: Materials in Medicine* **2010**, 10, 2637 - 2651.

Yoshida, H.; Klinkhammer, K.; Matsusaki, M.; Möller, M.; Klee, D.; Akashi, M., Disulfide-crosslinked electrospun poly( $\gamma$ -glutamic acid) non-wovens as reduction-responsive scaffolds. *Macromolecular Bioscience* **2009**, 9, (6), 568 - 574.

Klinkhammer, K.; Seiler, N.; Grafahrend, D.; Gerardo-Nava, J.; Mey, J.; Brook, G. A.; Möller, M.; Dalton, P. D.; Klee, D., Deposition of electrospun fibers on reactive substrates for *in vitro* investigations. *Tissue Engineering, Part C* **2009**, 15, (1), 77 - 85.

Gerardo-Nava, J.; Führmann, T.; Klinkhammer, K.; Seiler, N.; Mey, J.; Klee, D.; Möller, M.; Dalton, P. D.; Brook; G. A., Human neural cell interactions with orientated electrospun nanofibers *in vitro*. *Nanomedicine* **2009**, 4, (1), 11 - 30.

Grafahrend, D.; Lleixa Calvet, J.; Klinkhammer, K.; Salber, J.; Dalton, P. D.; Möller, M.; Klee, D., Control of protein adsorption on functionalized electrospun fibers. *Biotechnology and Bioengineering* **2008**, 101, (3), 609 - 621.

Schnell, E.; Klinkhammer, K.; Balzer, S.; Brook, G.; Klee, D.; Dalton, P.; Mey, J., Guidance of glial cell migration and axonal growth on electrospun nanofibers of poly- $\epsilon$ -caprolactone and a collagen/poly- $\epsilon$ -caprolactone blend. *Biomaterials* **2007**, 28, 3012 - 3025.

Dalton, P. D.; Grafahrend, D.; Klinkhammer, K.; Klee, D.; Möller M., Electrospinning of polymer melts: Phenomenological observations. *Polymer* **2007**, 48, 6823 - 6833.

Dalton, P. D.; Klinkhammer, K.; Salber, J.; Klee, D.; Möller, M., Direct *in vitro* electrospinning with polymer melts. *Biomacromolecules* **2006**, 7, 686 - 690.

K. Klinkhammer; E. Schnell; Dalton, P.; Klee, D.; Brook, G.; Mey, J.; Möller, M., Electrospun fibres of collagen-blended polycaprolactone for oriented cell growth. *DWI Reports* **2006**, 180, P17.

Klinkhammer, K.; Schnell, E.; Dalton, P. D.; Möller, M.; Mey, J.; Klee, D.; Brook, G., Elektrogenesponnene PCL/Kollagenfasern für orientiertes Zellwachstum zur Nervenregeneration. Electrospun PCL/collagen fibres for oriented cell growth in nerve regeneration. *Biomaterialien* **2006**, 7, (3), 175.

Klinkhammer, K.; Dalton, P.; Salber, J.; Klee, D.; Möller, M., Elektroverspinnung von PEO-*b*-PCL Blockcopolymer-Schmelzen zur Herstellung von Zellträgerstrukturen. Melt Electrospinning of PEO-*b*-PCL block copolymers for scaffold manufacturing. *Biomaterialien* **2005**, 6, (3), 187.

### **Conference contributions**

Klinkhammer, K.; Seiler, N.; Dalton, P.; Mey, J.; Brook, G.; Klee, D.; Möller, M., Substrates of electrospun polycaprolactone / collagen fibres for neurite guidance. Worldcongress of Biomaterials, 28. May - 1. Jun. 2008 in Amsterdam, Netherlands.

Klinkhammer, K.; Seiler, N.; Dalton, P.; Mey, J.; Brook, G.; Möller, M.; Klee, D., Neurite guidance by an *in vitro* system based on electrospun fibres on activated substrates. Biomedica, 16. - 18. Apr. 2008 in Maastricht, Netherlands.

Klinkhammer, K.; Seiler, N.; Schnell, E.; Dalton, P.; Mey, J.; Brook, G.; Klee, D.; Möller, M., Electrospun fibres of polycaprolactone and collagen for guided cell migration and axonal growth. 41. Jahrestagung der Deutschen Gesellschaft für Biomedizintechnik im VDE, 26. - 29. Sep. 2007 in Aachen, Germany.

Klinkhammer, K.; Seiler, N.; Dalton, P.; Möller, M.; Brook, G.; Mey, J.; Klee, D., Development of a system to test cell behaviour depending on chemical composition of electrospun fibres, fibre alignment and surface coating. 11<sup>th</sup> Euron PhD student day, 13. - 14. Sep. 2007 in Brüssel, Belgium.

Klinkhammer, K.; Schnell, E.; Dalton, P.; Mey, J.; Brook, G.; Klee, D.; Möller, M., Electrospinning of fibers from polycaprolactone and polycaprolactone/collagen blends for neuronal cell guidance. Annual Meeting of Society for Biomaterials, 18. - 21. Apr. 2007 in Chicago, Illinois, USA.

Klinkhammer, K.; Schnell, E.; Balzer, S.; Brook, G.; Dalton, P.; Klee, D.; Mey, J., Electrospinning of oriented nanofibers of collagen/poly- $\epsilon$ -caprolactone as a matrix for cell migration and neurite outgrowth in nerve regeneration. 7<sup>th</sup> Meeting of the German Neuroscience Society and 31<sup>st</sup> Göttingen Neurobiology Conference, 29. Mar. - 1. Apr. 2007 in Göttingen, Germany.

Klinkhammer, K.; Dalton, P.; Salber, J.; Klee, D.; Möller, M., Direct deposition of melt electrospun PEO-*b*-PCL fibres onto cells. VW-Symposium, 18. - 21. Mar. 2007 at Abtei Rolduc, Netherlands.

Klinkhammer, K.; Schnell, E.; Dalton, P.; Klee, D.; Brook, G.; Mey, J.; Möller, M., Electrospun fibres of collagen-blended polycaprolactone for oriented cell growth. ATC 2006, 29. - 30. Nov. 2006 in Aachen, Germany.

---

Klinkhammer, K.; Schnell, E.; Balzer, S.; Dalton, P.; Möller, M.; Brook, G.; Mey, J.; Klee, D., Electrospinning of polycaprolactone/collagen-fibres for oriented cell growth. 10<sup>th</sup> Euron PhD student day, 21. - 22. Sep. 2006 in Maastricht, Netherlands.

Klinkhammer, K.; Schnell, E.; Dalton, P. D.; Möller, M.; Mey, J.; Klee, D.; Brook, G., Elektrogenesponnene PCL/Kollagenfasern für orientiertes Zellwachstum zur Nervenregeneration. Electrospun PCL/collagen fibres for oriented cell growth in nerve regeneration. Jahrestagung der Deutschen Gesellschaft für Biomaterialien, 5. - 8. Sep. 2006 in Essen, Germany.

Klinkhammer, K.; Schnell, E.; Dalton, P.; Klee, D.; Brook, G.; Mey, J.; Möller, M., Electrospun fibres of collagen-blended polycaprolactone for oriented cell growth. 8<sup>th</sup> meeting of the sbii network, 1. Sep. 2006 in Liverpool, Great Britain.

Klinkhammer, K.; Dalton, P.; Salber, J.; Klee, D.; Möller, M., Elektroverspinnung von PEO-*b*-PCL Blockcopolymer-Schmelzen zur Herstellung von Zellträgerstrukturen. Melt Electrospinning of PEO-*b*-PCL block copolymers for scaffold manufacturing. Jahrestagung der Deutschen Gesellschaft für Biomaterialien, 7. – 8. Okt. 2005 in Würzburg, Germany.